

BIOLOGICALLY IMPORTANT COMPOUNDS IN SYNFUELS PROCESSES*. B. R. Clark, C.-h. Ho, W. H. Griest, and M. R. Guerin. Analytical Chemistry Division, Oak Ridge National Laboratory, P. O. Box X, Oak Ridge, Tennessee 37830.

Crude products, by-products and wastes from synfuel processes contain a broad spectrum of chemical compounds--many of which are active in biological systems. Discerning which compound classes are most important is necessary in order to establish effective control over release or exposure. Polycyclic aromatic hydrocarbons (PAH), multi-alkylated PAH, primary aromatic amines and N-heterocyclic PAH are significant contributors to the overall mutagenic activities of a large number of materials examined. Ames test data show that the basic, primary aromatic amine fraction is the most active. PAHs, multi-alkylated PAHs and N-heterocyclic PAHs are all components of the neutral fraction. In nearly all cases, the neutral fractions contribute the largest portion of the mutagenic activity, while the basic primary aromatic amine fractions have the highest specific activity. Neutral fractions are usually the largest (wt%) whereas the total basic fractions are small by comparison; thus, the overall greater contribution of the neutral fraction to the mutagenic activity of most samples. Biologically active constituents are isolated in preparative scale amounts from complex mixtures utilizing combinations of liquid-liquid extraction and various liquid chromatographic column-eluent combinations. Fractions are characterized using a combination of spectroscopic techniques and gas chromatography/mass spectrometry. (*Research sponsored by the Office of Health and Environmental Research, Department of Energy, under contract W-7405-eng-26 with the Union Carbide Corporation.)

THE ELEMENTAL COMPOSITION OF SHALE OILS. J. P. Fox. Energy and Environment Division, Lawrence Berkeley Laboratory, University of California, Berkeley, CA 94720.

The abundance of 47 elements were measured in 12 shale oils from LETC's controlled-state retort, 7 shale oils from LLL's 125-kg simulated in-situ retort and in oils from the Geokinetics, Occidental, Equity and Paraho processes using neutron activation analysis, x-ray fluorescence spectrometry and Zeeman atomic absorption spectroscopy. The elements studied include C, H, N, As, Se, Co, Ni, Fe, Mn, Zn, U, Cl, Na and others. The resulting data were analyzed to determine the effect of retort operating conditions on measured elemental abundances.

This paper compares the elemental abundances in oils from simulated, surface and in situ processes in the framework of retort operating conditions and discusses the potential environmental implications of observed trace element patterns. This investigation indicates that the major elements in shale oils (>10 ppm) are C, H, N, S, Fe, As, Cl and Na. The elements Al, Ba, Co, Cr, Cu, Hg, Mg, Mn, Mo, Ni, Se, V and Zn occur at concentrations of from 0.1 ppm to less than 10 ppm. All other elements studied occurred at less than 0.1 ppm in most oils. Striking differences were observed between the elemental abundances of Antrim, Moroccan and Green River shale oils.

ANALYSIS OF ENERGY WASTE EFFLUENTS FOR ORGANIC CHEMICALS USING THE MASTER ANALYTICAL SCHEME. Linda Sheldon, Shirley Yung, Roger Wiseman, Larry Michael, and Edo Pellizzari
Analytical Sciences Division, Chemistry and Life Sciences Group, Research Triangle Institute, P. O. Box 12194, Research Triangle Park, NC 27709.

A variety of analytical methods were tested during the development of a comprehensive scheme to identify and quantitate volatile organic chemicals in aqueous samples using high resolution gas chromatography/mass spectrometry/computer (GC/MS/COMP) as the major analytical tool. Volatile organics are defined as those compounds which will either elute from a GC column at 300°C in one hour or less or which may be derivatized to meet these criteria.

Highly volatile (bp <175°C), hydrophobic compounds were analyzed using a modified purge and trap procedure. Solvent extraction with pH adjustment served to concentrate the less volatile (bp >175°C) hydrophobic compounds. Ionic organics were concentrated by ion exchange, then chemically derivatized prior to gas chromatography. Lastly, volatile polar organics were concentrated by fractional distillation. As an alternative to direct aqueous injection, the distillate was injected onto a Tenax GC precolumn through a heated injection port, the water vented, and the organics were thermally desorbed into a gas chromatograph. For energy waste effluents, methods which gave a minimum detection limit of 10 ppb with 40% recovery were considered acceptable.

Developed methods were tested on a variety of spiked and unspiked sample waters including energy waste effluents. Specific problems with this sample matrix and test results will be presented. This research was supported by EPA Contract No. 68-03-2704.

TRACE ELEMENT BEHAVIOR IN THE SOLVENT REFINED COAL PROCESSES. R. H. Filby, S. R. Khalil,* and M. L. Hunt. Nuclear Radiation Center, Washington State University, Pullman, Washington 99164.

High sulfur coals contain significant quantities of trace metals which may have undesirable effects on liquefaction processes, on upgrading of derived syncrudes, or on the environment. A study of the fate of up to 35 trace elements in the SRC I and SRC II processes by neutron activation analysis (NAA) and atomic absorption spectroscopy (AAS) shows that significant emissions of toxic elements from the Fort Lewis, Washington 50 ton per day pilot plant (operated by Pittsburg & Midway Coal Mining Co.) occur and that, except for Hg in the SRC II process satisfactory material balances can be obtained for SRC I and SRC II processes. In the case of Hg in the SRC II process, and to a lesser extent As, Se and Sb, transport via gaseous streams has been demonstrated and can be related to the volatility and reactions of Hg^0 , HgS , H_2Se , As_4O_4 , etc. The NAA and AAS techniques and their application to the complex matrices encountered in coal liquefaction processes are discussed.

*Presently at University of Kentucky

CHARACTERIZATION AND MUTAGENICITY OF SHALE OIL FRACTIONS, Deborah S. Sklarew, Donald M. Schoengold, Richard A. Pelroy[†], Sylvia P. Downey, Barbara A. Vieux, James T. Cresto[†], Physical Sciences Dept. and Biology Dept.[†], Pacific Northwest Laboratory, operated for the Department of Energy by Battelle Memorial Institute

Product oils from several shale oil operations have been analyzed for organic compounds which are potential biological/environmental hazards. Two fractionation schemes have been compared both from an analytical and a biological point of view. The first method involves acid-base fractionation; the second uses partition chromatography on Sephadex LH-20. Fractions have been tested for mutagenicity in the Ames assay and those which gave positive results were further subdivided and analyzed by gas chromatography-mass spectrometry. In the case of the Sephadex LH-20 method, mutagenicity is concentrated in the methanol fractions; in the acid-base separation, mutagenicity is found in the basic and tar fractions.

COMPARISON AND CONTRAST OF TRACE ELEMENTS IN CRUDE SHALE OILS AND PETROLEUM

C. L. Wilkerson, D. S. Sklarew, J. C. Evans and J. S. Fruchter, Pacific Northwest Laboratory, Richland, WA 99352

The abundances and chemical forms of a large group of elements including the trace metals As, Co, Fe, Mo, Ni, Se, V and Zn were determined in three whole and fractionated shale oils obtained from Colorado and Utah oil shale reserves. The crude shale oils were representative product oils from an above-ground, a modified in-situ, and a true in-situ retorting process and were produced by pilot plant or larger sized facilities. Elemental abundances were determined by several modern analytical techniques including instrumental neutron activation analysis, energy dispersive X-ray fluorescence analysis, prompt γ -ray activation analysis, and plasma emission spectrometry. The analyses were compared to identify major differences between elemental partitioning yields of the various retorting technologies and were further compared and contrasted with reported elemental concentrations in petroleum. The elements As and Fe were found to be the most prominent trace metals in the shale oil matrix and As and Se levels were observed to be 1 to 2 orders of magnitude greater than those reported for petroleum.

ENVIRONMENTAL ORGANIC CHEMISTRY: THE ISOLATION AND IDENTIFICATION OF ORGANIC AND ORGANOMETALLIC COMPOUNDS FROM OIL SHALE RETORT WATERS.* Richard H. Fish and Mathilde J. Kland. Energy and Environment Division, Lawrence Berkeley Laboratory, University of California, Berkeley, CA 94720.

The complex nature of the inorganic, organic and organometallic contaminants found in oil shale retort waters is important to elucidate in order to evaluate the potential problems connected with the release of these compounds to the environment.

Our efforts have focused on more clearly defining the organic and the organometallic species, either synthesized or released during the retorting process, that eventually end up in the retort waters. Retort waters from LLL and LETC simulated in situ retorts and from Occidental's Logan Wash experiments were extracted with methylene chloride and the components separated and analyzed by a combination of dry column, thin layer and high performance liquid chromatography as well as capillary gas chromatography-mass spectrometry and nuclear magnetic resonance spectroscopy.

A discussion of the classes of organic and organometallic species identified, together with some of their toxicological and environmental implications, will be presented.

* Studies supported through the Department of Energy under contract no. W-7405-ENG-48.

INTERLABORATORY COMPARISON OF ENVIRONMENTAL ANALYSES ASSOCIATED WITH SYN-FUEL PRODUCTION, W. E. May, J. M. Brown, S. N. Chesler, F. R. Guenther, H. S. Hertz, L. R. Hilpert, R. N. Parris, K. L. Ritchie, and S. A. Wise, Center for Analytical Chemistry, National Bureau of Standards, Washington, DC 20234

In order to begin evaluating the state-of-the-art of the determination of pollutants associated with the production of alternate fuels, seven collaborative studies have been conducted by NBS. The aim of the five initial studies was to ascertain how well participating laboratories could perform the final quantitation step in a trace organic analytical scheme. The materials examined in these initial studies were two polynuclear aromatic hydrocarbon in hexane samples, a phenols in water sample, a phenols in hexane sample and a N-heterocyclic compounds (azaarenes) in hexane sample. Each of these samples contained between five and eight pure compounds, with each compound being present at the 1-100 $\mu\text{g/mL}$ (ppm) level.

The last two collaborative studies involved quantitative analyses of selected phenols, polynuclear aromatic hydrocarbons and N-heterocyclics in a shale oil and a solvent refined coal (SRC) material. Such analyses usually required a minimum of three steps: (1) Isolation of the analyte from the sample matrix; (2) Separation of the analyte from non-analyte interference; (3) measurement of detector response for the analyte and relating that to the concentration of the analyte in the original sample. The results of these collaborative studies will be reported and discussed along with methodologies developed at NBS for certifying the concentration of selected phenols, PAH and N-heterocyclics in alternate fuels.

ANALYSIS OF SULFUR HETEROCYCLES IN COAL-DERIVED PRODUCTS AND SHALE OILS* C. Willey
M. Iwao, T. A. Broadbent, R. N. Castle, and M. L. Lee, Department of Chemistry,
Brigham Young University, Provo, Utah 84602.

The carcinogenic activity demonstrated by complex mixtures of polycyclic aromatic compounds (PAC) has stimulated much effort by researchers to identify individual mixture components. Found in low concentrations among the mixture components of most PAC fractions from coal-derived products and shale oils are the sulfur heterocycles. Due to their low concentrations, an enrichment of the heterocyclic sulfur compounds is necessary for identification. A recently developed method to isolate the sulfur heterocycle fraction from a composite aromatic fraction has greatly aided efforts to separate and identify individual heterocyclic sulfur compounds by glass capillary gas chromatographic mass spectrometry.

In this study, the developed methodology for the enrichment and subsequent separation and identification of sulfur heterocycle fractions has been applied to selected coal gasification tars, coal liquids, and shale oils. Identification was accomplished through comparison of mass spectral and chromatographic retention data of mixture components with standard reference compounds.

Since few standard reference compounds of sulfur heterocycles are commercially available, compounds predicted by mass spectrometry to be present in enriched sulfur heterocycle fractions were synthesized. These compounds were used to obtain chromatographic retention data and for biological testing.

*This study was supported by the U.S. Department of Energy, Division of Biomedical and Environmental Research, Contract No. DE-AC02-79EV10237.

ENVIRONMENTAL HEALTH AND SAFETY ASPECTS OF SYNFUELS PROCESSING--AN OVERVIEW. E. J. Salmon, National Academy of Sciences, 2101 Constitution Avenue, Washington DC 20418 and H. Perry, Resources for the Future, 1755 Massachusetts Ave. Washington, DC 20036.

OBSERVATIONS ON THE POTENTIAL ENVIRONMENTAL EFFECTS OF SYNFUELS PRODUCTION. T. K. Janes, Environmental Protection Agency, Research Triangle Park, NC 27711

ENVIRONMENTAL IMPACT OF THE FORMATION OF A SYNFUELS INDUSTRY. M. J. Reilly, ESCO,
444 N. Capitol St. N. W. Washington DC 20001.

RISK ANALYSIS OF COAL UTILIZATION--SYNFUELS VS. DIRECT COMBUSTION. H. Inhaber,
Atomic Energy Control Board, Ottawa, Canada K1P 5S9.

THE IMPACT OF "NO ACTION". J. G. Seay, Institute of Gas Technology, 3436 S. State St. Chicago IL 60616.

ENVIRONMENTAL CONSIDERATIONS IN COAL GASIFICATION PLANT DESIGN. R. J. Feldman,
C. B. Foganan and N. R. Passow, The Lumax Company, Division of Combustion Engi-
neering, 1515 Broad St., Bloomfield NJ 07003.

ENVIRONMENTAL AND HEALTH ASPECTS OF COAL LIQUEFACTION PLANT DESIGN. C. R. Hoxley
Gulf Mineral Resources Company, 1720 S. Bellaire, Denver CO 80222

ASSESSMENT OF THE WATER BALANCE IN COAL CONVERSION PLANT DESIGN. II. Takash, C. S.
Kelley and W. G. Atkins, H. Mittelhauser Co., 5120 Belmont Rd. Suite G, Downers
Grove IL 60515.

TRANSPORTATION FUELS FROM SYNTHESIS GAS. R. H. Fischer and R. E. Hildebrand. U.S. Department of Energy, Office of Fossil Energy Programs, Division of Fossil Fuel Processing, Mail Stop E-338/Germantown, Washington, DC 20545.

ABSTRACT

The Department of Energy (DOE) has formulated a program to develop improved processes to convert synthesis gas from coal to quality transportation fuels. The program involves four elements.

1. Improved integration of gasification with liquefaction. This involves the use of low ratio H_2 to CO synthesis gas in the hydrocarbon formation step. Low ratio H_2 to CO can be converted to hydrocarbon by means of the Kolbel-Engelhardt reaction. The net result is considerable energy savings in steam.
2. Improved selectivity by use of shape selective catalyst. Normal Fischer-Tropsch reaction chemistry is subject to inherent limitations due to the chain growth mechanisms. Use of shape selective catalysts can result in circumvention of this limitation by the use of an intermediate that can be formed in high selectivity (methanol) or by inhibition of the chain growth mechanism.
3. Use of improved thermally efficient liquefaction reactors. Use of the liquid or slurry phase reactor can possibly result in single pass conversion, elimination of recycle, improved temperature control, and recovery of the heat of reaction at higher efficiency.
4. Production of methanol and fuel grade alcohol from low ratio H_2 -CO syn gas using liquid or slurry phase reactors.

The key to success in this effort will be a close integration of the gasification and synthesis steps so that the amount of steam and oxygen consumed by the total process will be minimized and the thermal efficiency maximized.

The initial contracts in this program are about to be signed and others are beginning negotiation. The goals of the program and this up coming work will be discussed.

EVIDENCE FOR ADSORBED HYDROCARBON INTERMEDIATES DURING THE INITIAL STAGES OF CO HYDROGENATION ON IRON

H.P. Bonzel and H.J. Krebs

Institut für Grenzflächenforschung und Vakuumphysik, Kernforschungsanlage Jülich, D-5170 Jülich, Germany

1. Introduction

Surface science techniques have been applied to the study of the surface properties of the transition metals Fe, Co, Ni and Ru /1-12/ and it is natural to extend the same approach to the study of Fischer-Tropsch synthesis (FTS) reactions on the same metal surfaces. However, reaction products in the adsorbed or gaseous phase apparently cannot be detected under vacuum conditions. Therefore, in order to utilize surface analytical techniques for the study of FTS, a combination of a surface analysis ultra-high vacuum system and an atmospheric reaction chamber has to be used, such as pioneered by Somorjai and coworkers /13, 14/.

In this paper we report on the use of such a combination apparatus of novel design with Auger electron (AES) and X-ray photoelectron spectroscopy (XPS) as analytical capabilities and a differential microreactor. The analysis of the reaction products is performed by gas chromatography (GC). Using this system we studied the hydrogenation of CO on polycrystalline iron foils and a Fe(110) single crystal at a total pressure of 100 kPa (= 1 bar \approx 1 atm) /15/.

2. Experimental

The experimental system, sketched in Fig. 1, consisted of a stainless steel ultra-high-vacuum (UHV) chamber pumped by an ion pump, and an attached sample transfer system containing a small micro-reactor. The UHV chamber shown on the left hand side of Fig. 1 operates at a base pressure of 1×10^{-8} Pa. This system (Leybold-Heraeus) features an ion sputter gun for surface cleaning, an electron gun, X-ray source and high resolution electron spectrometer for Auger electron (AES) and photoelectron (XPS) spectroscopies, and a quadrupole mass spectrometer for residual gas analysis. The sample is either a polycrystalline iron foil about 0.1 mm thick, or a Fe(110) single crystal, with an active area of 0.35 cm². It is situated at a cutout portion of a stainless steel rod of 2 cm diameter. This rod serves as a transfer mechanism between UHV chamber, micro-reactor and atmosphere. The Fe sample can be heated resistively up to 1400 K in vacuum and about 900 K in 100 kPa of a H₂/CO mixture. The temperature of the sample is measured by a sheathed Chromel-Alumel thermocouple attached to the underside of the sample.

The micro-reactor of about 4 cm³ total volume is a small section of the sample transfer system, Fig. 1. A mixture of CO and H₂ was passed continuously through this reactor at a rate of 50 cm³/min. The partial pressure ratio of CO to H₂ was fixed by adjusting the individual flow rates of these two gases before entering the mixing stage. Partial pressure ratios of CO to H₂ from 1:100 to 1:4 could be easily chosen.

The transfer of the Fe-foil from the UHV system into the micro-reactor was accomplished by pulling the sample rod until the sample was located inside the reactor. The sample could be moved to the atmospheric loading position in a similar way, and also back into the UHV chamber. The transfer time from the reactor into the UHV position including pump-down to 10^{-8} Pa was 45 seconds. The sample rod itself is water cooled such that during heating of the Fe sample inside the micro-reactor no parts other than the sample and the tip of the thermocouple get hot. During the catalytic rate measurements the hydrocarbon products were analyzed by gas chromatography. A 0.5 cm³ sample (loop volume) of the gas mixture was taken by the GC sample valve and passed over a 8 ft. Porapak Q column. The separated products were analyzed by a flame ionization detector.

The Fischer-Tropsch measurements were carried out in the following way: The

cleaned Fe sample was transferred from UHV into the micro-reactor where a steady state gas flow was already established. As soon as the sample came to a halt, the temperature was raised to the desired value as measured by the thermocouple. From this point on the time was measured and GC samples were taken periodically. At a later time the reaction was stopped by turning off the heating current. About 4 sec later the sample was transferred back to UHV for surface analysis by AES or XPS.

3. Results and Discussion

The measurements of FTS from CO and H₂ on Fe were carried out at a total pressure of 100 kPa (=1 atm) and CO/H₂ ratios of 1:100, 1:20 and 1:4. The temperature range investigated was 460-750 K. In all cases methane was the dominant product and its rate of formation time dependent. In order to check this time dependence, a series of GC reactivity measurements with a cycle of approximately 100 sec was carried out at the same temperature. Three examples of such curves are shown in Fig. 2 for a CO/H₂ ratio of 1:20 and different temperatures where the logarithm of the turnover number for methane is plotted as a function of time. These curves exhibit several interesting features: First, there is a strong rise in the methane rate of formation within the first 40-60 sec after reaching the reaction temperature. This rise signals the start of the reaction, and the apparent delay of about 30 sec prior to the rise (which is more obvious in a linear plot of rate versus time) represents the time it takes for the gas to flow from the reactor to the GC sampling valve. Second, there is a maximum in the rate of methane formation followed by a steady decline; both the position of the maximum and the slope of the decline depend on the temperature of the Fe-foil and the CO/H₂ ratio.

The occurrence of the maximum in these curves of Fig. 2 is connected with the known phenomenon of carbon accumulation on the Fe surface as a function of time /14,15/. The rate of carbon accumulation is faster, the higher the temperature or the higher the ratio of CO/H₂. However, the influence of the rate of carbon accumulation on the rate of CO hydrogenation is complicated due to different kinds of chemically bound carbon. We have measured the relative carbon concentration by XPS and present as an example the data in Fig. 3. This figure shows the carbon (1s) signal at different reaction times for similar experimental conditions as those of Fig. 2. In these experiments the Fe sample was moved into the micro-reactor for reaction for a short time, then into the UHV chamber for surface (AES or XPS) analysis, and back into the reactor for a continuation of the reaction.

The data in Fig. 3 illustrate the rapid increase in surface carbon concentration as a function of the reaction time and also a shift in the binding energy E_B of the C1s level from about 283.9 eV to 284.6 eV. Figure 4a shows the shift in E_B(C1s) versus time for a particular run at 530 K and CO/H₂ = 1:20. Figure 4b shows the corresponding integrated C1s peak area versus time. Note in Figs. 4a and 4b that the initial change in the plotted quantities, i.e. during the first 50 sec, is very rapid followed by a slower increase. It is tempting to associate this behaviour with the presence of different chemical carbonaceous species on the iron surface and with the rate of CH₄ formation.

Therefore we performed a number of experiments which were aimed at identifying the chemical nature of the carbonaceous surface phases after the CO/H₂ reaction. The procedure consists essentially in comparing the carbon Auger peak shapes and C1s binding energies of carbonaceous surface layers of known chemical origin (composition) with those of the surface phases generated by the hydrogenation of CO.

A total of three significantly different carbonaceous layers were observed after the hydrogenation reaction. Figure 5 shows the carbon Auger spectra of these three layers which we call the surface phases I, II and III, respectively. These spectra were obtained for CO/H₂ = 1:20. In comparing the Auger spectra of Fig. 5 one should in particular pay attention to the relative heights of the peaks labelled A, B and C. Other differences can be noted in the negative peak excursion at 270-285 eV. These, however, will not be referred to in this paper.

The carbon 1s spectra corresponding to the AES spectra in Fig. 5 showed different binding energies similar to those of Fig. 3. These measured C1s binding energies are listed in Table I together with the data for adsorbed acetylene, segregated carbidic and graphitic carbon.

Table I
C1s Binding Energies

Species	Binding Energy (eV)	
CO	285.9	} produced in UHV
C ₂ H ₂	283.9	
carbidity C	283.3	
graphitic C	285.0	
Phase I-CH _x	283.9	} after reaction
Phase II	284.2	
Phase III	284.7	

Surface phase I

The C1s binding energies of this surface phase and chemisorbed molecular acetylene are identical within experimental error. This fact suggests that surface phase I is a heavily hydrogenated carbon layer. A comparison of Auger data, Fig. 6, shows, however, a substantial difference for surface phase I and acetylene. On the other hand, a very good simulation of the surface phase I Auger spectrum is obtained when a carbidity surface carbon produced in UHV by heating the sample to 720 K for about 2 min is exposed to C₂H₂ at 400 K for 5 min (2×10^{-5} Pa). It is likely that under these conditions some decomposition of C₂H₂ into CH species will occur /16,17/. We propose therefore that the surface phase I consists mainly of carbidity carbon and CH species.

Surface phase II

At first sight the Auger spectrum of surface phase II, Fig. 5, appears to be identical to the spectrum of carbidity carbon segregated under UHV conditions. However, this is not the case. Figure 7 shows both spectra for a direct comparison, and it can be noted that the peaks B and C of these two spectra are shifted against each other by about 2 eV. The reason for this shift is presumably bonded hydrogen in the case of the surface phase II, as expected from the shift of 0.9 eV for the C1s spectra of UHV carbidity carbon and surface phase II carbon (see Table I). The fact that some hydrogen is necessary in order to generate the Auger peak of surface phase II is illustrated by the following experiment: Fe(110) with segregated carbidity carbon was exposed to C₂H₂ at 475 (2×10^{-5} Pa, 5 min). The Auger spectrum taken subsequently is shown as trace (c) in Fig. 7 and it has features identical to those of the surface phase II spectrum.

The amount of bonded hydrogen in the surface phase II is presumably less than in the CH_x layer, mainly for two reasons: (1) There is no shape change in the Auger peak relative to carbidity carbon, only an energetic shift; (2) the procedure of simulating phase II involves an C₂H₂ exposure at higher temperatures (475 K compared to 400 K for CH_x simulation) facilitating the dehydrogenation of C₂H₂. The surface phase II can thus be characterized as a carbidity carbon layer with bonded hydrogen.

Surface phase III

The carbon Auger peak of the surface phase III has a great similarity with that of graphitic carbon /18,19/. Figure 8 shows an Auger trace of graphitic

carbon on Fe(110) which was segregated to the surface by heat treating the crystal in UHV (625 K, 25 min). Looking at the relative peak heights A, B and C one can notice the same sequence as in the spectrum of phase III. In a procedure equivalent to those discussed in the previous sections we can also produce a phase III type carbonaceous layer by exposing the Fe crystal with carbidic carbon to C_2H_2 at about 580 K (2×10^{-5} Pa, 20 min). The Auger peak of this layer is shown as trace (b) in Fig. 8. For comparison the phase III peak is included as trace (c). All three traces (a) - (c) have very similar shapes but from a closer inspection of the energetic positions of the peaks it is apparent that peak B for the traces (b) and (c) is shifted to lower kinetic energies relative to that of trace (a). Since both layers characterized by (b) and (c) are originating from gas phase reactions involving hydrogen, it is reasonable to assume that this peak shift is indicative of bonded hydrogen.

Hydrogenation behavior

An interesting observation was made when the various carbonaceous layers were subjected to hydrogen atmosphere at elevated temperature. It was seen that the CH_x layer and the hydrogen containing carbidic carbon layer (phases I and II, respectively) could be readily removed by hydrogenation but that the graphitic layer was quite inert towards H_2 . An example of a hydrogenation of a mixed phase II/phase III layer is presented in Fig. 9. The total amount of carbon is seen to decrease but the binding energy shift from 284.4 eV to 284.9 eV indicates that carbidic carbon (phase II) is removed and graphitic carbon left behind on the surface.

The fast hydrogenation of surface phases I and II relative to the much slower removal of small amounts of graphitic carbon creates a possibility to separate the different phases in a mixed layer. Experiments of this kind showed that the total amount of carbon plotted for example in Fig. 4b could be broken up into a portion representing CH_x and carbidic carbon and a portion representing graphitic carbon. The first portion plotted versus time yields a maximum at about 30-50 sec similar to the maximum in Fig. 2. The second portion, graphitic carbon, increases steadily with time. We conclude that the maximum in reactivity is linked to the maximum in CH_x and carbidic carbon on the surface whereas the graphitic carbon acts as an inhibitor on the methanation as well as the Fischer-Tropsch reaction.

4. Conclusions

1. Layers of (UHV segregated) carbidic and graphitic carbon, molecularly adsorbed CO and C_2H_2 can be fairly well characterized by their respective carbon Auger peak fine structure and C(1s) binding energies.

2. Carbonaceous layers deposited by the CO hydrogenation reaction at 1 bar were analyzed by AES and XPS and could be classified by a comparison of carbon Auger line shapes and C(1s) binding energies with those of layers of known chemical composition.

3. A carbonaceous layer of particular interest formed in the initial phase of CO hydrogenation on Fe(110) was found to correspond to heavily hydrogenated carbidic carbon, most likely a CH_x phase. This phase is suggested to consist mostly of CH radicals.

4. The CH_x phase and carbidic carbon can be easily removed from the surface by hydrogenation; graphitic carbon is quite stable towards hydrogen at 1 bar and elevated temperatures.

5. The maximum in the time dependent methanation rate correlates with the maximum in CH_x and carbidic carbon; these latter species are important intermediates for the formation of methane and probably higher molecular weight products.

References

- /1/ K. Kishi and M.W. Roberts, J. Chem. Soc. Faraday Trans. I 71 (1975) 1715
- /2/ R.W. Joyner and M.W. Roberts, J. Chem. Soc. Faraday Trans. I 70 (1974) 1819
- /3/ K.Y. Yu, W.E. Spicer, I. Lindau, P. Pianetta and S.F. Lin, Surface Sci. 57 (1976) 157
- /4/ C.R. Brundle, IBM J. Res. Develop 11 (1978) 235
- /5/ G. Brodén, G. Gafner and H.P. Bonzel, Appl. Phys. 13 (1977) 333
- /6/ T.N. Rhodin and C.F. Brucker, Solid State Comm. 23 (1977) 275
- /7/ W. Erley and H. Wagner, Surface Sci. 74 (1978) 333
- /8/ G. Wedler, K.G. Colb, G. McElhiney and W. Heinrich, Appl. Surface Sci. 2 (1978) 30
- /9/ K.A. Prior, K. Schwaha and R.M. Lambert, Surface Sci. 77 (1978) 193
- /10/ R. Ku, N.A. Gjostein and H.P. Bonzel, Surface Sci. 64 (1977) 465
- /11/ H.P. Bonzel and T.E. Fischer, Surface Sci. 51 (1975) 213
- /12/ K.J. Singh and H. Grenga, J. Catal. 47 (1977) 328
- /13/ B.A. Sexton and G.A. Somorjai, J. Catal. 46 (1977) 167
- /14/ D.J. Dwyer and G.A. Somorjai, J. Catal. 52 (1978) 291 and J. Catal. 56 (1979) 249
- /15/ H.J. Krebs, H.P. Bonzel and G. Gafner, Surface Sci. (to be published)
- /16/ C.F. Brucker and T.N. Rhodin, J. Catal. 47 (1977) 214
- /17/ T.N. Rhodin, C.F. Brucker and A.B. Anderson, J. Catalysis (to appear)
- /18/ J.P. Coad and J.C. Rivière, Surface Sci. 25 (1971) 609
- /19/ C.C. Chang, Surface Sci. 25 (1971) 53

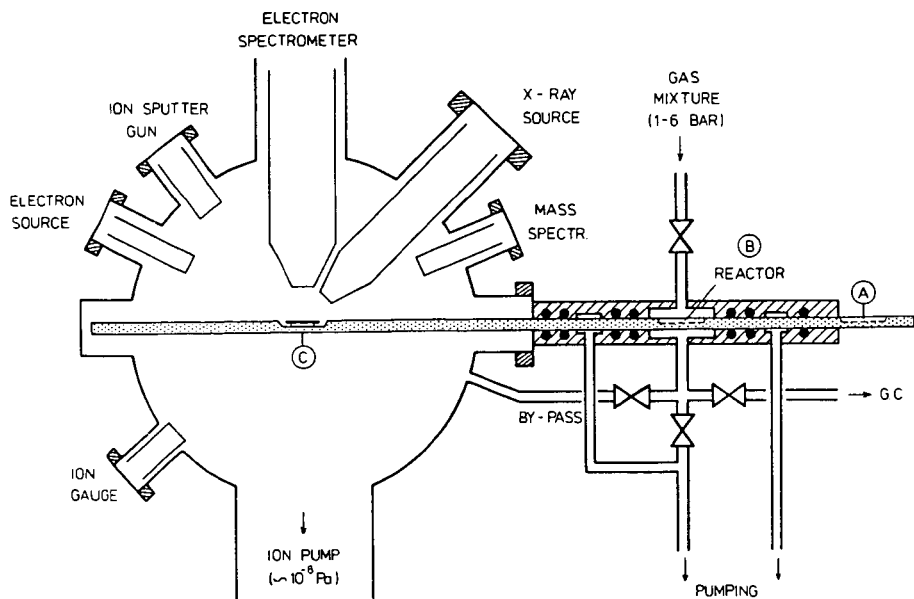


Figure 1: Schematic of UHV apparatus with attached sample transfer system and micro-reactor for catalytic rate measurements. The sample, located at the surface analysis position "C" in the center of the UHV chamber, can be moved by pulling the stainless steel rod, to the position "B" (reactor for chemical reaction) or position "A", the atmospheric loading position.

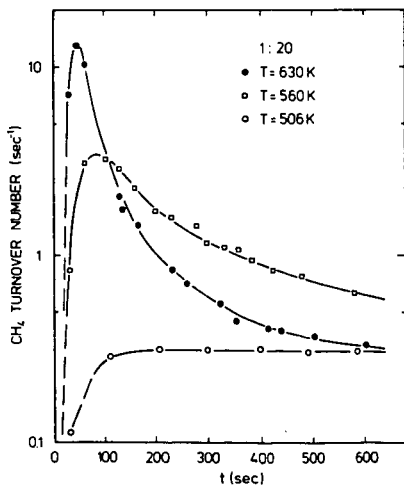


Figure 2: Semilog-plot of methane turnover number versus time for a CO/H_2 ratio of 1:20.

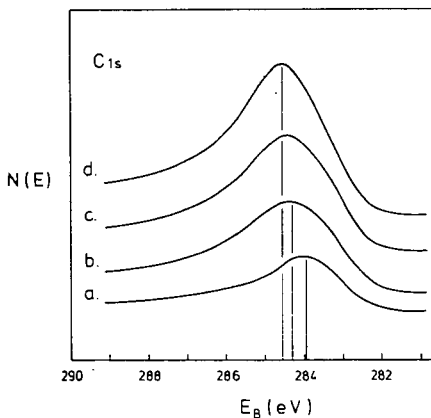


Figure 3: Carbon $1s$ XPS data after reaction, $\text{CO}/\text{H}_2 = 1:20$, $T = 530$ K, reaction times a) 3 sec, b) 23 sec, c) 83 sec and d) 600 sec. Note shift in maximum.

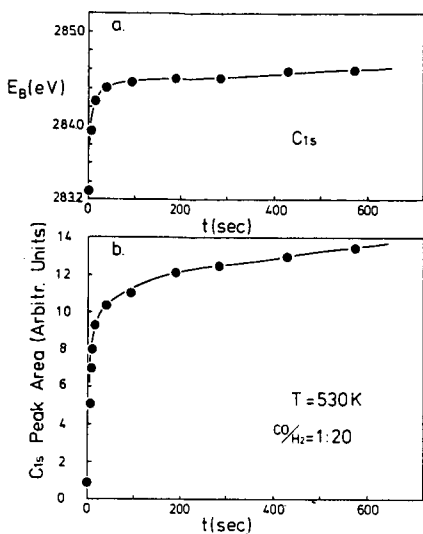


Figure 4: Same reaction data as in Fig. 3. (a) C_{1s} binding energy as a function of reaction time. (b) Integrated C_{1s} peak area (as a measure of surface carbon concentration) versus reaction time.

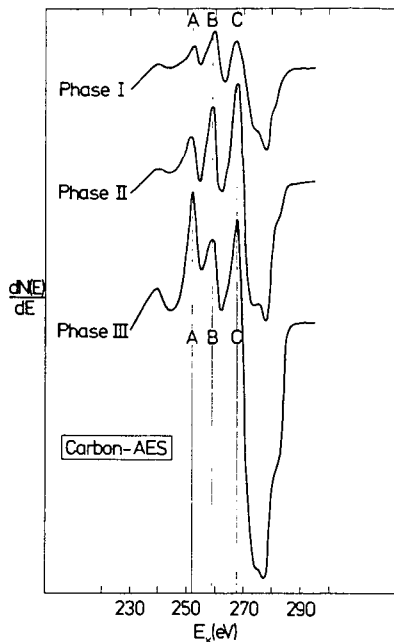


Figure 5: Carbon Auger spectra of the three carbonaceous surface phases formed after the CO/H₂ reaction at 1 bar and CO/H₂ = 1:20. Reaction conditions: Surface phase I - $T = 565 K$, $t = 15$ sec; surface phase II - $T = 615 K$, $t = 15$ sec; surface phase III - $T = 615 K$, $t = 90$ min.

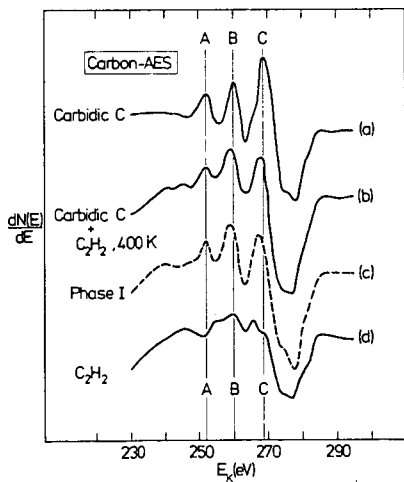


Figure 6: Carbon Auger spectra. (a) After heating the Fe(110) crystal in UHV at 720 K for about 3 min; (b) after exposure of the carbodic carbon on Fe(110) to 2×10^{-5} Pa C₂H₂ for 5 min at 400 K; (c) after reaction at 1 bar; (d) after exposing the clean Fe(110) crystal to C₂H₂ at room temperature (2×10^{-5} Pa, 5 min).

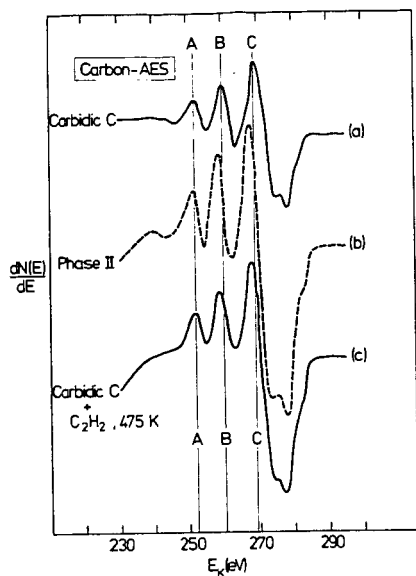


Figure 7: Carbon Auger spectra. (a) Fe(110) crystal was heated in UHV to 720 K for about 3 min; (b) after CO/H_2 reaction at 1 bar; (c) after exposing the surface produced under (a) to C_2H_2 at 475 K (2×10^{-5} Pa, 5 min).

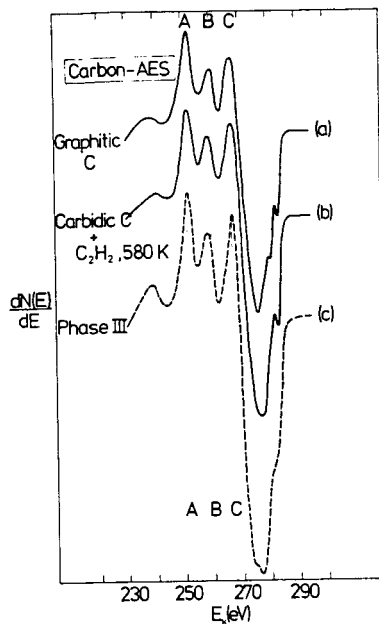


Figure 8: Carbon Auger spectra. (a) Fe(110) crystal was heated in UHV to 625 K for about 25 min; (b) after exposure of the Fe surface to C_2H_2 at 580 K (2×10^{-5} Pa, 20 min); after CO/H_2 reaction at 1 bar.

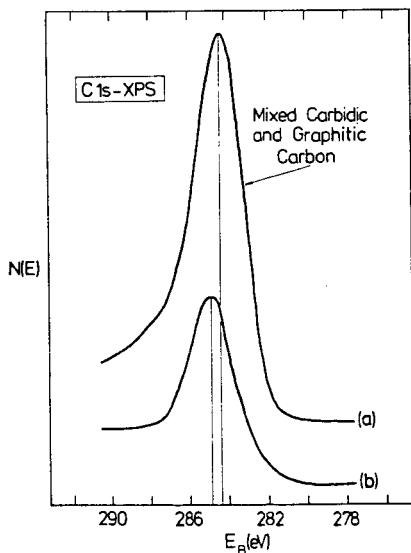


Figure 9: C1s spectra. (a) After CO/H_2 reaction at 1 bar and 630 K ($CO/H_2 = 1:20$, 10 min reaction time); (b) after hydrogenation of the surface under (a) at 1 bar, 630 K for 60 min.

CO HYDROGENATION OVER RHODIUM FOIL AND SINGLE CRYSTAL CATALYSTS:
CORRELATIONS OF CATALYST ACTIVITY, SELECTIVITY, AND SURFACE COMPOSITION

D. G. Castner,* R. L. Blackadar, and G. A. Somorjai

Materials and Molecular Research Division, Lawrence Berkeley Laboratory
and Department of Chemistry, University of California,
Berkeley, California 94720

*Present address: Chevron Research Company, P.O. Box 1627, Richmond,
California, 94802

ABSTRACT

CO hydrogenation at 6 atm over polycrystalline Rh foil and single crystal Rh (111) catalysts was investigated in a system where the surface structure and composition of the catalysts could be characterized both before and after the reaction. The reaction conditions ($H_2:CO$ ratio, reaction temperature, and surface pretreatment) were systematically varied to determine the optimum conditions for formation of oxygenated hydrocarbons. Initially clean Rh catalysts showed no structure sensitivity, primarily produced methane (90 wt%) at an initial rate of $0.15 \text{ molecules site}^{-1} \text{ sec}^{-1}$ at 300°C , and did not produce detectable amounts of oxygenated hydrocarbons. Preoxidation of the Rh catalysts (800 Torr O_2 , 600°C , 30 min.) resulted in dramatically increased initial rates, a larger fraction of higher molecular weight hydrocarbons, some structure sensitivity, and formation of methanol, ethanol, and acetaldehyde. The different Arrhenius parameters over the clean and preoxidized foils indicate that the methanation mechanism is different on these two surfaces. Decreasing the reaction temperature or $H_2:CO$ ratio increased the C_2H_4 to C_2H_6 ratio and shifted the product distribution towards higher molecular weight hydrocarbons.

INTRODUCTION

Reaction of H_2 -CO mixtures over the Group VIII metals usually yields a wide range of products, including alkanes, alkenes, and oxygenated hydrocarbons. In recent studies,^(1,2) Rh supported on SiO_2 showed a unique selectivity for production of the two-carbon oxygenated species acetaldehyde, acetic acid, and ethanol. Similar selectivity was shown at 1 atm on catalysts prepared by depositing Rh clusters on basic metal oxides.^(3,4) This contrasts with results for Rh foil⁽⁵⁾ and Rh supported on Al_2O_3 ,⁽⁶⁾ over which no oxygenated hydrocarbons were formed at 1 atm. A need therefore exists for studying CO hydrocarbons over well-characterized Rh at elevated pressures, under a variety of reaction conditions and surface pretreatments, to determine the conditions necessary for oxygenated product selectivity. We have measured reaction rates and product distributions over clean and pre-oxidized Rh foil and Rh(111) crystal surfaces at 6 atm and 250-400°C, with H_2 :CO ratios of 3:1 to 1:3. Surface structure and chemical composition were characterized using low-energy electron diffraction (LEED) and Auger electron spectroscopy (AES). The results will be compared to previous results on Rh catalysts.

EXPERIMENTAL

The apparatus and technique employed in these experiments are described elsewhere.^(5,7) Briefly, the reaction cell is located inside an ultra-high vacuum (UHV) chamber to allow ion sputter cleaning and surface characterization by LEED and AES immediately before and after reaction. After closing the cell, first the H_2 (99.9995% purity) and then the CO (99.99% purity,

Fe and Ni carbonyls removed in a dry ice trap) were admitted and circulated in the closed loop. Allowing a few minutes for mixing at room temperature, the reaction was then started by heating the Rh sample resistively. The buildup of products was monitored by a gas chromatograph using a Chromasorb 102 column and flame ionization detector. The reaction was stopped after times ranging up to 3 hr, by cooling to room temperature and pumping down to UHV, to measure changes in surface composition.

For preoxidized samples, the surface was heated to 600°C in 1 atm O₂ for 30 minutes inside the reaction cell. During this treatment, an epitaxial oxide was formed, and oxygen also dissolved into the bulk. The oxide layer was amorphous and had an O₅₁₀/Rh₃₀₂ AES peak intensity ratio of 0.5 to 0.6, although ratios up to 2.6 were obtained by oxidizing carbon-covered surfaces.

The initial turnover numbers (TN) were determined from a least squares fit to the initial slope of the product concentration vs. time curves. In the calculation, the atom density of the Rh(111) surface (1.6×10^{15} atoms cm⁻²) was used as the active site density. The same figure was also used for pre-oxidized samples, thus ignoring possible increases in surface area as well as a reduced Rh surface density on the oxide.

RESULTS

Fig. 1 shows the buildup of products during a typical run on clean Rh at 300°C and 3H₂:1CO. Results on the clean Rh foil and Rh(111) were identical. Under the above conditions, CH₄ was the main product (90 wt%) with initial TN 0.15 molecules site⁻¹ sec⁻¹. C₂ and C₃ hydrocarbons were formed, but no oxygenated hydrocarbons were detected. All rates of product formation, ex-

cept C_2H_6 , declined over the course of three hours. The AES spectra before and after reaction, in Fig. 2, show that small amounts of S and Cl and a monolayer of C built up on the surface during CO hydrogenation. AES peak intensities for these impurities remained nearly constant after the first 30 minutes, although the reaction rates continued to decline. The proximity of the Rh_{256} and Rh_{302} peaks prevented AES lineshape analysis to determine whether the carbon state was changing during this time.

Preoxidation of the Rh(111) crystal (see Figs. 3 and 4) greatly increased the initial TN's, shifted product distribution slightly to higher molecular weight, and resulted in the appearance of the oxygenated products methanol, ethanol, and acetaldehyde. The marked decrease in TN's during the first 30 minutes coincided with rapid loss of the epitaxial oxide. After this period, the near-surface oxygen concentration reached a low steady-state value, as shown in Fig. 5. Methane was still formed at a higher rate on the steady-state surface with oxygen than on the clean surface. Oxygenated products were formed during the entire three hours. Decreasing the temperature led to a further shift toward higher molecular weight and an increase in the C_2H_4 to C_2H_6 ratio, as shown in Figs. 6 and 7. During the CO-rich reactions acetaldehyde was the only oxygenated hydrocarbon produced. Also, two to four monolayers of carbon were deposited on the preoxidized Rh during CO-rich runs at $300^\circ C$, probably accounting for the increased poisoning rate (Fig. 6).

Results for preoxidized Rh foil were similar to those for preoxidized Rh(111) except for a small structure sensitivity shown in a lower CH_4 TN and larger C_2H_4 to C_2H_6 ratio. Also, ethanol formed a smaller fraction of the oxygenated products. In CO-rich runs, more carbon was deposited on the preoxidized foil than on preoxidized Rh(111), giving a faster poisoning rate.

The activation energy for methanation was found to be 12 kcal/mole on preoxidized foil, half the value (24 kcal/mole) found on clean Rh foil.⁽⁵⁾

DISCUSSION

Preoxidation of the Rh surfaces markedly changes their activity and selectivity, indicating that the chemical environment of the Rh atoms is important in determining their catalytic properties. This is consistent with the variability of supported Rh catalysts depending on their preparation.⁽¹⁻⁴⁾ The CH_4 formation rate depends directly on the oxygen concentration in the near-surface region, as shown in Table I. The lowest initial CH_4 production rate is obtained during CO hydrogenation over clean catalysts and the highest over the catalysts with an epitaxial oxide. An intermediate value is given by peroxidized surface which are flashed in vacuum prior to CO hydrogenation,⁽⁵⁾ resulting in a low near-surface oxygen concentration.⁽¹⁰⁾ The fact that CO_2 hydrogenation gives a higher CH_4 TN than CO hydrogenation under the same reaction conditions suggests that CO_2 oxidizes the catalysts during hydrogenation. CO_2 has been shown to dissociatively adsorb on Rh surfaces,^(8,9,11) and an oxygen AES signal was detected in the early stages of CO_2 hydrogenation over Fe.⁽¹²⁾

The changes in Arrhenius parameters, shown in Table II, strongly indicate that a change in mechanism is the cause of the increased CH_4 TN on preoxidized surfaces. In particular, a simple effect of surface area or active site density can be ruled out. The activation energy on the oxygen-treated surface is 12 kcal/mole, half that on the clean surface, 24 kcal/mole,⁽⁵⁾ and within experimental error of the value for CO_2 hydrogenation on clean Rh. This again

suggests oxidation by the CO_2 . Preexponential factors show a similar trend.

The effect of increasing pressure from 1 atm ⁽⁵⁾ to 6 atm (this study) was minor. The C_2H_4 to C_2H_6 ratio was smaller, presumably the result of the higher H_2 partial pressure increasing olefin hydrogenation. Also, the poisoning observed in this study at 6 atm was not observed at 1 atm. Possibly the effect of S and Cl impurities, or deactivation of C overlayers, is enhanced at high pressure. Behavior at 6 atm is in other respects similar to that at 1 atm ⁽⁵⁾ and agrees well with findings for supported Rh catalysts which produce hydrocarbons. ^(1,2,6) This indicates that metallic Rh or a complex of Rh and C is active in hydrocarbon formation, but that these surfaces do not provide the conditions necessary for oxygenated hydrocarbon formation, suggesting that a higher Rh oxidation state may be crucial to this process. Production of oxygenated hydrocarbons after the near-surface oxygen concentration reaches steady-state indicates that CO is the source of oxygen in these products, but bulk oxygen diffusing into the near-surface region is another possible source. We are undertaking isotopic labeling studies to resolve this question.

Varying the temperature and $\text{H}_2:\text{CO}$ ratio produces results that follow the trends predicted for a mixture of products in equilibrium, ⁽¹³⁾ that is, higher molecular weight and more unsaturated or oxygenated products are favored at low temperature, and the hydrogen-poor species C_2H_4 and CH_3CHO are favored at low $\text{H}_2:\text{CO}$ ratio. Thus thermodynamics seems to have relevance even though the overall $\text{CO}-\text{H}_2$ conversion to any of the products is far from equilibrium in our experiments. A possible explanation is that an initial slow step in the mechanism is followed by rapid combination and partial equilibration of hydrocarbon fragments.

REFERENCES

1. M. Ichikawa, Bull. Chem. Soc. Japan 51, 2268 (1978).
2. M. Ichikawa, Bull. Chem. Soc. Japan 51, 2273 (1978).
3. M. M. Bhasin, W. J. Bartley, P. C. Ellgen, and T. P. Wilson, J. Catal. 54, 120 (1978).
4. P. C. Ellgen, W. J. Bartley, M. M. Bhasin, and T. P. Wilson, 175th ACS Meeting, Los Angeles, Calif., Div. Petrol. Chem. Preprints 23, 616 (1978).
5. B. A. Sexton and G. A. Somorjai, J. Catal. 46, 167 (1977).
6. M. A. Vannice, J. Catal. 37, 449 (1975).
7. D. W. Blakely, E. I. Kozak, B. A. Sexton, and G. A. Somorjai, J. Vac. Sci. Technol. 13, 1091 (1976).
8. D. G. Castner, B. A. Sexton, and G. A. Somorjai, Surface Sci. 71, 519 (1978).
9. D. G. Castner and G. A. Somorjai, Surface Sci. 83, 60 (1979).
10. D. G. Castner and G. A. Somorjai, LBL-9288.
11. L. H. Dubois and G. A. Somorjai, LBL-8976 and LBL-9280.
12. D. J. Dwyer and G. A. Somorjai, J. Catal. 52, 291 (1978).
13. D. J. Dwyer, K. Yoshida, and G. A. Somorjai, 175th ACS Meeting, Los Angeles, Calif., Div. Petrol. Chem. Preprints 23, 521 (1978).

Table I. Comparison of initial methanation TN for CO and CO₂ hydrogenation in a batch reactor at 300°C over Rh and Fe catalysts. Methane TN is in molecules site⁻¹sec.⁻¹

Catalyst	Reaction Conditions	Surface Pretreatment	Initial CH ₄ TN at 300°C	Ref.
Rh foil	0.92 atm	clean	0.13	(5)
	3H ₂ :1CO	preoxidized ^(a)	0.33	(5)
Rh foil	0.92 atm	clean	0.33	(5)
	3H ₂ :1CO ₂	preoxidized ^(a)	1.7	(5)
Rh foil	6 atm	clean	0.15	this study
	3H ₂ :1CO	preoxidized ^(b)	1.7	
Rh(111)	6 atm	clean	0.15	this study
	3H ₂ :1CO	preoxidized ^(b)	4.6	
Fe foil	6 atm	clean	1.9	(12)
	3H ₂ :1CO	preoxidized ^(c)	18.7	(12)
Fe foil	6 atm 3H ₂ :1CO ₂	clean	10.9	(12)

(a) 15 min at 300°C in 700 Torr O₂, then heated to 1000°C in vacuum.

(b) 30 min at 600°C in 800 Torr O₂.

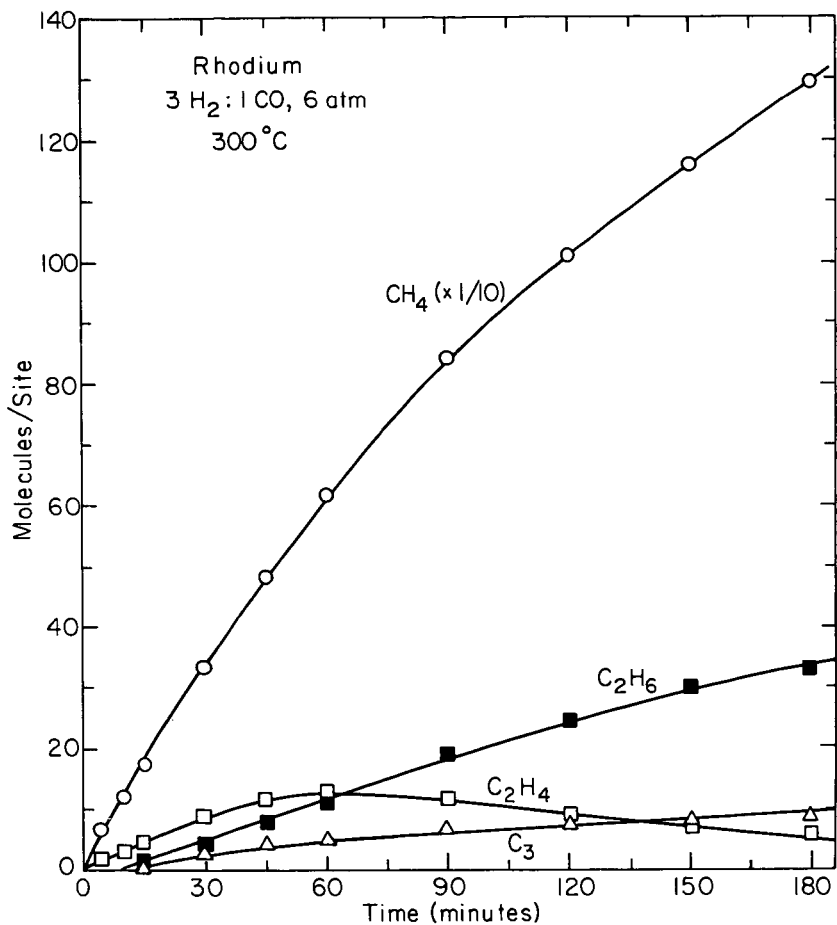
(c) 20 min at 300°C in 4 atm O₂.

Table II. Comparison of the Arrhenius methanation parameters ($TN = A e^{-E_a/RT}$) for CO and CO₂ hydrogenation over polycrystalline Rh foils. Units for TN and A are molecules site⁻¹sec⁻¹. E_a is in kcal/mole.

Reaction Conditions	Surface Pretreatment	CH ₄ TN at 300°C	A	E _a	Ref.
0.92 atm 3H ₂ :1CO	clean	0.13 ± 0.03	10 ⁸ (a)	24 ± 3	(5)
0.92 atm 3H ₂ :1CO ₂	clean	0.33 ± 0.05	10 ⁵ (a)	16 ± 2	(5)
6 atm 3H ₂ :1CO ₂	preoxidized ^(b)	1.7 ± 0.4	10 ⁵	12 ± 3	this study

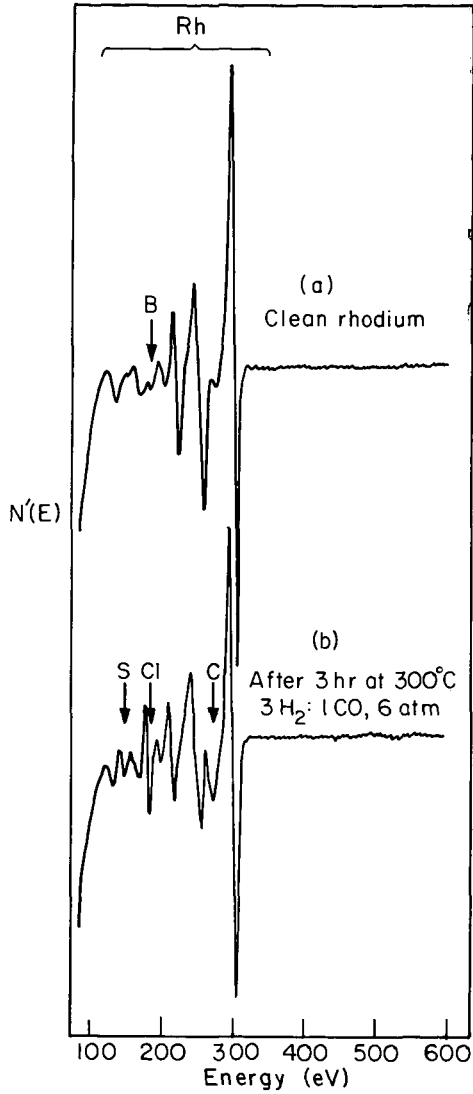
(a) determined from data in Ref. (5).

(b) 30 min. at 600°C in 800 Torr O₂.



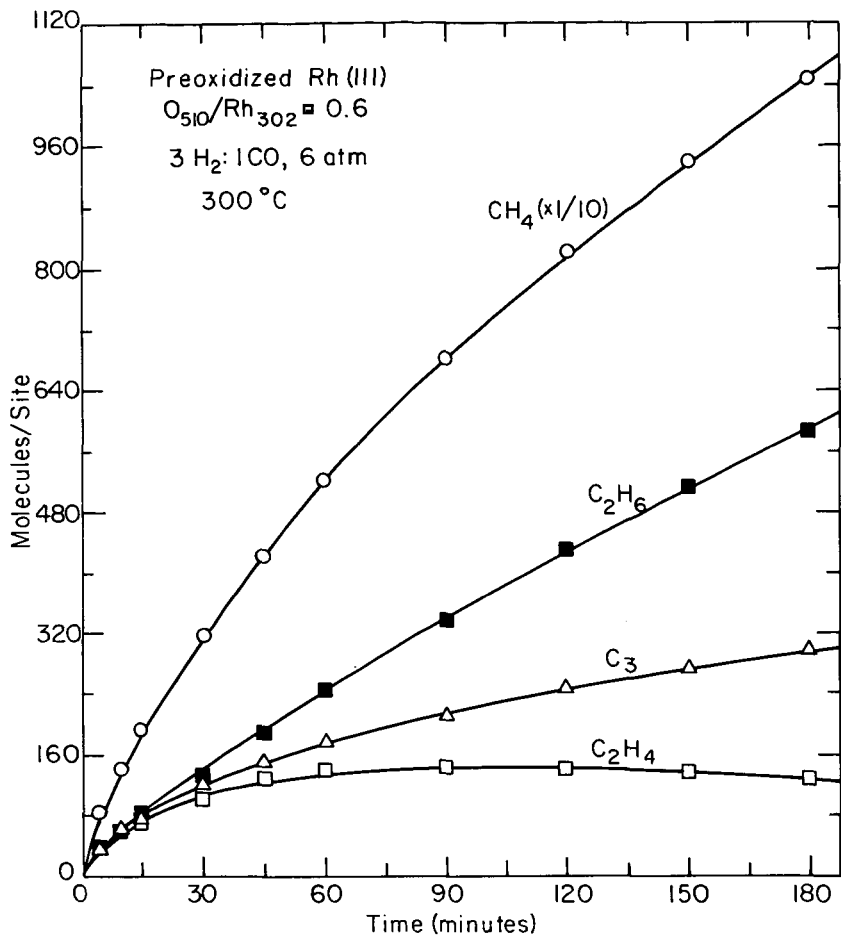
XBL 794-6130

Fig. 1. Buildup of the C_1 to C_3 hydrocarbon products during CO hydrogenation over initially clean Rh foil or Rh(111) catalysts at 6 atm, 300°C , and $3\text{H}_2:1\text{CO}$.



XBL 797-6655

Fig. 2. AES spectra of the initially clean Rh catalysts (a) before and (b) after 3 hr of CO hydrogenation at 6 atm, 300°C, and 3H₂:1CO.



XBL 794-6136

Fig. 3. Buildup of the C_1 to C_3 hydrocarbon products during CO hydrogenation over a preoxidized Rh(111) catalyst at 6 atm, $300^\circ C$, and $3H_2:1CO$.

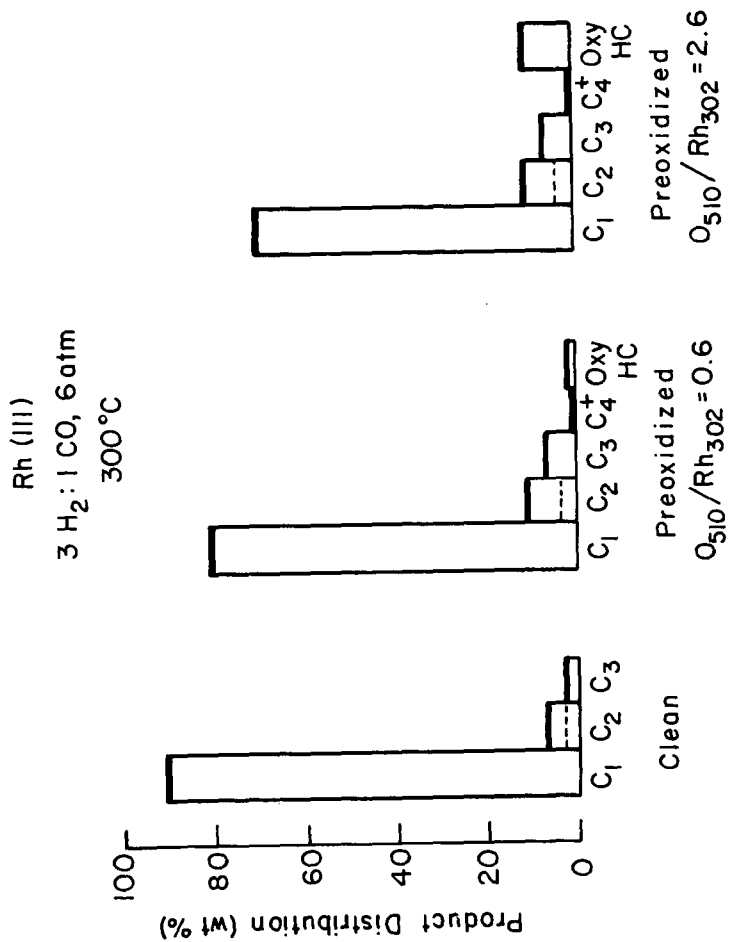
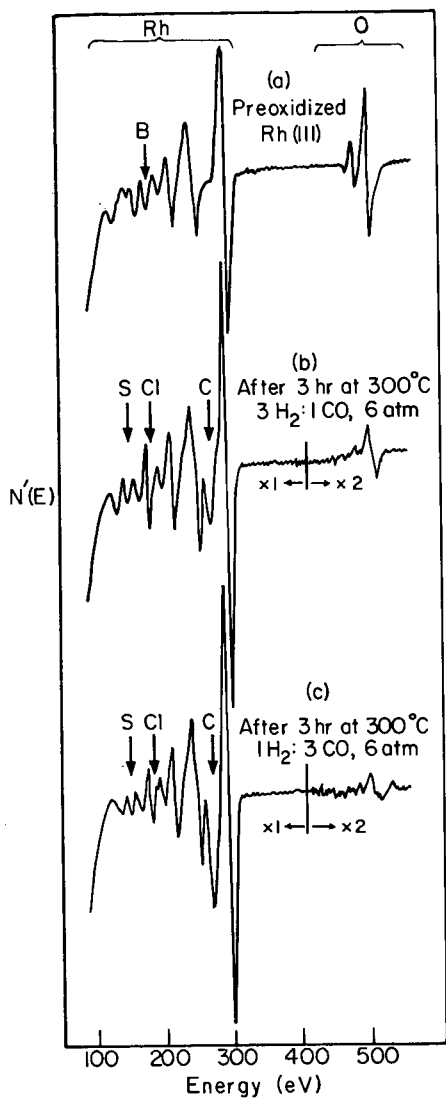


Fig. 4. The product distributions in weight percent after 2 hr of CO hydro-
genation over pretreated Rh(111) catalysts at 6 atm, 300°C, and
3H₂:1CO. Oxy HC is the sum of the CH₂OH, CH₃CH₂OH, and CH₃CHO frac-
tions. In the C₂ fraction the areas above and below the broken line
represent the C₂H₆ and C₂H₄ fractions.



XBL 797-6654

Fig. 5. AES spectra of the preoxidized Rh(111) catalyst (a) before and (b) after 3 hr of CO hydrogenation at 6 atm, 300°C, 3H₂:1CO, or (c) after 3 hr of CO hydrogenation at 6 atm, 300°C, 1H₂:3CO.

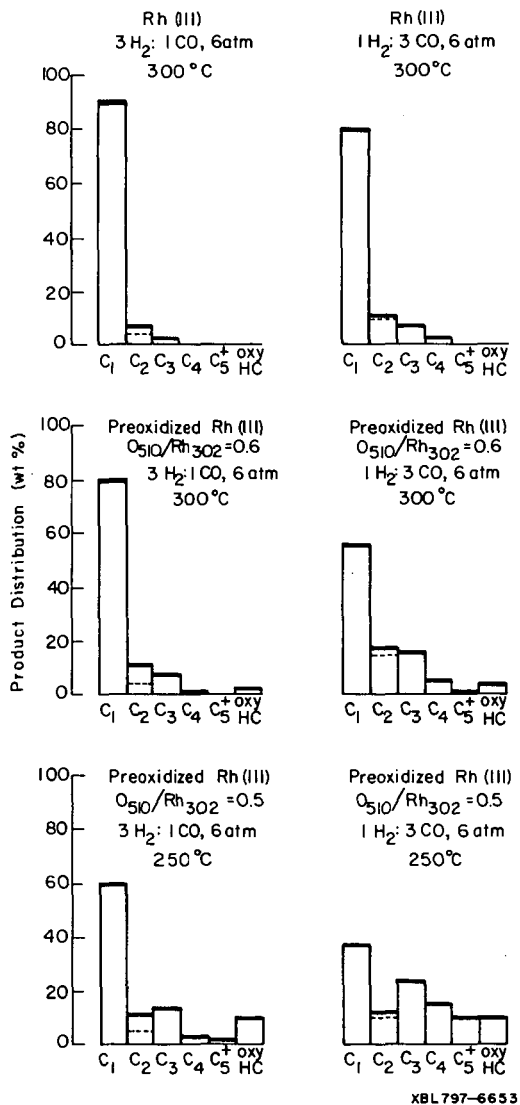
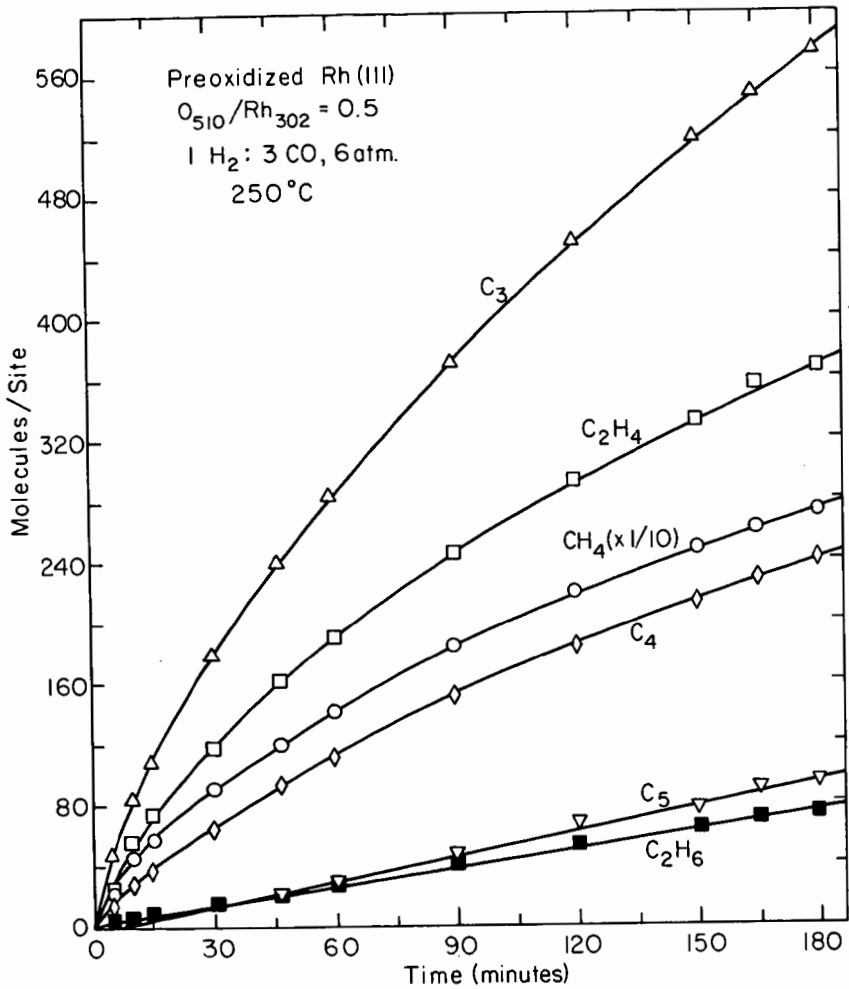


Fig. 6. Buildup of C₁ to C₄ hydrocarbon products during CO hydrogenation over a preoxidized Rh(111) catalyst at 6 atm, 250°C, and 1H₂:3CO.



XBL794-6129

Fig. 7. The product distributions in weight percent after 2 hr of CO hydrogenation over pretreated Rh(111) catalysts at various reaction conditions. See Fig. 4 for explanation of symbols.

CATALYTIC METHANATION OVER SINGLE CRYSTAL NICKEL AND RUTHENIUM:
REACTION KINETICS ON DIFFERENT CRYSTAL PLANES

R. D. Kelley and D. Wayne Goodman

Surface Science Division

National Bureau of Standards

Washington, D.C. 20234

Introduction

A specially designed ultrahigh vacuum system has been used to study the kinetics of the hydrogenation of CO over low surface area, single crystal catalysts. In a recent publication (1), we have reported reaction rate measurements for a Ni(100) catalyst and compared those results with kinetic data, derived from the literature, for small particle Ni supported on Al_2O_3 . There was remarkable agreement between the two catalyst systems in regard to specific reaction rates (the rate normalized to the number of surface metal atoms), the activation energy, and the product distribution. In the present report, we compare reaction rates measured on two crystal planes of Ni--the (100) and the close-packed (111)--and two crystal planes of Ru--the zig-zag, open (110) and the close packed (001). We also report the variation of the reaction rate and the surface carbon concentration with total pressure and with the $H_2:CO$ ratio. The surface carbon concentration (an active "carbide" carbon species) varies with the total pressure and with the reactant gas ratio. A striking correlation has been found between the surface carbide level and the catalytic reaction rate.

Experimental

The apparatus used for these studies consists of two connected ultrahigh vacuum chambers--one for surface analysis (Auger Electron Spectroscopy (AES)) and the other suitable for high pressure catalytic rate studies. A detailed description of the apparatus, the crystal cleaning procedure, and the techniques used to obtain kinetic rate data have been published (1). It should be noted that the number of metal surface atoms exposed to the reactant gas (used to normalize reaction rate data) is derived from the geometrical surface area of the annealed crystal and the appropriate surface atom density [Ni(100): 1.562×10^{15} atoms/cm²; Ni(111): 1.586×10^{15} atoms/cm²; Ru(110): 1.00×10^{15} atoms/cm²; Ru(001): 1.58×10^{15} atoms/cm²]. The Ru samples were cleaned using high temperature oxidation at 10^{-8} torr (2) followed by heating in vacuum to 1570K. (2)

Results and Discussion

The observation (1) that the rate of the reaction



(expressed as CH_4 molecules/surface site/sec) measured over a low surface area, single crystal catalyst is nearly identical to that measured over a supported small particle Ni catalyst (2) is a strong indication that there is little reactivity difference between those crystal planes commonly found in polycrystalline material (i.e., the low index planes). This expectation is confirmed in the data presented in Fig. 1, which is a plot of the specific rate (or turnover number) of CH_4 production versus the reciprocal temperature. The similarity between the open (100) and the close-packed (111) crystal planes of Ni is evident in both the value of the specific rate and the activation energy (24.7 kcal mole⁻¹ derived from the Ni(100) data). For comparison three sets of data for nickel (supported on alumina) catalysts are replotted from the literature. Thus for the $\text{H}_2 + \text{CO}$ reaction over Ni, there is essentially no variation in the reaction rate as the catalyst changes from small metal particles to bulk single crystal planes.

Analysis of an active crystal catalyst surface with AES indicates a low level of a carbon species and the absence of oxygen (1). Measurements of the rate of production of this surface carbon species (in pure CO) and the rate of reaction (in pure H_2) have indicated that both processes (i.e., the production and the removal of the surface carbon species) proceed at very similar rates. (3) A mechanism for the $\text{H}_2 + \text{CO}$ reaction consistent with the kinetic data and the finite surface carbon level during reaction was developed which involves the hydrogenation of an active carbon species formed from the dissociation of CO. Fig. 2a shows the changes in the reaction rate as the pressure is increased from 1-120 torr at a fixed $\text{H}_2:\text{CO}$ ratio. At low temperatures the rates fall on the same straight line at all pressures. As the temperature is increased a deviation from linearity is seen--the higher the pressure the higher the deviation temperature. Accompanying this non-linear rate behavior is an increase in the active carbon level on the surface of the catalyst crystal. We have proposed that this behavior (the departure from the linearity of the rate in Fig. 2a and the accompanying increase in the surface carbon level) is due to a decrease in the surface coverage of hydrogen and thus a decrease in the rate of hydrogenation of surface carbon. Fig. 2b shows similar data for a Ru(110) crystal. The variation of the reaction rate with pressure is very similar to the Ni(100) crystal--i.e., a departure from linearity of the rate and accompanying this departure an increase in the surface carbon level (see reference (4) for details of the AES measurement of carbon on Ru). We presume that the explanation of this behavior is the same offered for the Ni crystal. In fact, since the binding energy of H on Ru is lower than on Ni (2) the deviation from linearity should be expected at a lower temperature. This is particularly evident in the 1 torr data of Fig. 2a and 2b.

In addition to the rate data for the Ru(110) crystal, Fig. 2b also contains limited data for the basal plane of ruthenium, Ru(001). While the comparison is limited, it is clear that the $H_2 + CO$ reaction is quite similar in regard to the specific reaction rate and the activation energy for these two crystal planes of ruthenium.

The data of Fig. 2 indicate that the effect of the total pressure on the reaction rate is dependent on the temperature at which the measurements are made. Fig. 3 shows the variation of the specific rate as a function of pressure at two temperatures over a Ni(100) catalyst with the $H_2/CO = 4$. Many authors (5) have fitted reaction rate variation with pressure to a power rate law of the form

$$R_{CH_4} = A e^{-E/RT} p_{H_2}^x p_{CO}^y \quad 1)$$

The exponents, fitted from experimental data, have been used to derive information about the reaction mechanism (6). It is clear from Fig. 3 that, while power rate law exponents can be derived and used to scale rate data at fixed reaction conditions, such exponents are very sensitive to the reaction temperature. It is doubtful that any fundamental significance can be attached to values of the exponents derived at one temperature.

We have attempted to determine the dependence of the methanation rate on the partial pressure of both H_2 and CO . In conducting this study, we have measured the rate of CH_4 production with $H_2:CO$ ratios which varied from 0.1 to 1000 and with a total pressure which varied from 1 to 1500 torr. The results of this study indicate that even at one temperature a power rate law such as equation 1 is not adequate to describe the partial pressure dependence of the reaction rate. However, all reaction rate data measured over a Ni(100) catalyst can be correlated, on a smooth curve, with the concentration of "active" carbon on the Ni surface. Figure 4 is a plot of the measured carbon surface coverage and the measured specific reaction rate for various $H_2:CO$ ratios and total pressures at a temperature of 625K. It should be noted that the reaction rates are steady-state rates with no evidence for deactivation and that the carbon AES lineshape is always that of a "carbide" with no evidence for graphite formation. The estimate of carbon surface coverage from the AES carbon intensity is based on AES data obtained from a CO monolayer (4).

Since there is no pressure effect--in the pressure range of these measurements--in the rate of carbide production from pure CO (3) and since

at any $H_2:CO$ ratio an increase in pressure results in a decrease in surface carbon, we conclude that the data of Figure 4 is a manifestation of the change in the hydrogenation rate of the surface carbide with total pressure and with the $H_2:CO$ ratio. We have previously concluded (1) that the methanation reaction rate is determined by a delicate balance of the formation and removal of surface carbide and that neither of these processes are rate determining in the usual sense. Thus, as indicated in Figure 4 under reaction conditions unfavorable for the hydrogenation rate (e.g., low partial pressure of H_2 at a high temperature) the reaction rate should decrease and be accompanied by an increase in the surface carbon level. At lower temperatures the surface concentration of hydrogen (and thus the hydrogenation rate) becomes less strongly dependent on pressure. For example, the rate of CH_4 production for a 4:1 $H_2:CO$ ratio at 503K (plotted in Fig. 3) is only slightly dependent on pressure (from 1-1500 torr). The measured surface carbon level under these conditions is approximately 10% of a monolayer and does not change significantly over the entire pressure range.

Thus it appears that changes in temperature, H_2/CO ratio, and total pressure have a common effect on the methanation rate--namely, to change the surface concentration of hydrogen. Although these effects have been observed predominately on the Ni(100) crystal, the similarities between Ni and Ru with regard to reaction rate variation with pressure and with surface carbide level (Fig. 2) strongly suggest a similar explanation for ruthenium.

The results of these pressure studies suggest considerable caution in drawing the conclusion that crystallographic effects are absent in the methanation reaction over Ni or Ru. While this result appears valid under reaction conditions in which surface carbide level is low, as reaction conditions change effects due to diffusion of carbon, stability of the surface carbide, hydrogen surface concentration and other effects which can have a strong crystallographic dependence can become dominant factors influencing the reactivity.

FIGURE CAPTIONS

- Figure 1. Arrhenius plot comparing CH_4 synthesis on Ni(100), Ni(111), and supported Ni catalysts. Reaction conditions: 120 torr, $\text{H}_2/\text{CO} = 4$. Ni(111) - this work; Ni(100) - ref. (1); supported Ni - ref. 7.
- Figure 2. a.) Arrhenius plot of CH_4 synthesis on a Ni(100) catalyst at total reactant pressures of 1, 10, 120 torr. $\text{H}_2/\text{CO} = 4$.
b.) Arrhenius plot of CH_4 synthesis on a Ru(110) catalyst at total reactant pressures of 1, 10, 120 torr. $\text{H}_2/\text{CO} = 4$. Data at two temperatures for a Ru(001) catalyst at 120 torr is plotted with the symbol, x.
- Figure 3. Methane production rate (molecules/surface site/sec) versus pressure at 503K and 625K over a Ni(100) catalyst.
- Figure 4. Methane production rate (molecules/surface site/sec) at 625K over a Ni(100) catalyst versus surface carbon concentration (under steady state reaction conditions). The H_2/CO ratio and the total pressure (torr) for each point plotted is indicated in the insert.

REFERENCES

1. D. W. Goodman, R. D. Kelley, T. E. Madey, and J. T. Yates, Jr., accepted for publication in *J. Catalysis*.
2. D. W. Goodman, T. E. Madey, M. Ono, and J. T. Yates, Jr., *J. Catal.*, 50 279 (1977).
3. D. W. Goodman, R. D. Kelley, T. E. Madey, and J. M. White, accepted for publication in *J. Catalysis*.
4. D. W. Goodman and J. M. White, accepted for publication in *Surface Science*.
5. For example, M. A. Vannice, *J. Catal.*, 37, 449 (1975).
6. D. F. Ollis and M. A. Vannice, *J. Catal.*, 38, 514 (1975).
7. M. A. Vannice, *Catal. Rev. Sci. Eng.* 14(2), 153 (1976).

Fig. 1

Comparison of Rate of CH₄ Synthesis Over Ni Catalysts

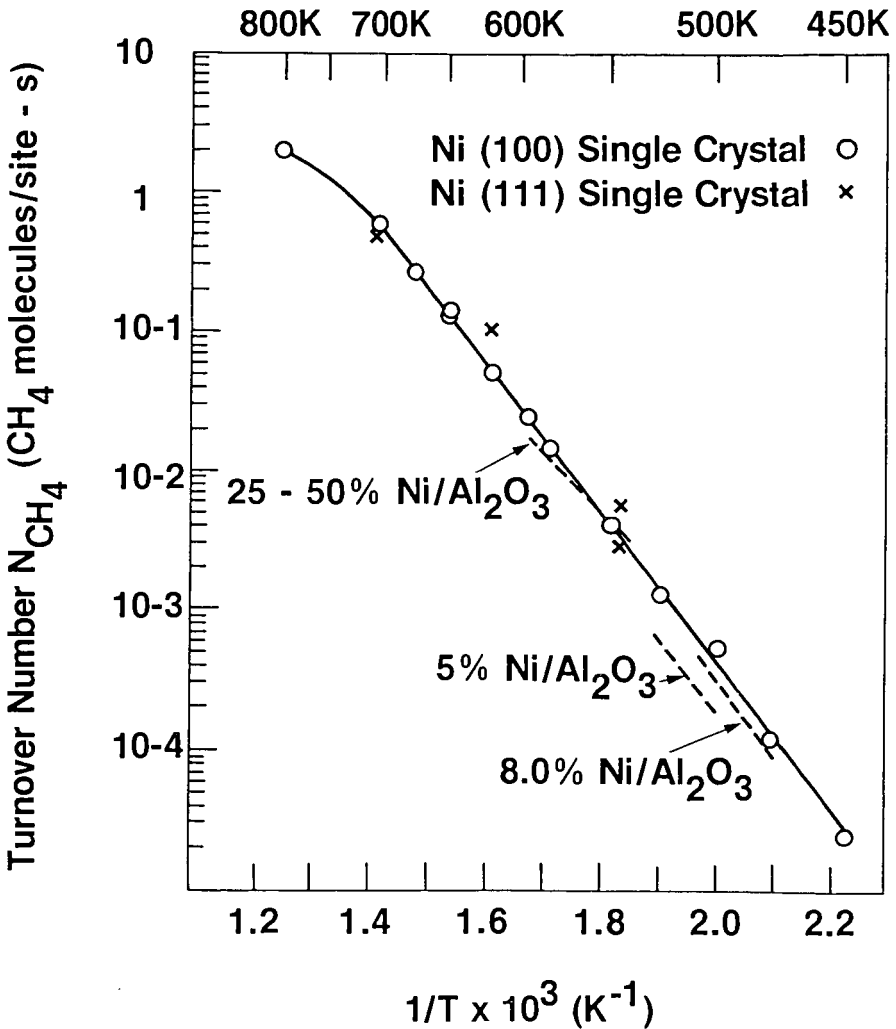


Fig. 2

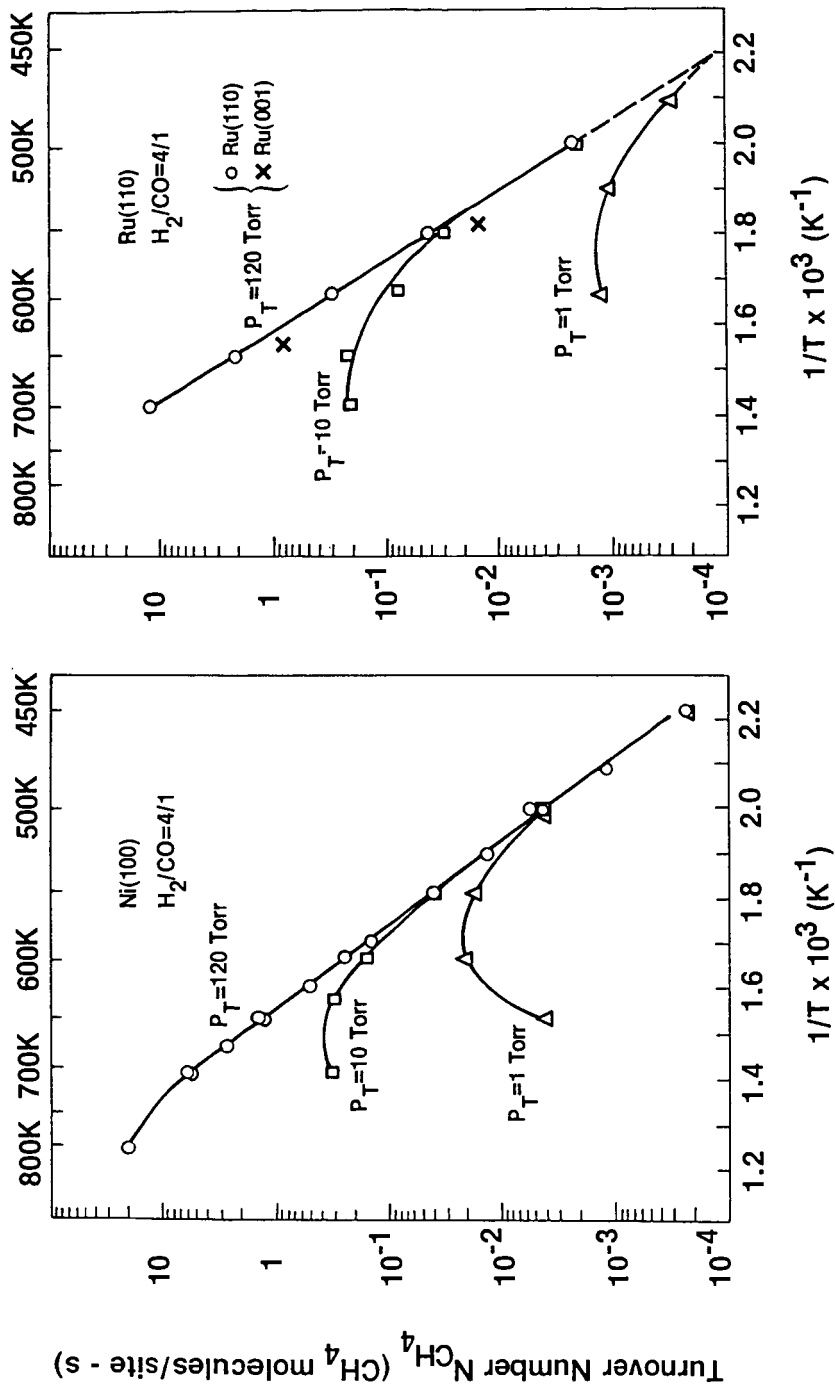


Fig. 3

Methane Production Versus Pressure Over A Ni(100) Catalyst

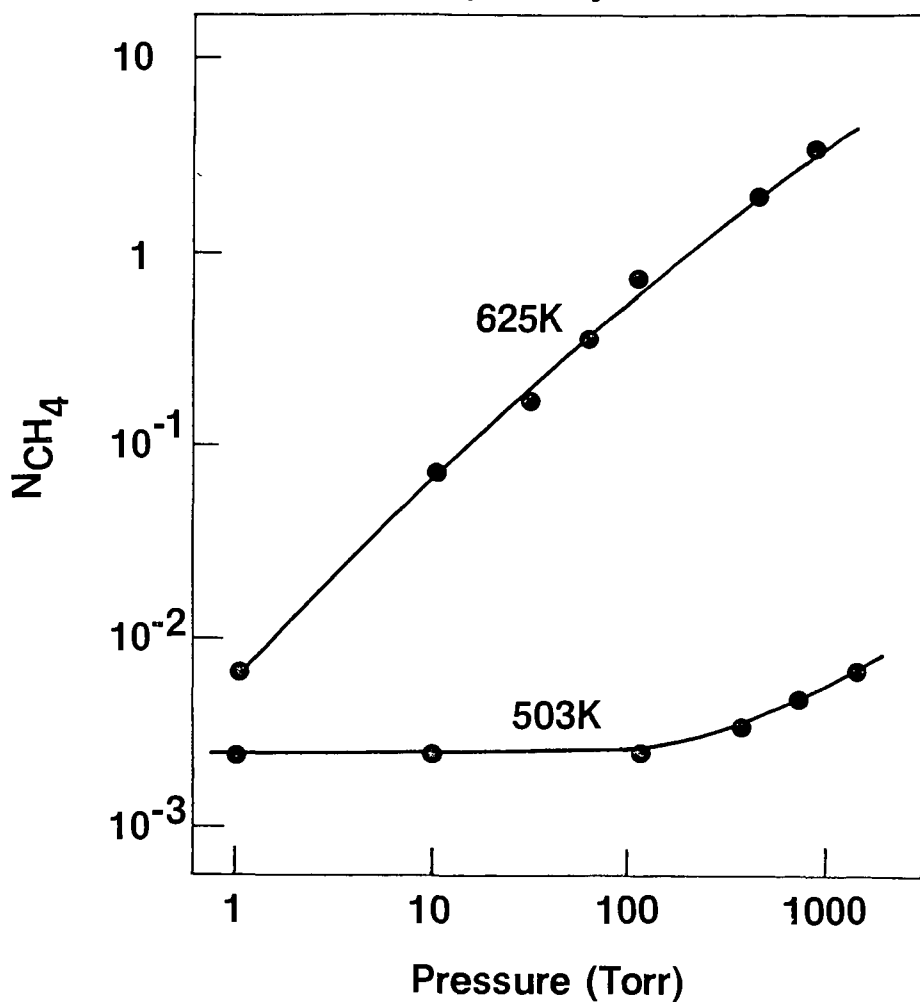
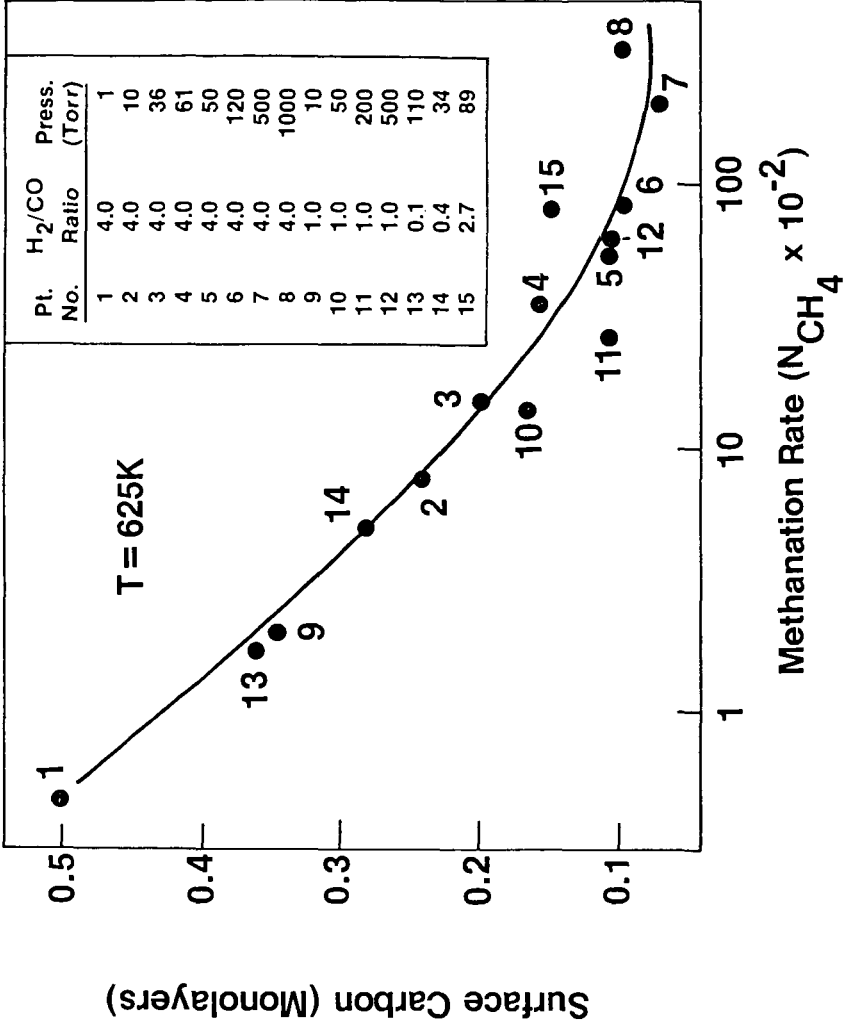


Fig. 4

Methanation Rate Versus Surface Carbon Level



THE EFFECTS OF POTASSIUM PROMOTION ON THE CHARACTERISTICS OF IRON FISCHER-TROPSCH CATALYSTS. H. Arakawa and A. T. Bell. Materials and Molecular Research Division, Lawrence Berkeley Laboratory and Department of Chemical Engineering, University of California, Berkeley, CA 94720.

The addition of potassium is well known to alter the performance of iron catalysts used for Fischer-Tropsch synthesis. The objectives of this investigation were to characterize the dependence of the activity, selectivity, and stability of alumina-supported iron catalysts on the K/Fe ratio and to seek explanations for the influence of potassium on the catalysts performance. Experiments were conducted with 20% Fe/Al₂O₃ catalysts containing 0 to 1 % of potassium. With increasing potassium content the catalyst activity decreased, the olefin to paraffin ratio of the product increased substantially, the methane selectivity decreased, and the catalyst stability was enhanced. The interpretation of these results will be discussed in terms of the influence of potassium on the adsorption of H₂, CO, and CO₂, and infrared observations obtained under reaction conditions.

DEACTIVATION BY CARBON OF NICKEL AND NICKEL-MOLYBDENUM METHANATION CATALYSTS

A. Douglas Moeller and Calvin H. Bartholomew

Brigham Young University
Department of Chemical Engineering
Provo, Utah 84602

INTRODUCTION

A serious problem in the catalytic methanation of coal synthesis gas is fouling of the catalyst by carbon deposition. This problem can be avoided by increasing the hydrogen content of the feed stream so that thermodynamic equilibrium is unfavorable toward carbon deposition (1); however, process economics favor minimizing hydrogen usage. Since most gasifiers produce a hydrogen deficient gas the application of a methanation catalyst which deposits carbon at negligible rates would be highly desirable, since it would eliminate the need for the shift reactor prior to methanation. Except for a few recent studies in this laboratory (2-5) there has been very little research to determine the effects of carbon deposition on activity or the kinetics and mechanism of carbon deposition on various catalysts during methanation. Such information would be valuable in determining the best catalysts and optimum operating conditions for methanation of hydrogen-poor synthesis gas.

A previous study in this laboratory (6) showed that Ni-Mo catalysts are promising for use in the BI-GAS process since they are as active as Ni but more resistant to sulfur poisoning. The present study was undertaken to determine the behavior of Ni and Ni-Mo catalysts under reaction conditions which are characteristic of combined shift/methanation and which favor massive carbon formation. The objectives of this study were to:

1. Determine the effects of carbon deposition on the activity of these catalysts under high temperature conditions (both low and high pressures) which promote carbon formation.
2. Determine if the carbon fouled catalysts could be regenerated by treatment in air or O_2 at high temperatures.

The results of activity, adsorption, carbon deposition and regeneration tests to accomplish these objectives are presented and discussed in this paper.

EXPERIMENTAL METHODS

Materials

Catalyst composition and suppliers are listed in Table 1. Catalyst preparation and pretreatment was the same as described previously (6).

Hydrogen gas (99.99% Whitmore) was purified using a Pd catalyst followed by a molecular sieve trap. Gases for the reaction mixtures, N_2 (99.99% Whitmore), CO (99.99% Matheson) CH_4 (99.97% Matheson), CO_2 (99.8% Whitmore) were used as delivered. The reaction mixture for the carbon deposition runs was passed through an activated charcoal trap heated to 473 K and a ZnO/molecular sieve trap heated to 353 K to remove any iron carbonyl and sulfur impurities before undergoing methanation. Catalyst presulfiding treatments were carried out using a 66 ppm H_2S in H_2 mixture prepared in this laboratory diluted to 9 ppm with hydrogen.

Procedure

H₂ Chemisorption. Prior to each test series, small samples (0.2-0.5 g) of reduced catalysts were rereduced at 773 K as previously described (6). H₂ adsorption isotherms were then measured at 298 K following procedures reported previously (7-9). H₂ chemisorption measurements were also performed following each series of tests to detect any changes in the catalyst surface area, and in the case of catalysts analyzed for carbon content H₂ chemisorption measurements were made directly after carbon deposition.

Specific Rate Measurement. Except for the fluidized bed tests specific rates were measured in a Pyrex, fixed-bed reactor at 498 K before and after the steady state carbon deposition runs and after regeneration in the same manner as in our previous study (6). Specific rate measurements for catalysts deactivated in the fluidized bed reactor were performed only after regeneration. Except for the measurements before and after high pressure carbon deposition these tests were performed with 0.2 to 0.6 gram samples and a reactant mixture consisting of 1% CO, 4% H₂ and 95% N₂. To avoid lengthy reduction and passivation steps, the specific rate measurements before and after the high pressure carbon deposition runs were carried out in the stainless steel high pressure reactor described previously (6) using 1 ml samples. The reactant mixture for these measurements was 4.3% CO, 5.6% H₂ and 90.1% N₂.

Steady State (24 h) Carbon Deposition Runs. After initial specific rate measurements, each catalyst was operated in a fixed bed for approximately 24 hours under steady state conditions at 723 K and pressures of 138 kPa or 2600 kPa to observe its behavior under severe carbon deposition conditions. Two samples of each catalyst were run at the lower pressure. One was used for regeneration tests and one was analyzed for carbon content. The space velocity for all steady state carbon deposition runs was 100,000 h⁻¹. Operation in the carbon deposition region of the equilibrium diagram was ensured by using a 4.2% CO mixture (in a N₂ diluent) and a H₂/CO ratio of 1.3. Figure 1 shows this composition on a carbon-hydrogen-oxygen triaxial plot along with our 1% CO mixture (H₂/CO = 4) and the BI-GAS nominal feed gas composition (H₂/CO = 1.4). Sample sizes were again 0.2-0.6 g for low pressure runs and 1 ml for high pressure runs. Reactant and product sampling was performed in the same way as in our previous in situ deactivation measurements (6).

Ni-Mo-Cu (0.57 g) and Ni-Mo (0.51 g) were operated in a fluidized bed reactor (6) for 24 hours at 723 K and 138 kPa. A fluidized bed was used in order to simulate more closely the BI-GAS process. The reaction mixture was a dilute BCR mixture of the following composition: 5.3% CO, 6.5% H₂, 1.6% CH₄, 3.6% CO₂, 83.0% N₂. These runs were repeated using fresh samples (0.5-0.6 g) and a 4.2% CO, 5.5% H₂, 90.3% N₂ mixture to obtain samples for carbon analysis.

Regeneration Tests and Passivation. Regeneration tests were performed with a 1-3% air in N₂ mixture at 138 kPa for catalysts deactivated at low pressure and a 1-4% O₂ in N₂ mixture at 2600 kPa for those deactivated at high pressure. In both cases the temperature was 573 K. Catalysts deactivated in a fluidized bed were also regenerated in a fluidized bed. During regeneration CO and CO₂ concentrations in the product stream were monitored continuously with the chromatograph for 15 to 30 minutes. After 30 minutes the CO₂ concentration was negligible indicating completion of carbon removal. The catalysts which had undergone either high pressure regeneration or low pressure fluidized bed regeneration were passivated with a dilute air/N₂ mixture and transferred to the fixed bed reactor cell to facilitate subsequent specific rate and H₂ chemisorption measurements.

Regeneration of the Ni catalyst was attempted using a 50% H₂O/H₂ mixture at 723 K and 2600 kPa for 6.5 hours, but it resulted in severe attrition and there was not enough catalyst left in the reactor to perform any meaningful tests. For this reason a dilute O₂/N₂ mixture at high pressure was used for regeneration of catalysts deactivated at high pressure.

Pre-sulfiding Runs. 0.5 ml samples of the Ni and Ni-Mo-Cu catalysts were loaded into the Pyrex fluidized bed reactor and re-reduced as discussed previously. The fluidized bed was used to assure uniform poisoning of the catalyst particles. These catalysts were then exposed to 375 ml/min of a gas mixture of 9 ppm H₂S in H₂ at 725 K for sufficient time to sulfide 50% of the catalyst surface (6). After exposure for the required time, the catalysts were cooled to room temperature and passivated. Activity tests were then run as described below.

RESULTS

Specific Rate and H₂ Chemisorption Measurements

Reaction rates per active site of catalyst, i.e. methane turnover numbers (N_{CH_4}), and product yields (fractions of converted CO occurring as various products) obtained in differential reactor tests of Ni, Ni-Mo, and Ni-Mo-Cu catalysts are presented in Table 2 along with H₂ chemisorptive uptakes.

The data in Table 2 show that all three catalysts suffered significant decreases in metal surface area measured by H₂ adsorption after carbon deposition at either low or high pressure. However, there were significant variations in the magnitude of changes observed for turnover numbers after carbon deposition at low pressure. The CH₄ turnover numbers of Ni and Ni-Mo-Cu did not change significantly while that of Ni-Mo dropped over 90%. CH₄ yield dropped for Ni and Ni-Mo but remained unchanged for Ni-Mo-Cu. Ni-Mo-Cu and Ni-Mo exhibited significant increases in CO₂ yield after carbon deposition, whereas Ni showed no significant CO₂ yield either before or after carbon deposition.

The catalysts also responded differently to regeneration. Ni and Ni-Mo regained activity after regeneration having CH₄ turnover numbers near those for the fresh catalysts; CH₄ yield was almost completely restored for Ni but only in part for Ni-Mo. Regeneration did not improve the activity or selectivity of Ni-Mo-Cu, but rather caused decreases in CH₄ and CO₂ yields. All of the sulfur-free catalysts apparently suffered a decrease in surface area after regeneration.

The results of differential runs for catalysts subjected to carbon deposition at high pressure demonstrated similar trends. That is, CH₄ turnover numbers as well as CH₄ yields decreased for all catalysts. In fact N_{CH_4} decreased by a factor of 2 for Ni and a factor of 10 for Ni-Mo-Cu and Ni-Mo.

Despite a decrease in surface area the regeneration treatment at high pressure with a dilute O₂ mixture seemed to greatly improve catalyst performance for all catalysts. CH₄ turnover numbers for the three catalysts ranged from 1.5 to 8 times the value before carbon deposition and CH₄ yields were 37 to 66 percent higher than pre-carbon deposition values. To determine if this effect was permanent the Ni catalyst was tested for an additional 20 hours at 623 K and space velocity of 100,000 h⁻¹ with 1% CO and H₂/CO = 4, after which the turnover number reverted to the pre-carbon deposition value.

Table 2 also shows the results of differential tests on two catalysts, Ni-Mo-Cu and Ni, which were pre-sulfided and exposed to carbon depositing environment at low pressure. These results show that carbon deposition is extremely detrimental to Ni-Mo-Cu when it has been previously exposed to H₂S. On the other hand Ni is

relatively unaffected showing similar activity performance to the non-sulfided catalyst. Both catalysts showed little change in H_2 uptake as a result of carbon deposition and/or regeneration. However, regeneration apparently caused a significant increase in CH_4 yield for pre-sulfided Ni.

Steady State (24 h) Carbon Deposition Tests

Values of CO conversion, rates of methane production and normalized activities are listed in Table 3 for Ni, Ni-Mo and Ni-Mo-Cu catalysts before and after 24 hour steady state tests at 773 K and $100,000 \text{ h}^{-1}$. Typical plots of normalized activity versus time are shown in Figures 2 and 3. Normalized activity is defined as the ratio of the instantaneous rate of methane production to the initial rate; the half life corresponds to a normalized activity of 0.5.

Based on the normalized activity after 24 hours the order of decreasing resistance to carbon deposition at low pressure was Ni, Ni (pre-sulfided), Ni-Mo-Cu, Ni-Mo, Ni-Mo-Cu (pre-sulfided). The order of increasing content of carbon deposited after 24 hours followed this same trend. However, when the Ni-Mo and Ni-Mo-Cu catalysts were operated in a fluidized bed, Ni-Mo maintained an activity of 0.38 compared to zero for Ni-Mo-Cu after the 24 hour carbon deposition test, even though 10 times more carbon was deposited on Ni-Mo compared to Ni-Mo-Cu. In fact, the Ni-Mo-Cu catalyst lost all measurable activity within 15 hours in the fluidized bed. The pre-sulfided Ni-Mo-Cu also deactivated very rapidly as shown in Figure 2. Figure 3 shows fairly significant fluctuations in the data at 8 hours for the Ni-Mo fluidized bed run. Maintenance of a steady flow during this run required constant attention, and this fluctuation can be attributed to flow variations during the evening and night hours when the run was unattended.

Data in Table 3 obtained at high pressure show that Ni-Mo lost no activity during the 24 hour period. Only a slight decrease in activity was observed for Ni, whereas the activity for Ni-Mo-Cu decreased by almost 40%.

For the low pressure fixed bed carbon deposition runs the decrease in normalized activity with time is represented best by the following expression:

$$a = \frac{a_0}{1 + \exp(-k a_0 \tau) [\exp(k_d [CO^0] t) - 1]} \quad 1)$$

where a = normalized activity at time t , a_0 = normalized activity at $t = 0$, k = reaction rate constant (h^{-1}), k_d = decay constant ($\text{l mol}^{-1} \text{h}^{-1}$), t = time (h), $[CO^0]$ = concentration of CO at bed entrance (mol l^{-1}), and τ = inverse space velocity (h). An expression for the half life ($t_{1/2}$) is obtained from Equation 1 by setting $a/a_0 = 0.5$ and rearranging. The result is

$$t_{1/2} = \frac{1}{k_d [CO^0]} \ln [\exp(k a_0 \tau) + 1] \quad 2)$$

Equations 1 and 2 were used to plot the solid lines in Figures 2 and 3 and to calculate the half lives shown in Table 3.

The data from the fluidized bed runs are correlated fairly well by the following expression after about 5 hours:

$$a = a_0 e^{-k_d t} \quad 3)$$

where the symbols have the same meaning as before. From Equation 3 the half life can be obtained as follows:

$$t_{1/2} = 0.693 (k_d)^{-1} \quad 4)$$

This expression was used to calculate the half lives of Ni-Mo and Ni-Mo-Cu in a fluidized bed which are shown in Table 3.

DISCUSSION

Effects of Carbon Deposition on Methanation Activity

Effects on Intrinsic Activity/Selectivity Properties. Several recent investigations of methanation over Ni, and Ru catalysts (10-12) have provided evidence that adsorbed carbon is an active reaction intermediate. McCarty and Wise (11) reported four types of carbon which are adsorbed on the Ni surface after exposure to CO. Two species designated α' -carbon and α -carbon (both atomic carbon) were easily removed by H_2 and another designated β -carbon (polymerized carbon) was about 1/100 as active toward H_2 . Graphitic carbon, the fourth type is apparently formed by high temperature conversion of the β -form. McCarty and Wise indicated that α -carbon (C_α) is slowly transformed to β -carbon (C_β) at temperatures above 600 K. Thus, carbon fouling of methanation catalysts is likely the result of C_β formation from C_α , the rate of transformation probably depending on the nature of the active site. The more active sites are more likely to promote both rapid deposition and gasification of C_α . If deposition occurs more rapidly than gasification, C_α will build up on the surface and C_β formation will be favored.

Assuming carbon is an active intermediate, the deactivation rate is then determined by the relative contributions of the rate of active carbon formation and the rate of gasification. The relationship between rates of carbon formation and gasification forms the basis of the following discussion of individual catalyst behavior under low pressure conditions. Apparently under the low pressure conditions of this study Ni shows very little deactivation and accumulates very little carbon. This behavior suggests that the rate of gasification equalizes the rate of deposition for nickel under these conditions. The small amount of carbon fouling that did occur appears to be mainly due to blockage or loss of sites since carbon deposition did not change the turnover number. The addition of Mo to Ni apparently favors the massive deposition of carbon as evidenced by the very significant loss of specific activity and greater carbon content of Ni-Mo. Indeed, recently obtained data from a gravimetric study in this laboratory (4,5) show that the rate of carbon deposition at 773 K on a 5.5% Ni-Mo/ Al_2O_3 catalyst is 5 times greater than for a 3% Ni/ Al_2O_3 catalyst. The major difference in behavior of these two catalysts appears to be the significantly higher rate of gasification of carbon for the 3% Ni/ Al_2O_3 . Perhaps Mo believed to be present as MoO_2 dissociates CO but not H_2 , thus catalyzing formation but not removal of C_α .

The addition of Cu to Ni-Mo appears to cause a reduction in the amount of C_α formed as indicated by the significantly lower turnover number of Ni-Cu-Mo. Consequently little C_β is formed, resulting in the relatively long half-life of Ni-Mo-Cu relative to Ni-Mo. Ponec (10,12) suggests that in order to dissociate adsorbed CO and form the active surface carbon species an ensemble of active Ni sites is necessary, and that addition of Cu, itself inactive towards methanation, dilutes the active Ni sites causing lower methanation activity of Ni-Cu catalysts as compared to Ni catalysts.

The change in selectivity observed for all catalysts after low pressure carbon deposition suggests some type of modification of the active sites. It is also reasonable to expect that a carbon covered surface will behave catalytically more like a metal carbide than a clean metal surface. This is supported by previous work of McCarty et al. (13,14) and Sexton et al. (15). In addition, massive deposits of carbon in filamentous form have been shown by previous workers to separate and encapsulate metal crystallites. Thus formation of large amounts of C_{β} may place the metal crystallites in a new support environment, the subsequent change in metal-support interactions inducing changes in activity/selectivity properties. In the case of bimetallic catalysts metal-carbon interactions may induce changes in surface composition which affect selectivity. Ponc (12), for example, presents evidence for the surface modification of a Ni-Cu film by repeated adsorption and temperature programmed desorption of CO.

The data in Table 2 suggest that carbon deposition at high pressure may increase the amount of C_{β} formed in the case of Ni and Ni-Mo catalysts. That is, the percentage decrease in CH_4 turnover number observed after high pressure carbon deposition is equal to or greater than that observed in the low pressure runs. This observation can be explained on the basis of CO partial pressure. At high pressure the minimum partial pressure of CO was 10 kPa (assuming 90% conversion) whereas the maximum partial pressure of CO in the low pressure carbon deposition tests was 6 kPa. At a higher partial pressure of CO the adsorption and dissociation of CO on the catalyst surface proceeds at a much greater rate (4,5). If the carbon formation rate is greater than the gasification rate more C_{β} will result.

Effects of Carbon Deactivation on Apparent Activity/Selectivity Properties in a Fixed Bed at High Temperature, Conversion Conditions. Even though considerable carbon fouling was evident, relatively little deactivation was observed during steady state deposition tests for most catalysts except Ni-Mo-Cu (see Figs. 2 and 3). This was particularly true at high pressure. This behavior indicates that only a portion of the active sites are necessary to maintain a high reaction rate. It is therefore reasonable to assume that in a fixed bed reactor most of the reaction takes place in a small zone at the entrance to the bed, creating a large concentration gradient over the reactor. In this small zone, the CO partial pressure is large and the rate of formation of C_{β} is high; further downstream the catalyst is subjected to a lower CO partial pressure and less C_{β} is formed. Thus a reaction zone is created which gradually moves downstream as the catalyst becomes fouled. Therefore, at high temperature, high conversion conditions and especially at high pressure, we would expect to observe very little deactivation until the reaction zone reaches the end of the bed. The catalyst would then exhibit an extremely rapid deactivation similar to the depletion of an ion-exchange column. Thus, the true deactivation behavior in a fixed bed at high temperatures and especially at high pressures is masked by heat and mass transfer limitations.

Ni-Mo-Cu exhibits a different type of behavior from the other catalysts at high pressure. During the first three hours a very rapid deactivation occurs. After this time the deactivation rate is similar to that observed during the low pressure carbon deposition run. The turnover number data in Table 2 and the larger amount of carbon for Ni-Mo-Cu relative to Ni (Table 3) suggest that the rate of gasification of the deposited carbon is slower at high pressure resulting in more C_{β} formation and more rapid deactivation. The presence of Cu probably inhibits the gasification step by limiting the area available for H_2 to adsorb and since higher CO partial pressure increases the rate of C_{α} formation, a net increase in C_{β} occurs. Ponc (12) showed that for CO adsorption on Ni-Cu/SiO₂ powder the surface Ni concentration increased with time. Assuming such a change in Ni-Mo-Cu, the increasing concentration of Ni on the surface would increase the rate of gasification with the net effect of slowing down the rate of C_{β} formation, thus accounting for the lower deactivation rate observed after three hours.

Effects of Pre-sulfiding. Separate gravimetric studies in this laboratory (4,5) have shown that pre-sulfiding the catalyst substantially reduces the gasification rate without significantly affecting the rate of inactive carbon deposition. The result is increased C_B formation (4,5) and more rapid deactivation of pre-sulfided Ni-Mo-Cu and Ni relative to the fresh catalysts (see Table 3).

Carbon Deposition in a Fluidized Bed. As might be expected Ni-Mo-Cu and Ni-Mo deactivated more rapidly in a fluidized bed than in a fixed bed due to more uniform exposure to the reaction mixture. However, Ni-Mo-Cu deactivated more rapidly than Ni-Mo, a result opposite to that obtained in the fixed bed. Perhaps this can be accounted for by the lower space velocities and lower conversions associated with the fluidized bed reactor. The rate of carbon formation is proportional to the partial pressure of CO. The lower conversion would translate to a higher CO partial pressure at the catalyst surface which would affect each catalyst differently because of their different compositions. Careful examination of the low pressure fixed bed data of Tables 2 and 3 reveals that Ni-Mo and Ni-Mo-Cu suffered approximately the same percentage loss of surface area, but that Ni-Mo contained ten times more carbon after the steady-state carbon deposition run. Thus under the higher CO partial pressure Ni-Mo-Cu might be expected to deactivate more rapidly than Ni-Mo since increased carbon deposition would have more effect on Ni-Mo-Cu. A possible additional effect is that under uniform exposure to the reactant mixture a greater modification of the surface occurred for Ni-Mo-Cu than for Ni-Mo. Since large concentration and temperature gradients are absent in the fluidized bed, these results are much more indicative of the true deactivation behavior. Moreover, they model better the behavior anticipated in the BI-GAS process.

Regeneration of Carbon Fouled Catalysts in Air/Oxygen

The restoration of activity following regeneration provides strong evidence that carbon fouled catalysts can be regenerated with dilute mixtures of air or oxygen. In fact, this may be the only practical approach since in industrial equipment the regeneration temperature is usually limited to 700 K, and significant carbon gasification by steam, H_2 or CO_2 does not occur at temperatures below 800 K (16,17). The increase in CH_4 turnover number for the catalysts after the high pressure dilute O_2 treatment was more than could be accounted for by simple removal of the deposited carbon. This could be the result of a surface modification by the O_2 treatment and/or a modification which occurred during reaction as discussed previously.

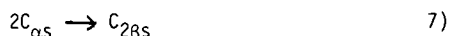
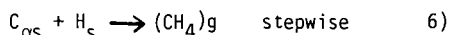
Palmer and Vroom (18) showed that the activity of nickel is increased by high temperature treatment with O_2 as a result of incorporating dissolved O_2 just below the surface. Sexton and Somorjai (15) reported similar results. Unfortunately this effect appears to be only temporary, since the specific activity of regenerated Ni/ Al_2O_3 returned to the same value as the fresh catalyst after 24 hours of reaction at 623 K $H_2/CO = 4$, a condition chosen to ensure that further deactivation did not occur.

Regeneration of methane activity by oxygen is not without a price, however. The results show an overall decrease in surface area after carbon deposition and regeneration of 18 to 71%. This surface area loss is undoubtedly a consequence of sintering and even loss of the catalyst crystallites themselves. Rostrup-Nielsen (19) reports that deposited carbon grows in long hollow filaments with the Ni crystallite at the end. Transmission electron microscopy studies in this laboratory (20) confirm this observation. The Ni crystallite is thus removed from the support by the carbon filament and when the carbon is removed by oxidation the crystallite is probably carried out of the reactor with the gas stream. In fact, chemical analysis of fresh and regenerated Ni/ Al_2O_3 samples revealed a 7% loss of nickel. It may be, therefore, impractical to regenerate carbon-fouled catalysts with air or oxygen since after a few cycles of deactivation and regeneration a large part

of the active surface of the catalyst would be gone. It depends, of course, on how much Ni is removed per treatment and the frequency of treatments.

A Model for Deactivation by Carbon

We propose a model to account for deactivation of nickel by β -carbon in a fixed bed during methanation. The proposed model for deactivation is a modification of that proposed by Wise et al. (21) for interaction of sulfur with Ni. A modification in the reaction mechanism is also made to account for the transformation of C_α to C_β and the loss of activity for surface reaction between C and H as the number of available nickel sites diminishes. Our proposed model is



where the subscript "s" denotes an adsorbed species. Since the α state represents single carbon atoms which are easily gasified and the β state represents poly-atomic carbon which is much less active it is reasonable to assume that the dimerization of single C_α atoms to C_β causes the deactivation observed for Ni and Ni bimetallic methanation catalysts.

According to our proposed model the rate of deactivation due to carbon fouling is proportional to the rate of C_β formation which is proportional to the net rate of C_α formation. The rate of C_α formation is in turn proportional to the partial pressure of CO and the activity of the catalyst. Assuming first order dependence on both of these variables, an expression for the deactivation rate can be written as $da/dt = -k_d[CO]a$ where k_d = deactivation rate constant, $[CO]$ = concentration of CO, a = normalized activity at time t . The deactivation model proposed by Wise et al. for sulfur poisoning (21) can be adapted by assuming the reaction rate to be first order in CO concentration and that there are no radial concentration gradients. Simultaneous solution of the deactivation rate expression and the equation of continuity in the z direction (direction of flow) yields Equation 1. The following expression also results if $z/V \ll 1$, where V is the velocity in the z direction.

$$\ln\left[\left(\frac{1}{1-x_{CO}}\right)-1\right] = \ln[\exp(k_a z/V)-1] - k_d [CO^0] t \quad (8)$$

By plotting $\ln\left[\left(\frac{1}{1-x_{CO}}\right)-1\right]$ versus time t , values for k and k_d can be determined from the intercept and slope respectively.

Equation 1 is plotted as a solid line in Figure 2 using these parameters. It fits the data very well for the low pressure fixed bed runs. A similar development assuming no concentration gradient in the z direction leads to the exponential relationship of Equation 3 for fluidized beds. Using Equations 1 and 3 we estimate that half of the active sites for Ni-Mo would be fouled in 37 days in a fixed bed and only 30 hours in a fluidized bed based on process conditions of $H_2/CO = 1.4$ and a space velocity of 3000 h^{-1} .

The fact that the proposed model for deactivation by carbon deposition predicts experimental behavior quite well indicates that it is consistent with the observed deactivation behavior -- i.e., the rate of deactivation increases as the partial pressure of CO is increased and decreases as the surface of the

catalyst is fouled by increasing accumulations of inactive carbon.

CONCLUSIONS

1. At 723 K and atmospheric pressure deactivation of nickel catalysts by carbon exhibited first order dependence on CO concentration (second order overall). Half-lives of Ni and Ni-Mo catalysts varied from 13-170 hours. Based on the specific intrinsic activities (CH_4 turnover numbers) after reaction under carbon depositing conditions the order of decreasing resistance to carbon deposition at low pressure was: Ni, Ni (pre-sulfided), Ni-Mo-Cu, Ni-Mo, Ni-Mo-Cu (pre-sulfided).

2. During reaction in a fixed bed at high temperatures and pressures little apparent deactivation was observed except in the case of Ni-Mo-Cu. The effects of deactivation were masked by the fast rate of reaction occurring in a portion of the bed. Thus the turnover numbers determined under reaction limited conditions reveal the true effects of deactivation.

3. Ni-Mo is more resistant to carbon deposition in a fluidized bed than Ni-Mo-Cu. The fluidized bed experiments provide more realistic indication of the true deactivation behavior because temperature and reactant concentrations are more uniform than in a fixed bed.

4. Pre-sulfiding the catalysts does not improve their tolerance to carbon deposition. In fact, pre-sulfiding Ni-Mo-Cu severely degraded its performance under severe carbon deposition conditions. It is believed that sulfur poisons the gasification of active carbon leading to a build up and transformation to inactive carbon.

5. A low pressure dilute air mixture at 573 K regenerates most carbon fouled catalysts. Using a dilute O_2 mixture at high pressure results in CH_4 turnover numbers and CH_4 yields which are temporarily higher than for fresh catalysts. Regeneration using air or O_2 results in a significant loss of surface area, but it may be the only practical method due to temperature limitations of industrial equipment.

ACKNOWLEDGEMENTS

The authors gratefully acknowledge financial support from Bituminous Coal Research, Inc. under their Contract No. EF-76-C-01-1207, U.S. Dept. of Energy; permission to publish catalyst data from the Climax Molybdenum Company of Michigan and the Harshaw Chemical Co.; and technical assistance from Dr. Robert Streeter of BCR.

REFERENCES

1. M.J. Whalen, "Carbon Formation in Methanators," Final Report to ERDA, FE-2240-10 (July 1976).
2. G.D. Weatherbee, G.A. Jarvi, and C.H. Bartholomew, Presented at the 85th National AIChE Meeting, June 4-8, 1978, Philadelphia.
3. C.H. Bartholomew, Final Report to DOE, FE-1790-9, Sept. 6, 1977.
4. D.C Gardner, M.S. Thesis, Brigham Young U., 1979.
5. D.C Gardner and C.H. Bartholomew, paper in preparation.
6. R.W. Fowler, Jr. and C.H. Bartholomew, I & EC Prod. Res. & Dev., in press.
7. C.H. Bartholomew, "Alloy Catalysts with Monolith Supports for Derived Gases," Quarterly Technical Progress Report to ERDA, FE-1790-1, (Aug. 6, 1975).
8. C.H. Bartholomew and R.J. Farrauto, J. Catal. 45, 41 (1976).
9. R.B. Pannell, K.S. Chung, and C.H. Bartholomew, J. Catal. 46, 340 (1977).
10. M. Araki and V. Ponec, J. Catal., 44, 439 (1976).
11. J.G. McCarty and H. Wise, J. Catal., 57, 406 (1979).
12. V. Ponec, Catal. Rev. - Sci. Eng., 18(1), 151 (1978).
13. J.G. McCarty and R.J. Madix, J. Catal. 38, 402 (1975).
14. J.G. McCarty and R.J. Madix, Surface Sci., 54, 121 (1976).
15. B.A. Sexton and G.A. Somorjai, J. Catal., 46, 167 (1977).
16. J.L. Figueirido and D.L. Trimm, J. Catal., 40, 154 (1975).
17. D.L. Trimm, Catal. Rev. - Sci. Eng. 16(2), 155 (1977).
18. R.L. Palmer and D.A. Vroom, J. Catal. 50, 244 (1977).
19. J.R. Rostrup-Nielsen, J. Catal. 27, 343 (1972).
20. D. Mustard and C.H. Bartholomew, paper in preparation, (1979).
21. H. Wise, B.J. Gikis, W.E. Isakson, J.G. McCarty, K.M. Sancier, S. Schechter, P.R. Wentrcek, and B.J. Wood, SRI, Final Report PERC-0060-8 (ERDA), Sept. 30, 1977.

TABLE 1
CATALYST COMPOSITIONS AND SUPPLIERS

Catalyst	Metal Composition (wt.%)			Bulk Density (g/cm ³)	Support ^b	Supplier
	Ni	Mo	Cu			
Ni	14			0.54	γ-Al ₂ O ₃ ^c Al ₂ O ₃ - SiO ₂ ^d Al ₂ O ₃	BYU Catalysis Lab Climax Moly. Corp. Harshaw Chem. Co.
Ni-Mo	10.9	19.8				
Ni-Mo-Cu	10	9 ^a	3			

a) wt.% MoO₃

b) Powder form

c) Kaiser SAS Medium; 0.32 cm spheres

d) Harshaw AL-1605P (91% Al₂O₃, 6% SiO₂)

TABLE 2

RESULTS OF DIFFERENTIAL REACTOR TESTS (498 K and 138 kPa)

Catalyst	Low Pressure Carbon Deposition ^a				High Pressure Carbon Deposition ^b			
	H ₂ Uptake ($\mu\text{mol/g}$)	$N_{\text{CH}_4}^c$ (s^{-1}) $\times 10^3$	Yield (%) ^d		H ₂ Uptake ($\mu\text{mol/g}$)	$N_{\text{CH}_4}^c$ (s^{-1}) $\times 10^3$	Yield (%)	
			CH ₄	CO ₂			CH ₄	CO ₂
<u>Ni</u>								
Pre-Carbon Deposition	163	2.4	69	0	163	1.5	52	14
Post Carbon Deposition	142	2.6	43	0	---	0.8	31	1
Post Regeneration	135	2.1	68	0	147	2.7	86	14
Post Regeneration + 20 h at 623 K	---	---	---	---	148	2.7 ^a	86 ^a	---
<u>Ni (Pre-Sulfided)</u>								
Pre-Carbon Deposition	89	2.0	66	19	---	---	---	---
Post Carbon Deposition	---	1.9	42	0	---	---	---	---
Post Regeneration	99	2.4	85	0	---	---	---	---
<u>Ni-Mo</u>								
Pre-Carbon Deposition	83	2.8	53	3	83	0.35	29	20
Post Carbon Deposition	51	0.16	13	26	---	0.04	6.5	71
Post Regeneration	24	2.5	23	21	22	2.6	40	42
Post Regeneration FBR	41	2.2	43	9	---	---	---	---

TABLE 2 - Continued

<u>Ni-Mo-Cu</u>									
Pre-Carbon Deposition	52	0.11	28	31	52	0.11	21	69	
Post Carbon Deposition	37	0.15	27	46		0.01	8.5	73	
Post Regeneration	30	0.11 ^e	21	30	46	0.31	32	34	
Post Regeneration FBR ^f	25	---	---	---	---	---	---	---	
<u>Ni-Mo-Cu (Pre-Sulfided)</u>									
Pre-Carbon Deposition	20	0.22	25	15	---	---	---	---	
Post Carbon Deposition	---	---	---	---	---	---	---	---	
Post Regeneration	18	---	---	---	---	---	---	---	

a) Conditions: 498 K, 138 kPa, 1% CO, H₂/CO = 4.

b) Conditions: 498 K, 138 kPa, 4.3% CO, H₂/CO = 1.3.

c) N_{CH₄} (turnover number) is the number of molecules produced per site per second.

d) Yield is percent CO converted which goes to CH₄/CO₂.

e) Too low to measure accurately.

f) FBR: Fluidized Bed Reactor run.

TABLE 3

RESULTS OF STEADY STATE (24 h) CARBON DEPOSITION TESTS (723 K, 138 or 2600 kPa, 100,000 h⁻¹)

Catalyst	% CO Conversion		Initial CH ₄ rate ($\mu\text{mol}/\text{cm}^3 \text{ cat. s}$)	Normalized ^a Activity after 24 h	Half life ^b (h)	Carbon Content after 24 h (wt%)
	Initial	Final				
<u>LOW PRESSURE</u>						
<u>Fixed Bed</u>						
Ni	41	43	14	1.05	170	0.6
Ni (P)	33	34	11	0.93	134	---
Ni-Mo	43	31	9.0	0.67	50	16.8
Ni-Mo-Cu	33	27	9.6	0.81	107	1.7
Ni-Mo-Cu (P)	13	2	3.6	0.10	13	---
<u>Fluidized Bed</u>						
Ni-Mo	61	23	7.7	0.38	33	7.2
Ni-Mo-Cu	32	0	4.6	0	2 ^c	0.6
<u>HIGH PRESSURE</u>						
Ni	94	91	36	0.99	---	---
Ni-Mo	81	83	21	1.05	---	---
Ni-Mo-Cu	81	52	25	0.63	---	---

a) Normalized activity = rate of CH₄ production divided by initial CH₄ production rate.

b) Half life = time at which normalized activity equals 0.5.

c) No activity after 15 h.

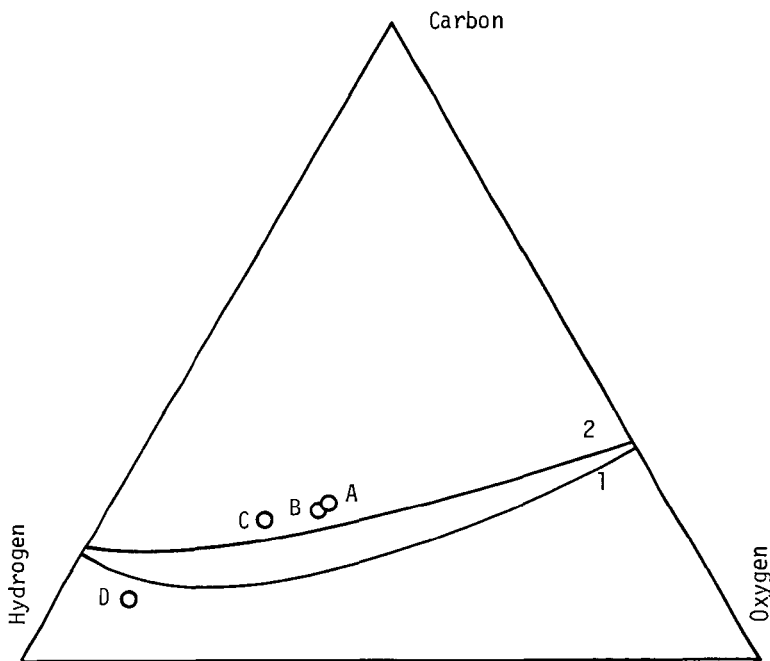


Figure 1. Equilibrium Diagram at 723 K and 138 kPa Showing BI-GAS and Test Feed Gas Compositions. A = BI-GAS, B = Fluidized Bed Runs, C = High and Low Pressure Runs plus some Differential Runs, D = Differential Runs. Curve 1 is the equilibrium curve based on graphite. Curve 2 is based on "non-ideal" carbon as reported by J.R. Rostrup-Nielsen in *J. Cat.* 27, 343-356 (1972).

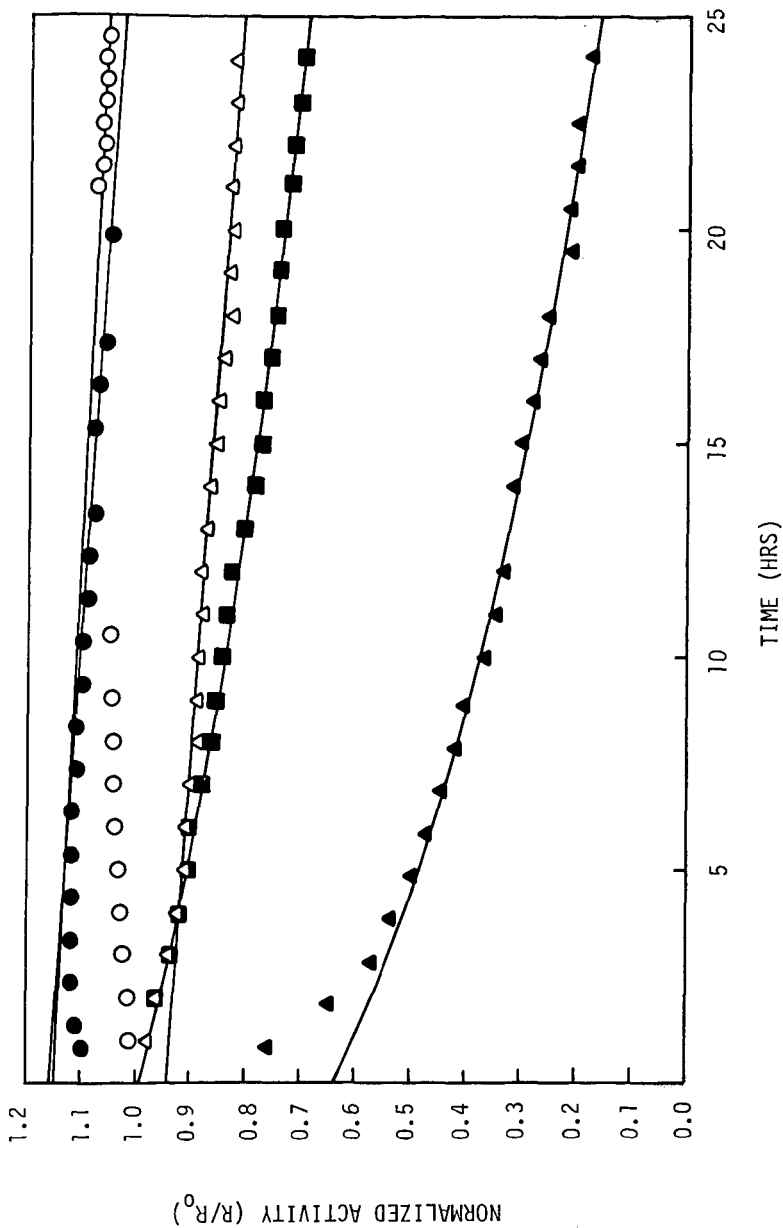


Figure 2. Variation of Normalized Activity with Time at Low Pressure: ○ = Ni, ● = Ni Pre-sulfided, Δ = Ni-Mo-Cu, ▲ = Ni-Mo-Cu (pre-sulfided), ■ = Ni-Mo. Solid lines represent correlation of data by expression:

$$a = \frac{1}{1 + \exp(-k_a \tau) \exp(k_d [CO^*] t) - 1}$$

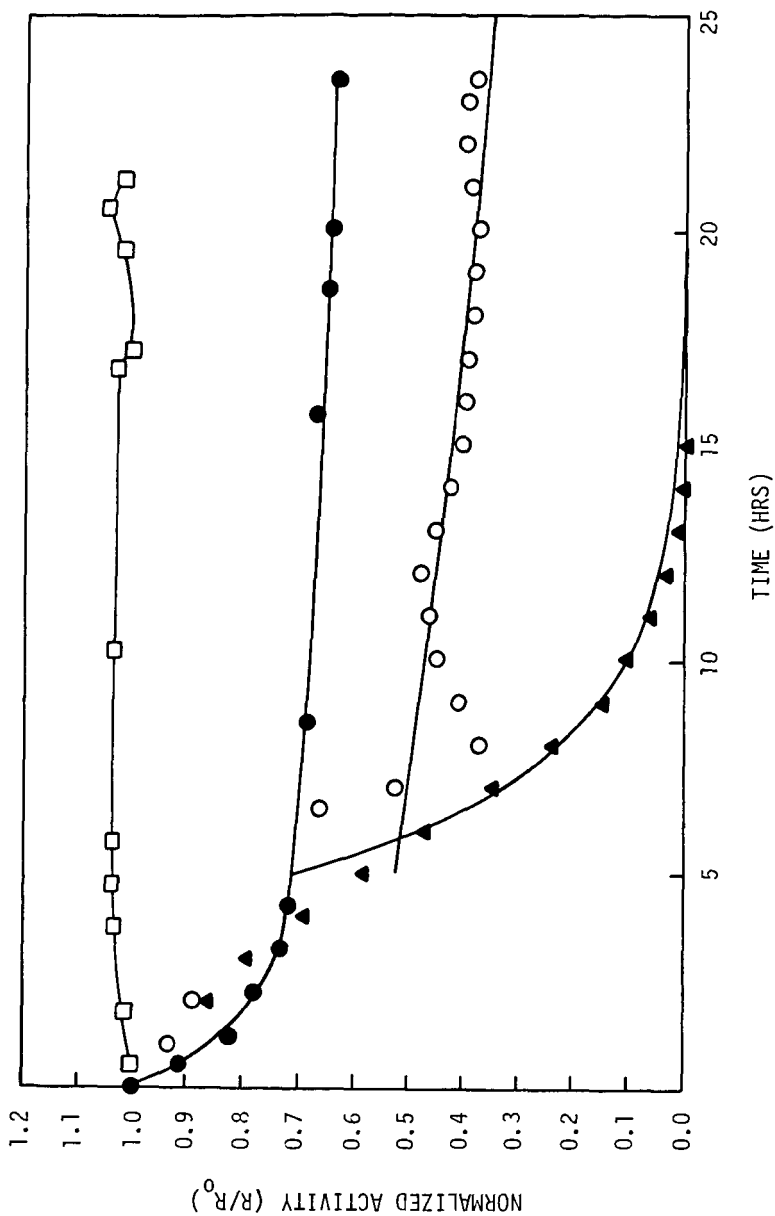


Figure 3. Variation of Normalized Activity with Time: \square = Ni-Mo high pressure run, \circ = Ni-Mo low pressure fluidized bed run, \bullet = Ni-Mo-Cu high pressure run, \blacktriangle = Ni-Mo-Cu low pressure fluidized bed run. Fluidized bed data after 5 hours are correlated by the expression $a = a_0 \exp(-k_d t)$.

Further Results on the Reaction of H_2/CO on Fused Iron
by the Transient Method

J. P. Reymond, P. Mériaudeau,
B. Pommier, and C. O. Bennett*

Laboratoire de Thermodynamique et Cinétique Chimiques
Université Claude Bernard, Lyon I
69621 Villeurbanne, France

Introduction

In a previous study (1) it has been proposed that the surface of a promoted fused iron catalyst is largely covered with carbon during the steady-state reaction of hydrogen and carbon monoxide (90% H_2 , 10% CO) at atmospheric pressure and 250°C. This same catalyst, a commercial ammonia synthesis catalyst (CCI), was also evaluated (at 2.0 MPa) in a more applied way in connection with the study of a scheme for energy storage in a central power plant (2, 3). It is now clear that it is necessary to consider that each catalyst (i.e., even the same metal on different supports) may operate for reactions of H_2/CO through a unique sequence of steps, or at least with a particular rate-determining step. Thus although the hydrogenation of surface carbon seems to be rate-limiting on iron (1), on ruthenium the dissociation of adsorbed CO has been proposed as rate limiting (4). The present work is a continuation of that of reference (1); this time the role of CO_2 and H_2O has been investigated, and interesting information has been obtained on the chain growth process.

Experimental

The reactor was made of 1/4-inch stainless steel tube and filled with 100 mg of catalyst (particles of 300 μm) mixed with 500 mg of glass beads of the same size. The reactor and the glass beads were confirmed to produce no products at the reaction conditions. Feed rates of H_2/CO (9/1) between 20 and 120 ml/min were explored but if not otherwise noted, 40 ml/min was used; the conversion was always less than 5% of the CO fed.

Hydrogen (99.99%, Air Liquide) was purified by a molecular sieve (5A) trap, followed by a deoxo reactor, followed by a second molecular sieve 5A. Carbon monoxide (99.9%, Air Liquide) was passed through a glass tube heated to 220°C to decompose carbonyls and then through a trap of activated carbon at 25°C.

Analysis of the reaction products was by gas chromatography. For the separation of the hydrocarbons, a Poropak Q (80-100 mesh) 6-m, 1/8-inch stainless steel column was used with a flame ionization detector. Column temperature was 195°C, and the carrier gas (He) was used at 30 ml/min. The CO_2 and H_2O were measured by a second identical Poropak Q column at 175°C, leading to a thermal conductivity detector. For the reaction conditions used, only alkanes were found among the hydrocarbon products.

Results

The Basic Reaction

After an initial reduction in flowing hydrogen at 60 ml/min for 60 hours at 500°C, the reactor is cooled to 250°C, and the feed is switched at time zero to 10% CO in H_2 . The curve 1 of Fig. 1 results. The deactivation is rapid and the production rate of methane passes through a maximum. A reactivation in H_2 at 500°C

* Now at University of Connecticut, Storrs, Connecticut 06268.

for 15 hours increases the activity of the catalyst to a level above what it was at the end of the first run, but below what it was at its maximum. This process continues with further reactivations, and Fig. 1 shows curves after 10 reactivations and after 20 reactivations. However, it was found that a short (30 min) treatment by oxygen at 500°C and 1 atm before the usual reduction by hydrogen produced a relatively stable catalyst, as shown by the curve O₂ of Fig. 1. The activity of the catalyst is obviously very sensitive to its state of oxidation and to the concentration of refractory carbon at or near its surface. It may be recalled that Matsumoto and Bennett (1) found that short treatments in helium at 250°C converted the active carbon intermediate to a form inactive at this temperature. Similar effects are observed for nickel (5).

Figure 2 shows the other hydrocarbons produced corresponding to the curve labelled O₂ on Fig. 1. The numbers by the curves are the steady-state rates of production divided by that for methane. These selectivities are insensitive to the activity level and are about the same for all the catalyst conditions of Fig. 1. Water and carbon dioxide are also produced, but these production rates are less reproducible. The catalyst has a fraction exposed of only about 5 percent, and it has been shown that the entire mass of iron is carburized (1). Thus small changes in carbon concentration in the bulk may produce CO₂ and H₂O at rates at least as high as the catalytic reaction. Figure 3 shows the history of a freshly reduced catalyst after exposure to CO/H₂ at 250°C, H₂ at 250°C, and finally H₂ programmed to 500°C. The first peak represents the removal of a surface carbon intermediate as methane, and the second large peak comes from the decarburization of the bulk of the catalyst. This result has already been discussed (1).

Another aspect of the reacting system can be seen in Fig. 4. Experiments were started with a feed rate of 120 ml/min, but the conversion (0.003 to CH₄) was not sufficient to obtain reliable analyses for H₂O and CO₂ by chromatography (thermal conductivity detector). The hydrocarbons, however, were analyzed correctly (flame ionization detector). When the conversion was increased (0.006 to CH₄) by reducing the feed rate to 20 ml/min, a much lower formation rate of methane was observed. This reduction in activity can only be explained by inhibition of the rates by products of the reaction; the reactant concentrations are of course almost unchanged. In other words, even at these low conversions the reactor is not truly differential.

We are thus led to investigate the effect of the products of reaction on the reaction rates, and these experiments will be described later. In order not to be misled by secular changes in the catalyst, a steady state condition is first established with 10% CO + H₂ feed. The feed is then changed to one containing H₂O, CO₂, etc. as desired, and finally it is changed back to 10% CO + H₂.

The base reaction has been studied at several temperatures (230°, 250°, 270°, and 300°C), and an activation energy of 20.4 kcal/mole is observed, similar to the value found at 2.0 MPa (2).

Influence of CO₂

To the reaction mixture 10% CO + H₂ was added 5% CO₂. The CH₄ production diminished by about 8%, and when the CO₂ was removed the methane formation rate regained its initial value. This effect is not sufficient to explain Fig. 4.

If the CO in the feed gas is replaced by CO₂, the methanation reaction continues at a lower rate, as shown in Table 1. The formation of higher hydrocarbons, however, is drastically reduced. The CO₂ is dissociatively adsorbed, but the surface oxygen concentration is increased.

Influence of Water

A concentration of 0.6% water vapor was added to the 10% CO + H₂ feed mixture at steady-state reaction, and Fig. 5 shows the result. The inhibiting effect of water is clear, and it is probable that the lower rates at higher conversion shown in Fig. 4 are explained by the increased water concentration at higher conversion.

It is also interesting to evaluate the capability of the steady-state catalyst surface to catalyze the shift reaction. Figure 6 indicates that when the H₂ in the 10% CO + H₂ mixture is replaced by 0.6% water, all production of hydrocarbons stops, and a large rate of CO₂ formation is observed. These results are further evidence of the power of the iron catalyst to adsorb dissociatively H₂ as well as CO.

Influence of Ethane

The addition of 10% C₂H₆ to the reactants does not change the rates of reaction. However, iron has some activity for hydrogenolysis (6). If the 10% CO + H₂ mixture is changed to 10% C₂H₆ + H₂, methane is formed at 0.65 μ mole/g min (see Fig. 7), less than 10% of a typical methanation rate.

Influence of Olefins

When 10% C₂H₄ + H₂ is fed to the reactor just after the reduction of the catalyst at 500°C, the curves of Fig. 7 are obtained. There is immediate production of methane, propane, n-butane, and n-pentane. Ethane is confounded with the large ethylene peak in the analysis by chromatography. The rates do not increase from zero as in Fig. 2. A switch to hydrogen (not shown on Fig. 7) produces no methane peak at 250°C, and programming the temperature to 500°C results in the production of only 4 μ moles of CH₄/g of iron. Thus the C₂H₄/H₂ mixture does not carburize the iron at 250°C. The reaction rates after 4 hours with ethylene are about twice those with CO, and the initial rates are an order of magnitude higher. Figure 7 shows also the switch from C₂H₄/H₂ to CO/H₂ and then to C₂H₆/H₂.

Figure 8 shows the usual curves for CO/H₂ over a reduced catalyst, followed by a switch to C₂H₄/H₂ over the now carburized catalyst. These results are consistent with the idea that the rate-determining step with CO is the hydrogenation of surface carbon. Subsequent chain growth occurs through CH₂ groups (or CH), and if these groups are formed directly from ethylene, the production rates of the products are higher; the rate limiting step coming from CO is no longer relevant. The C₂H₄/H₂ reaction occurs on iron, and after exposure of the catalyst to CO/H₂, much of the surface is covered with carbon, so the rate of CH₄ production with C₂H₄/H₂ of Fig. 8 is lower than that of Fig. 7.

Figure 9 shows the reaction of 10% C₃H₆ + H₂ over the reduced catalyst. The results are qualitatively the same as with ethylene. Butene-2/H₂ reacts as shown in Fig. 10, and butene-1/H₂ (always 90% H₂) gives rates that are all a bit lower than for butene-2, as shown. All these results emphasize that on the iron surface the CH₂ or CH fragments come rapidly to a steady state; the rates of production of the alkane products (no olefins were observed) are not appreciably influenced by the source of the CH₂ groups on the surface. However, there are some differences, as shown in Table 2, which gives the ratios of the production rates after 4 hours. Starting from a given olefin, the products are mostly of shorter chain length, and close to the chain length of the reactant. In any event, we are justified in supposing that, starting from CO/H₂, all the steps after CH₂ or CH formation are rapid, and little of the surface is covered by chain fragments at 250°C and 100 kPa.

Discussion

The new results of the present study confirm most aspects of the sequence of steps proposed by Matsumoto and Bennett (1). CO is adsorbed as C + O, and the freshly formed surface carbon is the most abundant surface intermediate; its hydrogenation by adsorbed hydrogen present as H is the rate-determining process. Carbon dioxide added to CO/H₂ is not strongly enough adsorbed to affect the rate appreciably. However, in the absence of CO, CO₂/H₂ makes methane at a lower rate; the surface is more oxidized, and the active C is present in lower concentration than in the presence of CO.

However, water can compete with CO for the surface, and it oxidizes the surface while reducing the active C coverage by forming CO₂. The high reaction rate of CO/H₂O to CO₂ rather than CH₄ shows the strong affinity of the surface of the iron catalyst for oxygen (Figs. 5-6).

We recall that the rate of hydrocarbon production over a freshly reduced catalyst rises from an initial value of zero. The carbon formed from CO reacts with the bulk iron of the catalyst, and the surface carbon necessary for hydrocarbon production gradually increases in coverage as the bulk of the iron is carburized to Fe₂C at 250°C. However, when C₂H₄/H₂ is passed over the reduced catalyst, no active C intermediate seems to be necessary. The rate starts at a maximum value, and the iron is not carburized. Thus the observed formation of CH₄ and C₃H₈ shown in Fig. 7 arises through a CH_n fragment. No oxygen is present. Iron thus behaves differently from cobalt, for which oxygen is apparently necessary for chain growth (7, 8).

When a CO/H₂ feed is changed to C₂H₄/H₂ (Fig. 8), the rate of hydrocarbon production is higher from ethylene than from CO. Methane is an important product from C₂H₄/H₂. This result is not inconsistent with the lack of ¹⁴CH₄ formed when ¹⁴C₂H₄ is added in small quantity to CO/H₂ (9). With CO present the C₁H_n groups must originate principally from CO, so that the added ¹⁴C will be concentrated principally in C_xH_y groups of x ≥ 2.

It is clear that the reaction of ethylene takes place on the iron surface, since the rate decreases as the inert graphitic carbon builds up (Figs. 7 and 8). It was shown previously (1) that the reaction from CO also occurs on the iron part of the surface; after steady state under CO/H₂, a brief exposure to H₂ alone and then a switch back to CO/H₂ leads to a temporary increase in the rate. If the exposure to hydrogen is long enough to decarburize some of the bulk, the subsequent CO/H₂ reaction rate is lowered as recarburization lowers the concentration of the active surface carbon.

A freshly reduced catalyst is carburized by the H₂/CO mixture in about an hour (recall that carburization in CO alone is much slower (1)). During this period the hydrocarbon formation rate gradually increases as the surface carbon concentration rises, as influenced by the bulk carbon (carbide) concentration. A switch to pure H₂ gives a methane peak, meaning that hydrogen reacts as H on the surface and that the surface coverage by C is high. The rate-determining process is the formation of CH_n from the surface C; subsequent chain growth is rapid and occurs through these groups, and the product distribution is determined by the rate of propagation and termination (desorption) of chains arising from CH_n. The presence of H₂O and to some extent CO₂ in the gas phase increases surface O at the expense of C and/or H, inhibiting the reaction. However, active surface carbon is gradually converted to inert (at 250°C) graphite, and activity slowly declines as the part of the iron covered with labile C decreases. For a much regenerated catalyst, oxygen followed by hydrogen cleans off a higher fraction of inert graphite than H₂ alone.

References

1. Matsumoto, H., and Bennett, C. O., J. Catal. 53, 331 (1978).
2. Atwood, H. E., and Bennett, C. O., Ind. Eng. Chem. Process Des. Dev. 18, 163 (1979).
3. Borghard, W. G., and Bennett, C. O., Ind. Eng. Chem. Product Res. Dev. 18, 18 (1979).
4. Dalla Betta, R. A., and Shelef, M., J. Catal. 49, 383 (1977).
5. McCarty, J. G., and Wise, H., J. Catal. 57, 406 (1979).
6. Montarnel, R., and Martino, G., Rev. Inst. Français du Pétrole 32, 367 (1977).
7. Gibson, E. J., and Clarke, R. W., J. Appl. Chem. 11 293 (1962).
8. Eidus, YaT., Zelinskii, N. D., and Ershov, N. I., Dokl. Akad. Nauk SSSR 60, 599 (1948).
9. Hall, W. K., Kokes, R. J., and Emmett, P. H., J. Am. Chem. Soc. 82, 1027 (1960).

Table 1
Reaction of CO₂ and H₂

Formation Rate, μ mole/g min.	Feed		
	Before		After
CH ₄	7.0	4.4	7.4
C ₂ H ₆	3.2	0.52	3.5
C ₃ H ₈	1.5	0.065	1.5

Table 2
Relative Production Rates
 (4 hours on stream)

Feed Mixture	$\frac{C_2}{C_1}$	$\frac{C_3}{C_1}$	$\frac{C_4}{C_1}$	$\frac{C_5}{C_1}$
10% CO + H ₂	0.6	0.29	0.10	0.02
10% C ₂ H ₄ + H ₂		0.15	0.06	0.001
10% C ₃ H ₆ + H ₂	0.49		0.087	0.002
10% butene-1 + H ₂	0.19	0.76		0.08
10% butene-2 + H ₂	0.20	0.92		0.09

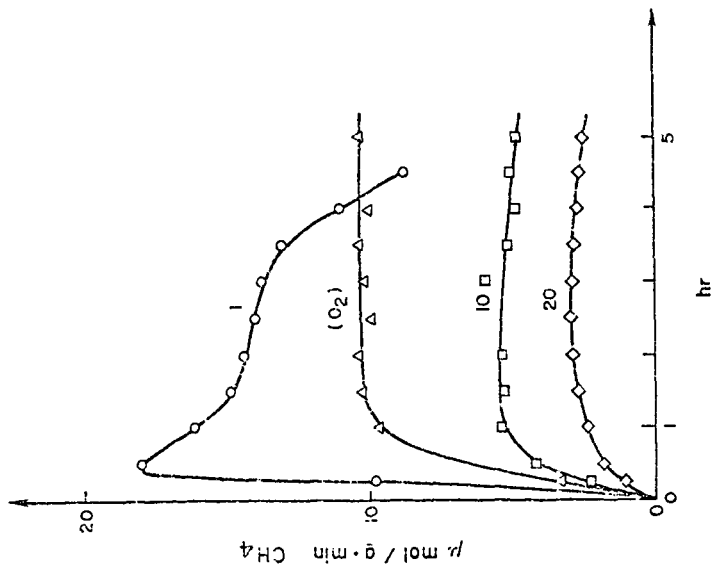


Figure 1

Rate of Reaction after Various Reactivations; Feed Rate, 120 ml/min.

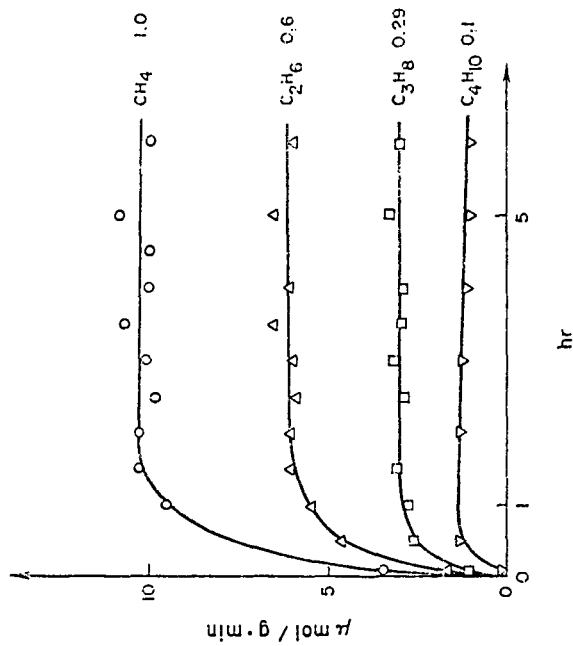


Figure 2

Formation Rates of Products.

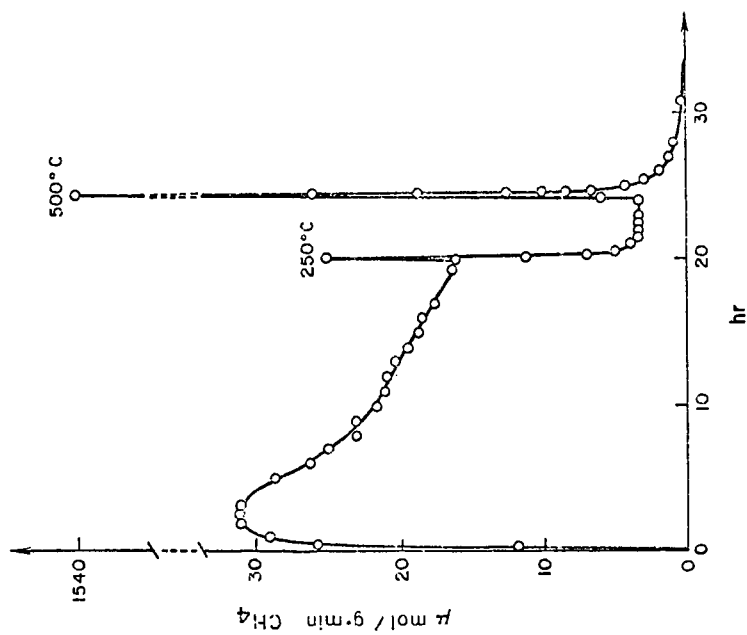


Figure 3

Hydrogenation of Surface Carbon.

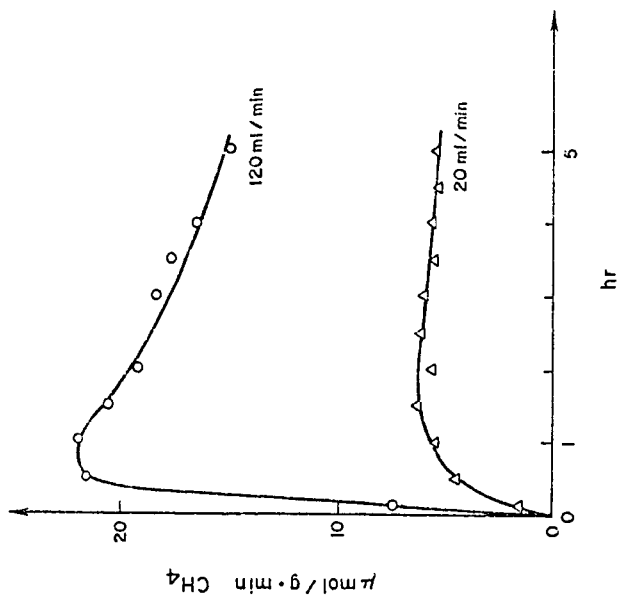


Figure 4

Effect of Flow Rate on Methane Formation.

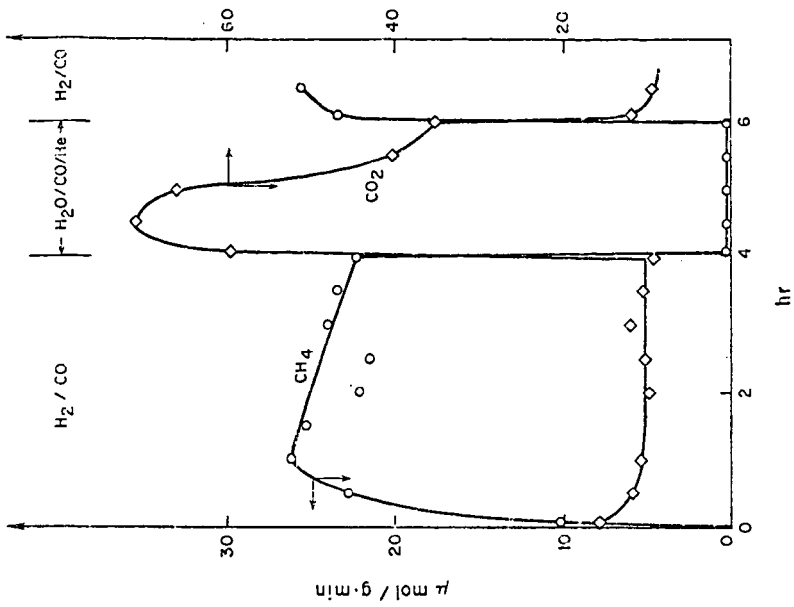


Figure 6

Reaction of Water and Carbon Monoxide.

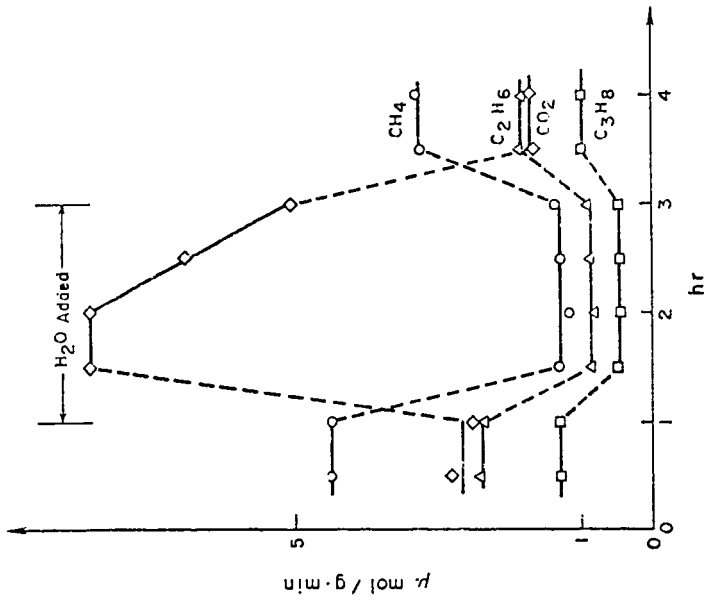


Figure 5

Effect of Water Vapor on the Reaction.

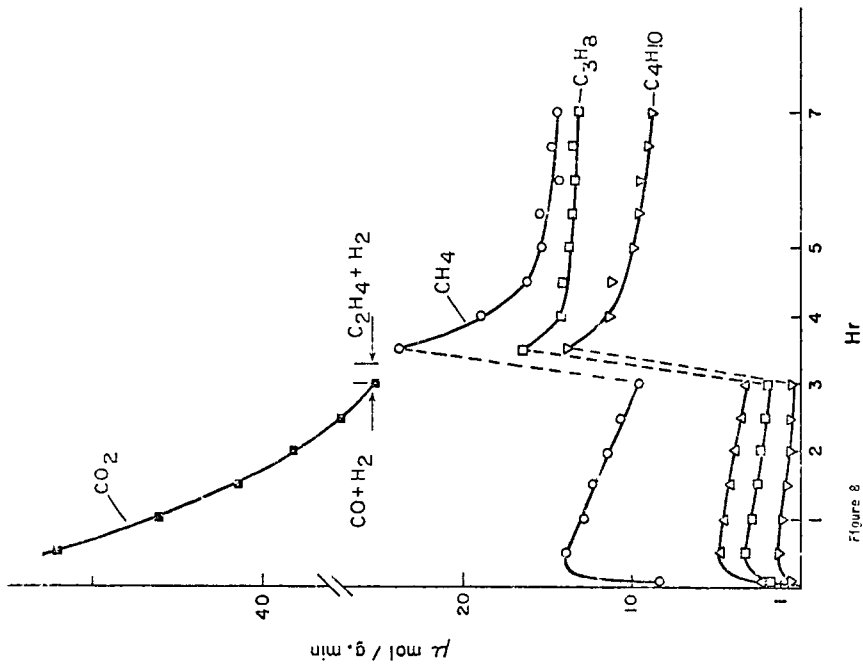


Figure 8

Reaction of Ethylene and Hydrogen on a Carburized Catalyst.

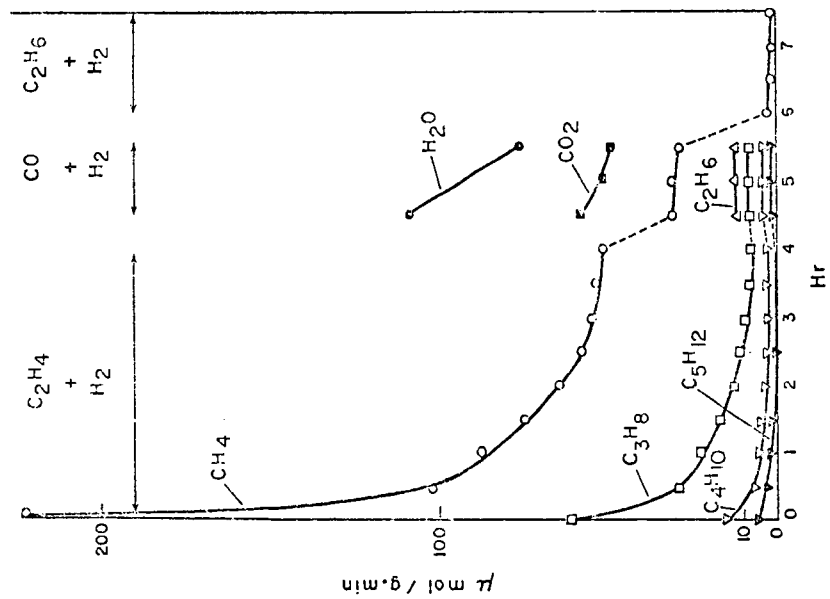


Figure 7

Reaction of Ethylene and Hydrogen on a Reduced Catalyst.

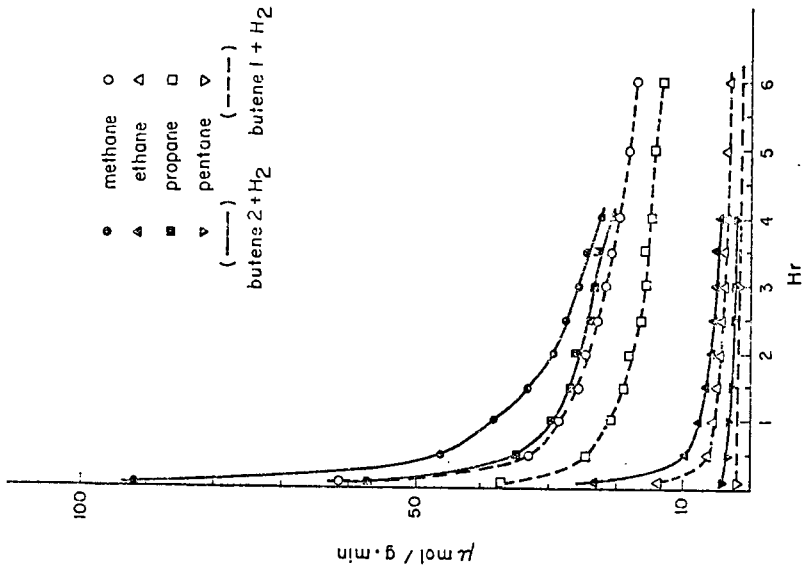


Figure 10

Reaction of Butene-1 and Butene-2 with Hydrogen.

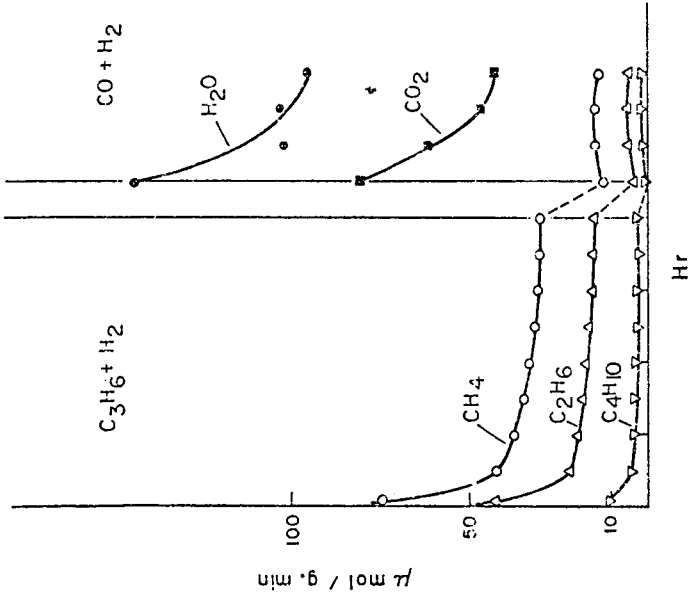


Figure 9

Reaction of Propylene and Hydrogen.

Synthesis Gas Reactions Using Catalysts Formed by Oxidizing Ni-Containing Intermetallic Compounds

H. Imamura and W. E. Wallace

Department of Chemistry
University of Pittsburgh
Pittsburgh, PA. 15260

I. Introduction

Intermetallic compounds containing rare earths or actinides in chemical union with the transition metals Fe, Co or Ni are transformed when exposed to synthesis gas at elevated temperatures into mixtures of rare earth or actinide oxides and elemental Fe, Co or Ni. It has been found that these mixtures are exceptionally active for syngas conversion (1-12). The converted alloys have been characterized by Auger spectroscopy (1,13), x-ray diffraction, ESCA (14) and electron microscopy (7). These studies showed that the surface regions consisted of transition metal nodules growing out of or dispersed on a substrate of rare earth or actinide oxide. The decomposed materials rather than the original alloy appear to be the catalytically active species for the reaction.

Additionally, it has been found that thorium-containing intermetallics such as ThNi₅ readily reacted with elemental oxygen to form a mixture of metallic Ni and ThO₂ (12). The oxidation of ThNi₅ occurred with a predominant formation of ThO₂ because of the strong chemical affinity of thorium for oxygen. During the oxidation reaction metallic Ni aggregates precipitated out in a fashion similar to that observed when the intermetallic is exposed to syngas. The reaction of ThNi₅ with a stoichiometric amount of oxygen required for the formation of thorium-supported Ni catalysts (Ni/ThO₂) brought about complete transformation into a mixture of Ni and ThO₂. This mixture had higher activity for methane formation by an order of magnitude than oxide-supported catalysts (15) prepared by conventional wet chemical procedures. Accordingly, it appears that the oxidation treatment of intermetallics constitutes a novel way for forming oxide-supported catalysts with high activity for syngas conversion.

In this work, the character of catalysts formed by the oxidation of several rare earth-nickel intermetallic compounds was studied in the manner used earlier to study the Th intermetallics. They were evaluated using x-ray diffraction, ESCA and CO chemisorption techniques. The resulting materials, which are probably new supported catalysts, were examined as syngas conversion catalysts.

II. Experimental

The intermetallic compounds (LaNi₅, CeNi₅, PrNi₅, NdNi₅, HoNi₅, ErNi₅ and ThNi₅) were prepared by induction melting the metal components in a water-cooled copper boat under an atmosphere of purified helium. These intermetallics were subjected to remelting several times or annealing at a prescribed temperature to insure homogeneity. The formation of the desired compounds was established by x-ray diffraction analysis.

The oxidation treatment of the intermetallics, which had been previously powdered in a porcelain mortar followed by outgassing, was conducted in the presence of oxygen at 610 mmHg. The amount of oxygen uptake by the compound was determined by the pressure drop in a closed system.

To establish the nature of the sample thus treated x-ray diffraction, x-ray photoelectron spectroscopy (ESCA) and CO chemisorption techniques were used.

Powder x-ray diffraction patterns were obtained using a Picker model 3488K diffractometer with Cu radiation. ESCA spectra were recorded on an AEI ES200 electron spectrometer using Al K α radiation (1486.6 eV). The spectrometer was operated at 12 KV and 25 mA with base pressure $<10^{-9}$ torr in the sample chamber. The binding energy was determined by reference to the contamination C 1s line at 285.0 eV. The CO chemisorption measurements were made at room temperature by means of an adsorption flow method (16). The procedures used have been described in detail previously (12).

III. Results and Discussion

1. Characterization of Catalysts Formed by Oxidation

X-RAY DIFFRACTION

The previous work (12) on the oxidation of thorium-containing intermetallic compounds showed that the oxidation reaction occurred in a stepwise fashion. At first, thorium in the alloy was oxidized largely to form the oxide, during which process finely divided Ni aggregates precipitated out on the resulting oxide surface. Accompanying this there was a remarkable enlargement in the surface area, by up to 200-fold. After completion of the oxidation of thorium further oxygen was taken up by the reaction of Ni to form NiO.

All the compounds studied in the present work readily reacted with considerable amounts of oxygen at 350°C. It was confirmed from x-ray diffraction studies that the oxidation steps approximated that of the thorium intermetallics just mentioned. For example, as depicted in Fig. 1, CeNi₅ was completely transformed into a mixture of Ni phase and CeO₂, i.e., Ni/CeO₂, when reacted with the stoichiometric amount of oxygen required to oxidize the Ce present in the alloy. When the CeO₂-Ni mixture was exposed to oxygen there was an additional uptake of oxygen. This occurred by the oxidation of Ni to form NiO. However, after reduction with hydrogen there was no evidence of NiO peaks in the pattern.

From x-ray line broadening measurements of the Ni (111) peak at $2\theta = 44.5$ (Cu K α radiation) it was possible to establish the Ni particle sizes dispersed on the resulting oxide using the Sherrer equation (18). As shown in Table 1, the particle sizes ranged from 90 to 350 Å. The particle sizes usually but not always showed an increase with increasing oxygen uptake for LaNi₅, CeNi₅ and ThNi₅.

ESCA

X-ray diffraction studies in the preceding section provided an overall image of the alloy transformed by the oxidation. ESCA measurements were made on the oxidized CeNi₅ to examine the chemical state of the surface species participating in the reaction. ESCA spectra of the oxidized CeNi₅ showed Ni, Ce, O and C signals within the probing depth of ESCA (several atomic layers). Confirming the results obtained by x-ray diffraction analysis, the Ce present in the surface region was found to exist largely in an oxide form. For Ni species the oxidized CeNi₅ (C-4) exhibited the Ni 2p_{3/2} peaks at 853.9 and 856.6 eV. These binding energies are characteristic of Ni and NiO, respectively (19). Hence Ni is present in the surface region, consisting of several atomic layers, as metal and oxide. Since the ESCA peak intensity is directly correlated with the surface concentration, the composition of the surface can be roughly established from the ESCA information. The intensity ratio of Ni 2p_{3/2} to Ce 3d_{5/2}, ~ 7.5 , indicates that the surface is largely metallic Ni.

Table 1. Characterization of Catalysts Formed by Oxidation

Precursor Intermetallic Compound	O ₂ Uptake (mmol/g)	Surface Area ^{a)} (m ² /g)	CO Chemisorption (μ mol/g)	Particle Size (Å)
LaNi ₅	-	0.10*	0.17*	
" (L-1)	1.71	0.55	1.2	90
" (L-2)	2.99	0.66	2.6	100
" (L-3)	6.57	3.5	7.1	100
CeNi ₅	-	0.08*	0.13*	
" (C-1)	2.32	1.1	4.8	110
" (C-2)	3.74	15.7	31.7	300
" (C-3)	4.47	25.4	45.7	200
" (C-4)	5.14	23.7	51.8	350
PrNi ₅	-	0.15*	0.10*	
" (P-1)	1.73	0.79	2.8	170
NdNi ₅ (N-1)	1.71	1.1	1.2	140
HoNi ₅ (H-1)	1.64	0.76	2.0	330
ErNi ₅ (E-1)	1.61	1.0	2.0	280
ThNi ₅	-	0.09*	0.2*	
" (T-1)	1.91	12.0	19.0	200
" (T-2)	3.35	18.0	105.7	270

a) Surface areas were measured at liquid nitrogen temperature by means of argon adsorption (17).

* These values were obtained for the original intermetallic compounds.

CO CHEMISORPTION

Although ESCA studies revealed existence of metallic Ni in the surface region, to obtain the information about the amount of metallic surface area or the number of active sites present on the surface room temperature CO chemisorption measurements were made. The results obtained are summarized in Table 1. It is informative to notice that the oxidized samples (L-1, C-1, P-1, N-1, H-1, E-1 and T-1) contain elemental oxygen corresponding to the complete formation of Ni/oxide assuming a stoichiometric reaction. It is evident that the oxidation led to an increase in the number of active sites along with a rise in the surface area. The extent of the increase was observed to be dependent upon the particular rare earth or actinide involved in the original compound. CeNi₅ and ThNi₅ exhibited striking changes in chemisorption during the stages of oxidation. CO chemisorption increases by up to 500-fold compared to the original compound were observed. In contrast, increases for LaNi₅ were much less pronounced. The differing behavior of CeNi₅ and ThNi₅ on the one hand and LaNi₅ on the other undoubtedly reflects important physicochemical differences. The most significant difference between LaNi₅ and the other two compounds is that La is trivalent and Ce and Th are quadrivalent. This leads to a different electron concentration and perhaps a difference in chemical stability. This may be responsible for variation in

behavior of the systems produced by oxidation, but the precise factors and their operation are as yet unclear.

2. Reaction of CO and H₂

The reaction was carried out in the range of 150 to 300°C over the alloys, which had been oxidized to varying extents. The data obtained are summarized in Table 2. Activity for the present reaction was represented by the rate of CO

Table 2. Activity of Various Catalysts

Precursor Intermetallic Compound	CO Conversion (%)	Activity (ml/sec.g)	T.N.x10 ³ (sec ⁻¹)
LaNi ₅ (L-1)	1.2	1.5x10 ⁻³	48
CeNi ₅ (C-1)	2.0	2.5x10 ⁻³	18
" (C-2)	1.0*	1.2x10 ^{-3*}	
" (C-3)	2.6*	3.7x10 ^{-3*}	1.7*
" (C-4)	5.0*	6.1x10 ^{-3*}	3.8*
PrNi ₅ (P-1)	1.8	2.2x10 ⁻³	26
NdNi ₅ (N-1)	0.5	6.1x10 ⁻⁴	19
HoNi ₅ (H-1)	1.6	2.0x10 ⁻³	31
ErNi ₅ (E-1)	4.2	5.2x10 ⁻³	59
ThNi ₅ (T-1)	9.0*	1.1x10 ^{-2*}	10.6*
" (T-2)	7.0(at 190°C)	3.5x10 ^{-2*}	5.6*

* The values correspond to the results measured at 205°C; the others were obtained at 275°C, except as noted.

consumption per gram-catalyst. This kind of comparison seems valid since the catalysts were used under very similar conditions. Taking into account the fact that the catalytically active species is metallic Ni dispersed on the surface, it is also of interest to specify the turnover number (T.N.), representing the specific activity per site. The turnover number as molecules CH₄ produced per site per second was determined from CO chemisorption measurements assuming a 1:1 ratio of a CO molecule to surface Ni atom in the surface complex. Among the catalysts studied the oxidized CeNi₅ and ThNi₅ exhibited exceptional activity (Table 2). The oxidized CeNi₅ and ThNi₅ showed T.N. measured at 205°C about an order of magnitude higher than conventional silica- or alumina-supported Ni catalysts (15). It is therefore apparent that the supported catalysts derived using the oxidation treatment of intermetallics are exceptionally active for the conversion of CO and H₂ to methane. T. Inui et al. (20) have reported that activity for methanation was substantially enhanced when ~3% rare earth oxide such as La₂O₃ or Ce₂O₃ was added to Ni-supported catalysts. It was found (21) that ThO₂ was also operative as a promoter for supported Ni catalysts.

It should be emphasized that the effectiveness of rare earth or actinide oxide-supported catalysts for syngas conversion is very dependent upon the preparation method. As noted in the Introduction, for example, a ThO₂-supported catalyst (6) prepared using the conventional impregnation procedure followed by calcining and reducing processes exhibited very poor activity compared to that obtained by the oxidation technique. It thus appears that the oxidation treatment of intermetallics plays a decisive role in formation of active catalysts and this method constitutes a new way of producing superior oxide-supported catalysts.

As shown in Table 2, for the oxidized CeNi₅ and ThNi₅ increase in the extent of oxidation results in an increase in the activity. There is a good correspondence between the CO chemisorption and activity and in this respect the present systems closely resemble behavior observed earlier for oxidized Ni₅Si₂ (22).

Hydrocarbon products in the reaction were largely methane. Small amounts of C₂ to C₄ hydrocarbons were also observed. Selectivity of hydrocarbon products over various oxidized alloys is listed in Table 3. The selectivity was determined in

Table 3. Selectivity of Catalysts

Precursor Intermetallic Compound	Conversion (%)	Composition (%)			
		C ₁	C ₂	C ₃	C ₄
LaNi ₅ (L-1)	1.8	92.0	7.0	1.0	-
CeNi ₅ (C-1)	3.4	86.3	7.0	5.3	-
" (C-4)	5.0	77.3	15.9	6.8	-
PrNi ₅ (P-1)	3.1	88.4	6.6	5.0	-
NdNi ₅ (N-1)	1.8	91.3	4.3	4.3	-
HoNi ₅ (H-1)	2.5	82.4	8.1	9.5	-
ErNi ₅ (E-1)	4.2	74.0	10.9	15.0	-
ThNi ₅ (T-1)	12.5	80.0	12.1	6.8	1.4

the conversion range below 10%. It is unclear from this study whether the selectivity is dependent upon extent of the total conversion. It is to be noted that the selectivity depends upon the nature of the rare earth or actinide in the precursor compound. Oxidized LaNi₅ revealed very high selectivity for methane formation. This accords with the observation of T. Inui et al. (20) referred to above.

References

1. V. T. Coon, T. Takeshita, W. E. Wallace and R. S. Craig, J. Phys. Chem. **80**, 1878 (1976).
2. A. Elattar, T. Takeshita, W. E. Wallace and R. S. Craig, Science **196**, 1093 (1977).
3. V. T. Coon, W. E. Wallace and R. S. Craig, in "The Rare Earths in Science and Technology," eds. G. J. McCarthy and J. J. Rhyne, Plenum Press, NY (1978), p. 93.
4. A. Elattar, W. E. Wallace and R. S. Craig, *ibid.*, (1978), p. 87.
5. W. E. Wallace, in Hydrides for Energy Storage, A. F. Andressen and A. J. Maeland, eds., Pergamon Press Inc. (1978), p. 33.
6. A. Elattar, W. E. Wallace and R. S. Craig, Advances in Chemistry, in press.
7. V. T. Coon, Ph.D. Thesis, University of Pittsburgh, August, 1977.
8. C. A. Luengo, A. L. Cabrera, H. B. MacKay and M. B. Maple, J. Catal. **47**, 1 (1977).
9. G. B. Atkinson and L. J. Nicks, J. Catal. **46**, 417 (1977).
10. A. Elattar and W. E. Wallace, in "The Rare Earths in Modern Science and Technology" (1979), in press.
11. A. Elattar and W. E. Wallace, Science, submitted.
12. H. Imamura and W. E. Wallace, J. Catal., submitted.
13. A. G. Moldovan, A. Elattar, W. E. Wallace and R. S. Craig, J. Solid State Chem. **25**, 23 (1978).

14. R. Chin, A. Elattar, W. E. Wallace and D. Hercules, *J. Catal.*, submitted.
15. M. A. Vannice, *J. Catal.* 37, 449 and 462 (1975); 40, 129 (1975); 44, 152 (1976); 50, 228 (1977).
16. H. L. Gruber, *Anal. Chem.* 34, 1828 (1962).
17. F. M. Nelsen and F. T. Eggertsen, *ibid.*, 30, 1387 (1958).
18. H. P. Klug and L. E. Alexander, in X-Ray Diffraction Procedures for Polycrystalline and Amorphous Materials, 2nd ed., p. 68, Wiley, NY (1974).
19. K. S. Kim and N. Winograd, *Surf. Sci.* 43, 625 (1974).
20. T. Inui, M. Funabiki, M. Suehiro and T. Sezume, *J.C.S. Faraday I* 75, 787 (1979).
21. S. Medsforth, *J. Chem. Soc.* 123, 1452 (1923).
22. H. Imamura and W. E. Wallace, *J. Phys. Chem.*, in press.

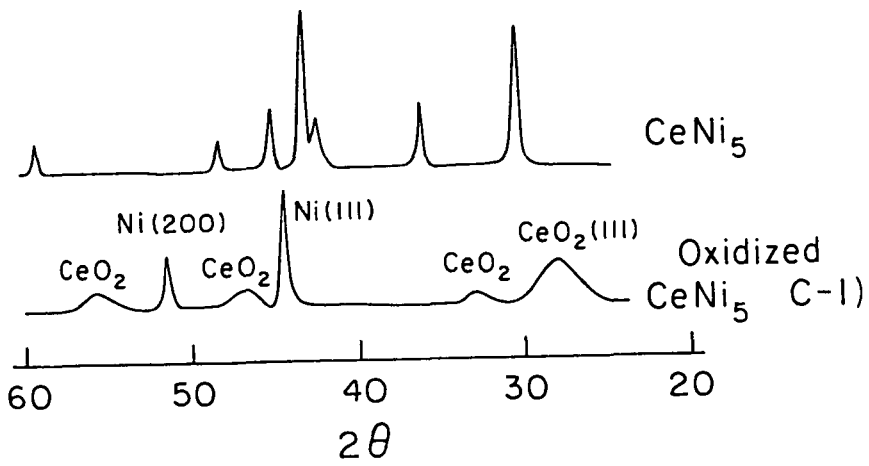


Fig. 1 Comparison of x-ray diffraction (Cu $K\alpha$ radiation) of the oxidized and original $CeNi_5$.

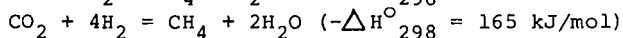
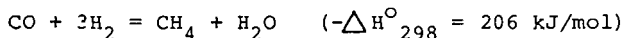
CATALYTIC ASPECTS OF HIGH TEMPERATURE METHANATION

Karsten Pedersen, Allan Skov and J.R. Rostrup-Nielsen

Haldor Topsøe Research Laboratories
Nymøllevej 55, DK-2800 Lyngby, Denmark

INTRODUCTION

Methanation of synthesis gas mixtures is an essential step in the manufacture of substitute natural gas (SNG):



The reactions are catalyzed by various metals of which supported nickel is preferred.

Methanation for SNG production is complex because the high concentrations of CO and CO₂ involved result in large potential temperature increases. This may cause sintering of the catalyst or for some cases a potential for carbon formation.

One solution is to include a recycle stream of product gas as a diluent. It is evident that this solution involves a loss of energy in the recycle operation, and that an economic process should allow minimum recycle. For an adiabatic process, however, this is equivalent to a large temperature increase.

Another solution is to carry out the methanation in a cooled reactor in which the heat of reaction is transferred from the reaction zone into a cooling medium, e.g. boiling water. For a cooled reactor, it appears advantageous to design for high "hot zone" temperatures, because this gives a better heat transfer.

When decreasing the operating temperature, the need for higher catalyst activity increases. Below a certain temperature the reaction will not "ignite". This problem may be aggravated because the catalyst having been exposed to the high temperature, may have to operate at the low temperature after ageing or poisoning of the catalyst at the reactor inlet.

Moreover, the steep temperature profile means that the operation temperature of a catalyst pellet may change 50-100°C within seconds in case of variations in load, recycle ratio and preheat temperature. This requires high mechanical stability of the catalyst.

Thus for adiabatic and for cooled reactors as well, in order to meet these process requirements, the catalyst should be active and stable both at high and low temperatures. This is a key problem to be solved when optimizing the methanation process for coal-based SNG.

The paper summarizes catalyst studies of important phenomena to be controlled in the development and use of an industrial catalyst meeting these requirements.

EXPERIMENTAL

The catalysts were studied in various test units. Sintering studies were performed in a tubular reactor ($D_i=32$ mm) in which various catalyst samples were exposed simultaneously to sintering at given temperature, pressure and atmosphere. Low temperature deactivation phenomena were studied in differential flow reactors ($D_i=0.8$ mm). The catalyst was used as 0.3 - 0.5 mm particles diluted with inert material. Standard activity tests, and determination of nickel surface areas were described earlier (1). The main part of the development work took place in a pilot plant with a 5 litre adiabatic reactor. The reactor had a full bed length (up to 2m) and operated at industrial mass velocities, leaving the reactor diameter as the only scale-up parameter. Catalyst samples from pilot tests were used for physical and catalytical examination.

RESULTS

Sintering

The methanation reaction on nickel requires a large ensemble of nickel atoms (2), and the specific activity is influenced by nickel crystallite size (3), by the composition of the support (4,5,6), and by non-linear poisoning effects (1). Therefore, the reaction appears sensitive to the structure of the catalyst and to its history of operation.

Sintering of the nickel crystals results in loss of surface area, and in principle recrystallization may change the nickel ensembles available, and hence cause a decrease of the specific activity. We showed previously (4,7) that heat treatment of nickel crystals on a stable low area ceramic support resulted in no sintering at 550°C over a period of 1000 hours, whereas the nickel surface area dropped to around 40 to 25% over the same period at 700°C and 850°C respectively, this result corresponds to the rule of Tammann, according to which sintering is expected above 0.5 times the melting point ($^\circ\text{K}$) (8) of the metal. The growth mechanism of supported metal crystals appears very complex (9,10). The growth rate might be influenced by the wetting properties of the metal to the support, and by the micropores of the support material. It was illustrated that the diffusion of a metal crystallite is impeded, when the size of the metal crystallite is of the order magnitude of the diameter of the pore (11,12). In general, the metal particles may hardly grow to a size larger than the pore diameter of the support. This means that a stabilized micropore system of the support effectively prevents sintering of the nickel crystals.

Nickel catalysts designed for low temperature operation are normally based on high area supports such as gamma alumina, silica, chromia, etc. These supports suffer from significant sintering, which may be accompanied by weakening when exposed to temperatures above 500°C (4,13). The sintering may be accelerated by high steam partial pressure (14). Figure 1 shows results from sintering tests at conditions for accelerated sintering (i.e. $\text{H}_2\text{O}/\text{H}_2=10, 30$ atm). Three catalysts are compared: a low area steam reforming catalyst, a high area low

temperature methanation catalyst ($\text{Ni}/\gamma\text{Al}_2\text{O}_3$), and the Topsøe methanation catalyst MCR-type. The MCR catalyst maintains a high total surface area and mechanical strength, whereas the $\gamma\text{Al}_2\text{O}_3$ based catalyst deteriorates. All catalysts show significant loss in nickel surface area at 800°C .

Carbon Formation

Thermodynamics predict carbon formation for methanation above a certain temperature, depending on feed composition and pressure. This may influence the minimum recycle ratio allowed, as illustrated in Figure 2. However, the thermodynamic data are influenced by the catalyst, because it modifies the structure of the carbon. This allows operation at conditions more critical than those, which correspond to the limit predicted on the basis of ideal graphite. We have shown previously (4,15) that this effect is favored by small nickel crystals in the catalyst.

In practice, this means that the so-called principle of equilibrated gas (1,4), (i.e. carbon formation when the gas shows affinity for carbon, after the establishment of the methanation and shift equilibria) predicts no carbon formation for methanation. The validity of this principle is indicated by the results in Table 1, obtained from thermogravimetric studies (1). The conclusion has been further confirmed by the experience in the pilot tests.

Low Temperature Problems

Low operating temperatures favor the adsorption of poisons, e.g. sulfur on the catalyst. We have shown that the effect of sulfur is strongly non-linear (1) reflecting that the methanation reaction is structure sensitive. This, and other studies (16,17), show that a sulfur content in the feed stream of less than 10 ppb is required to obtain a reasonable methanation activity after equilibration of the sulfur adsorption. Therefore, the effect of sulfur poisoning should rather be analysed in terms of a dynamic model for fixed bed adsorption (18).

The operation at a low recycle ratio or the straight-through operation in a cooled reactor, implies high partial pressures of carbon monoxide at the reactor inlet. This results in two problems.

At temperatures below 230°C , there is a substantial risk that carbon monoxide reacts with nickel, forming nickel carbonyl. Operation in this temperature range, with a partial pressure of carbon monoxide of 2.5 atm resulted in transport of nickel in the catalyst bed. Moreover, the formation of nickel carbonyl resulted in a drastic growth of the nickel crystals, up to particles of 20,000Å, thus exceeding, by large, the pore size of the catalyst support. This growth resulted in break-down of the catalyst. The forces involved appear much stronger than observed in thermal sintering of the nickel crystals, as described above.

Another result from operating with high partial pressure of carbon monoxide, appears to be a deactivation phenomenon, called β -deactivation developing slowly in some pilot tests, and being reflected by

the appearance of an inflection point in the axial temperature profile. Figure 3 illustrates the movement of the temperature profile, and that the β -deactivation disappears above a certain inlet temperature. The activity could be restored by treatment in hydrogen, as explained below.

The low temperature deactivation phenomena were further demonstrated by laboratory tests on a Ni/ η Al₂O₃ catalyst in a differential reactor. As shown in Figure 4, no deactivation was observed if CO was replaced by CO₂. The deactivation rate increases significantly with the CO/H₂ ratio and by the presence of sulfur. The role of sulfur on other deactivation phenomena was indicated in our earlier studies (1).

The MCR-2X catalyst shows much less deactivation than the Ni/ η Al₂O₃ catalyst. Analysis of the spent catalysts indicated by the growth of nickel crystals showed that the Ni/ η Al₂O₃ catalyst had also been exposed to carbonyl formation in contrast to the MCR-2X catalyst. The large influence of catalyst composition on deactivation rate and carbonyl formation was also reported by Vannice and Garten (6).

The β -deactivation is probably due to the formation of a less reactive carbon state on the nickel surface, which might be the β -state identified by Wise et.al. (19,20).

The situation corresponds to the deactivation observed in steam naphtha reforming at low temperatures (21), and to a general model for carbon formation on nickel (22). The adsorbed intermediate (α' -carbon) may either be gasified to methane (2,19) or be dissolved in nickel as carbon and form carbon whiskers (1), or be transferred into encapsulating carbon (β -carbon). For the present case, apparently the conversion of α' into β is too slow at very low temperatures, e.g. 250°C, whereas at high temperatures the rate of hydrogenation of β -carbon exceeds the transformation rate of α' into β -carbon (20). These effects are overlapped by the influence of the surface concentration of α' -carbon such as the hydrogenation rate of α' -carbon and the parameters governing the chemisorption of carbon monoxide. The CO chemisorption depends on the partial pressure of CO and the temperature at a given position in the reactor, and it is also affected by the composition of the catalyst (5).

MCR-2X Catalyst

The development program for methanation catalysts at Topsøe's laboratories aimed specifically at solving the problem of operating over a wide temperature range. The work resulted in the MCR-2X catalyst. The support has a stabilized micropore system that effectively prevents sintering of the nickel crystals. The resulting high nickel surface area and the absence of alkali (sometimes added to prevent carbon formation) led to the desired high methanation activity. The catalyst is mechanically stable at high as well as low temperatures. The stability was proven in pilot tests with a total run-time amounting to 15,000 hours. This included 8,000 hours operation at the same catalyst filling at a maximum temperature of 600°C. Data in Table 2 demonstrates the thermo-stability of MCR-2X reflected by an almost unchanged mechanical strength and total surface area. The activity stabilized after 1,000-2,000 hours.

The mechanical and chemical properties of MCR-2X also offer flexibility in providing the capability for regeneration of spent catalysts. Table 3 shows results from regeneration tests performed on samples taken after 4700 hours operation in the pilot plant. The carbonaceous film responsible for the β -deactivation can be removed simply by treatment in hydrogen, whereas sulfur is more difficult to remove. However, the catalyst easily withstands a high temperature oxidation and re-reduction, which will not only remove sulfur, but also result in redistribution of any sintered nickel crystals. As shown in Table 3, more than 50% of the original activity of a new catalyst can be regained by this method.

The properties of MCR-2X can be utilized in different process schemes optimized for the feedgas in question. The critical step is the first methanation stage, where the full potential of MCR-2X is utilized, MCR-2X allowing maximum practicable temperature increase from ca. 300°C to 700°C.

The mechanical sintering problem could be solved by using steam reforming catalysts, which will, of course, be active also for methanation. However, the nickel surface areas in most steam reforming catalysts are too small to provide adequate low temperature activity, thus dictating operating at higher reactor inlet temperatures. This will not necessarily influence the overall conversion in the reactor, which is fixed by the exit temperature. However, for adiabatic operation, the reduced temperature rise means a higher recycle energy consumption. In principle this can be overcome by increasing also the exit temperature, but this means a greater number of reactors because of the smaller conversion per reactor. This situation is illustrated in Figure 5, in which the operation, based on MCR-2X, is shown (solid line) in a simplified example involving three adiabatic reactors, corresponding to an overall conversion of 95%.

The process path, TREMP (Topsøe Recycle Methanation Process) is compared with alternative routes of high temperature methanation (dashed lines) based on a reforming type catalyst. A temperature of 450°C is assumed as the minimum inlet temperature for the reforming type catalyst. To achieve the same conversion of the first reactor as obtained in TREMP, a recycle ratio 2 times higher as in TREMP is required. This means higher energy consumption. If recycle is excluded, four reactor stages are necessary with reforming catalysts to obtain a conversion equivalent to that of the first TREMP reactor. Moreover, this solution is doubtful because of the excessively high exit temperature of the first reactor.

By the use of a combined bed of a non-nickel catalyst with MCR-2X, the inlet temperature can be decreased to 200°C, thus allowing a temperature increase of 500°C at a reduced recycle rate. The wide operating range of MCR-2X may be utilized in the design of boiling water reactors for methanation. With MCR-2X, design for "hot zone" temperatures of 700°C is realistic, since this leaves a good safety margin. An explorative test was made in the pilot plant in which MCR-2X was exposed to 780°C in the "hot zone". For simplicity the test was made in an air-cooled reactor. The inlet temperature was

300°C and after the hot zone, the reaction temperature was decreased to about 250°C. The tube wall temperature in the hot zone was between 300 and 400°C, which is close to the expected value in an industrial boiling water reactor. Measured and calculated temperature profiles are shown in Figure 6. No significant deactivation of the catalyst was observed at the test, which supports the possibility for designing for high hot spot temperatures, being important for optimum reaction and heat transfer conditions.

A special application of methanation is related to the Long Distance Energy Transport System NFE or ADAM/EVA system, which is being developed at the German Nuclear Research Center KFA-Jülich, in cooperation with Rheinische Braunkohlenwerke AG in Cologne. In this system (23,24), nuclear energy released in a helium-cooled high temperature reactor is transferred to steam reformer (EVA) with a hot helium as heating medium. The product is transported by pipeline to power plants in which the heat is recovered in a methanation plant (ADAM). The high exit temperature which can be accepted of MCR-2X makes it possible to raise superheated high pressure steam at the destination for electricity production as required in the NFE system. Topsøe has supplied the semi-commercial demonstration plant ADAM-1 to KFA - Jülich. The plant is based on three adiabatic methanation steps, and it is processing synthesis gas manufactured from up to 200 Nm³ per hour of natural gas (23). Figure 7 shows temperature profiles from an ADAM I run which was made by KFA in cooperation with Topsøe (25). MCR-2X was installed in the first two methanation steps, whereas the third methanator operated on MCR-4 which is a highly active low temperature catalyst.

CONCLUSIONS

The use of a nickel catalyst for methanation is limited to a minimum operating temperature because of the risk of carbonyl formation and deactivation, and to a maximum operating temperature because of sintering and in certain cases the risk of carbon formation. Between these temperature limits, the activity and stability of the catalyst determines the optimum layout of the methanation process. The Topsøe MCR-2X catalyst allows operation in the temperature range 250°C to well above 700°C. By combination with a non-nickel catalyst, the operation range can, for certain cases, be extended to 200 to 700°C. This capability of high temperature methanation offers the possibility of design for low recycle, or for optimum boiling water reactors.

REFERENCES

1. Rostrup-Nielsen, J.R., and Pedersen, K., J.Catal. (in press).
2. Araki, M., and Ponec, V., J.Catal. 44, 439 (1976).
3. Coenen, J.W.E., Schats, W.M.T.M., and van Meerten, R.Z.C. Bull.Sco.Chim.Belg. (1979) (in press).
4. Rostrup-Nielsen, J.R., "Steam Reforming Catalysts", Teknisk Forlag, Copenhagen 1975.

REFERENCES (Cont'd)

5. Schoubye, P., J.Catal. 14, 238 (1969).
6. Vannice, M.A., and Garten, R.L., J.Catal. 56, 236 (1979).
7. Rostrup-Nielsen, J.R., J.Catal. 21, 171 (1971)
8. Garner S.W., "Chemistry of the Solid State", Butterworths, London 1955, p 307.
9. Ruckenstein, E., and Pulvermacker, B., AIChE Journal 19, 356 (1973).
10. Wynblatt, P., and Tae-Moon, Ahn, "Sintering and Catalysis", Materials Science Research 10, 83 (1975).
11. Ruckenstein, E., and Pulvermacker, B., J.Catal. 37, 416 (1975).
12. Borisova, M.S., Fenelonov, V.B., Dzisko, V.A., Simonova, L.G., Kinet.Katal. 17, 653 (1976).
13. Williams, W., Butler, G.A., and Hammonds, J., J.Catal. 24, 352 (1972).
14. Levy, R.M., Bauer, D.J., Roth, J.F., Ind.Eng.Chem.Prod. Res. Develop. 7, 217 (1968).
15. Rostrup-Nielsen, J.R., J.Catal. 27, 343 (1972).
16. McCarty, J.G., Wentrcek, P.R., Wise, H. and Wood, B.J. DOE Contract 76-C-03-115, Annual Report Oct. 26, 1978.
17. Fitzharris, W.D., PhD Thesis, University of Delaware, 1978.
18. Christiansen, L.J., and Andersen, S., Proc. 6th Int. Symp. on "Chemical Reaction Engineering", Nice 1980 (in press).
19. McCarty, J.G., and Wise, H., J.Catal. 57, 406 (1979).
20. McCarty, J.G., Wentrcek, P.R., and Wise, H., in "Proc.Amer. Chem.Soc.Symposium", Chicago, Aug. 28-Sept. 2, 1977", p 1315.
21. Moseley, F., Stephens, R.W., Stewart, K.D., and Wood, J., J.Catal. 24, 18 (1972).
22. Rostrup-Nielsen, J.R., and Trimm, D.L., J.Catal. 48, 155 (1977).
23. Harms, H.G., Höhlelein, B., and Skov, A., Chem.Ing.Tech.(in press).
24. Boltendahl, V., Niessen, H.F., Theis, K.A., GWF-Gas/Erdgas, 117, 517 (1976).
25. Harms, H.G., Höhlelein, B., and Skov, A., Oil and Gas J. (submitted).

Table - 1

Carbon Formation, Thermogravimetric Tests

Experimental conditions re ref (1)
Catalyst, 13wt% Ni, $D_{Ni} = 300 - 3500 \text{ \AA}$

Carbon limits calculated from "principle of equilibrated gas"

	1	2
CO/H ₂	0,33	0,7
PCO atm	0,2	0,33
Temp. °C	400-470	400
Calc. carbon limits		
Carbon for (Temp. °C):		
Graphite	415 < T < 800	T < 1069
Catalyst ($D_{Ni} = 3500\text{\AA}$)	600 < T < 350	T < 684
Carbon Formation	No	Yes

Table - 2

High Temperature Stability of MCR2X

Results from Pilot Tests

Operation Time at Temp. h °C	BET Area m ² /g	H ₂ Area m ² /g	D_{Ni} Å
New MCR2X	52	7	220
8127 600	30	3	295
1895 600 followed by 860 700	35	3	345

Table - 3

Regeneration of MCR2X Catalyst

Samples from HTAS-run 5

Operating time at temp. h °C	Regeneration Conditions	Activation Conditions	Intrinsic Activity relative to unused cat.	
			Before	After
4800 290-385	H ₂ , 15h, 500°C	-	0.006	0.05
4800 290-385	H ₂ , 4h, 700°C	-	0.006	0.15
3900 280-300	H ₂ O, 16h, 700°C	800-850°C, 2h	0.025	0.42
3900 600	H ₂ O, 16h, 700°C	800-850°C, 2h	0.11	0.50

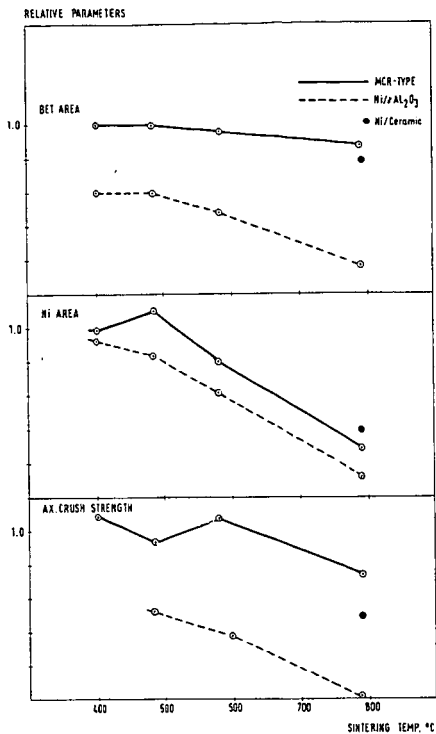


Figure 1

Sintering of Catalysts

30 kg/cm², H₂O/H₂=10, 140-170 hours
 MCR-type. BET-area = 33 m²/g
 Ni/γAl₂O₃. BET-area = 101 m²/g
 Ni/Ceramic. BET-area = 1.2 m²/g

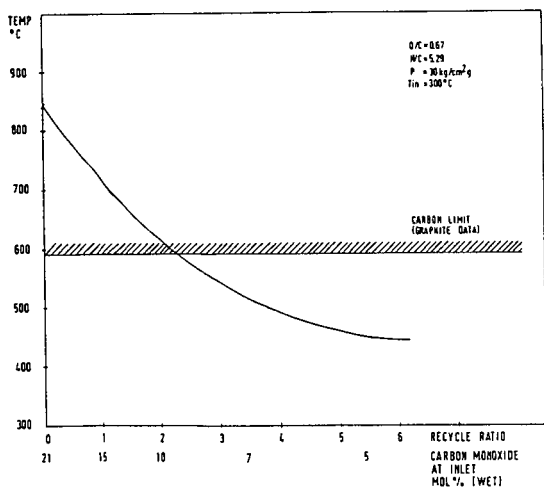


Figure 2

Carbon Limits

Recycle ratio and outlet temperature of adiabatic equilibration of gas. The example refers to a feed-gas containing 12 vol% CH₄. Correction for carbon-structure on catalyst moves carbon limits to 950-1050°C.

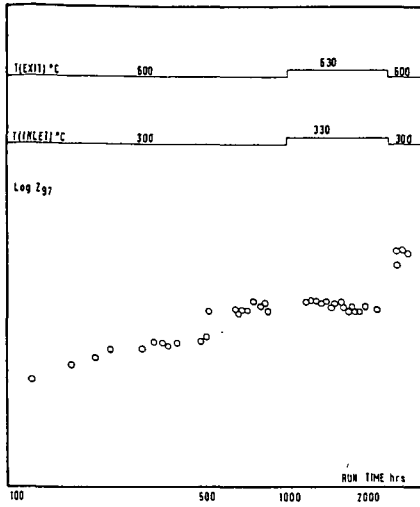


Figure 3

β -deactivation in Pilot Test

MCR-type catalyst.

$O/C = 1.$, $H/C = 6.$, $P = 30 \text{ kg/cm}^2\text{g}$,
 $PCO = 2 \text{ kg/cm}^2\text{g}$.

Z_{97} = axial distance from top of catalyst bed for 97% conversion of max. adiabatic ΔT obtained.

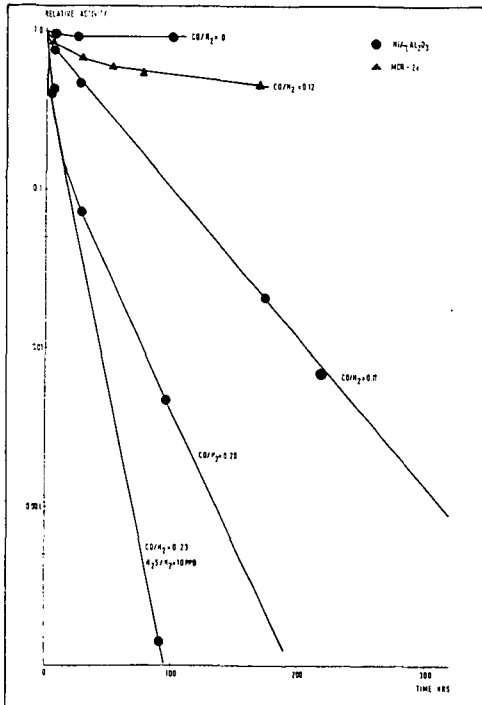


Figure 4

Low Temperature Deactivation

Laboratory Tests

300°C , $21.2 \text{ kg/cm}^2\text{g}$, $\text{NHSV} = 10^6 \text{ h}^{-1}$

Feedgas (vol%):

- H_2O (35)
- CO (0-11)
- CO_2 (5)
- H_2 (rest)

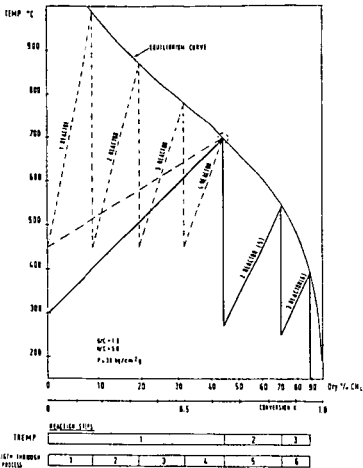


Figure 5

High Temperature Methanation
Simplified Example

Comparison of TRESP reaction steps (solid line) with reaction routes based on a reforming type catalyst (dashed lines).

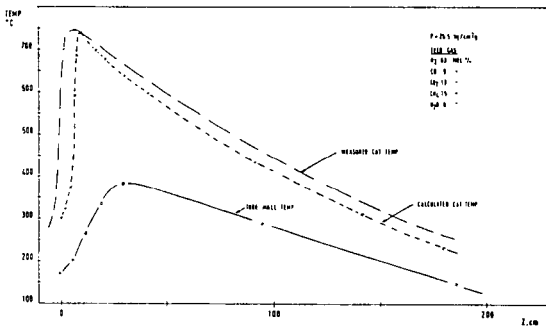


Figure 6

Explorative Pilot Test
with Air-cooled Reactor

Measured and calculated temperature profiles. The calculation model did not consider axial radiation in the bed, which explains the difference of the two profiles.

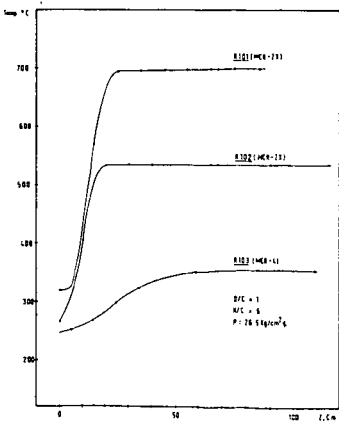


Figure 7

ADAM-1 Test Unit
Temperature Profiles

Applied Fischer-Tropsch Kinetics for a Flame Sprayed Iron Catalyst

W. J. Thomson, J. M. Arndt, and K. L. Wright

University of Idaho, Department of Chemical Engineering, Moscow, Idaho, 83843

INTRODUCTION

There has been a great deal of previous work done of Fischer Tropsch catalysis but until recently, very little rate data have been obtained other than semi-quantitative results. A great deal of the previous literature deals with the proposed and hypothetical mechanisms of Fischer Tropsch catalysis and its similarities/dissimilarities to SNG methanation. Despite the voluminous amount of work in this area there is still controversy as to whether deposited carbon or iron carbide (in the case of iron catalysts) is the active intermediate in the mechanistic scheme.¹ In addition to this there was a great deal of work accomplished at the Bureau of Mines in the 1940's and 50's concerning the behavior of Fischer Tropsch catalysis under various conditions.² Iron as well as cobalt and ruthenium have been proposed and studied as possible Fischer Tropsch catalysts.^{3, 4} There has also been considerable interest in the incorporation of various promoters in Fischer Tropsch catalysis in order to alter olefin-to-paraffin ratios, minimize CO₂ make, etc. An interesting study being conducted at the University of Utah⁵ is seeking to systematically alter various promoters in order to determine the best combination in order to achieve a maximum of C₂-C₅ hydrocarbons. A short review of Fischer Tropsch technology up to 1975 has been given by Shah and Perrotta.⁶

There have been two kinetic studies using iron catalysts for Fischer Tropsch applications.^{7, 8} Dry et. al.⁷ used a triple promoted iron catalyst in the pressure range of 10-20 atmospheres and at temperatures from 240-270C to determine the reaction orders of the CO consumption rate with respect to both hydrogen and CO. He employed a differential reactor with H₂-to-CO ratios varying from 1 to 7. They found that the reaction order with respect to CO was effectively zero but the reaction order with respect to H₂ was first order. Between 225 and 265C they also determined an activation energy of 16.8 Kcal/mole. However all their data were obtained by measurements of the CO₂ and water-make in the exit stream. By assuming that there was minimal oxygenated products (reasonable for iron

catalysts), then the summation of the CO₂ and water-make should equal the total CO consumption rate. In all cases the ratio of CO₂-to-water was less than 1 except at the highest temperatures (265C, where it equaled 1.15). Since the effect of increasing space velocity was to dramatically decrease the CO₂/H₂O ratio, they concluded that CO₂ was a secondary reaction produced by the water gas shift reaction. A more recent kinetic study was conducted by Atwood and Bennett.⁸ In this case they employed not only a tubular flow reactor but also an internally recirculated reactor (similar to the reactor employed here). They claimed in their paper that there was little difference in the reaction kinetics whether the recirculated reactor or the tubular flow reactor was employed. Based on our experience, it would appear that this was due to their minimal H₂ consumption (H₂ in excess) and a zero order dependency of the reaction with respect to CO (as reported by Dry et. al.⁷). In this case they reported that with the iron catalyst, the CO₂/H₂O ratio was significantly greater than one but it should be pointed out that the temperatures employed in this study ranged from 250C to 315C; that is, significantly higher than the temperatures used by Dry et. al.⁷ They proposed a kinetic expression which is based on the rate being dependent on the hydrogen concentration and the fraction of reduced iron present.⁹ A psuedo steady state balance between the oxidation of iron by H₂O and its reduction by CO leads to equation (1).

$$r_{CO} = \frac{k(P_{H_2})}{1 + b P_{H_2O}/P_{CO}} \quad (1)$$

Experimental data at three temperatures were used to determine the constants k and b as a function of temperature. However it should be pointed out that the term involving the ratio of water to CO partial pressures in the denominator was only important for a very few data points. Also, since a constant feed mixture with a H₂ to CO ratio of 2.0 was used and the authors report that the mole fraction of H₂ in the product stream was essentially

independent of carbon monoxide conversion, the H₂ partial pressure was close to a constant for all runs. Although the authors show an excellent fit when equation (1) is rearranged to the linear form of equation (2), note that the essentially constant hydrogen partial pressures and a small

$$\frac{P_{H_2}}{r} = \frac{1}{k} + \frac{b}{k} \frac{P_{H_2O}}{P_{CO}} \quad (2)$$

effect of the water-to-CO partial pressure would produce a constant rate at any temperature.

Two other rate expressions based solely on observation, have also been proposed.⁹ In one, the rate was observed to depend only on the partial pressure of H₂ (for conversions less than 60%) and, in the other an adequate correlation for cobalt was obtained by equation (3).

$$r_{CO} = \frac{k P_{CO} P_{H_2}^2}{1 + K_1 P_{CO} P_{H_2}^2} \quad (3)$$

Fischer-Tropsch synthesis is highly exothermic and consequently a good deal of attention has been spent on reactor design considerations. Designs ranging from slurry reactors to fluidized beds have been proposed² and, in the latter case, actually constructed.¹⁰ It is also common to utilize recycle reactors in order to restrict the temperature rise across the catalyst bed, but a heavy price must be paid in terms of compressor costs. A low pressure drop reactor utilizing parallel plates and inserts coated with catalyst was first proposed by DOE for the exothermic methanation reaction¹¹ and a similar design using iron catalysts for Fischer Tropsch has been discussed by Haynes, et. al.¹² The work reported here deals with an applied kinetics study utilizing this catalyst concept. While the scope of the project is concerned with product distributions as well as reaction rates, in this paper we will only focus on reactant and make-gas rates.

EXPERIMENTAL EQUIPMENT AND PROCEDURES

Berty Reactor System

All of the experiments were conducted in an internally recirculating reactor ("Berty" type) and a schematic of this equipment is shown in Figure 1. Hydrogen and CO are monitored separately via capillary flow meters equipped with pressure drop transducers and the flows are adjusted with the reactor on by-pass to obtain the desired inlet H₂-to-CO ratio and total flow. Once the desired ratio is obtained, a sample is sent for analysis via gas chromatography using a Carle Model 111 H gas chromatograph. The reactor is then put on stream and the H₂-CO mix is fed to the reactor. The exit stream leaving the reactor passes first through a "hot trap" (a condenser maintained at 120C) in order to condense waxes. The uncondensed portion of the stream then passes through a cold trap (at 0C) where water and oil are condensed. The gas effluent from this condenser passes into a knock-out pot to remove entrained liquids and then proceeds via a wet test meter to vent. Provisions are made to sample this exit gas stream on line and again, analysis is done via a Carle 111 H gas chromatograph. The reactor pressure is adjusted and maintained by means of a needle valve at the reactor exit. Temperatures within the reactor are measured just above and below the catalyst sample. The mass velocity across the catalyst surface can be adjusted by means of regulating the RPM of the magne-drive unit equipped with the Berty reactor. Typically at RPM's above 750 the temperature difference across the catalyst is within 2C and all data reported here were obtained at 1500 RPM.

The Carle Analytical Gas Chromatograph is equipped with an on-line hydrogen transfer tube so that reasonably accurate hydrogen peaks are obtained as part of the analysis. A 2.5 m poropak Q column at 105C was placed in a series-bypass mode with a 2.5 m molecular sieve column maintained at 30C. With the columns connected in series, H₂, CO and CH₄ pass through the poropak column and into the molecular sieve column where they are temporarily retained. A valve is then switched so that the molecular

sieve is bypassed and CO₂, H₂O and C₂-C₄ compounds are separated and analyzed. With the columns placed in series once again, analysis of H₂, CO and CH₄ takes place.

The iron catalyst, supplied by the Pittsburgh Energy Technology Center (PETC) of DOE, consisted of taconite which was plasma-sprayed to an average thickness of 0.56 mm on flat plates of iron substrate. It had a BET area of 2 m²/gm and a porosity of 0.48. The catalyst assembly consisted of 5 plates, each 7.6 cm high and of varying widths so as to be compatible with the draft tube size of the Berty reactor. The plates were bolted together with two threaded rods and the assembly and dimensions are shown in Figure 2. The catalyst was assembled, leak tested in He and then reduced by heating to 500°C in flowing H₂ over a 4-hour period and then holding at 450°C for 24 hours. Attempts were made to estimate the water make during reduction in order to determine the percentage reduction of the available iron. Unfortunately the slow reduction rate and consequent low H₂O concentrations did not allow for accurate measurements.

The need for a carburization pretreatment when using iron Fischer Tropsch catalysts has been the subject of a number of investigations.¹³ In this case we utilized a H₂/CO feed of 1.5 at 300°C and 1.6 MPa and ran for a total of 30 hours on-stream. This corresponded to the time at which the activity and product distribution stabilized. It should be pointed out however, that the catalyst was idled in H₂ at 300°C and 1.6 MPa at the end of each day's running. In addition the conversions varied during this pretreatment and, since the reactor behaves as a CSTR, the catalyst was exposed to varying H₂/CO ratios. This will be discussed below in more detail.

RESULTS

Prior to entering into a discussion of the results, it is important to emphasize the behavior of a CSTR reactor such as the one used here.

First of all, in discussing reaction rates or product distributions, it is the reactor *exit* conditions which are the independent variables. These are brought about by independent control of the inlet flow rate, inlet composition, reactor pressure, and temperature. Consequently, in the subsequent discussion only the exit conditions will be referred to. Another important factor is that, since a fixed bed catalytic reactor (\sim plug flow) will have catalyst exposed to both inlet and outlet conditions, it is important to obtain data over a wide range of conversions and inlet compositions. For example, in Fischer-Tropsch synthesis the H_2/CO ratio will generally increase as conversion increases. Thus it is important to vary the conversion as well as the inlet H_2/CO ratio so that a wide range of independent data are available for statistical analysis. In this work the CO conversions varied from 15% to 85% and the exit H_2/CO ratios were varied independently from 0.8 to 18. Total pressures ranged from 0.77 to 3.1 MPa and temperatures from 250C to 300C.

Induction Period

The fact that Fischer-Tropsch catalysts generally require an induction (or "carburation") period has already been mentioned. Proper carburation is thought to increase the catalyst lifetime and of course this is exceedingly important for commercial success. In our case, we wished to obtain rate data corresponding to the stable activity of the catalyst and we were unable to run continuously. Because of this latter restriction we followed a procedure of idling the catalyst in H_2 at 1.0 MPa whenever we were not running. Because of these differences we elected to utilize an alternate induction method which was more compatible with our day-to-day operation and which appeared to give the same stable activity¹⁴ as the more typical complex carburation procedure.

The procedure employed during the first 24 hours of induction was to expose the catalyst at 300C and 1.6 MPa pressure to a 1.5 H_2/CO mixture at an "exposure velocity" (J, volumetric flow rate at standard condition per unit superficial catalyst area) of 2.6 m/hr. Some of the results obtained

during this period are shown in Figure 3. First of all it should be noted that the conversion was very high during the first four hours on stream. This points to the importance of conducting Fischer-Tropsch catalyst screening tests only after the catalysts have been exposed to synthesis gas for at least four hours. Note that during the first 20 hours of induction, the conversion starts off low and builds up during the day's run. It was hypothesized that the H₂ idling procedure was effecting reduction of the active iron carbide so that the first few hours of the run are spent reforming FeC at the expense of hydrocarbon production. As a result, the inlet conditions were changed at 24 hours time-on-stream (TOS) to 3.1 MPa and H₂/CO = 2.0. As can be seen from Figure 3, once this change was made, the variation in daily conversions was markedly reduced and the catalyst reached apparent stability after about 35 hours TOS.

While the results in Figure 3 show only the total CO conversion, some mention ought to be made of the selectivity to C₅⁺ during this period. During the 24 hours TOS, the C₅⁺ weight fraction of total hydrocarbon make gradually increased on a daily basis from about 0.05 to 0.20. After this period the fraction remained essentially constant at about 0.25.

Product Distribution

In principle either CO₂ or H₂O can be produced from the chain growth which occurs during Fischer-Tropsch synthesis. However, CO₂ can also be produced via the reversible water gas shift reaction



Typically the CO₂ make was comparable to the CH₄ make at 250C and was 50 to 100% greater than CH₄ at 300C. If the CO₂ is produced from a side reaction such as equation (4), then one would expect an increasing CO/H₂ ratio with increased conversion. As Table I shows, this is indeed the case at both temperatures as long as the H₂/CO ratio is approximately constant. Also shown in Table I is the equilibrium parameter, ϕ , which is defined as

$$\phi = \frac{P_{\text{CO}_2} P_{\text{H}_2}}{K_{\text{eq}} P_{\text{CO}} P_{\text{H}_2\text{O}}} \quad (5)$$

and will of course be equal to 1.0 at equilibrium (K_{eq} is the equilibrium constant). It is apparent from the results shown in Table I that the water gas shift reaction is well removed from equilibrium at 250C but closer at 300C. Some measure of the reversible nature of the reaction rate can also be obtained from Table I. That is, at constant conversion the CO_2/H_2O ratio decreases as the H_2/CO ratio increases. This would indicate an inhibition of the forward reaction rate of equation (4) by increased product-to-reactant ratios.

Another important aspect of Fischer-Tropsch synthesis is the olefin-to-paraffin ratio of the hydrocarbon products. Table II shows the C_2H_4/C_2H_6 ratio as a function of the H_2/CO ratio and conversion at two temperatures. Note that this ratio decreases as conversion increases at both temperatures in agreement with Kugler's¹⁵ hypothesis that the main elements in chain growth are olefins, not paraffins. As expected, higher H_2/CO ratios also lower the C_2H_4/C_2H_6 ratio since these would tend to promote hydrogenation. Comparing the data at two temperatures, it can also be seen that higher C_2H_4/C_2H_6 ratios are favored at the lower temperature.

The experiments conducted during this portion of the investigation were designed primarily to obtain reaction rate data and since a large number of separate runs were required to accomplish this goal, the run times were generally restricted to 3 hours or less. Unfortunately this is not a sufficient length of time to obtain large enough quantities of oil for accurate measurements (the oil make varied from about 0.2 to 4.0 ml/hr). Nevertheless, some insight into the parameters which favor oil make can be obtained from the data shown in Figure 4. Here the weight fraction of C_5^+ (C_5^+ /total hydrocarbon make) is plotted as a function of conversion for different H_2/CO ratios at 250C. As expected, increasing conversions result in higher C_5^+ fractions (the chain has a chance to grow) and apparently higher H_2/CO ratios retard the formation of higher carbon numbers. Within the accuracy limitations of the data, the C_5^+ fraction did not appear to be a function of pressure at 250C. However this

was not the case at 300C where it was found that higher pressures tended to increase the C_5^+ fraction. Because of this, there were not enough 300C data at similar conditions in order to obtain a good comparison with the data at 250C. Nevertheless the results in Table III show a definite decrease in the C_5^+ fraction as the temperature increases from 250C to 300C.

Another parameter of interest in Fischer-Tropsch synthesis is the product distribution of the hydrocarbon make. During most runs a small but detectable wax was collected from the hot trap (see Figure 1) but the quantities were too small for accurate analysis. A number of oil-make samples were also subjected to GC-MS analysis and carbon numbers up to about 18 were detected with the highest weight fraction at C8 or C9. The major constituents of the oil were the normal paraffins with varying quantities of olefins and branched compounds at each carbon number. Little in the way of oxygenated compounds were detected.

A common analysis to which Fischer-Tropsch hydrocarbons are subjected is the so called "Schulz-Flory" distribution.¹⁶ In this case the log of the mass fraction of each species divided by its carbon number would plot linearly as a function of carbon number if Fischer-Tropsch synthesis follows equal probability chain growth. Such a plot, typical of the data collected here, is shown in Figure 5. As can be seen, while linear plots are obtained at low and high carbon numbers, there is a transition region between C₄ and C₈ which does not plot linearly. Since the C₁-C₄ compounds essentially remain in the gas phase and the C_5^+ compounds are collected in the liquid phase, it was first thought that the behavior in Figure 5 was due to a material balance error. However when various arbitrary errors were added, either to the gas or liquid quantities, the same type of plot resulted. Evidently the Schulz-Flory distribution does not apply over the complete carbon number range. It is interesting to note that similar results with this catalyst have been obtained at PETC using a tubular flow reactor.¹⁴

Reaction Rates

Ideally we would like to measure intrinsic reaction rates (that is, rates in the absence of all transport limitations) under proposed commercial operating conditions such as those used here. For Fischer-Tropsch synthesis this is difficult to do because of the production of higher carbon number oils which could saturate the catalyst pores and lead to the necessity of gaseous reactants having to diffuse through liquid filled pores. Although the thickness of the catalyst used here was only 0.56 mm, the very low diffusivities of gases in liquids ($\sim 10^{-5}$ cm²/sec) can still result in pore diffusion limited rates. This will be discussed in more detail below. For high reaction rates it is also possible to be limited by gas-solid transport phenomena. This was avoided in these experiments by increasing the reactor impeller speed until there was no separate dependency of the rate on impeller speed. This was found to occur at 750 rpm and, as mentioned earlier, all data were obtained at 1500 rpm.

Because of the possibility of pore diffusion limitations, the rate data were not subjected to thorough evaluations of various mechanistic kinetic expressions. In addition, because of the complexity of Fischer-Tropsch synthesis, it was decided to first attempt to analyze the rate of consumption of CO, independent of the species, produced. Consequently a simple power law model in terms of CO and H₂ partial pressures was evaluated but it did not provide for a sufficiently accurate correlation. Although a number of more complex models were found to give adequate correlations of the data it was found that the rate expression given by equation (1) gave as good a correlation as any. Specifically

$$r_{CO} = \frac{k P_{H_2}}{1 + b P_{H_2O}/P_{CO}} \quad (1)$$

with $k = 7.6 \times 10^3 \exp \left[\frac{-8820}{RT} \right] \quad (6)$

$$b = 0.40 \exp \left[\frac{1430}{RT} \right] \quad (7)$$

In these equations r_{CO} is expressed in terms of the superficial area of the catalyst, g moles/m²-hr, pressure is in atmospheres and temperature is in degrees Kelvin.

In comparing these values with those given previously by Atwood and Bennett⁸ for a potassium promoted fused iron catalyst, the major difference is in the apparent activation energy for k. Atwood and Bennett reported a value of 20.3 Kcal/mole whereas we observe a much lower value of 8.8 Kcal/mole. Again this might be due to strong pore diffusion effects since it is well known that for near first order kinetics, pore diffusion rate limitations will produce an apparent activation energy equal to one-half its true value. If this were the case, one would expect that equation (1) would not give as good a fit at the higher temperature. Figure 6 shows a plot of the predicted versus the measured values of r_{CO} and, as can be seen, the data scatter is definitely larger at 300C. In fact the average deviation at 250C was approximately 10% whereas it was 20% at 300C.

As already mentioned, CH₄ was the most significant product under all conditions. Consequently a separate determination was made of a rate expression which would describe its rate of formation. Due to the fact that CH₄ is only one of many products, no attempt was made to base the rate expression on kinetic mechanisms. Instead a simple power law model was employed and the results are shown in equation (8)

$$r_{CH_4} = 5.7 \times 10^4 \exp \left[\frac{-13,120}{RT} \right] P_{CO}^{-1/2} P_{H_2} \quad (8)$$

Here again the rate is given in moles/m²hr and the pressure in atmospheres. As expected, an increased rate of CH₄ production is favored by higher temperatures and higher H₂/CO ratios.

A similar attempt was made to obtain a suitable correlation for the rate of CO₂ production. Since it is hypothesized that the CO₂ is produced via the water gas shift reaction, it was anticipated that the rate here would depend on the partial pressures of CO and H₂O. Surprisingly however,

the rate was found to be independent of P_{CO} but rather to be dependent on the H_2O/H_2 ratio as shown in equation (9).

$$r_{CO_2} = 6.58 \times 10^7 \exp \left[\frac{-15,500}{RT} \right] \left(\frac{P_{H_2O}}{P_{H_2}} \right)^{1.3} \quad (9)$$

This could be explained in two ways: the reverse reaction rate is significant and strongly dependent on P_{H_2} ; and CO is in excess (since H_2O is a product of the primary synthesis reactions). The first portion of this explanation can not be proven but seems to be reasonable (strong H_2 adsorption could produce the same effect). Although the data used in obtaining equation (9) covered a wide range of CO/ H_2O ratios (0.2-12), there were only three runs (out of 62) with CO/ H_2O less than one. Since these runs had very high CO_2 production rates and high CO conversions, it is conceivable that the rate of CO_2 production does depend on P_{CO} when it is less than or equal to P_{H_2O} .

Diffusion Limitations

The possibility of strong pore diffusion effects has already been mentioned and the data for the CO consumption rate gives some evidence of its existence. However the rate expression for CO_2 production had an activation energy more typical of kinetic reactions and since it was found to depend on P_{H_2O} , the primary product of Fischer-Tropsch synthesis, it is somewhat surprising that it did not have a lower apparent activation energy. A possible explanation could be that the dominant reaction is methanation and, if it were much faster and in parallel with the other slower reactions, it could be the only pore diffusion limited reaction. Since equation (1) is based on the total CO consumption rate and CH_4 is the major product, this would explain the apparent discrepancy in the apparent activation energies in equations (6) and (9). Some support of this argument is given by the low activation energy associated with CH_4 production [equation (8)].

Whereas separate experiments to quantify the role of pore diffusion were not conducted, estimates of the effectiveness factor can be made provided there is some knowledge of the value of the effective diffusivity. Atwood and Bennett,⁸ assuming that CO diffusion in the liquid filled pores was limiting, used a value of 1.6×10^{-5} cm²/sec for a fused iron catalyst. Using this value and rearranging equation (1) to give an effective first order reaction, we estimate the effectiveness factor be about 0.30 at 300 C. Thus it appears that we have strong pore diffusion effects with respect to the CO consumption rate. This is probably due to the high rate of formation of CH₄ which was the major product (selectivity ~ 60%).

ACKNOWLEDGE

The financial support of this work by DOE under contract No. DE-AS22-78ET00260 is gratefully acknowledged.

REFERENCES

1. Ponec, V., CATAL. REV. - SCI. ENG., 18, p. 151 (1978).
2. Storch, H. H., M. Golumbic, and R. B. Anderson, "The Fischer-Tropsch and Related Syntheses," John Wiley & Sons, New York (1951).
3. Dent, A. L. and M. Lin, ACS Preprints, Div. of Petr. Chem., Anaheim, CA., 23, No. 2, p. 502, March 1978.
4. Everson, R. C., E. T. Woodburn, and A. R. M. Kirk, J. CATAL., 53, p. 196 (1978).
5. Yang, C. H. and A. G. Oblad, Preprints, Div. of Petr. Chem., Anaheim, CA., 23, No. 2, p. 513, March 1978.
6. Shah, Y. T. and A. J. Perrotta, I & EC PROD R & D, 15, p. 123 (1976).
7. Dry, M. E., T. Shingles, and L. J. Boshoff, J. CATAL., 25, p. 99 (1972).
8. Atwood, H. E. and C. O. Bennett, I & EC PROC. DES. DEV., 18, p. 163 (1979).
9. Anderson, R. B., in "Catalysis", p. 257, Vol. IV, Ed. by P. H. Emmett, Rheinhold Pub. Co., N.Y., 1956.
10. Chemical and Engineering News, Sept. 17, p. 13, 1979.
11. Demeter, J. J., Youngblood, A. J., Field, J. H., and Blenstock, D., U. S. BUR. MINES REPT. INV. 7033 (1967).
12. Haynes, W. P., Baird, M. J., Schehl, R. R. and Zarochak, M. F., Preprints, Div. Petr. Chem., ACS, 23, No. 2, p. 559, 1978.
13. Sancier, K. M., Isakson, W. E., Wise, H., Preprints, Div. of Petr. Chem., ACS, 23, No. 2, p. 545, 1978.
14. Schehl, R. R., Pitts Energy Tech Ctr., private communication.
15. Kugler, E. L., paper presented at the ADVANCES IN CATALYTIC CHEMISTRY, Snowbird, UT, Oct. 2-5, 1979.
16. Henrici-Olive, G., Olive, S., Angem. Chem. Int. Ed. Engl., 15, p. 136, 1976.

TABLE I
CO₂/H₂O MAKE AT TWO TEMPERATURES

	H ₂ /CO	X _{CO}	CO ₂ /H ₂ O	φ
250 C	2.24	.26	.14	.004
	2.25	.34	.25	.01
	2.16	.50	.37	.01
	5.9	.79	.42	.016
	8.9	.74	.27	.027
300 C	1.2	.60	1.9	.057
	2.8	.59	1.1	.077
	5.5	.62	0.6	.083
	3.6	.75	1.0	.091
	6.1	.79	1.0	.153
	7.3	.74	0.6	.110
	9.3	.76	0.45	.11

TABLE II
ETHYLENE/ETHANE MAKE AT TWO TEMPERATURES

	H ₂ /CO	X _{CO}	C ₂ H ₄ /C ₂ H ₆
250 C	1.5	.15	.14
	1.2	.21	.13
	2.24	.26	.092
	2.25	.34	.076
	2.16	.50	.050
	5.9	.79	.020
	8.9	.74	.012
300 C	1.05	.26	.096
	1.20	.41	.079
	1.20	.60	.028
	2.80	.59	.023
	5.50	.62	.012
	9.30	.76	.005

TABLE III
COMPARISON OF C₅⁺ FRACTION AT TWO TEMPERATURES

T(C)	X _{CO}	H ₂ /CO	P _T (MPa)	C ₅ ⁺ Fraction
250	.50	2.5	1.47	.31
300	.51	1.7	1.47	.12
250	.55	4.0	2.15	.18
300	.58	3.3	2.02	.10
250	.65	6.7	2.84	.13
300	.76	8.3	2.84	.07

FIGURE 1: SCHEMATIC OF EXPERIMENTAL EQUIPMENT

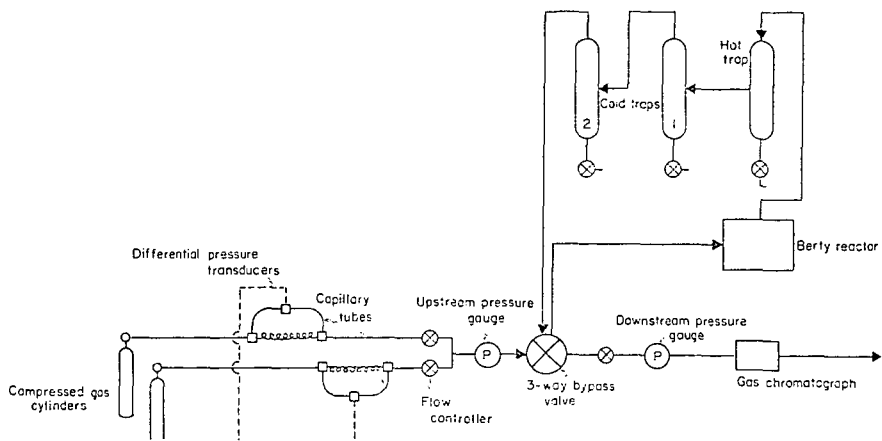


FIGURE 2: CATALYST ASSEMBLY

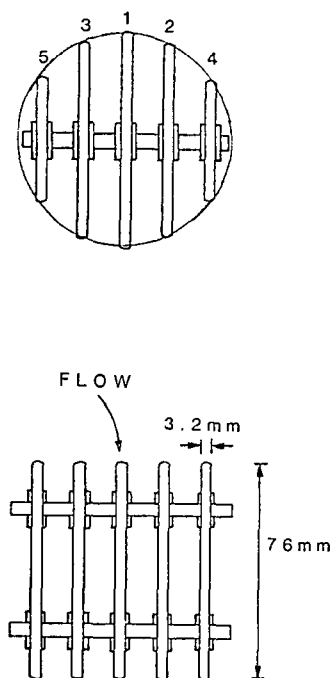


FIGURE 3: INDUCTION PERIOD: CONVERSION VERSUS TIME

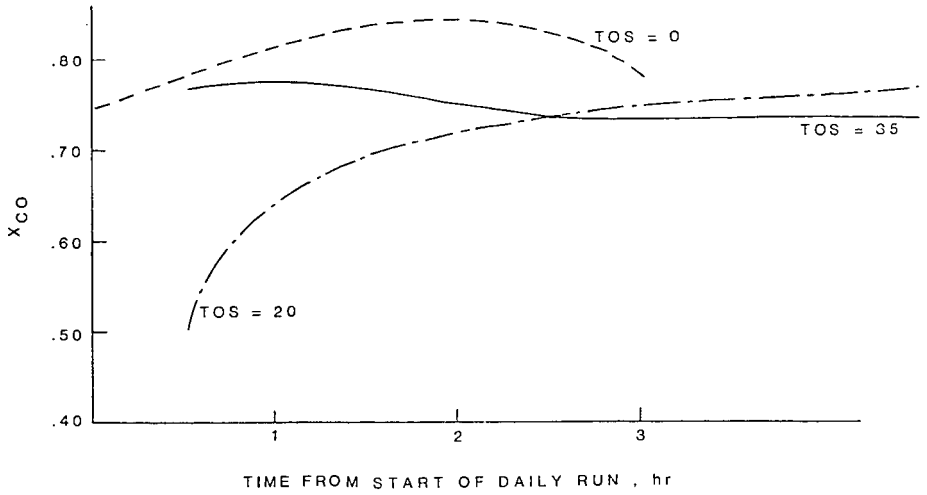


FIGURE 4: WEIGHT FRACTION C₅⁺ VS. X_{CO} (250C)

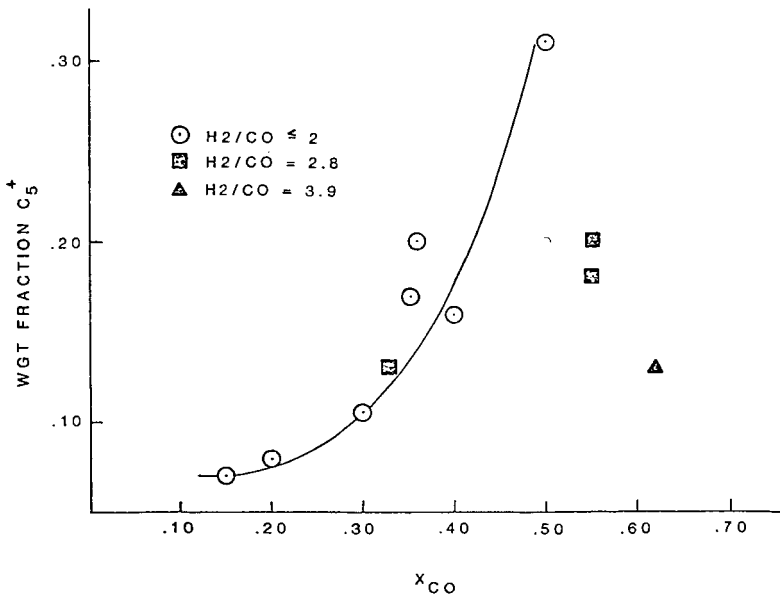


FIGURE 5: TEST OF SCHULZ-FLORY DISTRIBUTION

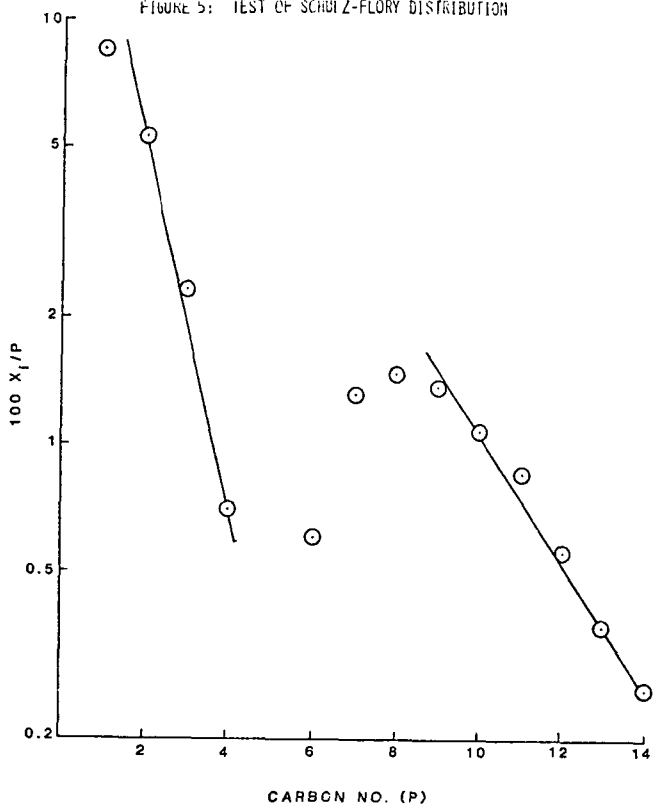
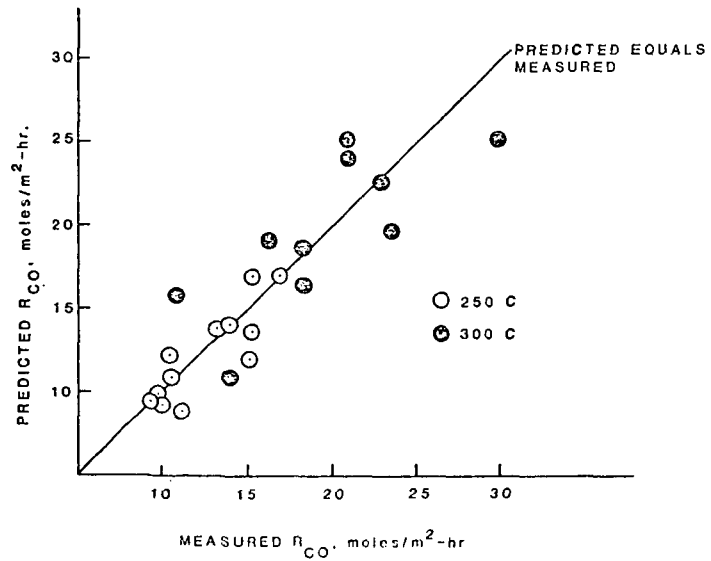


FIGURE 6: PREDICTED VS. MEASURED VALUES OF R_{CO}



Synthesis Gas Conversion to Gasoline Range Hydrocarbons
over Medium Pore Zeolite Catalysts Containing 3d-Metals and Bimetallics

V. U. S. Rao, R. J. Gormley, H. W. Pennline, L. C. Schneider and R. Obermyer*

Pittsburgh Energy Technology Center
4800 Forbes Avenue
Pittsburgh, PA 15213

and

*Department of Physics
Pennsylvania State University
McKeesport, PA 15132

Introduction

There is much current interest in the conversion of synthesis gas to gasoline range hydrocarbons using bifunctional zeolite catalysts (1,2). The medium pore (dia 6Å) zeolite ZSM-5 in combination with Fe was shown to yield a high fraction of aromatics in the product, resulting in a favorable octane number (≈ 90). The transition metal (TM) component catalyzed the hydrogenation of CO while the acid function of the zeolite led to an aromatic product. Owing to the medium size pores of ZSM-5 there was a fairly sharp cut-off, in the product distribution near the end of the gasoline range for the aromatic fraction.

In order to explore further the role of the TM component and the acidity of the zeolite on the product composition, experiments were performed in our laboratory on ZSM-5 impregnated with Fe and Fe-Co, and on Silicalite impregnated with Fe. Silicalite is a molecular sieve form (3) of SiO_2 .

A comparison of the crystallographic studies (4,5) on ZSM-5 and Silicalite, shows that the two zeolites possess very similar crystal structures. While the Si/Al ratio in ZSM-5 can be varied from 3 to ∞ , Silicalite has essentially no Al. Hence, it appears that Silicalite is the limiting form of ZSM-5 when the Al concentration is vanishingly small. Owing to the lack of cations which can be exchanged with protons, Silicalite has no acidity, while HZSM-5 is a highly acidic zeolite. Our investigations sought to find the difference in selectivity for synthesis gas conversion by ZSM-5 (Fe) and Silicalite (Fe) catalysts resulting from the above mentioned difference in acidity.

A further aim of the investigation was to investigate possible difference in selectivity between ZSM-5 (Fe) and ZSM-5 (Fe-Co) catalysts, resulting from the different 3d-electron concentration of the TM component. Magnetic studies (TMA) were performed to characterize the TM component and particularly to detect the formation of bimetallic Fe-Co clusters.

Experimental

The zeolites were prepared using methods described in the literature (3,6). The metal component was introduced by gradually adding the metal nitrate solution to the zeolite until incipient wetness was reached. The impregnation with the metal nitrate solution was carried out for an hour under vacuum in order to enable the nitrate solution to enter the pores of the zeolite. The material is initially dried with constant stirring over a boiling water bath, and further dried in air at 110°C for 12 hours. It is then pelleted to yield tablets 3mm in diameter. In the case of the Silicalite based catalysts, about 10% by weight of an amorphous silica such as Ludox AS-40 was added as a binder before the pelletization step.

The catalysts were tested for synthesis gas conversion in both a fixed bed microreactor and a Berty (continuous flow stirred tank) reactor (7). The latter is shown in Figure 1. The catalyst pellets were loaded into the 2-inch diameter CFSTR chamber and retained by glass wool with a screen. Impeller speed was 1240 rpm. Excellent bed temperature control was obtained by a modification which involved the installation of a coil in the head of the reactor through which air could flow for faster heat removal.

A schematic diagram of the reactor system is shown in Figure 2. Synthesis gas with a H_2/CO -ratio of either 2/1 or 1/1 would pass through a carbon trap and enter the reactor. Liquid and solid hydrocarbon products are collected in a hot trap usually maintained at 150° C and in an ice trap. This series of traps are alternated and drained periodically. Product gases are metered and then flared.

The tablets of the zeolite impregnated with TM were reduced in flowing H_2 at 21 bar and 450° C for 24 hrs. They were then carbided with synthesis gas at 7 bar and 250° C for 24-48 hrs to yield the active catalyst. The gas phase product (C_1 - C_4 hydrocarbons) was analyzed by gas chromatography. The liquid product was separated into paraffins, olefins, aromatics and oxygenates by column chromatography using FIA detection.

Results and Discussion

(a) Influence of Zeolite Acidity:

The results obtained in the Berty reactor on the catalysts ZSM-5 (11.1 wt% Fe) and Silicalite (13.6 wt% Fe) are shown in Table 1. It is apparent that a high percentage of aromatics is obtained from the ZSM-5 (11.1% Fe) catalyst, while the product from the Silicalite (13.6% Fe) catalyst has a low aromatic fraction but much higher olefin and oxygenate fractions. It is thus apparent that the acid function of ZSM-5 based catalyst is responsible for the conversion of the olefins and oxygenates to aromatics. The aromatic fraction imparts a high octane number to the product.

(b) High Olefin Yields from Silicalite Based Catalysts:

The interesting aspect of the product slates from the Silicalite based catalysts was the high percentage of olefins in both the gas and liquid phase products. When promoted with potassium, the Fe containing Silicalite catalyst yielded a large C_2 - C_4 olefin fraction as seen in Table 2. The C_2 - C_4 olefin fraction from Silicalite² (7.8% Fe, 0.9% K) in a fixed bed microreactor² is compared with that from a precipitated Fe-Mn catalyst of Kolbel et al (8), known for its very high olefin yield. It is seen that the olefin yields from the two catalysts are quite comparable. The Silicalite (7.8% Fe, 0.9% K) catalyst yields a much higher C_2 - C_4 olefin/paraffin ratio than the precipitated Fe-Mn catalyst and hence is of potential commercial interest. The mechanism for the enhancement of olefin production on adding K as a promoter has been discussed by Dry et al. (9).

(c) Influence of Transition Metal Component on Product Composition:

The addition of cobalt to Fe containing ZSM-5 catalyst was found to result in a marked change in product composition as seen from the Berty reactor study results in Table 3. It is seen that the incorporation of cobalt into the catalyst results in (a) reduction in the wasteful shift conversion as seen from the decrease in CO_2 in the product (b) lowering of the aromatic fraction to about 10% of the C_5^+ fraction. However, the octane number remained at a relatively high value of 81, despite the decrease in the aromatic fraction. Hence, the impregnation of zeolites with bimetallic TM clusters provides a promising means of altering the extent of shift conversion and the composition of the liquid product. Changes in the aromatic fraction with TM component was an unexpected result since aromatization is normally associated with the acidity of the zeolite. It is possible that some of the cobalt is attached to the Al sites in the zeolite, reducing its acidity. Further studies on this subject are necessary.

(d) Magnetic Studies:

The magnetic properties of TM impregnated zeolite catalysts have been investigated between 77K and 923K in applied fields up to 21 kOe. Samples of ZSM-5 (11.1% Fe), ZSM-5 (5.6% Fe, 4.5% Co) and Silicalite (13.6% Fe) were magnetically analyzed after each of the impregnation, reduction and carburization steps and after use as a catalyst.

The reduced samples of ZSM-5 (11.1% Fe) and Silicalite (13.6% Fe) indicate that Fe is in the metallic state with 86% and 85% reduction, respectively. Thermo-magnetic analysis (TMA) of carbided ZSM-5 (11.1% Fe), show it to be in the high Curie point form (10) of the Hägg carbide. TMA analysis reveals the used ZSM-5 (11.1% Fe) to be the hexagonal close packed (hcp) carbide form of Fe_7C , and the used Silicalite (13.6% Fe) to be the high Curie point form of the Hägg carbide.

The TMA of ZSM-5 (5.6% Fe, 4.5% Co) shows that the reduced, carbided, and spent samples have large magnetic moments (1.94, 2.04 and $2.61 \mu_B$ per TM atom respectively, at room temperature) and high Curie points ($> 900^\circ C$), which cannot be accounted for on the basis of individual Fe and Co particles. The magnetic data indicate the composition to be that of a Fe-Co alloy (11). Hence, we conclude that the difference in selectivity between ZSM-5 (11.1% Fe) and ZSM-5 (5.6% Fe, 4.5% Co) catalysts can be attributed to the presence of bimetallic TM clusters in the latter, with consequent changes in the average number of 3d-electrons per TM atom.

(e) TM Cluster Size and Bifunctional Catalysis:

To determine TM particle size in the bifunctional catalysts CO adsorption studies were performed to determine the TM surface area. These studies showed that the TM clusters had an average diameter of 100-110 Å. Owing to the limitations connected with CO adsorption for estimating metal surface areas, the above may be considered to be approximate values of the TM cluster diameter. Hence, the majority of the TM clusters must reside outside of the pores of the zeolite. We believe that the bifunctional catalytic behavior of these catalysts results from high interparticle diffusivity relative to intracrystalline diffusivity (12).

Conclusions

Our experiments lead to the following conclusions:

- (1) Zeolite acidity plays an important role in the formation of aromatics from synthesis gas by bifunctional catalysts as strikingly evidenced in a comparison of the product slates from ZSM-5 (11.1% Fe) and Silicalite (13.6% Fe).
- (2) The transition metal component impregnated into the zeolite plays an important role in selectivity as seen from the liquid phase products from ZSM-5 (11.1% Fe) and ZSM-5 (5.6% Fe, 4.5% Co). In this context, zeolites containing bimetallic clusters are of special interest.
- (3) Silicalite impregnated with Fe and promoted with K has an exceptionally high selectivity for the production of C_2-C_4 olefins from synthesis gas.

Acknowledgements

We wish to thank R. R. Schehl and B. D. Blaustein for useful discussions, S. S. Pollack for x-ray diffraction analyses, M. F. Ferrer for FIA chromatographic studies, A. Elattar of the University of Pittsburgh for CO adsorption measurements, and W. Picking of Gulf Research for measuring octane numbers.

Table 1. - Comparison of Products from ZSM-5 (11.1% Fe) and Silicalite (13.6% Fe) Catalysts with $H_2/CO=2$, and $P=21$ bar.

Catalyst	ZSM-5 (11.1% Fe)	Silicalite (13.6% Fe)
Temperature, °C	300	280
CO Conversion, %	68.2	39.4
H_2 Conversion, %	38.7	16.5
Space Velocity (h^{-1})	1500	1350
<u>Product Composition (%)</u>		
CO_2	52.0	51.1
H_2O	19.4	22.1
CH_n + oxygenates	28.6	26.9
<u>Hydrocarbon and Oxygenate Composition (%)</u>		
CH_4	54.1	26.5
C_2H_4, C_2H_6	1.1, 15.0	2.5, 15.0
C_3H_6, C_3H_8	2.1, 6.3	10.8, 7.2
C_4H_8, C_4H_{10}	0.0, 4.5	4.8, 4.8
C_5^+ and oxygenates	16.9	25.0
<u>Composition of C_5^+ and oxygenates (%)</u>		
Aromatics	72	4
Olefins	3	41
Saturates	24	33
Oxygenates	1	22
%Gasoline range (BP <204° C)	75	77
Research octane No.	96	36

Table 2. - Conversion of Synthesis Gas to Olefins in Fixed Bed Reactors, Using Silicalite (7.8% Fe, 0.9% K) Compared with That Using a Precipitated Fe-Mn Catalyst of Kolbel et al (8).

Catalyst	Silicalite (7.8% Fe, 0.9% K) (our)	Precip. Fe-Mn (Kolbel et al)
Pressure (bar)	21	14
Temperature (°C)	280	290
H_2/CO Ratio	0.9	0.8
Space Velocity (h^{-1})	1300	353
<u>Product Composition (CH_n + Oxygenates) %</u>		
CH_4	8.6	12.1
C_2H_4	8.2	7.6
C_2H_6	0.4	4.9
C_3H_6	19.3	17.3
C_3H_8	<0.2	2.1
C_4H_8	8.6	15.2
C_4H_{10}	<0.2	3.1
C_2-C_4 Olefins	36.1	40.1
C_2-C_4 Paraffins	<0.8	10.1
C_5^+ and oxygenates	55.1	47.8
C_2-C_4 Olefins	>45.1	4.0
C_2-C_4 Paraffins		

Table 3. - Product Compositions from the Catalysts ZSM-5 (11.1% Fe) and ZSM-5 (5.6% Fe, 4.5% Co), in a Bertly Reactor, Showing the Influence of cobalt addition to the Catalyst.
 Process Condition: $H_2/CO = 2$, $P = 21$ Bar and $GHSV = 1000$ hr^{-1}

Catalyst	ZSM-5 (11.1% Fe)	ZSM-5 (5.6% Fe, 4.5% Co)
Temperature	300	280
CO Conversion, %	68.2	37.8
H ₂ Conversion, %	38.7	41.3
Space Velocity	1500	1400
<u>Product Composition (%)</u>		
CO ₂	52.0	9.8
H ₂ O	19.4	51.8
CH _n + Oxygenates	28.6	38.4
<u>Hydrocarbon and Oxygenate Composition (%)</u>		
C ₁₋₄ hydrocarbons	83.1	74.3
C ₅₊ and Oxygenates	16.9	25.7
<u>Composition of C₅₊ and Oxygenates (%)</u>		
Aromatics	72	10
Olefins	3	46
Saturates	24	37
Oxygenates	1	7
% Gasoline range (BP 204° C)	75	94
Research octane No.	96	81

References

1. C. D. Chang, W. H. Lang and A. J. Silvestri, *J. Catal.* 56, 268 (1979).
2. P. D. Caesar, J. A. Brennan, W. E. Garwood and J. Ciric, *J. Catal.* 56, 274 (1979).
3. R. W. Grose and E. M. Flanigen, U. S. Patent 4,061,724 (1977).
4. G. T. Kokotailo, S. L. Lawton, D. H. Olson and W. M. Meier, *Nature* 272, 437 (1978).
5. E. M. Flanigen, J. M. Bennett, R. W. Grose, J. P. Cohen, R. L. Patton, R. M. Kirchner and J. W. Smith, *Nature* 271, 437 (1978).
6. R. J. Argauer and G. R. Landott, U. S. Patent 3,702,886 (1972).
7. J. M. Berty, *Chem. Engr. Prog.* 70, 68 (1974).
8. H. Kolbel, M. Ralek and K. D. Tillmetz, Proc. 13th Intersoc. Energy Conv. Eng. Conf., Society of Automot. Engineers (1978), p. 482.
9. M. E. Dry, T. Shingles, L. J. Boshoff and G. J. Oosthuizen, *J. Catal.* 15, 190 (1969).
10. K. M. Sancier, W. E. Isakson and H. Wise, Preprints, Div. of Petroleum Chemistry, ACS, 23 (2), 545 (1978).
11. R. M. Bozorth, "Ferromagnetism", Van Nostrand, New York, 1951, pp. 190-209.
12. P. B. Weisz, *Adv. Catal.* 13, 137 (1962).

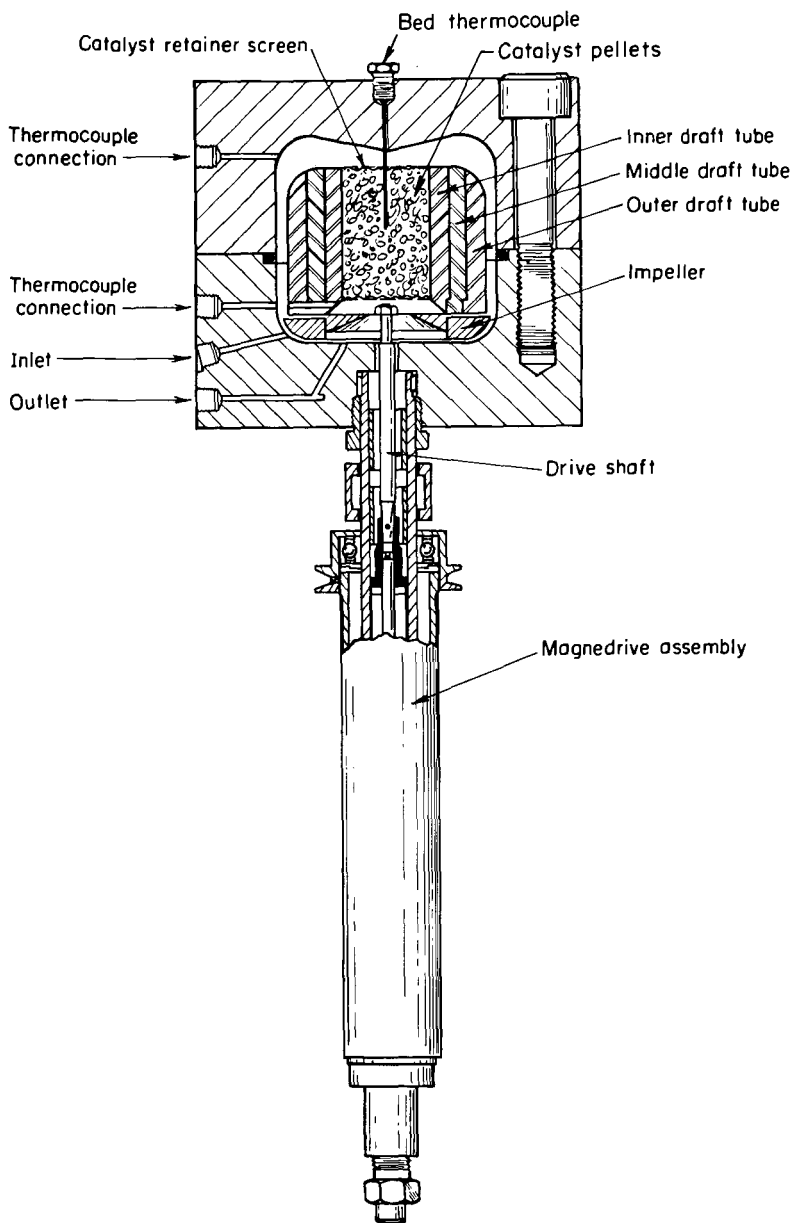


Figure 1. - Bertly Reactor (CFSTR)

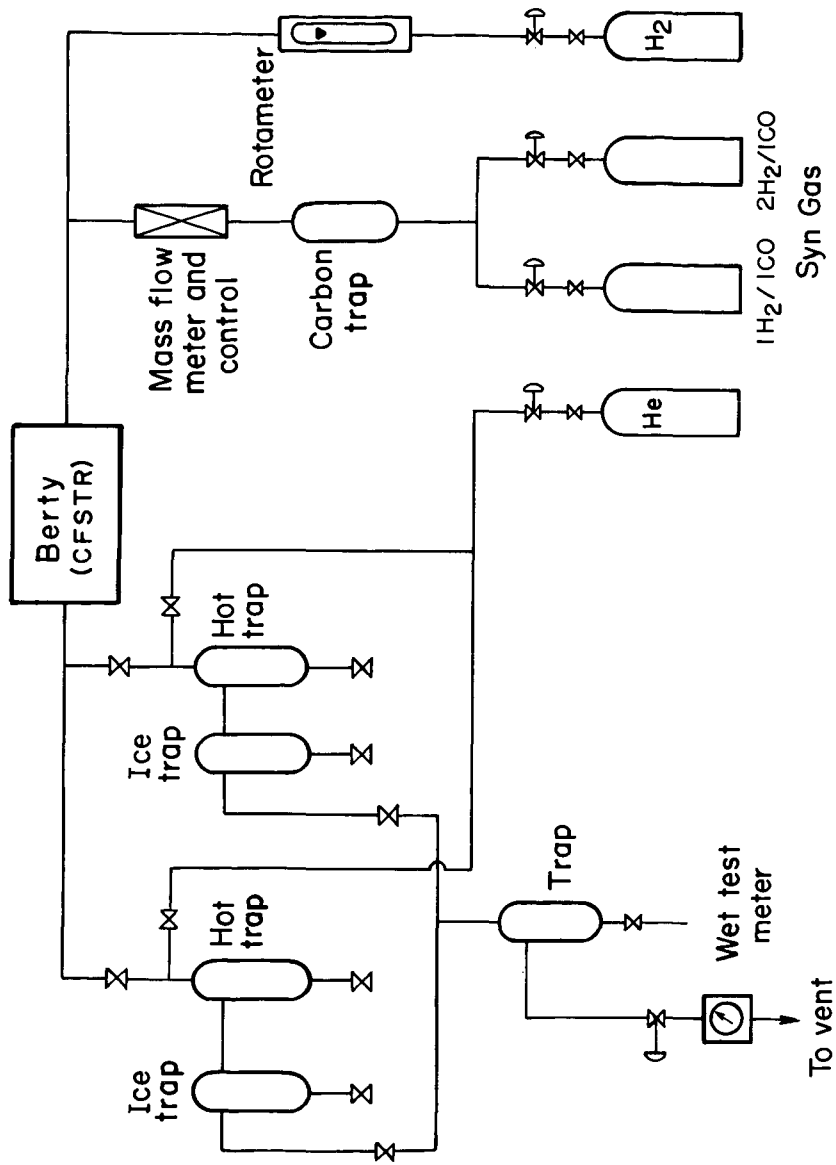


Figure 2. - Flow Diagram for Bertly Reactor System

THE HYDROGENATION OF CARBON MONOXIDE OVER UNSUPPORTED IRON-MANGANESE CATALYSTS FOR THE PRODUCTION OF LOW-MOLECULAR WEIGHT OLEFINS. Y. S. Tsai, A. G. Oblad and F. V. Hanson, Department of Fuels Engineering, 320 W. C. Browning Building, University of Utah, Salt Lake City, Utah 84112.

The hydrogenation of carbon monoxide for the production of low molecular weight (C_2 - C_4) olefins has been investigated over unsupported iron-manganese catalysts. A series of fifteen catalysts of different iron/manganese ratio were prepared and evaluated.

The screening tests were conducted in a fixed-bed, bench-scale reactor. The standard catalyst evaluation conditions were 473-523 K, 500 psig, 2/1 H_2/CO ratio and a gas hourly space velocity $1.08 \text{ cm}^3\text{g}^{-1}\text{s}^{-1}$. The most promising catalyst with regard to the C_2 - C_4 hydrocarbon yield was composed of 2.2 parts of manganese per 100 parts of iron.

Four of the catalysts, $Mn/Fe=2.2$, $Mn/Fe=8.4$, $Mn/Fe=63$ and $Mn/Fe=278$ were selected for an extended process variable investigation. The olefin yield increased with increasing reaction temperatures, with decreasing space velocity and with decreasing H_2/CO ratio. The dependence of the olefin yield on reactor pressure reported in the literature was not observed in this investigation. The activation energy in the temperature range 473-523 K was 20-30 kcal mol^{-1} .

A MODEL FOR THE ISOTHERMAL PLASTOMETRIC BEHAVIOR OF COALS

William G. Lloyd, Henry E. Francis, Morgan R. Yewell, Jr.

Institute for Mining and Minerals Research, University of Kentucky,
P. O. Box 13015, Lexington, KY 40583

Raymond O. Kushida and Vega D. Sankur

Jet Propulsion Laboratory, California Institute of Technology
Pasadena, CA 91103

Introduction

The plasticity of bituminous coals in the range 350-500°C is of critical importance in thermomechanical fluidization such as is required for coal pumping by heated screws (1-3) and in hydrogenolysis in the absence of added solvent (4,5). The fact that the optimum reaction temperatures for three major current liquefaction technologies are nearly identical (6) and are close to the fluidity maxima for many plastic coals suggests that the processes comprising coal "melting" are critically important to hydroliquefaction. More generally, coal plasticity is obviously involved in caking problems (7-10).

The most widely used method of measuring coal plasticity was developed by Gieseler (11). With minor modifications this remains a standard procedure (12); its relationship to other measurements has been discussed elsewhere (13). This method measures the resistance of a mass of well-packed pulverized coal to the rotation of a rabble-arm stirrer which is driven through a constant-torque clutch. At low temperatures the solid mass completely immobilizes the stirrer shaft. In the standard Gieseler procedure the coal is heated at a uniform rate of 3°C/min. As the coal begins to soften -- typically at about 390°C -- the stirrer shaft commences to turn slowly. As temperature increases the coal becomes more fluid and the shaft turns more rapidly, eventually achieving a maximum rate. The coal melt -- actually a heterogeneous mixture of solids, molten phase and gaseous pyrolyzate -- then undergoes a thickening or "coking"; the stirrer shaft turns progressively more slowly, and eventually stops. Gieseler data are recorded in units of dial divisions per min (ddpm), where 100 ddpm = 1 shaft rotation per min. For three bituminous coals of varying plasticity the standard Gieseler data are shown in Table 1.

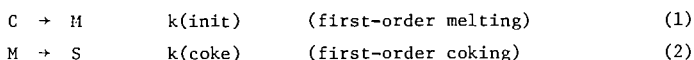
The Isothermal Model

It is often useful to study phenomena under isothermal conditions. Gieseler plastometry lends itself to such studies, since sample warmup time in the standard crucible (2-3 min.) is short in comparison with the usual melting/coking time scale (20-120 min.). Isothermal Gieseler plastometry has been explored by Fitzgerald (14,15) and by Van Krevelen and coworkers (16,17). A plot of $\log(\text{ddpm})$ against time shows a long linear coking region (14,15).

Figure 1 (open circles) shows the isothermal plastometric curves at 410-2°C obtained with the three coals described in Table 1. Both the maximum fluidities

and the periods of fluidity are seen to vary substantially among these coals.

The linearity of the coking slopes has been interpreted to imply a sequence of first-order reactions (14-17):



where C, M and S represent the meltable portion of the original coal, the fraction which is molten (metaplast), and the fraction which is resolidified (coked). This scheme gives rise to the rate law:

$$d[M]/dt = k_i[C] - k_c[M] \quad (3)$$

There are two problems with this scheme. First, it does not generate model curves which resemble observed curves. Specifically, it predicts the rate of increase of fluidity during the softening process to decelerate progressively, while in fact this increase is exponential with time over most of the melting period. Second, this scheme specifically assumes that Gieseler fluidity is a linear measure of the molten fraction or metaplast; but that assumption is mistaken, as we will show.

For the purpose of more closely modeling the actual isothermal curves we propose a second melting process, such that the rate of increase of fluidity is dependent upon the concentrations of both metaplast and unmelted fraction:



The rate law now acquires a third term:

$$dF/dt = k_i[C] + k_m[C][M] - k_c[M] \quad (5)$$

(We use F for fluidity, rather than [M] for metaplast, on the left-hand side). The virtue of Equation 5 is that, for most isothermal runs, it can provide a fairly good fit to the experimental data, and therefore can define the experimental curves in terms of numerical constants associated with the melting and coking processes. The solid points in Figure 1 are values generated by the Equation 5 model, using the values given in Table 2. It is a characteristic of this model that the experimental points in the vicinity of maximum fluidity tend to be higher than those generated by the model. This may reflect formation of gas bubbles, which lead to anomalously high experimental readings.

In applying this model, the least-squares melting and coking slopes are calculated from the experimental data; we use all data between 1 ddpm and one fourth the maximum observed fluidity. The extrapolated maximum fluidity (emf) and the time of maximum fluidity are taken from the intersection of these slopes.

From these determinations, approximate values for the model constants can be estimated empirically from the cubic equations:

$$\frac{m(\text{melt})}{k(\text{melt})} = -0.3179 + .71507 \times R - .15991 \times R^2 + .012348 \times R^3 \quad (6)$$

$$\frac{m(\text{coke})}{k(\text{coke})} = -0.6934 + 1.1504 \times R - .26779 \times R^2 + .020826 \times R^3 \quad (7)$$

$$\ln[k(\text{init})] = -16.127 + 2.8478 \times P - .25098 \times P^2 + .005726 \times P^3 \quad (8)$$

where $m(\text{melt})$ and $m(\text{coke})$ denote the melting and coking slopes, $R = m(\text{melt})/m(\text{coke})$, and $P = [(m(\text{melt}) + m(\text{coke})) \times t(\text{max flu})]$. These equations give fairly good fits when $k(\text{melt})$ is in the range 0.5 to 4 min.^{-1} and $k(\text{coke})$ is in the range 0.2 to 1.5 min.^{-1} . To relate the conceptual molten fraction $[M]$ to the observed ddp, the emf from a model curve is compared with that from the experimental curve. For example, Ohio #9 seam coal at 411° has an experimental emf of 81.3 ddp, and a calculated emf (using the k values of Table 2) of $[M] = 0.683$. When each datum in the model curve is multiplied by the factor 81.3/0.683, the model fluidities are converted to units of ddp. [Detailed procedures and programs for these estimates are available from the authors.]

Effect of Temperature

Isothermal curves were obtained upon Kentucky #11 seam coal at five additional temperatures, in the range 400-460°C. Values of the model constants are given in Table 3. An Arrhenius plot of the model constants $k(\text{melt})$ and $k(\text{coke})$ is shown in Figure 2. For this coal the value of the apparent E_a for $k(\text{melt})$ (best 5 of 6 data) is 173 ± 13 kJ; that for $k(\text{coke})$ (also best 5 of 6) is 228 ± 6 kJ. Viscosities commonly show an analogous "activation energy of viscosity" (18,19). The apparent E_a of maximum fluidity is approximately 600 kJ, high when compared with those for asphalt (120-150 kJ) and glass (390-400 kJ) (20,21).

When the temperature dependencies for the parameters of this model have been estimated from the data of Table 3, isothermal curves may be calculated for any interpolated temperature, or for any extrapolated temperature close to the range of experimental data. Figure 3 shows a family of fluidity envelopes for the Kentucky #11 seam coal, based upon data calculated for the range 392-468°C. Each curve is an "isofluidity" envelope, open at the top. Figure 3 is read along horizontal (isothermal) lines. At 430° this coal exhibits a plastic period (fluidity greater than 1 ddp) from 2 to 30 min., and has a fluidity exceeding 100 ddp from 5 to 20 min. This projection, which will afford markedly different envelopes for different coals, may find use in applications in which the plastic properties of bituminous coals are important.

Discussion

The organic structures of coals are numerous and varied. Bonds which thermally cleave at useful rates at 390-400°C (dissociation energies of 210-230 kJ) are not the same as those cleaved at 460° (240-260 kJ). A major reason for isothermal measurements is to control this variable.

Gieseler fluidity can be related to viscosity units by calibrating with standard fluids. Measurements with the plastometer used in this study and with

appropriate standards (22) in the range 500 - 10,000 poise yield a linear calibration:

$$\ln(\text{poise}) = 16.2789 - 0.96787 \ln(\text{ddpm}) \quad (9)$$

with a correlation coefficient of .9997. Actual coal melts are heterogeneous (7,16), pseudoplastic (23), and viscoelastic in their later coking stages (24). It is nevertheless useful to interpret Gieseler fluidities as estimates of true viscosities.

Nicodemo and Nicolais (25) and Fedors (26) have shown the viscosity of Newtonian suspensions of solids to conform to the expression:

$$\eta/\eta_0 = \exp(a\phi) \quad (10)$$

where η , η_0 , and ϕ are the suspension viscosity, solvent viscosity, and solids fraction. Data obtained by Lee (27) show the logarithm of the maximum fluidity of coal blends to vary linearly with composition. These observations are telling us the same thing: that the logarithm of fluidity, not fluidity itself, is a direct measure of the molten fraction. If we assume that a fluidity of 1 ddpm corresponds to the maximum solid fraction ϕ_{\max} , we can project the relationship:

$$\ln(F) = \ln(F^0) \cdot \left[1 - \frac{\phi}{\phi_{\max}} \right] \quad (11)$$

To use Equation 11 we need estimates of ϕ_{\max} and of the fluidity of pure metaplast, F^0 . The maximum solid fraction in a random dispersion of monodisperse spheres is 0.63 (28,29). This fraction is higher for polydisperse spheres (30) and for some size distributions may be as high as 0.9 (31). For coal melts we will assume a value of ϕ_{\max} of 0.80. If the extrapolated maximum fluidity of the Pittsburgh #8 seam sample at 412° (1.0 x 10⁶ ddpm) is taken as a rough estimate of F^0 , we can estimate solid fractions in other coals from fluidities at this temperature. Fluidities of 10, 100, 1,000 and 10,000 ddpm indicate solid fractions of approximately .67, .53, .40 and .27. The minimum values of ϕ for Ohio #9 and Kentucky #11 samples in Table 2 are approximately 0.55 and 0.41.

The linearity of log(F) with ϕ has mechanistic implications as well. The left-hand of Equation 3 is more accurately expressed as $d \ln[M]/dt$. The curves of Figure 1 show linear increases of metaplast with time in the early stages, and linear decreases of metaplast with time (zeroth order kinetics) in the later coking stages.

Extrusion pumping of coals in the plastic state entails substantially isothermal operations for residence times of a few minutes in the screw (1-3). Several coals, including those of the present study, have been extruded with no difficulty in JPL's 1.5-in. coal pump. Two coals which showed very little plasticity (less than 2 ddpm) were not extrudable (3). The isothermal plastometry profiles may prove to be a useful tool in predicting behavior in coal pumps. Recent evidence of the substantial effect of pressure upon observed plasticity (10) indicates that this variable should be considered in future work.

Acknowledgments

Christopher England (Jet Propulsion Laboratory) first suggested this study. This work was performed for the coal pump development project, Jet Propulsion Laboratory, California Institute of Technology, under Contract no. 954920. The coal pump project is supported by the Department of Energy through an agreement with the National Aeronautics and Space Administration.

References

- (1) P. R. Ryason and C. England, *Fuel*, 57, 241 (1978).
- (2) V. Kevorkian and F. J. Cumings, U. S. Patent 4,106,997 (1978).
- (3) W. J. Schatz, E. G. Carpenter, C. S. Daksla, C. England, S. P. Feinstein, R. O. Kushida, D. W. Lewis, W. G. Lloyd and V. D. Sankur, "Coal Pump Development - Phase I Feasibility Report", JPL 5030-235, Jet Propulsion Laboratory, California Institute of Technology, Pasadena, September 1978.
- (4) H. E. Mehesch, *Erdoel, Kohle, Erdgas, Petrochem.*, 31, 323 (1978).
- (5) Y. Sato, K. Imuta and T. Yamakawa, *Fuel*, 58, 322 (1979).
- (6) B. Gates, *Chemtech*, 1979, 97.
- (7) D. W. Van Krevelen, "Coal", Elsevier Publishing Co., Amsterdam, 1961, pp 263ff.
- (8) R. Loison, A. Peytavy, A. F. Boyer and R. Grillot, in H. H. Lowry, ed., "Chemistry of Coal Utilization", supplementary vol., John Wiley & Sons, New York, 1963, pp 177ff.
- (9) S. V. Sobolev and E. M. Taitis, *Khim Pererab. Topl.*, 30, 68 (1974).
- (10) M. Kaiho and Y. Toda, *Fuel*, 58, 397 (1979).
- (11) K. Gieseler, *Gluckauf*, 70, 178 (1934).
- (12) ASTM Method D 2639-74, Amer. Soc. for Testing and Materials, Philadelphia, PA, 1974.
- (13) R. Loison, et al., ref. (8), pp 152-69.
- (14) D. Fitzgerald, *Trans. Faraday Soc.*, 52, 362 (1956).
- (15) D. Fitzgerald, *Fuel*, 35, 178 (1956).
- (16) D. W. Van Krevelen, F. J. Huntjens and H. N. M. Dormans, *ibid.*, 462 (1956).
- (17) H. A. G. Chermin and D. W. Van Krevelen, *ibid.*, 36, 85 (1957).

- (18) E. N. da C. Andrade, *Nature*, 125, 309 (1930); E. N. da C. Andrade, "Viscosity and Plasticity", Chemical Publishing Co., Inc., New York, NY, 1951.
- (19) S. Glasstone, K. J. Laidler and H. Eyring, "The Theory of Rate Processes", McGraw-Hill Book Co., Inc., New York, 1941, pp 480ff.
- (20) P. B. Macedo and A. Napolitano, *J. Chem. Phys.*, 49, 1887 (1968).
- (21) H. E. Schwyer and R. W. Lodge, *Ind. Eng. Chem., Prod. Res. Develop.*, 13, 202 (1974).
- (22) Cannon Instrument Co., State College, PA 16801.
- (23) P. L. Waters, *Fuel*, 41, 3 (1962).
- (24) D. Fitzgerald, *ibid.*, 36, 389 (1957).
- (25) L. Nicodemo and L. Nicolais, *Polymer*, 15, 589 (1974).
- (26) R. F. Fedors, *ibid.*, 16, 305 (1975).
- (27) H. C. Lee (Kaiser Steel Corp.), private communication.
- (28) G. D. Scott, *Nature*, 188, 908 (1960).
- (29) R. F. Fedors, *J. Colloid Interface Sci.*, 46, 545 (1974).
- (30) R. F. Fedors, *Polymer*, 20, 225 (1979).
- (31) S. Feinstein (Jet Propulsion Laboratory), private communication.

Table 1
Properties of Three Bituminous Coals

Seam source	Ohio #9 Noble Co.	Kentucky #11 Webster Co.	Pittsburgh #8 (from METC)
Proximate: ¹			
moisture	2.15%	1.97%	0.79%
ash	18.87	8.34	8.65
vol. matter	39.40	41.19	40.85
fixed carbon	39.58	48.50	49.71
Ultimate: ²			
carbon	79.41	82.21	84.83
hydrogen	5.30	5.43	5.49
nitrogen	1.13	1.36	1.44
sulfur	5.38	3.52	2.92
oxygen ³	8.78	7.48	5.33
Heating value ²	14,010 Btu/lb	14,770 Btu/lb	15,290 Btu/lb
Free swelling index	3	7	7½
Petrographic analysis ¹			
exinoids	2.1%	5.1%	4.0%
vitrinoids	70.1	76.3	75.3
other reactives	1.9	1.2	0.9
inert macerals	12.9	11.0	13.7
ASTM Gieseler plastometry			
softening T	398°C	392°C	372°C
coking T	462°	474°	485°
max flu T	435°	435°	(414-459°)
max fluidity	114 ddpm	6240 ddpm	>>25000 ddpm

¹ As received.

² Moisture- and ash-free basis.

³ By difference.

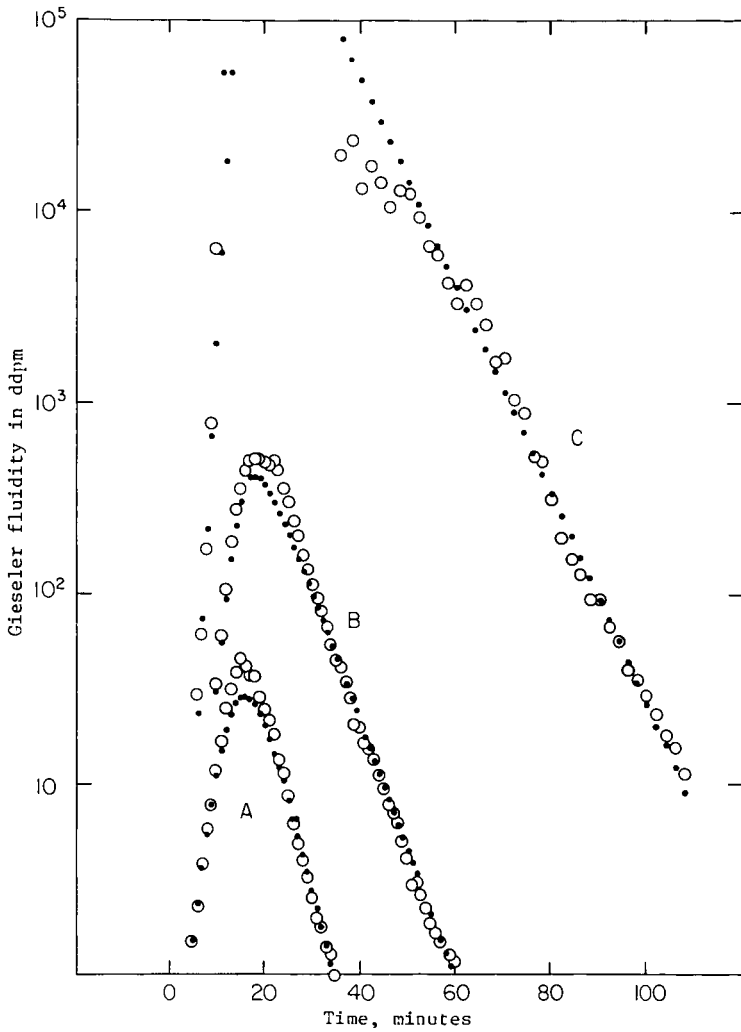


Figure 1. Isothermal plastometric curves of three bituminous coals. A - Ohio #9 seam (Noble Co.) at 411°C. B - Kentucky #11 seam (Webster Co.) at 410°C. C - Pittsburgh #3 seam (from IETC) at 412°C. Open circles are experimental data; solid points are calculated by the three-parameter model (values given in Table 2).

Table 2

Characteristics of Three Isothermal Plastic Curves at 410-412°C

	Ohio #9 <u>411°C</u>	Kentucky #11 <u>410°C</u>	Pittsburgh #8 <u>412°C</u>
Melting slope	0.425	0.621	1.084
Coking slope	-0.216	-0.151	-0.125
Maximum fluidity, ddpm ¹	81	896	1.0 x 10 ⁶
Time of maximum fluidity ¹	14.3 ₄	15.4 ₂	15.7 ₅
<u>Calculated values:²</u>			
k(init)	6.0 x 10 ⁻⁴	4.3 x 10 ⁻⁵	3.4 x 10 ⁻⁸
k(melt)	0.77	0.79	1.24
k(coke)	0.35	0.16	0.125

¹ By extrapolation of melting and coking slopes.

² Using the three-parameter model described in text. Dimensions of k(init) and k(coke) are min⁻¹; k(melt) is min⁻¹ mass fraction⁻¹.

Table 3

Effect of Temperature upon the Isothermal Plastic Curves of Kentucky#11 Seam Coal (400-460°C)

<u>Temperature, °C</u>	<u>400.</u>	<u>410.</u>	<u>425.5</u>	<u>440.</u>	<u>449.9</u>	<u>460.</u>
Melting slope	0.172	0.621	1.35	1.60	2.57	5. ₃
Coking slope	-0.069	-0.151	-0.325	-0.67 ₉	-1.11	-1.5 ₆
Maximum fluidity, ddpm ¹	44	896	2.58E4	3.34E4	8.89E4	2.21E6
Time of maximum fluidity ¹ , min.	25.8 ₂	15.4 ₂	11.1 ₄	8.1 ₂	6.3 ₀	4.1 ₃
<u>Calculated values:²</u>						
k(init)	1.2E-3	4.3E-5	1.9E-6	3.0E-6	6.5E-7	4.3E-7
k(melt)	0.26	0.79	1.74	2.49	4.05	7. ₁
k(coke)	0.083	0.158	0.339	0.84 ₈	1.40	1.6 ₆

¹ By extrapolation of melting and coking slopes.

² See Table 2, footnote 2.

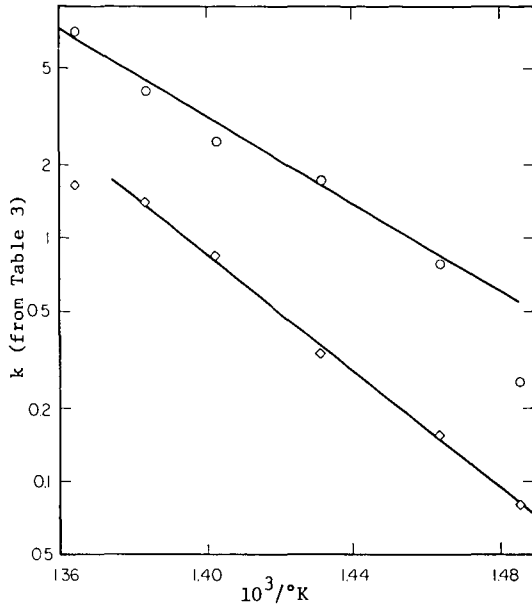


Figure 2. Arrhenius dependency of the model constants $k(\text{melt})$ (circles) and $k(\text{coke})$ (diamonds) for Kentucky #11 seam coal

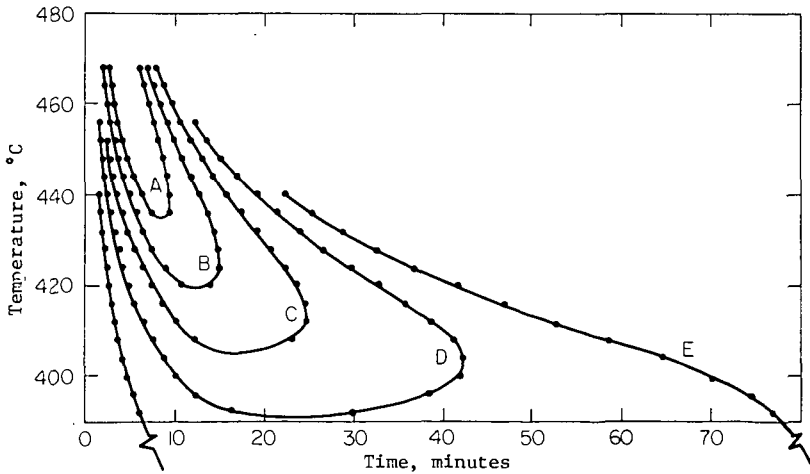


Figure 3. Isothermal fluidity envelopes for Kentucky #11 seam coal
 A - 10^4 ddpm. B - 10^3 ddpm. C - 10^2 ddpm. D - 10 ddpm. E - 1 ddpm

PITCH RESIDUES FROM UPGRADING OF BITUMEN AND HEAVY OILS AS ADDITIVES IN COKE MAKING:
INFLUENCE OF PITCH PROPERTIES

K. Belinko, L.A. Ciavaglia, B.N. Nandi and J.M. Denis,

Energy Research Laboratories
Canada Centre for Mineral and Energy Technology,
Department of Energy, Mines and Resources,
c/o 555 Booth Street, Ottawa, Ontario K1A 0G1

INTRODUCTION

Impending shortages of good coking coals throughout the world have prompted a series of investigations at CANMET (Canada Centre for Mineral and Energy Technology) into the utilization of western Canadian marginal coking coals in the production of metallurgical grade coke. One possible way to do this is to add residual pitch from thermal hydrocracking of bitumen and heavy oils to such coals (1). This pitch has been found to be an excellent additive for up-grading low fluid, low volatile, inert-maceral rich coals. The pitch acts as a fluidity-enhancing agent, and by interacting with the vitrinite of the coal, augments the supply of reactive carbon necessary for bonding together of inert macerals.

The purpose of this publication is to add further insight into the role of pitch in carbonization of coal/pitch blends. Pitches derived from thermal hydrocracking of bitumen at different degrees of severities were utilized for this purpose. This provided a means of assessing the properties of the pitches in the carbonization process without changing the basic chemical nature of the parent material.

EXPERIMENTAL

The properties of the pitches derived from thermal hydrocracking of Athabasca bitumen under various operating conditions are given in Table 1. These four pitches were produced under different degrees of severity during the process A being characteristic of pitch obtained under relatively mild conditions and D, of pitch obtained at high severities. A relation was found to exist between the degree of severity during hydrocracking and the various properties listed in Table 1 (e.g. CCR, aromaticity, softening point).

TABLE 1
Physical and Chemical Properties of Pitches

		Pitch			
		A	B	C	D
Volatile matter	%	73.1	64.8	53.5	44.6
Ash	%	1.8	2.3	3.2	5.8
Softening temperature	°C	50	95	105	135
Conradson carbon residue	%	34.7	42.2	50.7	64.6
Specific gravity		1.10	1.13	1.16	1.24
Benzene-insolubles*		2.6	4.2	11.6	20.6
Asphaltenes	%	37.2	44.6	48.1	55.2
H/C		1.32	1.19	1.09	0.94
Sulphur	%	5.58	5.63	6.33	4.85
Aromaticity**	%	38.2	49.4	56.3	69.8

* Ash-free basis, ** ¹³C NMR analysis

The coal used was a western Canadian, low fluid, high rank bituminous coal having a relatively high concentration of inert macerals. Proximate, ultimate and petrographic analyses of this coal are given in Table 2.

TABLE 2

Properties of the Coal

<u>Proximate Analysis</u>		(dry basis)
Ash	%	9.8
Volatile matter	%	21.2
Fixed Carbon	%	69.0
<u>Ultimate Analysis</u>		
Carbon	%	78.9
Hydrogen	%	4.3
Sulphur	%	0.8
Nitrogen	%	1.3
Oxygen (by diff.)	%	4.9
Ash	%	9.8
<u>Petrographic Analysis</u>		
Vitrinite	vol. %	51.8
Semi-fusinite	vol. %	34.2
Fusinite	vol. %	11.2
Micrinite	vol. %	2.6
Exinite	vol. %	0.2
Mean reflectance in oil, R_o		1.17

Coal/pitch blends with varying pitch concentrations were prepared and their fluidities determined by means of a Gieseler plastometer. The fluidities of the various blends are reported in Table 3. A value representing the concentration of pitch which can potentially interact with the coal during carbonization, C_p , is also given in Table 3. C_p was calculated on the following basis:

$$C_p = \left(\frac{\text{Concentration of pitch}}{\text{in the coal-pitch blend}} \right) \times \left(\frac{\text{wt. \% CCR in}}{\text{the pitch}} \right) \quad 1)$$

where CCR is the Conradson carbon residue (2) and approximates the contribution of carbonaceous material made by the pitch to the blend during carbonization.

The various coal/pitch blends were carbonized using a canister coking technique developed at CANMET (3). The blends were packed to a bulk density of 801 kg/m³ into perforated tin plate canisters 29.3 cm long and 7.6 cm in diameter. Twenty cans, each containing a different blend were side-charged into CANMET's 250-kg moveable wall coke oven.

The relative strengths of the cokes produced from the canister test were determined by a small sample tumbler test developed by Bituminous Coal Research (BCR) (4) and are reported in Table 3. These strength indices are a measure of size reduction in tumbled coke particles and therefore a large index corresponds to a weak coke.

Optical examinations of the various cokes were made with a Leitz reflected light microscope using an oil immersion lens. The micrographs were taken at 600X magnification using partially crossed nicols.

TABLE 3

Carbonization Data for Coal Pitch Blends

		Concentration of Pitch in Blend wt %					
		0	5	8	10	14	16
<u>Pitch A</u>							
Contribution of carbon from pitch, C_p	%	Nil	1.5	2.4	3.1	4.1	4.7
Fluidity of blend	dd/min	Nil	1.9	6.1	6.4	36	28
BCR* strength index		N/A**	49.0	36.4	38.2	37.4	38.1
<u>Pitch B</u>							
Contribution of carbon from pitch, C_p	%	Nil	2.1	3.3	4.1	5.7	6.6
Fluidity of blend	dd/min	Nil	1.5	5.7	7.1	120	530
BCR* strength index		N/A**	53.8	35.3	34.5	37.3	35.8
<u>Pitch C</u>							
Contribution of carbon from pitch, C_p	%	Nil	2.6	4.1	5.0	7.1	8.2
Fluidity of blend	dd/min	Nil	1.1	5.0	13.0	370	400
BCR* strength index		N/A**	52.7	36.7	36.9	39.0	40.3
<u>Pitch D</u>							
Contribution of carbon from pitch, C_p	%	Nil	3.3	5.2	6.5	9.1	10.4
Fluidity of blend	dd/min	Nil	1.0	4.0	6.8	260	1150
BCR* strength index		N/A**	57.8	43.1	35.1	41.3	45.1

* Bituminous Coal Research Inc., Pittsburgh, P.A.

** A non-agglomerated char was produced

RESULTS AND DISCUSSION

A photograph showing two representative cokes from the canister test is shown in Fig. 1. The coke shown at the top was produced from coal with no pitch additive and was poorly agglomerated. The coke at the bottom was agglomerated and hard and was typical of cokes produced from coal/pitch blends. The former coke could not be evaluated by the BCR tumbler test because of its non-agglomerated character. The strength indices of the cokes produced from coal/pitch blends are given in Table 3.

The strengths of the cokes produced from blends containing pitch A and pitch B were not found to vary significantly for pitch concentrations above 5%. On the other hand, additions of more than 10% pitch in coal/pitch C and coal/pitch D blends were found to be detrimental to coke strength. The influence of pitch concentration on coke strength was therefore more pronounced for pitch obtained from high severity thermal hydrocracking runs. It would be difficult to predict an exact optimum pitch concentration based solely on the results reported in Table 4 for coal/pitch D blends.

Coal/pitch blends having C_p values in excess of about 7% produced cokes of progressively weaker strengths. The Conradson carbon residue (CCR) contents of pitches A and B were sufficiently low to permit additions of up to 16% pitch to the coal without C_p values of the blend exceeding 7%. This would account for the lack of a minimum in BCR strength index for cokes produced from blends containing pitch

A and pitch B within the concentration range investigated.

Fluidity data for the various blends are summarized in Table 3. A marked increase in the fluidity of the blends was observed for pitch concentrations greater than 10%. The increase in fluidity was generally found to be more pronounced for pitch obtained from high severity thermal hydrocracking runs. This perhaps suggests that there is a better interaction between pitch and the vitrinite of the coal in cases where the pitch was treated under more severe conditions during thermal hydrocracking. It is evident from Table 1 that pitch aromaticity is directly related to the degree of severity during thermal hydrocracking. The interaction between the pitch and the vitrinite may therefore be related to the aromaticity of the pitch:

Based on some of the arguments presented above, the following relationship was found to be consistent with the data in Table 3:

$$\text{BCR strength index} = 26.47 + 1.75 C_p \exp \frac{0.97}{A^{3/2} F}; \quad 1.5 \leq C_p \leq 10.4 \quad 2)$$

Where C_p is defined according to Equation 1), A is the aromaticity of pitch determined by ^{13}C NMR and F is the fluidity of the coal/pitch blend. Equation 2) is plotted in Fig. 2 and was found to have a coefficient of correlation of 0.89.

According to Equation 2), the BCR strength index of a coke produced from a coal/pitch blend is not only dependent on the value of C_p , but also on the fluidity of the blend. Low values of C_p in the blend appear to be desirable in achieving good coke strength provided the fluidity of the blend is sufficiently high to make the exponential term in the equation approach unity. Once the exponential term has approached unity, additional increases in C_p may only contribute to a deterioration in coke strength. The inter-relationship between C_p and fluidity borne out by Equation 2) emphasizes the need for controlled fluidity in ensuring a uniform and efficient distribution of the binding material throughout the coal during carbonization. This is demonstrated, for instance, in the case of 5% addition of pitch D to the coal, Table 3. Although the C_p value was relatively high, low fluidity prevented proper distribution of the binding material in the coal during carbonization; consequently, a weak coke was produced.

In order to confirm this dependence on fluidity, a series of microscopic examinations was made on the cokes produced from the canister test. The coke produced from the coal with no pitch additive was found to be poorly bonded. Inert macerals were segregated within the coke structure with little or no binding material surrounding them (Fig. 3). Coal/pitch blends produced cokes of varying qualities depending on values of C_p and fluidity. Three specific cases were chosen to demonstrate this dependence: (i) coal + 5% pitch D, (ii) coal + 10% pitch D and (iii) coal + 16% pitch D.

In case (i), coal + 5% pitch D, some degree of bonding was observed between inert macerals, but the bonding was generally discontinuous and sporadic. This is exemplified for instance in Fig. 4. It is noteworthy that for blends having similar C_p values but higher fluidities, e.g. coal + 10% pitch A, bonding was found to be considerably more uniform than that shown in Fig. 4. The difference in bonding can therefore be attributed to the fluidity of the respective blends.

The coke produced from case (ii), coal + 10% pitch D, was found to exhibit excellent bonding. The binding material was uniformly and continuously distributed throughout the coke and the inert macerals were embedded within the coke matrix, Fig. 5. These observations were consistent with the relatively good BCR strength index obtained for this coke.

The deterioration in coke strength observed for case (iii), coal + 16% pitch D, was attributed to the development of micro-cracks within the coke structure, Fig. 6. The mechanism by which these cracks form is not well understood, but could perhaps result from an excess of binding material between the inert macerals of the coal, thereby weakening the overall structure.

From the three cases considered, it is evident that coke strength can be correlated to the micro-structure of the cokes. The coke quality appears to be a complex function of the amount of pitch added, the physico-chemical properties of the pitch and the fluidity of the coal/pitch blend.

It should be emphasized that the arguments presented in this paper apply specifically to inert-maceral rich, low fluid, high rank coals. Equation 2) has so far only been tested for this particular type of coal. It is possible that other coals may yield results that do not conform exactly to this equation. For instance, the coal used in this work had no inherent fluidity, and consequently a term for the fluidity of the coal itself does not appear in the equation. However Equation 2) does demonstrate the strong inter-relationship between the contribution of binding material made by the pitch and the fluidity of the blend.

CONCLUSIONS

High rank coals from western Canada which are rich in inert macerals, generally require a pitch additive to produce metallurgical grade coke. Pitch concentration in the coal/pitch blend dictates both the amount of binding material made available to the coal and the fluidity of the blend. Both these parameters depend on the physico-chemical properties of the pitch and on the extent of interaction between the pitch and the coal.

In order to produce good quality coke from a coal/pitch blend, the blend must possess sufficient fluidity to ensure a uniform and continuous distribution of binding material throughout the coal. Inert macerals of the coal must be adequately wetted and bonded together. Optimum coke strength is achieved when pitch is added in sufficient amount to generate a controlled fluidity with enough binding material to agglomerate the coke. If added in large amounts, the pitch can have deleterious effects on the resultant coke. The reason why too much pitch weakens the structure is not well understood, but appears to be related to the development of microcracks within the coke matrix.

ACKNOWLEDGEMENTS

The authors wish to thank B.H. Moffatt and S.E. Nixon for their technical assistance during the course of this work. Thanks are also due to W. Gardiner and his staff for their assistance in carrying out carbonization tests.

REFERENCES

1. Belinko, K., Ciavaglia, L.A. and Nandi, B.N. "Energy for industry", Ed. P.W. O'Callaghan; Pergamon Press (London); pp. 79-89 (1978).
2. American Society for Testing and Materials; Part 23, D-189 (1975).
3. Montgomery, D.S. and Nandi, B.N. Fuels Research Centre Divisional Report 73/11; Department of Energy, Mines and Resources, Ottawa, Canada (1973).
4. Moses, R.G. Bituminous Coal Research Inc., Monroeville, Pennsylvania; Personal Communication.

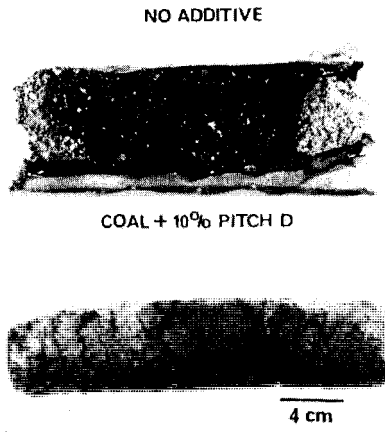


FIGURE 1: High Temperature Cokes Produced From Canister Tests

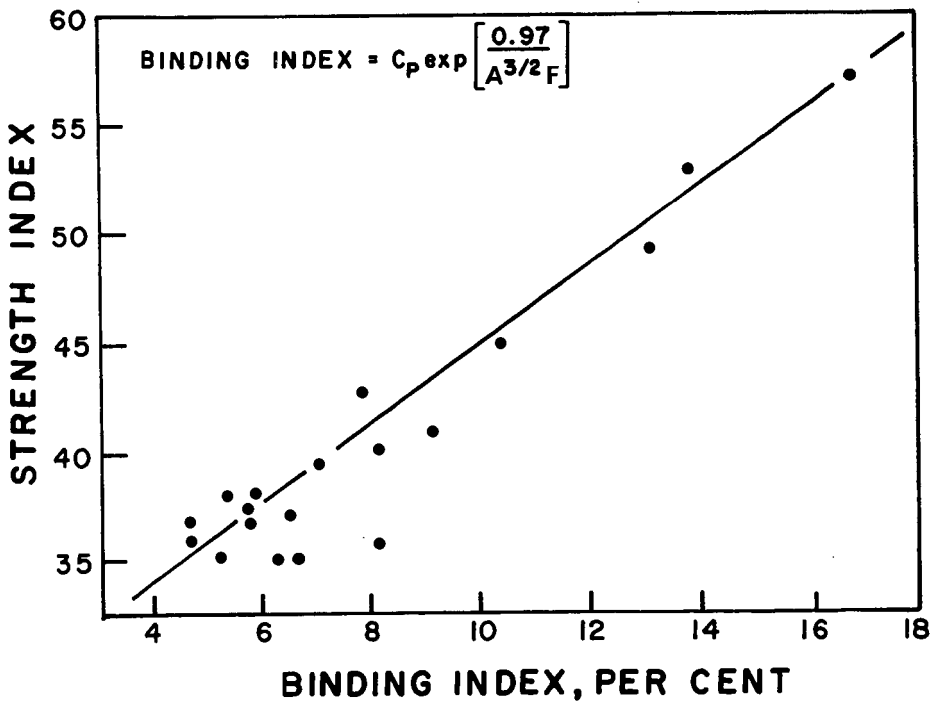


FIGURE 2: Relative Strength Indices for Various Coal/Pitch Blends

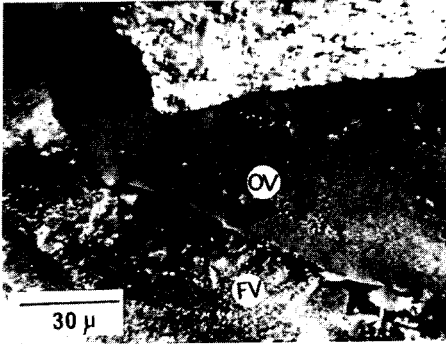


FIGURE 3: Optical Micrograph of Coke Produced from Coal With No Additive Showing Poor Bonding Between Fused Vitrinite (FV) and Oxidized Vitrinite (OV)

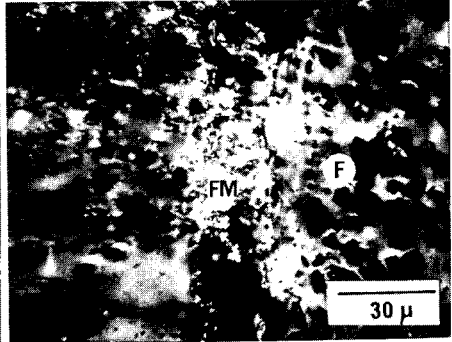


FIGURE 4: Optical Micrograph of Coke Produced from Coal + 5% Pitch D Showing Discontinuous Bonding of Fused Mass (FM) With Fusinitic Structure (F)

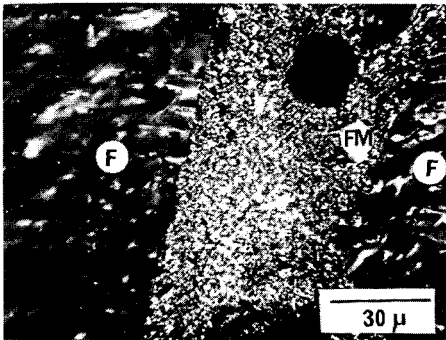


FIGURE 5: Optical Micrograph of Coke Produced from Coal + 10% Pitch D Showing Excellent Bonding of Fusinitic Structure (F) by Fused Mass (FM)

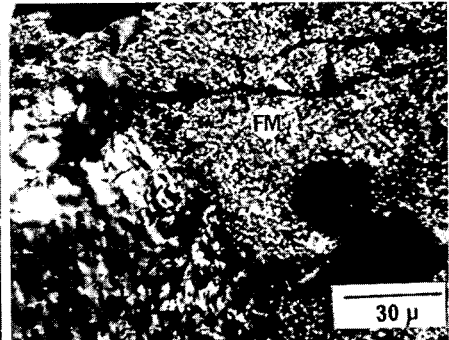


FIGURE 6: Optical Micrograph of Coke Produced From Coal + 16% Pitch D Showing Development of Microcracks Within Fused Mass (FM)

SYNTHETIC FUELS - PITFALLS AND PROMISE. Fred Schulman. Energy Systems Technology Corp., 927-15th St., N.W., Washington, D.C. 20005

Technical process improvements and policy restraints on OPEC's ability to increase oil prices at will are two essential components of a viable synthetic fuels industry. One without the other spells frustration and failure. The Arab oil embargo of 1973-74 and the subsequent five-fold increase in petroleum prices led to multibillion dollar programs to develop synthetic fuels. Expectations of a great new synthetic fuels industry were unfulfilled as prices and costs rose toward their equivalent-value-to-oil. Cost differentials in favor of imported oil continue to increase year by year despite many chemical and engineering innovations. For example, estimated costs of producing shale oil rose from \$7 per bbl in 1973 to \$30/bbl today. When the OPEC cartel raised oil prices another 54% last June, it became even more important to encourage domestic oil production and to develop energy alternatives. OPEC's new prices will force the base price of synthetic fuels to rise to \$46-50 by 1983. Rising feedstock costs imperil the domestic petrochemical industry and endanger chemical exports. This paper details some of these problems and suggests a number of energy policy actions aimed at establishment of the domestic fuels industry on a sound basis.

Development of a Simulated Catalyst Aging Technique

J.F. Kriz and M. Ternan

Energy Research Laboratories
Canada Centre for Mineral and Energy Technology
Department of Energy, Mines and Resources Canada
Ottawa, Canada
K1A 0G1

INTRODUCTION

Under hydrocracking conditions, heavy oils produce deposits that accumulate on the catalyst surface. By poisoning and by hindering accessibility of the active sites, these deposits cause fouling of the catalyst. Material that is so deposited is either originally present in the feed, such as heavy metals and minerals, or is formed during hydrocracking, such as coke. Not all deposits deactivate the surface at the same rate. It was established by repeated regeneration that rapid fouling under typical bitumen hydrocracking conditions is caused primarily by coke formation (1). To obtain a longer-lasting formulation, catalyst development should therefore focus on types that resist coke formation. Such an effort would involve a systematic approach to catalyst production based on information obtained in aging tests.

To determine the true aging characteristics, actual processing conditions must be maintained because they affect product formation and thereby also the process of deactivation. However, a serious disadvantage of aging tests under actual processing conditions is that they are slow and thus consume a great deal of time and manpower. The time involved becomes critical if aging characteristics are required for a large number of catalysts. It is the purpose of this report to describe a technique that simulates catalyst aging and provides preliminary information in a much shorter time.

EXPERIMENTAL EQUIPMENT AND MATERIALS

A bench-scale fixed-bed reaction system was used, in which the bitumen mixed with hydrogen flowed up through the catalyst bed continuously. Liquid and vapour were separated in receiver vessels. The equipment was previously described in detail (2) but the following modifications were made to accommodate the particular requirements of the present study (3):

1. Bitumen was stored in a heated hopper from which it could be fed through taps into two 1000-mL burettes in a heated plastic cabinet. With a light positioned behind the cabinet and the inside of the cabinet heated to about 75°C, it was possible to monitor the feed level in the burettes. A Milton Roy "Constametric" pump, model number TCP 43-43 TJ, was used to feed the bitumen through heated lines into the reactor. A pressure gauge was placed at the pump outlet to monitor pressure at the pump head.
2. To reduce the reactor volume, a stainless steel insert was machined to fit it, reducing the inside diameter to 1.27 cm from 2.54 cm but maintaining length at 30.5 cm.

The catalyst selected for comparative runs was a commercial type Harshaw 0603T with 3 wt % CoO and 12 wt % MoO₃ supported on alumina in the form of cylindrical 3.2-mm pellets. About 150 g of this catalyst represented a full reactor load but only about 30 g could be loaded with the insert. The rate of aging was evaluated using Athasbasca bitumen obtained from Great Canadian Oil Sands Limited at Fort McMurray, Alberta. Properties of the feedstock are listed in Table I.

TABLE I

Properties of Athasbasca Bitumen

Specific gravity	1.009 (15/15 ^o C)	Benzene insolubles	0.72 wt%
Sulphur	4.48 wt%	Carbon	86.36 wt%
Ash	0.59 wt%	Hydrogen	10.52 wt%
Conradson Carbon Residue	13.3 wt%	Nitrogen	0.45 wt%
Pentane insolubles	15.5 wt%	Pitch (525 ^o C+)	51.5 wt%

OPERATING CONDITIONS

The conditions that affect catalyst deactivation in a continuous flow system are temperature, hydrogen pressure, hydrogen flow rate and liquid space velocity. The hydrocracking process consists of a number of complex reaction steps, initially involving various constituents of bitumen. Catalytic processes on active surface sites participate in some of the reaction steps.

Although it would be difficult, because of complexity of the reactions, to predict accurately the impact of changes of any processing condition, some overall effects can be derived from the fundamentals of reaction kinetics. The rate of individual reaction steps varies with temperature and concentration of reactants. Cracking reactions are endothermic and accelerate with increasing temperature, whereas hydrogenation reactions accelerate with increasing hydrogen pressure. Coke formation depends on the rates of cracking and dehydrogenation, followed by polymerization. Therefore coke formation accelerates with increasing temperature and decreasing hydrogen pressure.

The conditions for "simulated aging" were chosen by performing a series of screening experiments to investigate the effect of variations in space velocity and temperature. The effect of hydrogen pressure on catalyst aging was studied previously using a different experimental system (4). In the present study, the hydrogen pressure was maintained constant at 13.9 MPa for all tests, which is within the practical range for hydrocracking. A satisfactory effect could not have been achieved by varying only space velocity; an increase in temperature was also necessary to reduce aging time sufficiently. After some preliminary experimentation, optimum deactivation conditions were found to prevail with a space velocity of 5 h⁻¹ and at a temperature of 495^oC.

The following series of tests under different operating conditions are documented in the present report:

Series 1

True or base deactivation rates were measured at 450^oC and at a liquid volumetric space velocity of 1 h⁻¹ based on the reactor volume packed with the catalyst pellets. The corresponding feed rate was 152 mL h⁻¹ as no insert was placed in the reactor. The hydrogen flow rate was maintained at 35.6 cm³ s⁻¹ at STP. This test is referred to as true aging and was run continuously for 56 hours, and then periodically in five - to eight-hour intervals, totalling about 200 hours in all. Analyses were performed on samples of the liquid product accumulated in two to five hours of operation.

Series 2

High space velocity tests were performed under the same conditions as for true aging - 13.9 MPa, 450°C, and without insert - except for a different arrangement of space velocities. Catalyst aging was carried out in two 12-hour periods during which space velocity was maintained at 5 h⁻¹, and the hydrogen flow at 95 cm³ s⁻¹ at STP. The level of activity, initially and after each 12-hour period was determined by changing the space velocity to 1 h⁻¹, the hydrogen flow to 35.6 cm³ s⁻¹ at STP for two hours and analyzing the liquid sample that accumulated during these two hours.

Series 3

Simulated deactivation rates were measured at high temperature and high space velocity. This test was run at 495°C and a liquid volumetric space velocity of 5 h⁻¹. The insert was placed in the reactor and the corresponding feed rate was 181 mL.h⁻¹. The hydrogen flow rate was maintained at about 70 cm³ s⁻¹ at STP. The series was referred to as simulated aging and was run continuously for 32 hours. The liquid product that accumulated during each hour of operation was withdrawn for analysis.

Series 4

A link between simulated aging and true aging was sought by additional tests in the following manner. The simulated aging conditions were applied for a period of time and were then changed to match the true aging conditions for approximately two hours during which two liquid samples were obtained. The run was then terminated, the reactor re-loaded with a fresh catalyst, and the test was repeated for a different time period under simulated aging conditions. Three different time periods - 2, 4 and 6 hours, respectively - under simulated aging conditions were examined. No insert was placed in the reactor and the simulated aging test was run at 495°C with the feed₃ rate of 760 mL.h⁻¹, space velocity of 5 h⁻¹, and the hydrogen flow rate at 70 cm³ s⁻¹ at STP.

Several processing conditions were applied differently in each series of tests. For instance, in Series 2, the space velocity was five times greater than in Series 1, whereas the gas flow rate was only about three times greater. In Series 1, the gas flow:feed ratio was lower than in Series 3, but higher than in the simulated aging in Series 4. In addition, the length:diameter ratio was increased in Series 3 by placing the insert in the reactor, thereby increasing the linear velocity:space velocity ratio through the catalyst bed. The use of the insert and varying flow regime resulted from experience with the experimental system and facilitated smooth operation. The changes made were necessary to prevent the reactor plugging and to maintain temperature profiles within the catalyst bed.

The impact of increasing temperature and space velocity is discussed in the next section of this report. Variations in hydrogen flow are not considered significant for the purpose of this investigation, because an excess of hydrogen was used in all experiments and because hydrogen flow seemed to exhibit only a small effect on product formation (5).

RESULTS AND DISCUSSION

True Aging

The deactivation pattern is shown in Fig.1 in terms of an increase in the specific gravity of the liquid product and an increase in its sulphur content. It can be predicted by extrapolation that further deactivation would

be recorded beyond 200 hours of operation. However, it can be seen that deactivation is more rapid in the early stages of the test than in the later stages. Since deactivation decelerates with time, the curves in Fig.3 may eventually level off, indicating a constant activity. The decelerating deactivation is in agreement with results of a previous study which also showed that this leveling-off is relatively more pronounced and takes place earlier with increasing hydrogen pressure (4). Whether a state of constant activity in fact exists is not known as the patterns in Fig.1 cannot be extrapolated with any precision. Furthermore, tests carried out continuously for longer than 200 hours of operation are necessary to determine deactivation patterns that are unaffected by start-up and shut-down procedures. These long-term tests are to be performed on a special testing system presently under construction.

High Space Velocity

The results of the high space velocity tests included analytical data on liquid product samples obtained for both high and base space velocities of this series. The results for the base space velocities served as a measure of deactivation after completing a period with high space velocity. The deactivation is indicated in the left-hand side of Fig.1,

A five-fold increase in feed rate had an insignificant effect on the rate of deactivation. One could rationalize this finding by assuming that lower conversions caused by reduced residence time would compensate for the greater feed rate in relation to coke formation. However, a more detailed analysis would reveal that the relationship between the space velocity and the rate of deactivation may be more complex, mainly because of the multicomponent structure of the reaction system. The concentration of reaction constituents depends on the rates of their formation and depletion. Thus the total yield of a component may not be a monotonic function of the residence time. If some coke precursors react faster than others, then their participation in total coke formation depends on the space velocity, a change in which may consequently be reflected in both the quantity and the quality of the coke deposits. In addition to chemical phenomena, mechanical regeneration may take place whereby particles of coke are detached from the surface by abrasion or by dissolution of the binding carbonaceous material. Should a similar process take place while bitumen is used, it would be enhanced by increasing the space velocity.

The high space velocity series indicated that the desired effect could not be established by changing the space velocity at base temperature. To accelerate aging substantially, the catalyst fouling was simulated at a higher reaction temperature. The term simulated aging is used to emphasize the severe consequences of the change in temperature.

Simulated Aging

The results of the simulated aging tests are shown in Fig.2. The activity dropped rapidly in the first period of the run, leveled off, and remained approximately constant beyond 15 hours of operation.

The performance under simulated aging reflected the effect of both high temperature and high space velocity. The performance seemed to be more sensitive to temperature, particularly with respect to the pitch fraction of the bitumen. The initial high pitch conversion observed could result from molecular weight reduction or growth. Molecular growth would result in precipitation of coke, most of which would be retained on the catalyst surface and reactor walls. The molecular weight reduction by cracking would generate compounds having a lower boiling point than those contained in the pitch. It

is apparent that, whereas both of the latter processes have taken place simultaneously, the growth rate was much smaller because the amount of coke formed accounts for only a fraction of the pitch converted. However, the high temperature of simulated aging compared with true aging shifted the balance towards coke formation as reflected in rapid catalyst deactivation.

Less extensive hydrogenation under simulated aging conditions, indicated by a low H:C ratio, was presumably due to a high aromatic carbon content. An analysis by Fourier Transform C-13 N.M.R. indicated that the unsaturated carbon represented about 30% of the total carbon in the initial product of simulated aging compared with about 20% of that of true aging. The following reasons may be considered to account for changes in the aromatic carbon content. More extensive splitting of side chains from aromatic rings caused by the higher temperature could have yielded more gas in the product. Apart from hydrocracking reactions, the higher temperature also shifts the naphthenes-aromatics equilibria towards formation of aromatics (6). In addition to the temperature effects, the high space velocity of simulated aging may have hindered the extent of hydrogenation because of the shorter contact time.

Link between Simulated and True Aging

Since the rate of deactivation under simulated aging conditions could not easily be related to the rate of deactivation under true aging conditions, a series of experiments was performed in which a link was sought between simulated and true aging. The purpose of these experiments was to measure the level of activity under true aging conditions after the catalyst had been subjected to simulated aging conditions for a certain period of time, and then to graphically estimate the time in which the catalyst would deteriorate enough to reach this level of activity while being subjected to true aging conditions.

The activity levels determined for three different time periods under simulated aging are marked on the right-hand side of the curves in Fig.1. By applying these results it was estimated that 2 hours of operation under simulated aging conditions would correspond to about 50-70 hours under true aging, and similarly, 4 hours to 100-150 hours, and 6 hours to 150-200 hours. Hence, assuming that simulated aging is approximately 30 times faster than true aging, one could extrapolate the pattern of true aging and speculate that it would level off in about 400 hours of operation.

Estimating the link between true and simulated aging in Fig.1 is an approximation only. However, it is apparent that by using simulated aging conditions, the deactivation was accelerated sufficiently to proceed substantially in a very short time. It is expected that by applying this method to a number of catalysts, preliminary information can be obtained by comparing their deactivation patterns such as the one shown in Fig.2. This information would then be available either in addition to the true aging data, or for use with catalysts on which true aging tests are not warranted.

ACKNOWLEDGEMENTS

The authors wish to express their sincere appreciation to R.W. Taylor for modifying the experimental system and to L. Galbraith for technical assistance.

REFERENCES

1. McColgan, E.C. and Parsons, B.I. "The hydrocracking of residual oils and tars. Part 6: Catalyst deactivation by coke and metals deposition"; Department of Energy, Mines and Resources, Mines Branch (since renamed Canada Centre for Mineral and Energy Technology (CANMET)) Research Report R273; 1974.
2. O'Grady, M.A. and Parsons, B.I. "The hydrogenation of Alberta bitumen over cobalt molybdate catalyst"; Department of Energy, Mines and Resources, Mines Branch, Research Report R194; 1967.
3. Kriz, J.F. and Ternan, M. "Development of a simulated catalyst aging technique"; Energy, Mines and Resources, Canada, CANMET Report 78-24; 1978.
4. Ranganathan, R., Logie, R.B. and Denis, J.M. "Catalytic hydrocracking of Athabasca bitumen in a fluidized bed reactor - effect of pressure on catalyst decay"; Energy, Mines and Resources, Canada, CANMET Report 77-40; 1976.
5. Merrill, W.H., Logie, R.B. and Denis, J.M. "The effect of hydrogen recycle rate on the non-catalytic hydrocracking of G.C.O.S. separated bitumen"; Department of Energy, Mines and Resources, Mines Branch; Divisional Report FRC 72/115-PPE; 1972.
6. Gully, A.J. and Ballard, W.P. "Hydrogenation of catalytic cracking charge stocks"; Adv Pet Chem Refin (New York, Interscience, Publishers) 7:240-282; 1963.

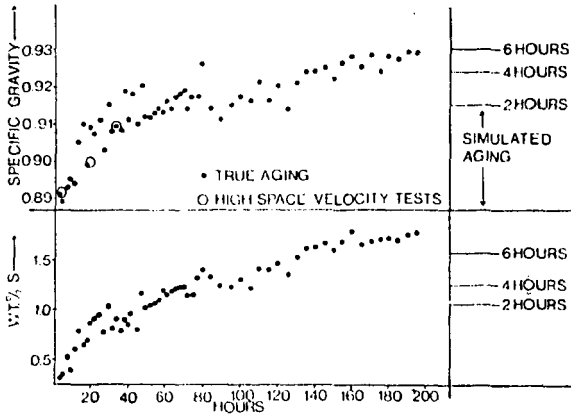


Fig.1 Specific gravity (15/15°C) and sulphur content (wt %) in the liquid product versus time on stream (h) during true aging. O indicates high space velocity experiments. Activity levels on right-hand side relate to different time periods under simulated aging.

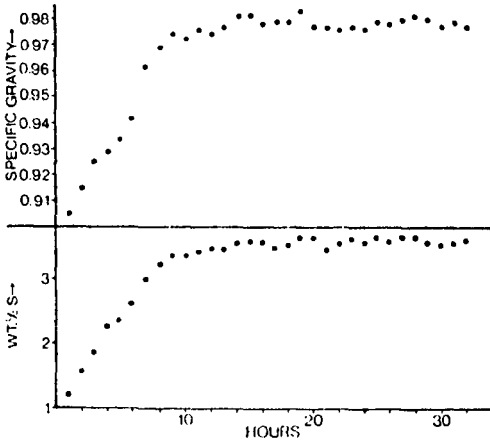


Fig.2 Specific gravity (15/15°C) and sulphur content (wt %) in the liquid product versus time on stream (h) during simulated aging.

REMOVAL OF ORGANIC SULFUR FROM COAL: THE USE OF LIQUID SULFUR DIOXIDE

Duane F. Burow and Boris M. Glavincevski

Department of Chemistry, University of Toledo, Toledo, Ohio 43606

ABSTRACT

The utility of liquid SO_2 for the removal of organic sulfur from several Eastern bituminous coals has been explored. Reactions were carried out in sealed fritted glass tubes at elevated temperatures; after subsequent washing, the coal was analyzed for sulfur content. Approximately 40% of the organic sulfur could be removed in these simple exploratory experiments. In addition, comminution of most of the coals occurred and a portion of the coal was extracted. The extract from selected coals was characterized by thin-layer chromatography, by nmr (^1H and ^{13}C) and infrared spectroscopy, and by field-ionization mass spectrometry. For comparison, extractions with phenol and *p*-cresol, under similar conditions, were also examined. The results of these preliminary investigations warrant further research to establish optimum conditions for the removal of sulfur compounds from coal by treatment with liquid SO_2 and to facilitate removal of residual SO_2 from the coal.

INTRODUCTION

Solvent extraction has been extensively used for compositional characterization of coals.^{1,2} Several existing coal refining processes³⁻⁵ use solvent treatment, along with pressurized hydrogen to facilitate some degree of desulfurization. Treatment with liquid SO_2 has been successfully used to remove organic sulfur compounds from petroleum on a commercial scale.⁶ The ability of liquid SO_2 to disintegrate various coals has been exploited to produce low-sulfur coal powders via release of pyrite.⁷ Utilization of liquid SO_2 treatment of coal for the removal of organic sulfur, however, has not been investigated. In this paper we report the results of a set of preliminary experiments in which the effectiveness of liquid SO_2 for removal of organic sulfur from bituminous coals PSOC 194, 267, 270, and 319 was investigated.

EXPERIMENTAL

Procedures for the manipulation and preparation of the sulfur dioxide (Matheson, anhydrous) have been described previously.^{8,9} Coal samples were obtained from the Coal Research Section, Pennsylvania State University. All other materials were of commercial origin and used as received.

Reactions were carried out in borosilicate glass tubes fitted with a medium-porosity fritted glass filter to provide two chambers of ca. 20 mL capacity each. The chambers were terminated with glass tubing of different sizes: one end permitted introduction of lump (ca. 1 cm) coal and the other end facilitated easy sealing under vacuum. For reactions at elevated temperatures, these tubes were placed in a Parr model 4641 autoclave reactor.

In a typical experiment, the reaction tube was charged with a coal sample (ca. 5 g) sealed on one end, and thoroughly evacuated. After distillation of sulfur dioxide (ca. 8 mL) into the tube at -78°C , the reaction tube was cooled to -196°C and sealed at the other end. Upon warming to room temperature, the tube, along with others, was placed in the autoclave and the autoclave was evacuated. The autoclave was then charged with ca. 100 mL of liquid SO_2 to provide backing pressure for the reaction tubes at elevated temperatures, closed, and heated at ca. $4^{\circ}\text{C}/\text{min}$ to the reaction temperature. After maintenance of the reaction temperature for 60 min, the autoclave was cooled, depressurized, and opened. Each reaction tube was then inverted in a cold bath at -78°C to separate the liquid SO_2 from the coal by filtration via the internal frit. The red to orange colored liquid SO_2 solution was frozen, the tube was opened, the coal was transferred to another container, and all volatile materials were allowed to evaporate over a two hour period. The viscous, oily extract remaining after evaporation of the liquid SO_2 was retained for subsequent analysis. The treated coal was washed for analytical purposes in a Buchner funnel with sequential aliquots of distilled water, acetone, water, 3.8 M nitric acid, water, and acetone until no yellow color was observed in each wash liquid. The coal was then dried at 110°C and analyzed for sulfur. In separate washing experiments with the raw coals, no yellow color was observed in the wash liquids; subsequent sulfur analyses of the coal indicated that only inorganic sulfur was removed from the raw coal by this wash procedure.

For comparison of the results of these coal/liquid SO_2 experiments, two other types of experiments were also run. Authentic samples of iron pyrite were treated with liquid SO_2 and liquid $\text{SO}_2/\text{H}_2\text{O}$ mixtures at 100°C using procedures analogous to those described above; no apparent reaction occurred. Samples (ca. 4 g) of PSOC 267 were treated with 10 mL of phenol and *p*-cresol in sealed tubes at 181° and 200°C , respectively. The coal was subsequently washed in a Buchner funnel with distilled water and acetone, dried at 110°C , and analyzed for sulfur.

All sulfur analyses, at least in triplicate, were accomplished with a Fisher model 470 sulfur analyser. Field-ionization mass spectra were obtained on a Varian model MAT CH5 spectrometer with sample temperatures from 120° – 280°C . The ^1H and ^{13}C nmr spectra were recorded on a JEOL FX90Q Fourier transform spectrometer fitted with a broadband probe and deuterium lock. Samples were in CDCl_3 solution with internal TMS reference. Infrared spectra of the extract (thin film on NaCl plates) were recorded on a Perkin Elmer model 621 spectrometer. Thin-layer chromatography of the extract was carried out with the nmr sample solutions using silica gel (Si-30) plates. Elution was accomplished with 10% acetone/hexane, 30% acetone/hexane, and absolute ethanol; either I_2 vapor or phosphomolybdic acid (5% w/v in ethanol) was used to develop the plates.

RESULTS AND DISCUSSION

Precombustion desulfurization of coal has been a topic of immense interest and importance^{10,11} since it offers an alternative to installation and operation of expensive post-combustion scrubbers for conventional combustion systems. Although a variety of processes are available for precombustion removal of inorganic sulfur compounds, practical procedures for removal of covalently bound organic sulfur are relatively uncommon. Thus, application of novel chemical approaches to the problem would appear to be appropriate. Early reports¹² of the ability of liquid SO₂ to disintegrate a variety of coals and to extract a portion of the coal along with our previous experience with this solvent suggested investigation of the utility of liquid SO₂ as a means of removing organic sulfur from coal. If successful, such a procedure would utilize a pollutant to remove the source of that pollutant.

Liquid sulfur dioxide is recognized as an excellent solvent for aromatic, heterocyclic, and alkyl sulfides⁸ which can be derived from coal.^{1,2,13} As a liquid, SO₂ is not easily oxidized or reduced and the adducts responsible for its solvent properties are both thermally and hydrolytically labile;⁸ thus any contamination of the coal by residual sulfur dioxide should be readily eliminated. Although other interactions and reactions will be considered in future reports, only reactions based on the mild Lewis acid characteristics of liquid SO₂ are of importance here. Thus, the reaction of significance is summarized by Eq.1:



Products from this reaction are usually highly colored and highly soluble in liquid SO₂.⁸ Physical disintegration of the coal by liquid SO₂, probably via similar donor-acceptor reactions with aromatic, amine, and oxygen containing functional groups, would serve to promote the reaction in Eq.1. It should be emphasized that frequently, the chemical properties of liquid SO₂ can be significantly altered by the presence of cosolvents;⁸ often, undesirable side reactions occur in such mixed media.

The characteristics of the bituminous coals utilized in these preliminary investigations are given in Table I; our sulfur analyses are given in parentheses. PSOC 267 and 270 were chosen since they contain significant amounts of organic sulfur but little pyritic sulfur which might confuse interpretation of preliminary results. Our analyses of PSOC 270 reveal that, although the lumps in our sample had the composition indicated in Table I, the fines in our sample had a sulfur content of ca. 6% with the additional sulfur being pyritic. All results reported here concern the lump coal of PSOC 270. For comparison, PSOC 194 which contains both pyritic and organic sulfur and PSOC 319 which contains only pyritic sulfur were also examined. Use of the fritted glass reaction tubes facilitated observation of reactions, isolation of the extracted material, and rapid examination of several coals and reaction conditions.

The results are summarized in Table II. At room temperature, liquid SO₂ readily wets each of the coals and begins to develop a yellow color upon contact. The yellow color becomes more intense upon standing and changes to intense orange or red-orange after heating. The color indicates the dissolution of donor-acceptor compounds formed between the solvent and coal constituents; the increasing intensity accompanies

an increasing concentration of these adducts. Disintegration of coal lumps was observed for PSOC 267, 270, and 319; the extent of disintegration increases progressively in the order listed. Although lumps of PSOC 194 were not disintegrated, close examination revealed appreciable swelling and expansion along fissures. It should be realized that the only mechanical agitation used during these experiments was a mild shaking of the tubes to initially mix the materials. At this stage, there does not appear to be an obvious pattern which links maceral content to degree of disintegration.

Inspection of Table II reveals that significant amounts of SO_2 are retained on the coal (Exp. 1). Effective removal of this residual SO_2 is essential. Mild heating (110°C) and washing with water or aqueous detergent solutions were less effective than the wash solution used in Exp. 2. When used alone, organic solvents are more effective than mineral acid or base (compare Exp. 2 and 3 with Exp. 4, 5, and 6). The utility of washing with the organic liquids for removal of the yellow SO_2 adducts increases in the order: hexane, benzene, CCl_4 , ethanol, and acetone. A sequence of washes using acetone, water, and HNO_3 (Exp. 7) effectively removes the residual SO_2 in most cases. Since the wash sequence was carried out during a filtration operation contact time with the HNO_3 was insufficient to appreciably modify the coal material itself; separate wash experiments using the acetone, water, HNO_3 sequence with the raw coal (PSOC 267 and 270) itself indicated that no appreciable mass change occurred and that no yellow materials were obtained under these wash conditions. Where pyrite is not present, the sulfur content of the coal after this wash sequence represents the organic sulfur remaining in the coal after the liquid SO_2 treatment. For PSOC 267 and 270, ca. 37% and 25%, respectively, of the organic sulfur can be removed by simple treatment of the lump coal with liquid SO_2 . Grinding the lump coal PSOC 270 (-60 mesh) improves the percentage organic sulfur removal to ca. 48%. Present results with coals containing pyrite are less easily interpreted since the wash sequence probably does not completely remove the pyrite. Furthermore, in separate experiments with authentic pyrite samples, it was demonstrated that neither liquid SO_2 nor liquid $\text{SO}_2/\text{H}_2\text{O}$ mixtures react with pyrite. For PSOC 319, where virtually all the sulfur is pyritic, the measured value of 1.6% sulfur after SO_2 treatment probably represents pyrite which is not removed in the wash sequence. For PSOC 194, the measured value of 2.1% sulfur after liquid SO_2 treatment more than likely represents both unreacted organic and pyritic sulfur. With PSOC 194, the failure of liquid SO_2 to disintegrate the coal probably limited extraction of the organic sulfur by the SO_2 .

Extraction of powdered PSOC 267 with phenol and *p*-cresol resulted in 52% and 66%, respectively, removal of organic sulfur compared to 37% by liquid SO_2 . The results of the extractions with phenol and *p*-cresol are similar to those reported elsewhere for other coals.

Although these results with liquid SO_2 are not as impressive as those with phenol and *p*-cresol, it has been demonstrated that organic sulfur can be removed by extraction with liquid SO_2 . It is also important to note that optimum conditions for liquid SO_2 extraction and for residual SO_2 removal have as yet to be established. Furthermore, these preliminary results when compared with other worker's results¹⁰ for a variety of organic solvents, are sufficiently encouraging to indicate that treatment with liquid SO_2 should be investigated further. Experiments to define conditions

more carefully and to investigate the use of appropriate reagents that will enhance the removal of sulfur compounds from coal by liquid SO₂ are underway.

The material obtained by evaporation of the SO₂ extraction liquid comprises 5-10% of the original coal. Most of this oily extract dissolves in chloroform, acetone, and concentrated HCl; this material is only partially soluble in benzene and is insoluble in hexane. Very finely divided particulate matter, observed to be in suspension in the chloroform and acetone solutions appears to resemble high molecular weight material obtained by Larsen and Choudhury¹³ during their investigation of the effectiveness of coal depolymerization reactions. Although it is likely that liquid SO₂ under these conditions merely extracts lower molecular weight material already in the coal, some small degree of depolymerization could also be occurring.

Thin-layer chromatography of the liquid SO₂ extract from PSOC 267 was carried out using a chloroform solution for deposition and eluted with progressively more polar solvents; long-wavelength UV illumination was used to observe fluorescence in the samples. Although no distinct bands were developed upon elution, three definite fractions that differ by polarity of constituents were apparent on the plates. Several conclusions can be drawn from these TLC experiments. The complete sample contains easily oxidizable functions. All alkyl functions are attached to aromatic residues. The less conjugated (blue fluorescent) fraction is less polar than the more conjugated (orange fluorescent) fraction. A very polar fraction, not transported by any eluent used, is even more highly conjugated (red fluorescent). These observations are consistent with the types of structures¹⁴ known to exist in coals as well as with the spectroscopic measurements to be described next.

The field ionization mass spectrum of the liquid SO₂ extract from PSOC 267 is illustrated in Fig. 1; the corresponding spectrum of the extract from PSOC 270 is similar in several features. The molecular weight distribution in these spectra are not as broad nor is the average molecular weight as high as might have been expected.¹⁴ The presence of very finely divided particulate matter, which presumably has higher molecular weight components that are not volatilized under the measurement conditions, could be responsible for such observations. The spectra contain striking patterns in which the mass difference among major components is 14 amu. These patterns suggest the presence of a variety of CH₂ containing structures. It is tempting to assign another pattern near m/e = 184 to dibenzothiophene since it strongly resembles that obtained with an authentic dibenzothiophene sample. The lack of high resolution mass spectral data, however, makes such an assignment pure speculation at this stage.

The infrared spectrum of the liquid SO₂ extract of PSOC 267 (neat, thin film) is shown in Fig. 2. It is apparent that the extract contains O-H, N-H, aromatic and aliphatic C-H groups, a variety of substituted aromatic structures, and probably ethers. There is no evidence of either residual SO₂ or of organic structures containing SO₂ substitution; no procedures other than evaporation of the liquid SO₂ under ambient conditions were used to process this extract.

Proton and ^{13}C (proton noise decoupled) nmr spectra of the liquid SO_2 extract of PSOC 267 are shown in Fig. 3. Qualitatively, the proton spectrum resembles that of CS_2 extracts of other bituminous coals as reported by Retcofsky and Friedel;¹⁵ our assignments follow those of these workers. The signals with $\delta < 1.8$ are assignable to alkyl type protons, those with $2.0 < \delta < 3.5$ are assignable to benzylic type protons and those with $6.9 < \delta < 8.8$ are assignable to aromatic type protons; the signal at $\delta \text{ ca. } 4.8$ is attributed to phenolic and alcoholic type protons. Integrated intensities provide the following distribution of protons: 20.9% aromatic, 1.9% -OH, 32.1% benzylic, and 45.1% other alkyl types. It would appear that the alkyl-H/aromatic-H ratio is higher for this extract than for CS_2 extracts of bituminous coals with similar carbon content (84.6% C in PSOC 267).

The ^{13}C nmr spectrum reveals further detail concerning the types of structures found in the liquid SO_2 extract of PSOC 267 since assignments are readily made by reference to the work of Fischer *et al.*¹⁶ Features in common with both SRC extracts and methylnaphthalene extracts of bituminous coal are found in the liquid SO_2 extract. The sharp signal at 14.1 ppm is assigned to terminal methyl groups on aliphatic side chains, that at 19.8 ppm to unhindered aryl methyl groups, and those at 22.7 and 31.9 ppm to α and β methylene carbons, respectively, on tetralin type structures. The sharp, dominant resonance at 29.7 ppm is readily assigned to methylene carbons in $\text{Ar-CH}_2\text{-CH}_2\text{-Ar'}$ groups whereas the weaker signals at 32.6, 37.4, and 39.2 ppm are characteristic of single methylene carbons bridging aromatic structures. The broad, low field band with a higher field asymmetry is typical of a composite of aromatic type carbons. Individual sharp signals within this band correspond to alternate polynuclear aromatics that are partially substituted.¹⁶ The apparent absence of signals at even lower fields from carbon atoms without proton substituents is attributed to lack of NOE enhancement for these nuclei.

Thus the liquid SO_2 extract of PSOC 267 has been shown to contain coal constituents similar to those obtained by extraction with common organic solvents. Although an abundance of alkyl groups (methyl and especially methylene) is found in the carbon structures as illustrated by the infrared, ^{13}C nmr, and mass spectra, it is not clear whether this is representative of PSOC 267 composition or is a consequence of the properties of liquid SO_2 . Less is known about the composition of heteroatom compounds in the extract: OH, NH and probably ether groups are apparent but available spectral data do not reveal other groups such as might be found in organic sulfur compounds. Unfortunately, the spectra obtained are not sensitive to divalent sulfur containing organic structures and reliable elemental analyses were precluded by lack of sufficient material. Since better characterization of this extract may eventually provide clues concerning the ability of liquid SO_2 to remove organic sulfur compounds, such efforts are to be made.

In summary, preliminary experiments have demonstrated that liquid SO_2 can be used to remove organic type sulfur compounds from bituminous coals and that the liquid SO_2 extract contains coal components similar to those found by extraction with organic solvents. The ability of liquid SO_2 to disintegrate some coals and to fracture others has been confirmed. Conditions to optimize the removal of sulfur compounds from coal and to facilitate removal of residual SO_2 from the coal are under investigation.

ACKNOWLEDGEMENTS

The support of this research by the Department of Energy, under Contract No. ET-78-G-01-3316, is gratefully acknowledged.

REFERENCES

1. D.W. van Krevelen, "Coal: Typology, Chemistry, Physics, and Constitution", Elsevier, Amsterdam, 1961.
2. H.H. Lowry, "Chemistry of Coal Utilization", Wiley, New York, 1945, Vol. 1, Chapter 19.
3. R.M. Baldwin, J.O. Golden, J.H. Gary, R.L. Bain, and R.J. Long, in "Coal Processing Technology", American Institute of Chemical Engineers, New York, Vol. 2, p. 128 (1975).
4. R.P. Anderson, ibid., p. 130.
5. S. Morooka and C.E. Hamrin, Jr., Chem. Eng. Science, 34, 521 (1979).
6. L.F. Audrieth and J. Kleinberg, "Non-Aqueous Solvents", Wiley, New York, 1953, Chapter 11.
7. W.K.T. Gleim, U.S. Patent 4, 120, 664, 1978.
8. D.F. Burow, "Sulfur Dioxide" in The Chemistry of Non-Aqueous Solvent Systems, J.J. Lagowski, Ed., Vol. 3, 1970, p. 138.
9. D.F. Burow, Inorg. Chem., 11, 573 (1972).
10. R.A. Meyers, "Coal Desulfurization", Marcel Dekker, New York, 1977.
11. "Coal Desulfurization", T.D. Wheelock, Ed., ACS Symposium Series No. 64, ACS, Washington, D.C., 1977.
12. F. Fischer and W. Gluud, Chem. Ber., 49, 147 (1916).
13. J.W. Larsen and P. Choudhury, J. Org. Chem., 44, 2856 (1979).
14. "Organic Chemistry of Coal", J.W. Larsen, Ed., ACS Symposium Series No. 71, ACS, Washington, D.C., 1978.
15. H.L. Retcofsky and R.A. Friedel in "Spectrometry of Fuels", Plenum, New York, 1970, Chapter 6.
16. P. Fischer, J.W. Stadelhofer, and M. Zander, Fuel, 57, 345 (1978).

TABLE 1. Characteristics of Bituminous Coals Treated with Liquid SO₂

	COAL (PSOC NO.)			
	194	267	270	319
Type	HVB	HVA	HVA	LV
Origin	OH	VA	AL	PA
Macerals (%/v)				
Vitrinite	73.3	60.9	68.1	85.5
P. Vitrinite	12.6	5.3	3.2	4.2
Micrinite	3.3	15.6	9.1	1.0
Fusinite	2.2	8.7	8.6	4.3
S. Fusinite	2.3	3.4	4.6	4.0
Resinite	3.6	1.5	0.8	0.0
Sporinite	1.8	3.2	5.0	0.5
Elemental Analysis (DAF)				
%C	78.23	84.63	83.34	86.49
%H	5.56	5.58	5.55	4.57
%N	1.72	2.53	1.74	1.61
%O(diff)	10.97	5.18	6.59	0.16
%S(total)	3.51	2.08 (1.967) ^a	2.77 (2.682) ^a	7.17
organic	1.26	2.01	2.70	0.10
pyritic	2.19	0.02	0.02	7.00
sulfatic	0.07	0.05	0.05	0.07

^aAnalyses done in this work.

TABLE 2. Experimental Results

Sample (PSOC No.)	Exp. No.	Solvent ^a	Reaction Temp. (°C)	Wash	%S	Organic Sulfur Removed
270						
lump	1	SO ₂	150	-	5.756	
lump	2	SO ₂	150	1.5M NaOH, H ₂ O	3.802	
lump	3	SO ₂	150	3M HCl, H ₂ O	3.522	
lump	4	SO ₂	150	H ₂ O, C ₆ H ₆	2.682	
lump	5	SO ₂	100	CCl ₄	2.602	
lump	6	SO ₂	100	acetone	2.316	
lump	7	SO ₂	150	multiple ^b	2.005	25%
lump	8	SO ₂ /C ₆ H ₆ ^c	100	-	3.089	
lump	9	SO ₂ /C ₆ H ₆ ^c	100	multiple ^b	1.992	25%
powder ^d	10	SO ₂	75	multiple ^b	1.397	48%
267						
lump	11	SO ₂	75	multiple ^b	1.241	37%
powder ^d	12	phenol	180	H ₂ O, acetone	0.9394	52%
powder ^d	13	p-cresol	200	H ₂ O, acetone	0.6580	66%
194						
lump	14	SO ₂	100	multiple ^b	2.134	
314						
lump	15	SO ₂	100	multiple ^b	1.584	

a. For liquid SO₂ reactions, 60 min reaction time was used and for organic solvent reactions, 5 hr was used.

b. The multiple wash consisted of the use of sequential aliquots of acetone, H₂O, 3.8 M HNO₃, H₂O, acetone (see text).

c. The SO₂/benzene solution was ca. 1:1 (vol).

d. Lump coal was crushed and ground to -60 mesh.

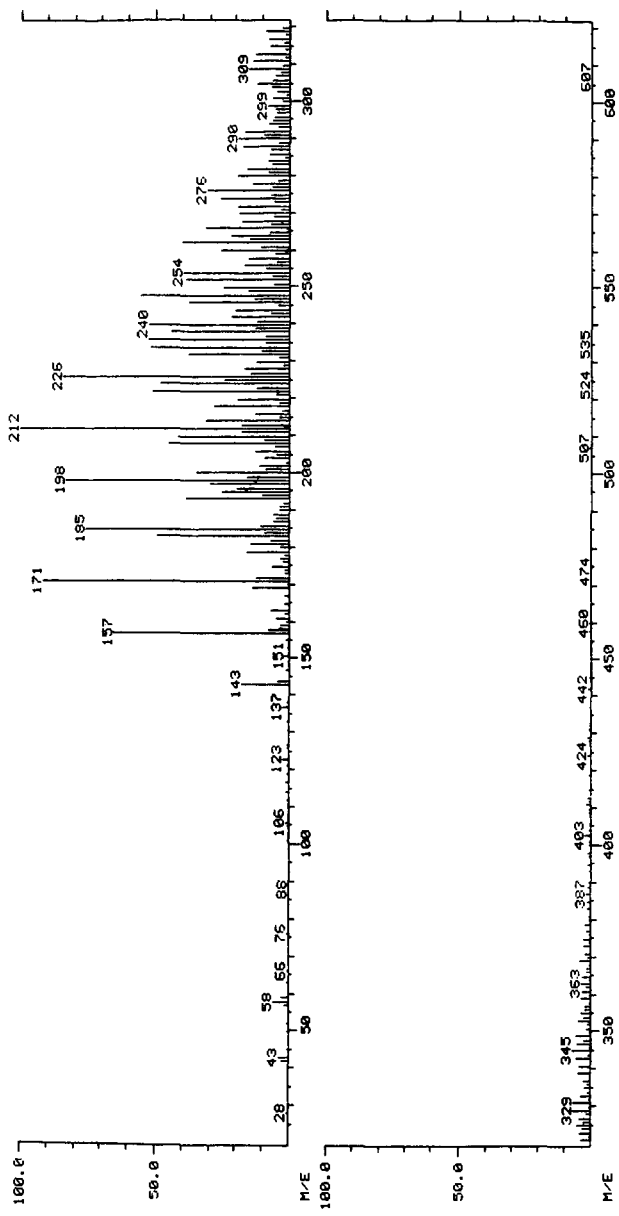


FIGURE 1. Field ionization mass spectrum of the liquid SO₂ extract of coal PSOC 267.

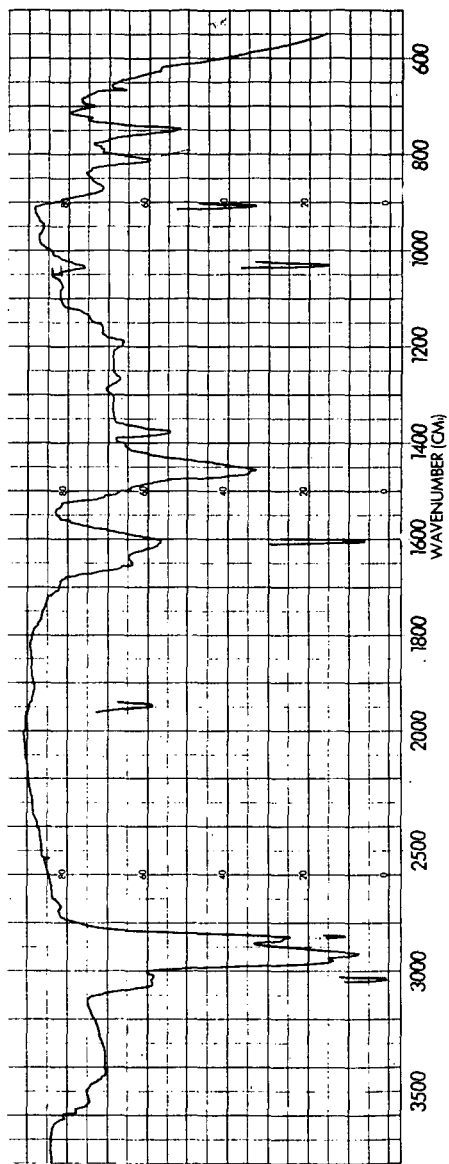


FIGURE 2. Infrared spectrum of the liquid SO₂ extract of coal PSOC 267.

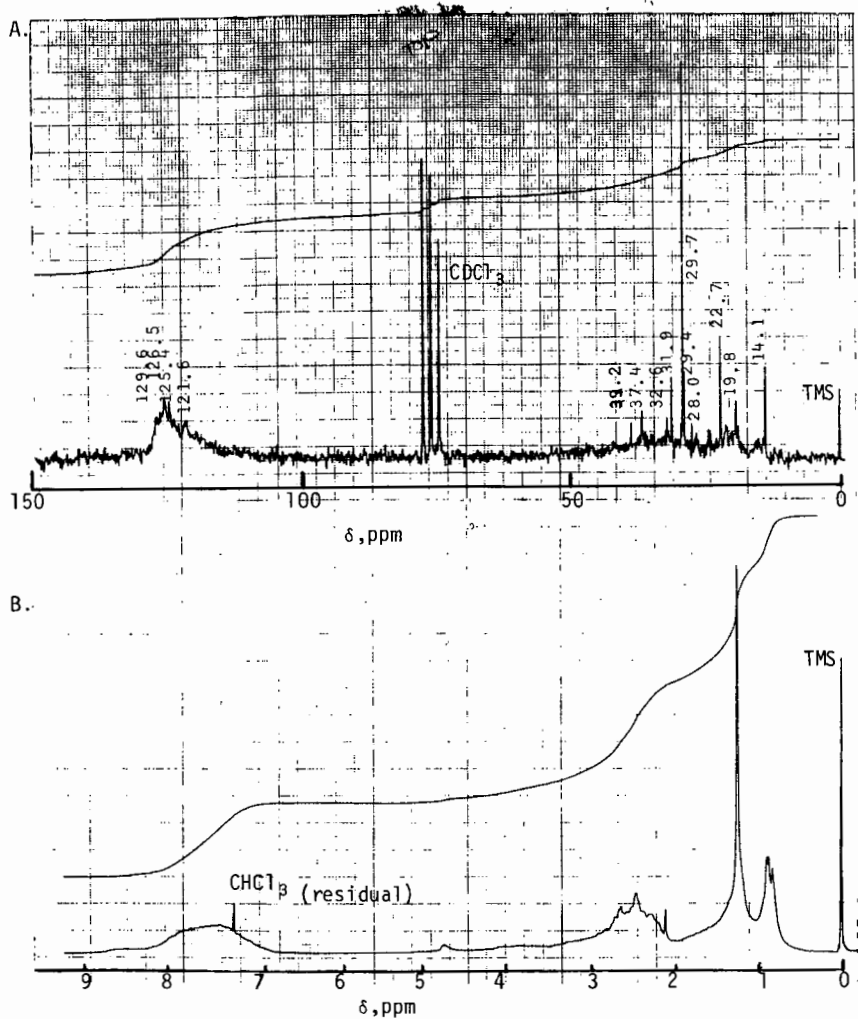


FIGURE 3. Nuclear magnetic resonance spectra of the liquid SO_2 extract of coal PSOC 267 (CDCl_3 solution, 5 mm tube). A. ^{13}C nmr spectrum, proton noise decoupled, 2000 pulses B. ^1H nmr spectrum, 10 pulses.

Evaluation of Oxydesulfurization Processes for Coal
I. The Effect of the Ames Process on Model Organosulfur Compounds

L. W. Chang, W. F. Goure, T. G. Squires, and T. J. Barton

Ames Laboratory, US DOE and Department of Chemistry
Iowa State University
Ames, Iowa 50011

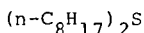
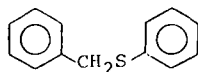
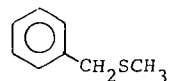
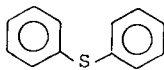
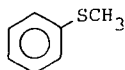
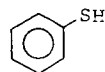
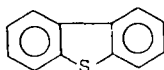
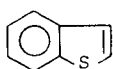
INTRODUCTION

One of the main obstacles to the use of coal as an alternate energy source is that it contains sulfur which contributes to air pollution when the coal is burned. It is estimated that only few percent of coals in the United States will be able to meet EPA SO₂ emission standards (1). Although some chemical procedures have been reported to be effective for desulfurization of coals, most, if not all, of the sulfur that is removed is inorganic. There is little information about what actually happens to the organic sulfur when coals are subjected to these process conditions. A major reason for this ignorance is the lack of information about the nature and distribution of the organosulfur functional groups in the coal.

Recently, several workers have reported that organic sulfur as well as inorganic sulfur can be removed by oxidative processes (2-6). Wheelock, *et. al.* (2) reported that under the following conditions: 150°C, 200 psig O₂, 0.2M aq. Na₂CO₃, 1 hour; up to 40% of the organic sulfur can be removed from coal without significantly reducing the recovery of combustible organic matter.

In this paper we wish to report our evaluation of the effectiveness of this Ames process in the desulfurization of coal. Instead of using coal, model organosulfur compounds were subjected to Ames process conditions. Our approach is based on the assumption that a definitive knowledge of the organosulfur functional groups and their distribution in coal is not a prerequisite for investigating the viability of desulfurization processes. Thus, it is sufficient to measure the propensity of a representative spectrum of organosulfur model materials toward desulfurization under process conditions.

In our study, the following organosulfur compounds have been subjected to Ames process conditions either by themselves or in the presence of coal. For comparison, some model sulfur compounds were also run under the same conditions except that nitrogen was used in place of oxygen. The results of our study are summarized in Tables I and II.



EXPERIMENTAL

Reactions in the Absence of Coal

The reactions were run either in an 1 liter or a 300 ml autoclave. In a typical run, approximately 5 g (for the 1 liter autoclave) or 1 gram (for the 300 ml autoclave) of organic sulfide was placed in a glass liner of an autoclave. After adding 300 ml (1 liter autoclave) or 50 ml (300 ml autoclave) of 0.2M aqueous sodium carbonate solution, the reactor was sealed, flushed with N_2 , and heated as rapidly as possible to 150°C. After the reactor had equilibrated at 150°C (10-15 minutes), the system was pressurized to 200 psig with oxygen and the reactor was flushed with a slow stream of oxygen for 3 minutes. A cold trap was connected to the vent tube of the autoclave to collect the starting sulfide (usually a small amount) which escaped from the reactor during the flushing process (the collected sulfide was combined with the reaction mixture in the autoclave after the reaction). The reactor was then sealed, and temperature (150°C), stirring (1500 rpm) and pressure (200 psig) were maintained for one hour. During the initial pressurization and the first 20-30 minutes of the reaction, cooling of the reactor with water was sometimes required.

After one hour, the heater was turned off; the reactor was cooled to room temperature and the contents were poured into a beaker. The reactor and the glass liner were washed with benzene and with water. The reaction mixture and these washings were combined and extracted with benzene, and the benzene extract was dried (Na_2SO_4) and filtered. To the reactions run in the 300 ml autoclave an internal standard was added directly to the dried benzene extract and the solution was analyzed by gas chromatography (GC) to determine the quantity of starting sulfide left and volatile compounds formed in the reaction. GC response factors for the sulfides, products and the standards were generated in the form of calibration table using standard solutions containing the sulfide, products and the standard. For the reactions run in the 1 liter autoclave, the volume of dried and filtered benzene extract was adjusted to 500 ml, and a 50 ml of aliquot of the benzene solution was withdrawn. An internal standard was added to the 50 ml solution; the solution was analyzed with GC.

The extracted aqueous layer of the benzyl phenyl sulfide or the benzyl methyl sulfide reaction mixture was acidified with concentrated hydrochloric acid, and washed with benzene. The benzene washings were dried (Na_2SO_4) and flash evaporated to afford a residue which NMR and IR analysis showed to be benzoic acid. The remaining aqueous layer was evaporated to dryness, and the residue was analyzed by NMR, IR, and UV spectroscopy.

Reaction in the Presence of Coal Under Oxygen or Under Nitrogen Atmosphere

The coal used was Iowa coal (Lovilia, 200 mesh) and was dried at 110°C overnight. The reactions in the presence of coal were run in a 300 ml autoclave. The reaction procedures were the same as those mentioned above except that ca 4.0 g of coal was added to the reaction mixture for each run. After the reaction, the reaction mixture and washings were combined and filtered, and the filtrate was extracted with benzene. The coal collected with filtration was washed with acetone, then benzene several times. The benzene and the acetone-benzene extracts were combined, dried (Na_2SO_4) and analyzed with GC using internal standards.

RESULTS AND DISCUSSION

Tables I and II demonstrate that among the model compounds that we studied, only thiophenol and compounds containing a benzylic sulfide linkage were oxidized to an appreciable extent. Thiophenol was converted to phenyl disulfide which was resistant to further oxidation. Benzyl phenyl sulfide was oxidized and cleaved to give benzaldehyde, benzoic acid and benzenesulfonic acid; benzyl methyl sulfide gave similar results. The other model compounds were unreactive under the Ames process conditions either by themselves or in the presence of coal. Even in the presence of coal, more than 70% of the starting sulfide was recovered. The reduced recoveries of starting

Table I. Reaction Results of Compounds Run Under the Ames Process Conditions in the Absence of Coal^a

<u>Compound</u>	<u>Recovered Yield (%) of Starting Sulfide</u>	<u>Product</u>
Benzothiophene	87	-----
Dibenzothiophene	96	-----
Thiophenol	0	Phenyl Disulfide
Phenyl sulfide	98	-----
Phenyl methyl sulfide	89	-----
Benzyl methyl sulfide	36	Benzoic acid Benzaldehyde Methanesulfonic acid
Benzyl phenyl sulfide	29	Benzoic acid Benzaldehyde Benzenesulfonic acid
N-Octyl sulfide	90	-----

^a Ames process conditions: 150°C, 200 psig O₂, 0.2M aqueous Na₂CO₃, 1 hour.

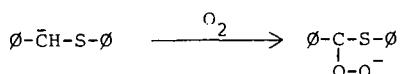
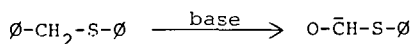
Table II. Reaction Results of Compounds Run Under the Ames Process^a Condition in the Presence of Coal^b

<u>Compound</u>	<u>Recovered Yield (%) of Starting Sulfide</u>	
	<u>N₂^c</u>	<u>O₂^d</u>
Dibenzothiophene	83	76
Phenyl sulfide	76	74
Benzyl methyl sulfide	75	13
N-octyl sulfide	--	82

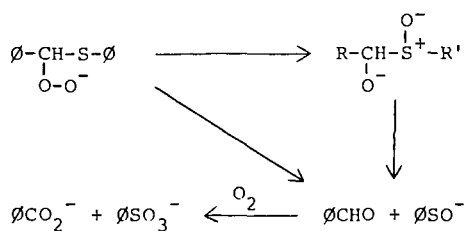
^a Ames process conditions: 150°C, 200 psig O₂, 0.2M aqueous Na₂CO₃, 1 hour. ^b Iowa Lovilia Coal. ^c Reaction run under nitrogen atmosphere. ^d Reaction run under oxygen atmosphere.

materials in the presence of coal (see Table II) can be attributed to absorption of the organosulfur compound by the microporous structure of coal and the mechanical loss associated with working up the reaction mixture. This hypothesis was confirmed by the correspondingly low recoveries of starting sulfides from reactions run in the presence of coal under nitrogen atmosphere--an inert atmosphere. Furthermore, no oxidation products were detected in the reaction mixtures. Clearly, of the compounds investigated thus far, only benzyl sulfides and thiophenol underwent any chemical reaction, and (the benzyl sulfides were the only compounds in which carbon sulfur bond cleavage occurred.

The base-catalyzed reaction of compounds containing a benzylic sulfide linkage with molecular oxygen has been studied under a variety of conditions. Wallace *et. al.* (7) reported that benzyl phenyl sulfide can be oxidized with molecular oxygen in 2M potassium *t*-butoxide-HMPA at 80°C to yield benzoic acid. The authors proposed that the reaction proceeded via the formation of an α -carbanion followed by reaction between the ion and oxygen.



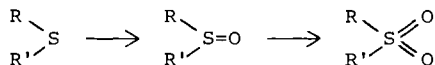
The resulting α -peroxide anion can then decompose in either a stepwise or concerted manner to form benzaldehyde and benzenesulfenate which are oxidized to the corresponding carboxylic and sulfonic acids. In the first step of this mechanism, the α -carbanion is stabilized by the d-orbital of the adjacent divalent sulfur atom.



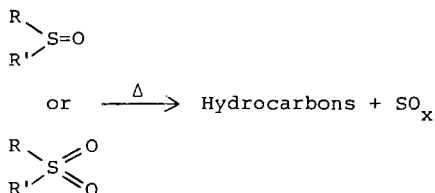
We believe that a similar mechanism is involved in the oxidation of benzyl phenyl sulfide under Ames process conditions.

Oxydesulfurization of the organic sulfides in coal has been formulated as a two-step process (8): 1. Selective oxidation of the sulfur to sulfoxides and sulfones with the latter as the favorable product; and 2. Thermal decomposition of the oxidation products, usually under basic conditions.

Step 1.



Step 2.



In this formulation, the reaction is initiated by oxidation of the sulfur and, in fact, is made possible by this oxidation which results in polarization and weakening of the carbon to sulfur bonds (8).

We find no evidence to support this hypothesis; oxidation of the sulfur was detected only in thiophenol and in the benzyl sulfides. In the first case, oxidation of mercaptans to disulfides is a facile reaction known to occur under conditions such as the Ames process. No further oxidation of the disulfide was detected. In the latter case, we submit that carbon-sulfur bond cleavage is initiated by oxidative attack at the benzyl position instead of at sulfur. This postulate is supported by our recent discovery that, under Ames process conditions, fluorene was oxidized rapidly and quantitatively to fluorenone while dibenzothiophene was removed unchanged from the same reaction mixture.

Oxidation of benzylic carbon hydrogen bonds in preference to sulfur would have a substantial impact on the development of processes for the oxydesulfurization of coal. We intend to investigate this phenomenon and explore methods for reducing or reversing the ratio of benzylic to sulfur oxidation.

ACKNOWLEDGEMENTS

This work was supported by the U. S. Department of Energy, contract No. W-7405-Eng-82, Division of Fossil Energy, budget code AA-10-03-03.

REFERENCES

1. J. A. Cavallaro, M. T. Johnston, and A. W. Deurbrouck, "Sulfur Reduction Potential of the Coals of the United States; A Revision of Report of Investigations 7633," RI 8118, U. S. Bureau of Mines, 1976.
2. T. D. Wheelock, R. T. Greer, R. Markuszewski, and R. W. Fisher, "Advanced Development of Fine Coal Desulfurization and Recovery Technology," Annual Technical Progress Report, Oct. 1977 - Sept. 1978. IS-4688 prepared for DOE-Fossil Energy, by Ames Laboratory, Iowa State University, Ames, Iowa. April, 1979.
3. R. A. Meyers, "Coal Desulfurization," Marcel Dekker, Inc., New York (1977).
4. P. S. Ganguli, G. C. Hus, G. R. Gavalas, and S. H. Kalfayan, Am. Chem. Soc., Div. Fuel Chem., Preprint, 21, 118 (1976).
5. S. S. Sareen, R. A. Giberti, P. F. Irminger, and L. J. Petrovic, AIChE Symp. Ser., 73, 183 (1977).
6. S. Friedman and R. P. Warzinski, J. Eng. for Power, 99, 361 (1977).
7. T. J. Wallace, H. Pobiner, F. A. Baron, and A. Schriesheim, J. Org. Chem., 30, 3147 (1965).
8. A. Attar and W. H. Corcoran, Ind. Eng. Chem., Prod. Res. Dev., 17, 102 (1978).

HIGH-PERFORMANCE LIQUID CHROMATOGRAPHY SEPARATION
OF OLEFIN, SATURATE, AND AROMATIC HYDROCARBONS IN HIGH-BOILING
DISTILLATES AND RESIDUES OF SHALE OIL

John F. McKay and D. R. Latham

Laramie Energy Technology Center, DOE, P. O. Box 3395, Laramie, Wyo. 82071

ABSTRACT

A high-performance liquid chromatography (HPLC) method has been developed for the separation of olefin, saturate, and aromatic hydrocarbons found in high-boiling distillates and residues of shale oil and in whole shale oils. The dual-column chromatographic system uses silica gel in one column and silica gel coated with silver nitrate in a second column. Separated fractions are analyzed by infrared and carbon-13 nuclear magnetic resonance spectrometry to demonstrate the validity of the separation. The time required for a separation is about two hours. The separations are reproducible, and recovery of material after separation is generally better than 90 percent. The olefin, saturate, and aromatic fractions obtained from a separation are suitable for further analysis.

INTRODUCTION

As increased amounts of shale oil are processed together with petroleum, it becomes increasingly important to have methods available for the analyses of shale oil. A fundamental difference in the composition of shale oil and petroleum is that shale oil contains three major hydrocarbon compound types--olefins, saturates, and aromatics--while petroleum contains only saturates and aromatics. Olefins, because they are hydrogen deficient and unstable, cause problems in the processing of shale oil that are not encountered in the processing of petroleum. They are also of special interest because the amounts, and perhaps kinds, of olefins in shale oil are related to the retorting conditions that produce the shale oil. Techniques for the analysis of saturates and aromatics in petroleum are well known; however, methods for determining olefin, saturate, and aromatic hydrocarbons in the heavy distillate and residue portions of shale oil are needed.

Many techniques for the determination of olefins, saturates, and aromatics have been reported in the literature (1-11). The methods usually involve liquid chromatography with silica gel (3, 4, 10) or liquid chromatography combined with chemical reactions (1, 11, 12). The methods work well in the analytical applications for which they were designed--primarily the determination of hydrocarbon types in light distillates. Difficulties, such as incomplete separation of compound types, often arise when the methods are applied to the analyses of heavier hydrocarbon fractions. The purpose of the work discussed in this paper is to extend the analysis of olefin, saturate, and aromatic hydrocarbons to the high-boiling distillate and residue fractions of shale oil. Several requirements were established for a satisfactory analytical method: 1) the determination should be fast; 2) the results should be reproducible; 3) the samples should have minimum exposure to air, light, and heat; and 4) the separated hydrocarbon types should be chemically unaltered and therefore suitable for further analyses.

This paper describes a dual-column high-performance liquid chromatography (HPLC) method for the separation and determination of olefin, saturate, and aromatic hydrocarbons in high-boiling distillate and residue fractions of shale oil. The method can also be used to separate hydrocarbon types in whole shale oils. The dual-column technique uses silica gel to separate aromatic hydrocarbons from olefin and saturate hydrocarbons and silica gel coated with silver nitrate to separate olefin from satu-

rate hydrocarbons. Cyclohexane is used as solvent for the hydrocarbon samples. The time required for a separation is about two hours.

EXPERIMENTAL

Apparatus

Shale oil distillates and residues were obtained using an ASCO (Arthur F. Smith Co.) 2-in. Rota-Film (wiped-wall) still. Acids, bases, and neutral nitrogen compounds were removed from the samples using a gravity-flow glass column (2.5 cm x 90 cm) packed in three sections with anion resin, cation resin, and ferric chloride/Attapulugus clay. The column was wet-packed using cyclohexane.

Hydrocarbon separations were made using a dual-column system in a Waters Associates AGC/GPC-202 liquid chromatograph equipped with refractive index and ultraviolet detection units. The first column contained silica gel, and the second column contained silica gel coated with silver nitrate. Both columns were stainless steel (7.8 mm i.d. x 61 cm) and were supplied with 5-micron fritted end fittings. Infrared spectra were recorded on a Perkin-Elmer model 621 spectrophotometer, and carbon-13 NMR spectra were obtained using a Varian CFT-20 spectrometer.

Materials

Amberlyst IRA-904 anion-exchange resin (Rohm and Haas) was used for removal of acids, and Amberlyst A-15 cation-exchange resin (Rohm and Haas) was used for removal of bases. Attapulugus clay, 50/80 mesh (Engelhard Minerals and Chemical Corp.) coated with ferric chloride (Baker and Adamson) removed neutral nitrogen compounds from the samples. The preparation of resins and ferric chloride/Attapulugus clay has been described (13).

Silica gel 60G (E. Merck) for thin-layer chromatography was used as received to separate aromatics from saturates and olefins. The same silica gel coated with 20 percent silver nitrate (Baker and Adamson) separated saturates from olefins. The silver nitrate-coated gel was prepared by dissolving the silver nitrate in water, mixing the solution with silica gel, and removing the water on a rotary evaporator. The gel was activated at 110°C for 12 hours. Cyclohexane, benzene, and methanol were commercial HPLC-grade solvents from various suppliers and were used as received.

Shale Oil Samples

The shale oils used in this study were produced by in situ and aboveground retorting processes (14). The Site 9 oil was obtained from the Laramie Energy Technology Center (LETC) in situ experiment near Rock Springs, Wyo. The 150-ton retort oil is from the LETC simulated in situ 150-ton retort near Laramie, Wyo. Paraho and Superior oils are from aboveground retorts located at Anvil Points, Colo., Cleveland, Ohio, respectively.

Distillation of Shale Oils

Crude shale oils that had been centrifuged to remove particulate matter and water were distilled using a wiped-wall still. The still was operated at 20 torr to remove oil boiling below 210°C (corrected to atmospheric pressure). Distillate fractions boiling from corrected temperatures of 210 to 370°C and 370 to 535°C were obtained at lower pressures and increased temperatures. The residue was recovered material that did not distill at 250°C (corrected) and 0.2 torr. The residue was actually exposed to a temperature of 250°C for only a few seconds so that thermal degradation was minimal.

Preparation of Hydrocarbon Samples

A sample (1 g) of distillate, residue, or whole shale oil was dissolved in cyclohexane (100 ml) and passed through a gravity-flow glass column containing successive beds of anion (80 g) and cation (80 g) resins and ferric chloride/ Attapulugus clay (100 g). The column was washed with cyclohexane (500 ml) to recover the hydrocarbons. The cyclohexane was removed from the hydrocarbons using a rotary evaporator.

Preparation and Assembly of HPLC Columns

A reservoir column was attached to an empty HPLC column, and both columns were filled with dry silica gel or silver nitrate/silica gel (about 20 g). Cyclohexane was then pumped through the system to wet and compress the packing material into the HPLC column. The reservoir column was then detached. Columns packed using this technique contained 15 g of gel wetted with cyclohexane, and the gel was uniformly distributed in the column. After a separation, the silver nitrate/silica gel column could be reactivated by washing with cyclohexane (100 ml). The silica gel column was not reusable. Figure 1 shows the dual-column assembly, chromatograph, and detectors.

Column Calibration

During routine analyses, the cut point for the separation of saturates and olefins from aromatics on the silica column was made according to elution volume. The proper elution volume was established prior to the separations by passing samples through the silica gel column and monitoring the separation with ultraviolet and refractive index detectors. Once the proper elution volume had been established, the detectors were removed from the chromatographic system.

Separation Procedure

A routine separation was made in the following manner. A shale oil hydrocarbon sample (200 mg), dissolved in cyclohexane (1 ml), was placed on the silica gel column, and cyclohexane was pumped through the two columns for 40 minutes at a rate of 1 ml/min and a pressure of about 350 psig. Under these elution conditions aromatics are retained on column 1, while saturates and olefins pass through to column 2. Valves between the columns and a second solvent reservoir allowed continued pumping cyclohexane through the second column where olefins and saturates were separated. Saturates were eluted with cyclohexane from the silver nitrate column with continued pumping for 30 minutes at 1 ml/min. Olefins were then eluted from the silver nitrate column by pumping benzene/cyclohexane, 20/80 percent, through the column for 30 minutes at 1 ml/min. Simultaneously, benzene/methanol, 40/60 percent, was pumped through the first column for 60 minutes to elute aromatics. The total separation time was about 2 hours.

DISCUSSION

Identification of Hydrocarbon Types

Infrared and carbon-13 NMR spectrometry were used to analyze the hydrocarbon fractions prepared by the dual-column chromatographic system. The analyses demonstrate the validity of the separations. Both spectrometric techniques have special analytical advantages and limitations; when used together they permit a satisfactory analysis of the hydrocarbon fractions.

The fractions of saturates, olefins, and aromatics were first examined using infrared spectrometry. Two absorption bands were used to analyze the fractions: 1) the mono-olefin stretching band at 1630 cm^{-1} to identify olefins and 2) the aromatic ring carbon-carbon stretching band at 1600 cm^{-1} to identify aromatics. Saturates have no absorption bands in the infrared that distinguish them from other hydrocarbon types.

An example of the use of infrared spectrometry in analyzing hydrocarbon fractions presented in Figure 2, which shows the partial infrared spectrum of the total hydrocarbons from a 210-370°C distillate together with the partial infrared spectra of separated fractions. In Figure 2a, both mono-olefin and aromatic absorption may be seen in the spectrum of the total hydrocarbons. Figures 2b, 2c, and 2d show that a separation of aromatics, olefins, and saturates has been achieved. Only trace amounts of aromatics absorbing at 1600 cm^{-1} can be observed in the spectrum of the saturates (Fig. 2d) and olefins (Fig. 2c). Olefins are observed in only the olefin fraction (Fig. 2c).

In general, infrared spectrometry is a very useful method for analyzing the hydrocarbon fractions because it is fast and sensitive. It does, however, have limitations. First, in a mixture of hydrocarbon types, saturates cannot be distinguished from olefins or aromatics. Second, use of the 1630 cm^{-1} band does not allow the detection of conjugated di- and tri-olefins. Third, infrared analyses of complex mixtures of olefins cannot be quantitative because the molar absorptivities of individual olefinic compounds are quite variable. The correct value of molar absorptivity to use in an infrared calculation involving Beer's law is not known.

Carbon-13 NMR spectrometry was used to complement infrared spectrometry in the analyses of separated fractions. These data confirmed infrared data and provided additional information about the hydrocarbon types, especially the olefins.

Figure 3 shows carbon-13 NMR spectra of saturates (Fig. 3a), olefins (Fig. 3b), and aromatics (Fig. 3c) from a 370-535°C hydrocarbon concentrate. For quantitative determination of olefins, the spectral region of interest is between 110 and 140 ppm relative to tetramethylsilane (TMS). Saturates show no carbon-13 absorption in this region. Olefins show absorption bands between 114 and 138 ppm (15, 16); the position of absorption is dependent upon the type of olefin. Alpha olefin bands are observed at 114 and 138 ppm, while internal olefins have absorption bands between 114 and 138 ppm. Aromatic carbons are seen as a broad, symmetrical absorption envelope centered at about 128 ppm. Figure 3a shows that, in this particular separation run, the saturates contain 1 or 2 percent of another hydrocarbon type, probably aromatics. Olefins are observed only in the olefin fraction, not in the saturate or aromatic fractions. Trace amounts of aromatics appear to be in the olefin fraction, confirming the infrared data.

Carbon-13 NMR is useful not only because it aids in judging the quality of separation that has been achieved but also because it provides detailed information about molecular structure. For example, in an olefin mixture, the number of double bonds of an average olefin molecule can be calculated if the average molecular weight of the olefin mixture is known and if the ratio of aliphatic/olefinic carbons can be measured by carbon-13 NMR. However, carbon-13 NMR also has limitations. First, in a mixture of hydrocarbons, saturates cannot be distinguished from olefins and aromatics. Second, olefins may not be observable in a concentrate of saturates or aromatics if the amount of olefins is lower than about 3 or 4 percent. Third, with carbon-13 spectrometry alone, it may be difficult to distinguish between internal olefins and aromatics; in such a case ultraviolet analyses are useful.

Infrared and NMR analyses established that saturate, olefin, and aromatic compound classes were separated into three discrete fractions by the dual-column system. This allowed the quantitative determination of each class to be made gravimetrically.

Separation Results

a. Hydrocarbons in High-Boiling Distillates and Residues. - The dual-column method was used to separate hydrocarbons from three different boiling ranges of four shale oils. The results of the separations are shown in Table 1. All data were obtained gravimetrically. Duplicate determinations were made to show the reproducibility that

can be expected with the separation technique. In most cases the reproducibility is similar to that experienced in the silica gel separation of saturate and aromatic hydrocarbons in petroleum. The cause of the poor reproducibility experienced in some runs is not known. The recovery of separated hydrocarbon types was generally better than 90 percent.

From a characterization point of view, the data in Table 1 show some interesting trends. First, distillates and residues from the Site 9 in situ oil and the 150-ton retort oil contain smaller amounts of olefins and larger amounts of saturates than the other oils. Thus, it appears that the Site 9 and 150-ton retort oils were produced under milder retorting conditions than the Paraho and Superior oils. Second, the distributions of hydrocarbon compound types as related to distillation temperature can be seen. For example, in the Site 9 oil, the aromatics increase as the distillation temperature increases. The olefins are constant in the distillates and increase in the residue. These changes are at the expense of saturates which decrease as the distillation temperature increases.

b. Hydrocarbons from Whole Shale Oils. - The dual-column method permitted the fast determination of saturates, olefins, and aromatics in whole shale oils. The results of the separations are shown in Table 2. Both reproducibility and recovery values are similar to those seen in the separation of distillates and residues. Unknown amounts of light hydrocarbons from the whole shale oils were lost during the solvent-removal procedure.

SUMMARY AND CONCLUSIONS

An HPLC method has been developed for the separation of saturates, olefins, and aromatics in high-boiling distillates and residues of shale oil and in whole shale oils. The dual-column chromatographic system uses silica gel in one column and silica gel coated with 20 percent silver nitrate in a second column. The time required for a separation is about two hours. The separations are reproducible; recovery of material after separation is generally better than 90 percent. The saturate, olefin, and aromatic fractions obtained from a separation are suitable for further analyses.

ACKNOWLEDGMENTS

The authors thank Mr. Shawn C. Tapley for the chromatography work, Dr. Daniel A. Netzel for the carbon-13 NMR analyses, and Dr. Shuang-Ling Chong for helpful discussions.

DISCLAIMER

Mention of specific models or brand names of equipment is made for information only and does not imply endorsement by the Department of Energy.

LITERATURE CITED

1. H. L. Johnson, and R. A. Clark, *Anal. Chem.*, 19, 869 (1947).
2. G. U. Dinneen, J. R. Smith, and John S. Ball, *Petroleum Refiner*, May 1950.
3. G. U. Dinneen, J. R. Smith, R. A. Van Meter, C. S. Allbright, and W. R. Anthony, *Anal. Chem.*, 27, 185 (1955).
4. E. L. Saier, A. Pozefsky, and N. D. Coggeshall, *Anal. Chem.*, 26, 1258 (1954).
5. H. B. Jensen, J. R. Morandi, and G. L. Cook, *Preprints, ACS Div. Petrol. Chem.*, 13 (2), 898 (1968).

6. J. R. Morandi and H. B. Jensen, *J. Org. Chem.*, 34, 1889 (1969).
7. H. B. Jensen, R. E. Poulson, and G. L. Cook, *Preprints, ACS Div. Fuel Chem.*, 15 (1), 113 (1971).
8. R. E. Poulson, H. B. Jensen, J. J. Duvall, F. L. Harris, and J. R. Morandi, *Proc. 18th Annual ISA Analysis Instrumentation Symposium, San Francisco, Calif., May 1972*, p. 193.
9. J. R. Morandi, D. G. Earnshaw, and H. B. Jensen, *Abstracts, Pittsburgh Conference on Analytical Chemistry and Applied Spectroscopy, Cleveland, Ohio, March 1972*, p. 170.
10. *ASTM Book of Standards, 1975, Part 24, Method D 2003-64*, p. 144.
11. L. P. Jackson, C. S. Allbright, and R. E. Poulson, *Anal. Chem.*, 46, 604 (1974).
12. L. P. Jackson, C. S. Allbright, and R. E. Poulson, "Analytical Chemistry of Liquid Fuel Sources: Tar Sands, Oil Shale, Coal, and Petroleum," Peter C. Uden, Sidney Siggia, and Howard B. Jensen, Ed., *Advances in Chemistry Series 170, American Chemical Society, Wash., D. C. 1978*, p. 232.
13. D. M. Jewell, J. H. Weber, J. W. Bunker, Henry Plancher, and D. R. Latham, *Anal. Chem.*, 44, 1391 (1972).
14. G. L. Baughman, *Synthetic Fuels Data Handbook, 2nd Ed., Cameron Engineers, Inc., 1978, Denver, Colo., 80210*.
15. R. A. Friedel, and H. L. Retcofsky, *J. Amer. Chem. Soc.*, 85, 1300 (1963).
16. D. A. Netzal, D. R. McKay, R. A. Heppner, F. D. Guffey, S. D. Cooke, and D. L. Varie, *Proc. EPA Oil Shale Symposium: Sampling, Analysis, and Quality Assurance, Denver, Colo., March 26-28, 1979*.

TABLE 1. - Hydrocarbon separation results of distillates and residues

Sample	Wt. percent of total hydrocarbon fraction			Percent recovery
	Saturate	Olefin	Aromatic	
150-ton, 210-370°C dist.	64	5	19	88
"	63	7	20	90
370-535°C dist.	61	6	29	96
"	59	7	34	100
>535°C residue	45	11	43	99
"	45	11	38	94
Site 9, 210-370°C dist.	70	5	17	92
"	72	6	23	101
370-535°C dist.	64	6	24	94
"	59	5	29	93
>535°C residue	48	8	40	96
"	40	10	47	97
Paraho, 210-370°C dist.	25	27	30	82
"	36	23	26	85
370-535°C dist.	38	24	34	96
"	31	23	35	89
>535°C residue	19	10	48	77
"	23	13	44	80
Superior, 210-370°C dist.	25	29	30	84
"	27	36	28	91
370-535°C dist.	32	21	42	95
"	32	22	42	96
>535°C residue	27	22	47	96
"	31	19	48	98

TABLE 2. - Hydrocarbon separation results of whole shale oils

Shale oil sample	Wt. percent of hydrocarbons from total oil			Percent recovery
	Saturate	Olefin	Aromatic	
150-ton retort	53	17	22	92
"	40	21	22	83
Site 9 retort	46	18	18	82
"	55	15	20	90
Paraho retort	41	27	24	92
Superior retort	41	26	32	99
"	36	31	28	95

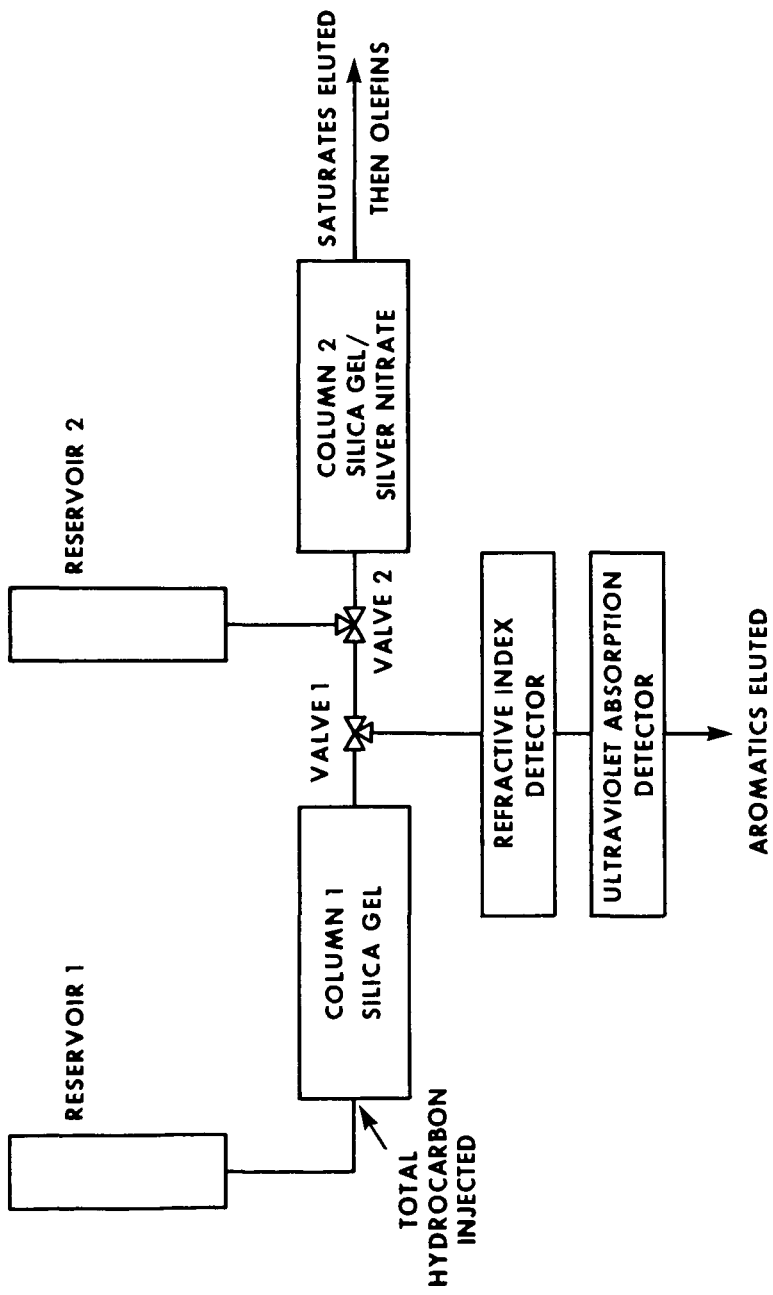


FIGURE 1. HPLC apparatus

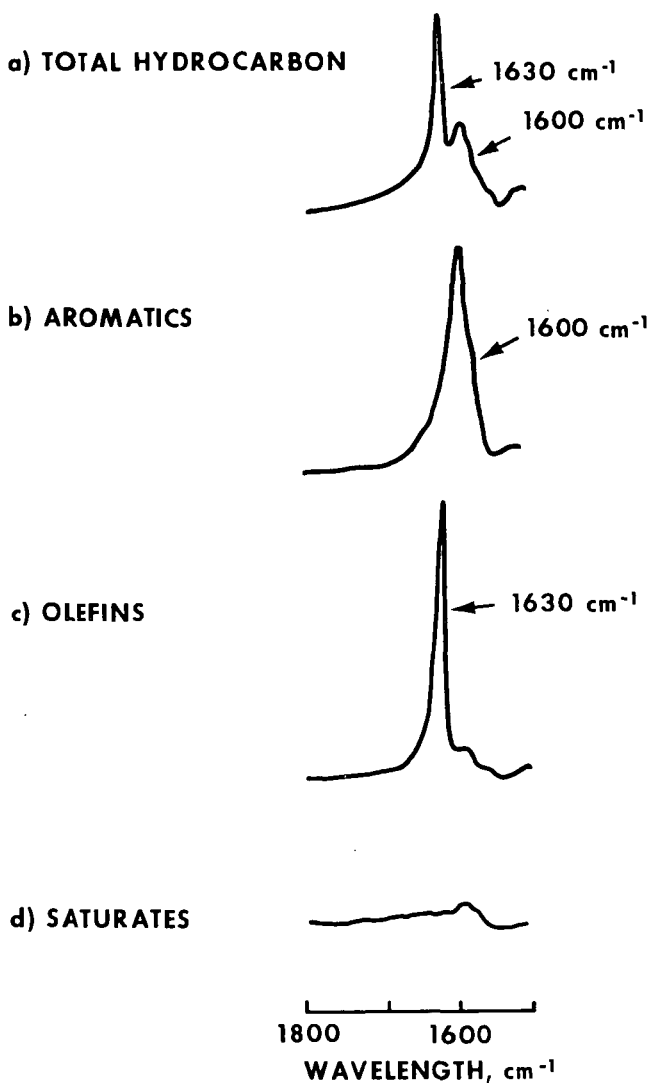


FIGURE 2. Partial infrared spectra of shale oil 210-370°C distillate total hydrocarbon and fractions

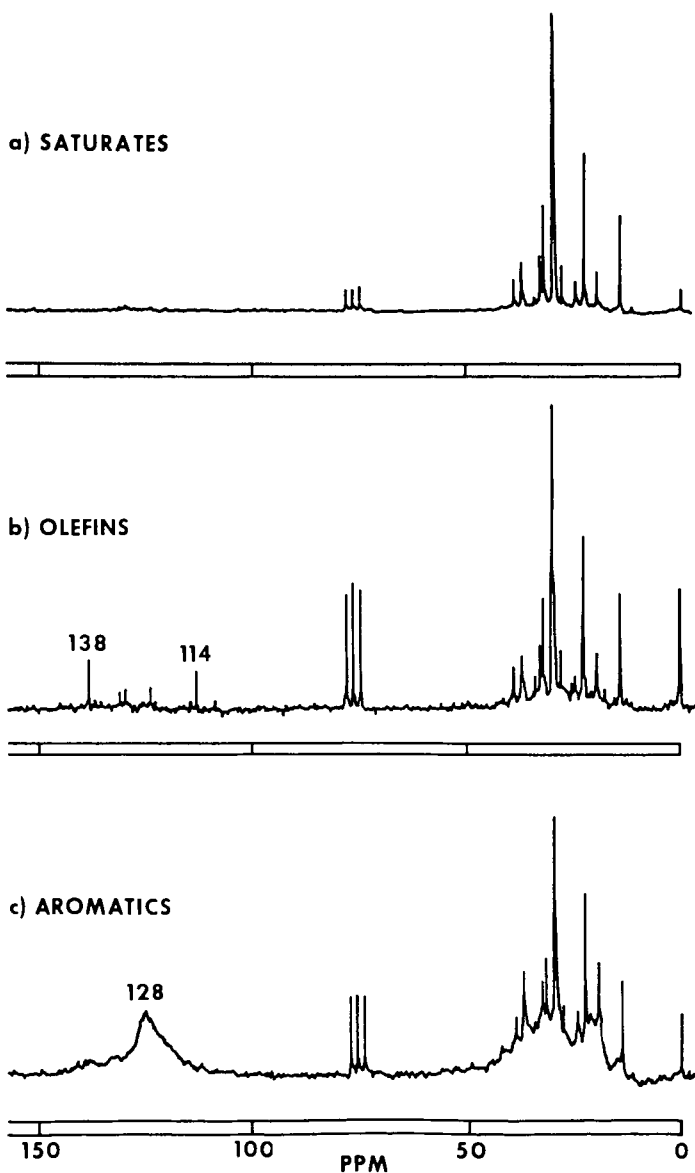


FIGURE 3. Carbon-13 NMR spectra of hydrocarbon fractions from Paraho 370-535°C distillate

LOW TEMPERATURE CLEAVAGE REACTIONS OF ILLINOIS NO. 6 COAL

Frank R. Mayo, David H. Buchanan,¹ and Lee A. Pavelka

SRI International, Menlo Park, California 94025

This paper presents a progress report on our efforts to determine the kinds and proportions of single bond in Illinois No. 6 coal that can be broken below 100°C. The principal obstacle to the use of present liquefaction processes is the high cost of plants that would employ the required high temperatures and pressures. Our work deals only with low-temperature processes near atmospheric pressure. It has focused on (1) the asphaltol fraction of Illinois No. 6 coal, which is the pyridine-soluble, toluene-insoluble fraction that comprises about two-thirds of the 15% of coal that can be extracted by pyridine, and (2) the pyridine-extracted coal, which is about 85% of the initial dry coal, and which represents the essence of the liquefaction problem.

Oxidations

Previous work by Huntington et al² described the effects on the same two substrates of (1) AIBN-initiated oxidations in pyridine solution at 50°C, and (2) refluxing with alcoholic KOH (78°) without oxygen. Either reagent would reduce the number-average molecular weight (\bar{M}_n , by vapor-phase osmometry) of the asphaltol by nearly 50% but sequential treatment with both reagents produced little additional effect, as if the two reagents were affecting similar bonds. Only about 10% of the extracted coal was made soluble in pyridine, but some substrate became soluble in alcoholic KOH.

NaOCl oxidation of very finely divided extracted coal in water suspension at 30° and pH 13 has been much more effective in dissolving this material.³ 76% of the carbon in the extracted coal has been converted to black acids (\bar{M}_n about 1000) soluble in aqueous base, and 7% to water-soluble acids; 4% of the initial carbon was undissolved; the remaining 12% is presumably in carbon oxides. Oxygen oxidation of extracted coal in water suspension at pH 13 and 50° is much slower but has led to 85% dissolution of the coal and recovery of 66% of the original coal in black acids. Oxidations of asphaltol, well dispersed in water at pH 13, gave better results: with NaOCl at 30°, 99% dissolution and 93% of the carbon in black acids; with oxygen at 50°, 98% dissolution and 80% of the carbon in black acids.

These oxidations in water suspension at pH 13 and oxidations with AIBN and oxygen in pyridine solution² at 50°C appear to proceed by different mechanisms. In radical-initiated oxidations of extracted coal, the H/C ratio decreases from .73 to .69, as if benzylic hydrogen were being removed preferentially. However, in both NaOCl and oxygen oxidations of both asphaltol and extracted coal in water, H/C increases somewhat, notwithstanding replacement of some H by O, suggesting preferential removal of aromatic groups. Possibly some hydroxylated aromatic rings are sites of attack. The principal products, black acids, from oxygen and NaOCl oxidations in water at pH 13 have similar compositions.

Cleavages of Asphaltols

Results of cleavages of asphaltols, probably at ether links, are summarized in Figures 1 and 2. Each half of each table starts from the center with asphaltol with slightly different \bar{M}_n . In general, reactions were run under nitrogen, and at room temperature except as noted. Products were sometimes separated by solubility but always washed free of reagents and solvents and dried in an Abderhalden drier at <0.001 torr, usually at 140°C in Figure 1, usually at 76°C in Figure 2. (The only need for 140° drying seems to be with samples that contain pyridine or amines and have not been acid-washed.) \bar{M}_n s were determined by VPO in pyridine, in which all products were soluble, at concentrations of 0.5 to 3g/L. Keys to abbreviations and

arrangement of data are given in Figure 2. Thus, molecular weights of products are in the middle of each second line of each block of data.

Experiments in the upper left quarter of Figure 1 show that eight extractions of asphaltol with 5% KOH at room temperature resulted in solution and recovery of 9% of soluble carbon. 23% of the original C was lost, at least partly as water-soluble and/or volatile products. Molecular weight reductions without heating parallel those at 78°.2

Reactions of asphaltol with benzylamine (lower left quarter in Figure 1), and then drowning the reaction in ether or methanol, resulted in part of the asphaltol becoming soluble in these solvents and a decrease in \bar{M}_n of about one-half. Treatment of the ether-insoluble product with alcoholic KOH resulted in fractionation of the product but not further degradation. The butylamine-methanol combination appears to behave similarly.

Pyridine hydroiodide in pyridine at room temperature decreases the \bar{M}_n of asphaltol to one-half to one-third of the original (upper right in Figure 1). This experiment was run on the premise that pyridine hydroiodide would be an acid in pyridine, which is an excellent solvent for asphaltol. However, methyl iodide was nearly as effective as HI. Asphaltol was treated with methyl iodide at room temperature in the hope of making sulfonium as well as pyridinium salts. The product was then heated to 140° at reduced pressure in the expectation of splitting out methyl iodide from pyridinium salts (without net coal bond cleavage) and conversion of the original sulfides to methyl sulfides and coal alkyl iodides, with net cleavage of sulfide bonds. However, the reduction in \bar{M}_n from 1250 to 660 is surprisingly high, since the 1.7% S content corresponds to only 0.66 S/asphaltol molecule, of which most is expected to be in heterocyclic aromatic rings. A somewhat greater reduction in \bar{M}_n is reported for a duplicate experiment in Figure 2. It is therefore possible that I⁻ alone may be able to cleave ether links, a conclusion to be supported in discussion of Figure 2. Thus, abilities of Me₃SiI⁴ and of hexamethyldisilazane plus ME₃SiCl (the latter intended for trimethylsilylation⁵) to cleave asphaltols may be due as much or more to halide ions generated as to the original reagent.

We tried sodium in liquid ammonia as an ether-cleaving reagent, but found that addition of sodium in liquid ammonia to a cold solution of asphaltol in butylamine gave better control, less reduction of the asphaltol, and a decrease in \bar{M}_n by nearly 50%. Treatment of this product with pyridine hydroiodide (right center of Figure 1) then gave further reduction in molecular weight. However, our data suggest that combination of the sodium and HI reactions gave no more cleavage than HI alone.

Figure 2 summarizes cleavage reactions of two other asphaltols with HI (check of Figure 1 experiment), HBr, toluene sulfonic acid, and some metal salts, all (except the MeI experiment) in pyridine solution. The other acids, even at 50°, are not as effective as HI at room temperature, but zinc bromide, and especially zinc chloride and LiI·H₂O,⁶ have given more molecular weight reduction than any of the acids. However, all of these reactions have apparently resulted in incorporation of pyridine in the products, as shown by the high recoveries and high nitrogen contents. Some products also lose weight slowly and persistently on heating at 140° in vacuo. A possible explanation is that cleavage of an aryl alkyl ether by metal halide gives metal phenolate and alkyl halide; some of the latter then reacts with pyridine solvent to give unstable quaternary pyridinium salts. However, the remarkable reactivity of these reagents at low temperatures may be associated with the use of pyridine as solvent.

Conclusions

This progress report shows that asphaltol from Illinois No. 6 coal can be extensively degraded at or near room temperature by several acidic and basic reagents and by some oxidizing and reducing agents, with good to excellent recovery of original

carbon. These agents appear to attack ether links, or maybe aromatic rings in oxidations at pH 13, but as yet we know of no precedent for reactions of aliphatic amines or alcoholic KOH with ethers at these temperatures. To determine the proportions of various kinds of breakable single bonds in Illinois No. 6 coal, we plan to carry out further degradations on asphaltol by combinations of reagents, and then extend the most promising of these reactions to extracted coal. We expect that this kind of information will provide the basis for new and economical approaches to coal liquefaction, which will employ much milder conditions and much less expensive processes and plants.

Acknowledgement

Most of the research described here was supported by the U.S. Department of Energy under Contract No. ET-78-C-01-3293.

References

- (1) Present address, Department of Chemistry, Eastern Illinois University, Charleston, IL, 61920.
- (2) J. G. Huntington, F. R. Mayo, and N. A. Kirshen, *Fuel*, 58, 24 (1979).
- (3) F. R. Mayo and N. A. Kirshen, *Fuel*, in press.
- (4) M. E. Jung and M. A. Lyster, *J. Org. Chem.*, 42, 3761 (1977).
- (5) S. Friedman, M. L. Kaufman, W. A. Steiner, and I. Wender, *Fuel*, 40, 33 (1961).
- (6) I. T. Harrison, *Chem. Communications*, 1969, 616.

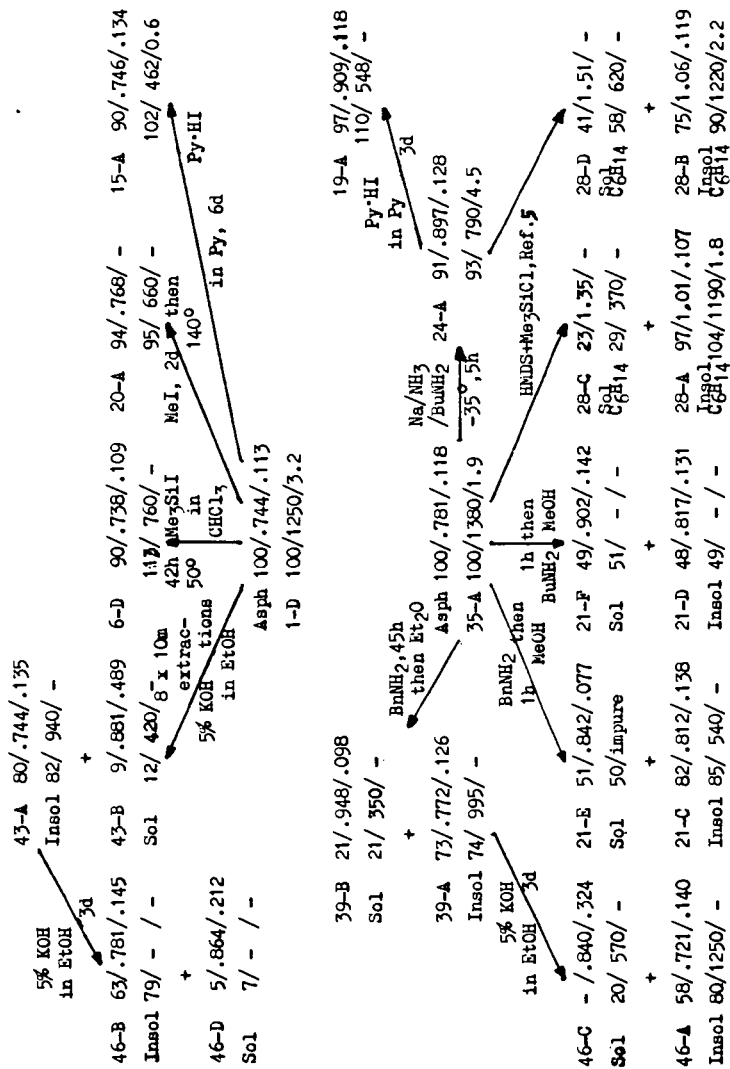
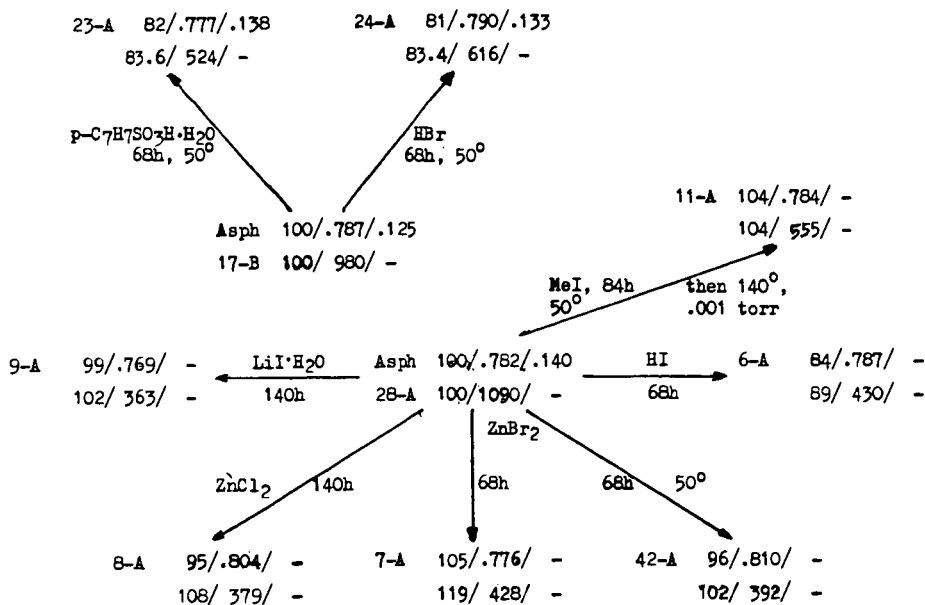


Figure 1. Cleavages of asphaltols, at room temperature, except as noted. Key and abbreviations are in Figure 2.



Key to arrangement of data:

Sample Atom % C/ H/C / O/C
 ↑
 Yield
 ↓
 No. Wt. % / \bar{M}_n /eq.OH/mole

Abbreviations:

As = asphaltol
 Bn = benzyl
 Bu, Et, Me = n-butyl, ethyl, methyl
 HMDS = hexmethyldisilazane
 d, h, m = days, hours, minutes

Figure 2. Cleavages of asphaltols in pyridine solution (except with MeI) and at room temperature (except as noted otherwise).

OXYDESULFURIZATION OF COAL TREATED WITH METHYL IODIDE --
IMPLICATIONS FOR REMOVAL OF ORGANIC SULFUR

R. Markuszewski, C.-K. Wei^a, and T. D. Wheelock

Ames Laboratory, USDOE, and
Department of Chemical Engineering
Iowa State University,
Ames, Iowa 50011

Introduction

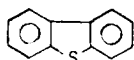
In the chemical desulfurization process being developed at the Ames Laboratory, coal is leached with a dilute solution of sodium carbonate containing dissolved oxygen under pressure and at elevated temperature. For many coals, most of the inorganic sulfur can be removed, and the organic sulfur content can be reduced by 25-40% (1,2). In some instances, as much as 70% of the organic sulfur has been removed. An essential piece of information in evaluating the effectiveness of a process for the removal of organic sulfur is the identity and reactivity of the various sulfur functions grouped under the term "organic sulfur."

Although much data is available on the content and distribution of the so-called pyritic, sulfatic, and organic sulfur in various coals, relatively little has been published on the nature and abundance of the organic sulfur groups in coal. Essentially no data are available on the reactivity of such functional groups under oxidizing conditions, such as those found during oxydesulfurization. In fact, no completely satisfactory method exists as yet for the direct determination of organic sulfur in coal, although a few methods are being developed. These methods are based either on microprobe analysis (3,4), or on low-temperature ashing of the organic components of coal (5), or on their thermokinetic reduction to hydrogen sulfide (6). As a routine, however, organic sulfur is still being determined as the difference between the total sulfur and the amount of the inorganic (i.e., pyritic plus sulfatic) sulfur, according to ASTM procedures.

Attempts to identify and quantitatively determine organic sulfur functions in coal have been few. On the basis of very sparse data, it is generally assumed that the organic sulfur in coal can be described almost completely by the following classes:

^a Present address: Dept. of Chemical Engineering, University of Minnesota, Minneapolis, MN 55455

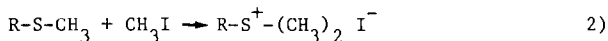
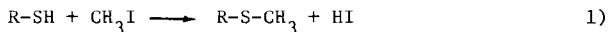
- Class 1. Aliphatic or aromatic thiols (mercaptans, thiophenols): R-SH, Ar-SH
- Class 2. Aliphatic, aromatic, or mixed sulfides (thioethers): R-S-R, Ar-S-Ar, R-S-Ar
- Class 3. Aliphatic, aromatic, or mixed disulfides (bisthioethers): R-SS-R, Ar-SS-Ar, R-SS-Ar
- Class 4. Heterocyclic compounds of the thiophene type: e.g., dibenzothiophene



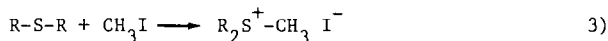
It is generally assumed that any chemical desulfurization process that can remove organic sulfur will do so because of the reactivity of compounds in Class 1, 2, and 3. Heterocyclic compounds in Class 4 are extremely stable to chemical attack and high temperature.

The fundamental approach in this study is based on the different reactivity of methyl iodide toward different organosulfur functions to produce sulfonium compounds. The general scheme of reactions for the various classes of sulfur groups can be summarized as follows (7):

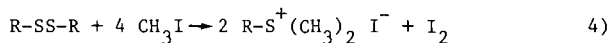
1. Mercaptans:



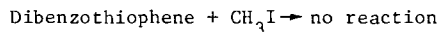
2. Sulfides:



3. Disulfides:



4. Heterocyclic compounds:



The reaction of coal with methyl iodide was used previously (8) to determine the thioether content of coal by measuring the uptake of iodine, presumably associated as iodide with the sulfonium compounds. But the iodine uptake is not a true measure of the thioether content because other compounds, notably heterocyclic nitrogen compounds, can also react resulting in uptake of iodine. To overcome this difficulty, the sulfonium compounds were washed out with a solvent like acetone, and the decrease in the sulfur content was then taken as the indicator of the thioether content (7). A similar procedure was adopted in this work.

Experimental

Materials

The coal used in this study was a high-volatile bituminous coal from the Star mine in Mahaska County, Iowa. The coal was pulverized, screened using U.S. Standard sieves, dried, and analyzed for ash, heating value, and sulfur distribution by ASTM procedures.

Fresh methyl iodide was used directly from the reagent bottle. In some experiments, the reagent was cleaned by shaking with mercury, but no significant difference was noticed in the results.

Methyl Iodide Reaction

A slurry of 20 g coal and 30 ml methyl iodide was placed in a large test tube, covered with foil, and allowed to stand for 3 days at room temperature. The slurry was then filtered and washed with about 2 l. acetone to remove reaction products and unreacted methyl iodide, until the test for iodide (silver nitrate) was negative. The treated coal was dried and analyzed again. Qualitative tests for residual iodide in the treated coal (hydrogen peroxide treatment followed by extraction of iodine into a benzene layer) showed only traces of iodide. The methyl iodide treatments were repeated on enough coal samples to provide a stock of treated coal to be used for the oxydesulfurization experiments.

Oxydesulfurization of Coal in Autoclave

The coal (40 g) was leached for 1 hr with 400 ml solution in a 1-liter autoclave described previously (1). The leaching was done at 150°C under 50 or 200 psia oxygen partial pressure. For non-oxidizing conditions, a partial pressure of 50 psia nitrogen was used. Water or 0.2 M sodium carbonate was used as the leaching solution. The residues from the alkaline leaching step were leached for a second time, also for 1 hr at 150°C, using water, 0.1 M sulfuric acid, 0.1 M phosphoric acid, or 0.2 M sodium carbonate in a nitrogen atmosphere.

Calculations

In order to account for the different levels of ash in the various coal residues, the sulfur content was converted from weight percent to pounds of sulfur per million Btu. This conversion, in effect, allowed the comparison of the organic sulfur content in the organic (i.e., combustible) portion of the coal.

In a few cases, the heating value was not actually determined but was calculated using a formula (1), based on the assumption that the ash-free heating value is relatively constant for the same coal, regardless of the treatment conditions.

Results and Discussion

Removal of Sulfur by the Methyl Iodide Treatment

The results of treating coal with methyl iodide are presented in Table 1. Based on the pounds of sulfur per million Btu, the methyl iodide treatment removed, on the average, 48.3% of the organic sulfur. This seems to indicate that at least one-half of the organic sulfur is in the class that is reactive toward methyl iodide. Since thiophenic compounds are unreactive and disulfide groups react too slowly at room temperature, the reactive portion of the organic sulfur is probably of the sulfide and mercaptan classes.

Further tests were run by treating mineral pyrite with methyl iodide under similar conditions and then washing with acetone. No reaction was observed; the sulfur content was unaffected. Also, simple washing of coal with 2 l. of acetone (without prior methyl iodide treatment) did not alter significantly the ash content, heating value, and sulfur distribution of the coal.

Another possible explanation for the reduction of the organic sulfur may be offered if methyl iodide simply methylates the coal, thus increasing its organic content and decreasing the sulfur content by "dilution." If this observation were a reflection of a methylating effect, then the heating value should have increased, the ash content should have decreased, and the "dilution" should apply to all types of sulfur in coal. Yet the changes in ash content, heating value, and weight recovery were insignificant; and the pyritic and sulfatic sulfur values were fairly constant. It seems, therefore, that organic sulfur was really removed by this procedure. It is not known, however, by what mechanism the sulfonium salts are washed away.

Removal of Sulfur by Oxidative Leaching

The results of leaching the methyl iodide-treated coal are presented in Table 2. The sulfur content should be compared not only to that of the initial coal but also to that of the methyl iodide-treated coal in Table 2. It can be seen that leaching with alkali only, (sample No. 016D), in the absence of oxygen, did not have any effect on the sulfur content. When leaching in the presence of oxygen, the total sulfur content decreased, largely because of a decrease in the inorganic sulfur content. The total sulfur content was lower when higher oxygen partial pressures were used or when the leaching solutions were alkaline. The organic sulfur content was relatively constant, although it appeared slightly higher under non-alkaline conditions when water only was used as the leachant.

In Table 3 results are presented for desulfurization experiments in which a second leaching step was added after the first leaching step with an alkaline solution. The additional leaching was done in a non-oxidizing nitrogen atmosphere, using water, sulfuric acid, phosphoric acid, or sodium carbonate solutions. Aside from one run which appears to be anomalous, the total sulfur content did not seem to be reduced by the second leaching step.

The organic sulfur content, however, appears to be slightly higher than that obtained after one leaching step, under alkaline conditions and in the presence of oxygen. It may be possible that under the nitrogen atmosphere of the second step, some of the pyrite may be converted to elemental sulfur. Such a conversion would be characterized by a decrease in the pyritic sulfur, an increase in the organic sulfur, but no change in the total sulfur. Such a conversion would also be favored by acidic conditions.

Methyl Iodide Treatment of Oxydesulfurized Coal

The results in Table 4 show the effect of methyl iodide treatment on Star coal that had been precleaned by a float-sink technique and subsequently leached for 1 hr with 0.2 M sodium carbonate at 150°C under 50 or 200 psia partial pressure of oxygen. By comparison with the sulfur values in Table 1, the cleaning and leaching apparently removed only the inorganic sulfur, leaving the organic sulfur content largely unaffected. Leaching at higher oxygen partial pressure seemed to remove more total sulfur.

Curiously, subsequent treatment of the leached coal with methyl iodide did not seem to remove any organic sulfur as it did when applied to the raw, unleached coal (see Table 1). This lack of reactivity may be due to physical changes in the coal caused by the high temperature (150°C) of the leaching. Alternatively, the chemical leaching may have caused a conversion of reactive organosulfur groups into unreactive groups. Perhaps also the difference in the particle size (-200 mesh in this set of experiments compared to -150/+200 mesh in previous experiments) can be a contributing factor.

Conclusions

Treatment of coal with methyl iodide followed by extensive washing with a solvent to remove the reaction products has been used to remove approximately one-half of the organic sulfur content in an Iowa high volatile bituminous coal. The pyritic and sulfatic sulfur content was not affected by the methyl iodide treatment. Washing the coal with solvent only did not produce any effect either. On the basis of chemical reactions reported in the literature, it is assumed that the reactive sulfur groups that were removed by this treatment may be organic sulfides or mercaptans.

Subsequent leachings of the methyl iodide-treated coal under various conditions of oxydesulfurization did not reduce further the organic sulfur content. The inorganic sulfur content, however, was reduced by the oxydesulfurization steps. It can be assumed that all the reactive and accessible organic sulfur was removed by the methyl iodide treatment, and further chemical desulfurization was directed only against the inorganic sulfur.

When the coal was first precleaned by a float-sink technique and then leached by the oxydesulfurization procedure, the organic sulfur content was not affected by subsequent treatment with methyl iodide. This lack of reactivity of the organic sulfur toward methyl iodide may be caused by physical or chemical changes in the coal brought about by the high temperature or chemical nature of the oxydesulfurization process.

Acknowledgment

This work was performed under Contract No. W-7405-eng-82 with the U.S. Department of Energy, Division of Fossil Energy.

References

1. Wheelock, T. D., Greer, R. T., Markuszewski, R., and Fisher, R. W., Annual Technical Progress Report, Oct. 1, 1977 - Sept. 30, 1978, IS-4668, Ames Laboratory DOE, Iowa State University, Ames, IA, (April, 1979)
2. Markuszewski, R., Chuang, K.-C., and Wheelock, T. D., Proceedings: Symposium on Coal Cleaning to Achieve Energy and Environmental Goals (Sept. 1978, Hollywood, FL), Vol. II, p. 1039, EPA-600/7-79-098b, April 1979.
3. Harris, L. A., Yust, C. S., and Crouse, R. S., Fuel 56, 456 (1977).
4. Raymond, R. and Gooley, R., Scanning Electron Microscopy, 1978/I, O. Johari, ed., SEM, Inc., AMF O'Hare, IL, 93 (1978).
5. Paris, B., Chap. 3 in Coal Desulfurization: Chemical and Physical Methods, T. D. Wheelock (ed.), ACS Symposium Series 64, Am. Chem. Soc., Washington, D.C., 1977.
6. Attar, A. and Dupuis, F., Am. Chem. Soc. Div. of Fuel Chem. Preprints 23(2), 44 (1978).
7. Angelova, G. K. and Syskov, K. I., Izv. Akad. Nauk SSSR, Met. Topl., No. 5, 153 (1959).
8. Postowsky, J. J. and Harlampovich, A. B., Fuel 15(8), 229 (1936).

Table 1. Effect of methyl iodide (MeI) treatment and acetone (Me₂CO) washing on sulfur content of coal.^a

No. ^b	Treatment	H.V., Btu./lb.	Ash, %	S Content, lb./10 ⁶ Btu.				S Redn., %	
				Tot.	Pyr.	Sulf.	Org.	Org.	Tot.
001D	None	12579	8.34	2.02	0.98	0.15	0.89	--	--
029D	Me ₂ CO	12495	8.95	2.06	1.08	0.20	0.78	--	--
003	MeI + Me ₂ CO	12552	8.29	1.68	1.08	0.17	0.43	50.6	16.8
004	MeI + Me ₂ CO	12490	8.46	1.62	1.18	0.14	0.30	66.3	19.8
005	MeI + Me ₂ CO	12506	8.57	1.78	1.04	0.10	0.64	28.1	11.9
Ave (of 003, 004, 005)		12516	8.44	1.70	1.10	0.14	0.46	48.3	15.8

^aStar coal (-150/+200 mesh).

^b"D" denotes average of duplicate analysis.

Table 2. One-step oxydesulfurization of MeI - treated coal.^a

Sample No. ^b	Leach soln.	O ₂ psia	H.V., Btu./lb.	Ash, %	S Content, lb./10 ⁶ Btu.				
					Tot.	Pyr.	Sulf.	Org.	Org.
001D	-- None	--	12579	8.34	2.02	0.98	0.15	0.89	
Ave. of 003, 004, 005	-- MeI	--	12516	8.44	1.70	1.10	0.14	0.46	
013	H ₂ O	50	12046	6.75	1.28	0.44	0.17	0.67	
006	Na ₂ CO ₃	50	10220	12.90	1.21	0.52	0.16	0.53	
014D	H ₂ O	200	11818	6.68	1.06	0.20	0.12	0.75	
012	Na ₂ CO ₃	200	11787	13.02	0.91	0.39	0.08	0.44	
016D	Na ₂ CO ₃	0 ^c	12245	7.41	1.63	0.95	0.11	0.57	

^aStar coal (-150/+200 mesh), treated with MeI and then leached 1 hr at 150°C with H₂O or 0.2 M Na₂CO₃ under 50 or 200 psia O₂.

^b"D" denotes average of duplicate analysis.

^cNon-oxidizing atmosphere of 50 psia N₂ partial pressure.

Table 3. Two-step desulfurization of MeI - treated coal.^a

Sample No. ^b	2nd step Leach	H.V., Btu./lb.	Ash, %	S Content, lb./10 ⁶ Btu.			
				Tot.	Pyr.	Sulf.	Org.
1st Leach Step with 0.2 M Na ₂ CO ₃ under 50 psia O ₂							
018D	H ₂ O	11119	14.28	1.30	0.67	0.03	0.60
020D	0.1 M H ₂ SO ₄	11529	6.72	1.24	0.46	0.05	0.73
023	0.1 M H ₃ PO ₄	11479	12.26	1.31	0.53	0.03	0.63
024D	0.2 M Na ₂ CO ₃	9042	13.33	1.20	0.52	0.07	0.61
1st Leach Step with 0.2 M Na ₂ CO ₃ under 200 psia O ₂							
027D	H ₂ O	11763 ^c	9.32	0.86	0.21	0.05	0.60
035D	0.1 M H ₂ SO ₄	11614 ^c	6.03	1.03	0.30	0.08	0.65
031D	0.1 M H ₃ PO ₄	11478 ^c	12.27	1.16	0.52	0.05	0.59
033D	0.2 M Na ₂ CO ₃	9831	19.65	1.20	0.65	0.08	0.47

^aStar coal (-150/+200 mesh), treated with MeI and then leached 1 hr at 150°C with 0.2 M Na₂CO₃ under 50 or 200 psia O₂. For 2nd step, leached 1 additional hr at 150°C under 50 psia N₂ with indicated leach solution.

^b"D" denotes average of duplicate analysis

^cH.V. calculated.

Table 4. Methyl iodide (MeI) treatment of leached coal.^a

Sample No. ^b	Treatment	H.V., Btu./lb.	Ash, %	S Content, lb./10 ⁶ Btu.			
				Tot.	Pyr.	Sulf.	Org.
060D	Leached under 50 psia O ₂	9162	9.53	1.29	0.24	0.05	1.00
062D	MeI treatment of Sample 060D	11370	10.63	1.26	0.24	0.01	1.01
064	Leached under 200 psia O ₂	10810	11.71	1.04	0.11	0.02	0.91
065D	MeI treatment of Sample 064	11534	10.56	0.96	0.10	0.01	0.85

^aStar coal (-200 mesh) precleaned and leached 1 hr at 150°C with 0.2 M Na₂CO₃ under 50 or 200 psia O₂.

^b"D" denotes average of duplicate analysis.

MOLECULAR COMPONENTS OF COAL AND COAL STRUCTURE. D. Bodzek and A. Marzec. Department of petroleum and Coal Chemistry. Polish Academy of Sciences. 44-100 Gliwice, 1 Maja 62 St. Poland.

High volatile bituminous coal was extracted at room temperature by means of 18 solvents having their electron-donor /DN/ and -acceptor /AN/ properties quantitatively determined. Extracts were analysed by field ionization and high resolution mass spectrometry. Extractable compounds having molecular masses in 200-600 a.m.u. range constitute 30% wt. of coal organic material. Hydrocarbons / $C_n H_{2n-6}$ up to $C_n H_{2n-34}$ /, nitrogen compounds /CHN, CHN_2 , CHN_3 /, oxygen compounds /CHO, CHO_2 / and nitrogen-oxygen compounds /CHNO, CHN_2O , $CHNO_2$, CHN_2O_2 , CHN_3O / were identified in the extracts. On the basis of extraction data /extract yields, solvent DN and AN numbers/ and MS analysis the conclusion has been drawn that extractable compounds are bonded to coal macromolecular network by electron-donor-acceptor bonds. These bonds are destroyed during extraction by substitution activity of solvents. Solvent substitution capabilities depend on their donor and acceptor numbers.